
NORTH ATLANTIC TREATY
ORGANIZATION



AC/323(AVT-237)TP/862

SCIENCE AND TECHNOLOGY
ORGANIZATION



www.sto.nato.int

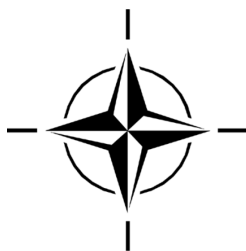
STO TECHNICAL REPORT

TR-AVT-237

Benchmarks in Multidisciplinary Optimization and Design for Affordable Military Vehicles

(Référentiels d'optimisation et de conception
pluridisciplinaires pour des véhicules
militaires abordables)

Final Report of NATO RTG AVT-237.



Published September 2019

Distribution and Availability on Back Cover





STO TECHNICAL REPORT

TR-AVT-237

Benchmarks in Multidisciplinary Optimization and Design for Affordable Military Vehicles

(Référentiels d'optimisation et de conception
pluridisciplinaires pour des véhicules
militaires abordables)

Final Report of NATO RTG AVT-237.

The NATO Science and Technology Organization

Science & Technology (S&T) in the NATO context is defined as the selective and rigorous generation and application of state-of-the-art, validated knowledge for defence and security purposes. S&T activities embrace scientific research, technology development, transition, application and field-testing, experimentation and a range of related scientific activities that include systems engineering, operational research and analysis, synthesis, integration and validation of knowledge derived through the scientific method.

In NATO, S&T is addressed using different business models, namely a collaborative business model where NATO provides a forum where NATO Nations and partner Nations elect to use their national resources to define, conduct and promote cooperative research and information exchange, and secondly an in-house delivery business model where S&T activities are conducted in a NATO dedicated executive body, having its own personnel, capabilities and infrastructure.

The mission of the NATO Science & Technology Organization (STO) is to help position the Nations' and NATO's S&T investments as a strategic enabler of the knowledge and technology advantage for the defence and security posture of NATO Nations and partner Nations, by conducting and promoting S&T activities that augment and leverage the capabilities and programmes of the Alliance, of the NATO Nations and the partner Nations, in support of NATO's objectives, and contributing to NATO's ability to enable and influence security and defence related capability development and threat mitigation in NATO Nations and partner Nations, in accordance with NATO policies.

The total spectrum of this collaborative effort is addressed by six Technical Panels who manage a wide range of scientific research activities, a Group specialising in modelling and simulation, plus a Committee dedicated to supporting the information management needs of the organization.

- AVT Applied Vehicle Technology Panel
- HFM Human Factors and Medicine Panel
- IST Information Systems Technology Panel
- NMSG NATO Modelling and Simulation Group
- SAS System Analysis and Studies Panel
- SCI Systems Concepts and Integration Panel
- SET Sensors and Electronics Technology Panel

These Panels and Group are the power-house of the collaborative model and are made up of national representatives as well as recognised world-class scientists, engineers and information specialists. In addition to providing critical technical oversight, they also provide a communication link to military users and other NATO bodies.

The scientific and technological work is carried out by Technical Teams, created under one or more of these eight bodies, for specific research activities which have a defined duration. These research activities can take a variety of forms, including Task Groups, Workshops, Symposia, Specialists' Meetings, Lecture Series and Technical Courses.

The content of this publication has been reproduced directly from material supplied by STO or the authors.

Published September 2019

Copyright © STO/NATO 2019
All Rights Reserved

ISBN 978-92-837-2186-4

Single copies of this publication or of a part of it may be made for individual use only by those organisations or individuals in NATO Nations defined by the limitation notice printed on the front cover. The approval of the STO Information Management Systems Branch is required for more than one copy to be made or an extract included in another publication. Requests to do so should be sent to the address on the back cover.

Table of Contents

	Page
List of Figures	xiii
List of Tables	xvii
AVT-237 Membership List	xix
Executive Summary and Synthèse	ES-1
Chapter 1 – Introduction	1-1
1.1 Background and Justification	1-1
1.2 Objectives	1-1
1.3 Topics Covered	1-2
1.4 Deliverables and/or End Product	1-2
1.5 Team and Resources	1-2
Chapter 2 – Documentation Standards for MDO Benchmarks	2-1
2.1 Documentation Standards: Benchmark Executive Summary	2-1
2.2 Documentation Standards: Benchmark Details	2-2
2.3 Documented Benchmarks	2-4
Chapter 3 – Benchmark: Efficient Supersonic Air Vehicle (ESAV)	3-1
3.1 Benchmark Executive Summary	3-1
3.1.1 Qualitative Optimization Problem Statement	3-1
3.1.1.1 Design Variables	3-1
3.1.1.2 Objective Function(s)	3-1
3.1.1.3 Constraint Function(s)	3-1
3.1.2 Description of Analyses/Disciplines/Theory/Fidelities Involved	3-1
3.1.3 MDO Approach (Algorithm/Architecture)	3-2
3.1.4 Implementation Details	3-2
3.1.4.1 Analysis Software	3-2
3.1.4.2 Optimization Software	3-2
3.1.4.3 Hardware	3-2
3.1.4.4 Human Effort	3-2
3.1.5 Results	3-2
3.1.5.1 Initial Design (Design Variables, Objectives, Constraint Values)	3-2
3.1.5.2 Optimized Design (Design Variables, Objectives, Constraint Values)	3-3
3.1.5.3 Observations	3-3
3.1.6 Technical and Financial Improvements/Benefits of Using MDO vs. Traditional Design Methods	3-3
3.1.7 References; Web Resources; Science Connect Link; and Validation Data Location	3-3
3.2 Benchmark Details	3-3
3.2.1 High-Level	3-3

3.2.2	Multidisciplinary Analysis (MDA)	3-4
3.2.2.1	Implementation Details of Analyses and Corresponding Responses Used to Formulate MDO Objective and Constraint Functions	3-4
3.2.2.2	Practical Concerns	3-7
3.2.3	MDO Problem Definition Details	3-7
3.2.4	MDO Algorithm	3-8
3.2.5	MDO Results	3-8
3.2.6	Technical and Financial Improvements/Benefits of Using MDO vs. Traditional Design Methods	3-12
3.2.7	References; Web Resources; Science Connect Link; and Validation Data Location	3-12

Chapter 4 – Benchmark: Common Research Model (CRM) 4-1

4.1	Benchmark Executive Summary: CRM Effort One	4-1
4.1.1	Qualitative Optimization Problem Statement	4-1
4.1.1.1	Design Variables	4-1
4.1.1.2	Objective Function(s)	4-2
4.1.1.3	Constraint Function(s)	4-2
4.1.2	Description of Analyses/Disciplines/Theory/Fidelities Involved	4-2
4.1.3	MDO Approach (Algorithm/Architecture)	4-2
4.1.4	Implementation Details	4-2
4.1.4.1	Analysis Software	4-2
4.1.4.2	Optimization Software	4-2
4.1.4.3	Hardware	4-2
4.1.4.4	Human Effort	4-2
4.1.5	Results	4-2
4.1.5.1	Initial Design (Design Variables, Objectives, Constraint Values)	4-3
4.1.5.2	Optimized Design (Design Variables, Objectives, Constraint Values)	4-3
4.1.5.3	Observations	4-4
4.1.6	Technical and Financial Improvements/Benefits of Using MDO vs. Traditional Design Methods	4-4
4.1.7	References; Web Resources; Science Connect Link; and Validation Data Location	4-4
4.2	Benchmark Executive Summary: CMR Effort Two	4-4
4.2.1	Qualitative Optimization Problem Statement	4-4
4.2.1.1	Design Variables	4-4
4.2.1.2	Objective Function(s)	4-5
4.2.1.3	Constraint Function(s)	4-5
4.2.2	Description of Analyses/Disciplines/Theory/Fidelities Involved	4-5
4.2.3	MDO Approach (Algorithm/Architecture)	4-6
4.2.4	Implementation Details	4-6
4.2.4.1	Analysis Software	4-6
4.2.4.2	Optimization Software	4-6
4.2.4.3	Hardware	4-7
4.2.4.4	Human Effort	4-7
4.2.5	Results	4-7
4.2.5.1	Initial Design (Design Variables, Objectives, Constraint Values)	4-7
4.2.5.2	Optimized Design (Design Variables, Objectives, Constraint Values)	4-7
4.2.5.3	Observations	4-7
4.2.6	Technical and Financial Improvements/Benefits of Using MDO vs. Traditional Design Methods	4-7

4.2.7	References; Web Resources; Science Connect Link; and Validation Data Location	4-7
4.3	Benchmark Executive Summary: CMR Effort Three	4-8
4.3.1	Qualitative Optimization Problem Statement	4-8
4.3.1.1	Design Variables	4-8
4.3.1.2	Objective Function(s)	4-8
4.3.1.3	Constraint Function(s)	4-8
4.3.2	Description of Analyses/Disciplines/Theory/Fidelities Involved	4-9
4.3.2.1	Analysis Model	4-9
4.3.3	MDO Approach (Algorithm/Architecture)	4-10
4.3.4	Implementation Details	4-10
4.3.4.1	Optimization Algorithm	4-10
4.3.4.2	Analysis Software	4-11
4.3.4.3	Optimization Software	4-11
4.3.4.4	Hardware	4-11
4.3.4.5	Human Effort	4-11
4.3.5	Results	4-11
4.3.5.1	Initial Design (Design Variables, Objectives, Constraint Values)	4-11
4.3.5.2	Optimized Design (Design Variables, Objectives, Constraint Values)	4-12
4.3.5.3	Observations	4-12
4.3.6	Technical and Financial Improvements/Benefits of Using MDO vs. Traditional Design Methods	4-13
4.3.7	References; Web Resources; Science Connect Link; and Validation Data Location	4-13
4.4	Benchmark Executive Summary: CRM Effort Four	4-13
4.4.1	Qualitative Optimization Problem Statement	4-13
4.4.1.1	Design Variables	4-13
4.4.1.2	Objective Function(s)	4-13
4.4.1.3	Constraint Function(s)	4-14
4.4.2	Description of Analyses/Disciplines/Theory/Fidelities Involved	4-15
4.4.2.1	Analysis Model	4-15
4.4.3	MDO Approach (Algorithm/Architecture)	4-15
4.4.4	Implementation Details	4-16
4.4.4.1	Optimization Algorithm	4-16
4.4.4.2	Analysis Software	4-16
4.4.4.3	Optimization Software	4-16
4.4.4.4	Hardware	4-16
4.4.4.5	Human Effort	4-16
4.4.5	Results	4-16
4.4.5.1	Initial Design	4-18
4.4.5.2	Optimized Design	4-18
4.4.5.3	Observations	4-18
4.4.6	Technical and Financial Improvements/Benefits of Using MDO vs. Traditional Design Methods	4-18
4.4.7	References; Web Resources; Science Connect Link; and Validation Data Location	4-19
Chapter 5 – Benchmark Executive Summary: Coupled Hydrostructural Optimization of a 3-D Hydrofoil		5-1
5.1	Benchmark Executive Summary	5-1
5.1.1	Qualitative Optimization Problem Statement	5-1

5.1.1.1	Design Variables	5-2
5.1.1.2	Objective Function(s)	5-2
5.1.1.3	Constraint Function(s)	5-2
5.1.2	Description of Analyses/Disciplines/Theory/Fidelities Involved	5-3
5.1.3	MDO Approach (Algorithm/Architecture)	5-3
5.1.4	Implementation Details	5-3
5.1.4.1	Analysis Software	5-3
5.1.4.2	Optimization Software	5-3
5.1.4.3	Hardware	5-3
5.1.4.4	Human Effort	5-3
5.1.5	Results	5-4
5.1.5.1	Initial Design (Design Variables, Objectives, Constraint Values)	5-4
5.1.5.2	Optimized Design (Design Variables, Objectives, Constraint Values)	5-4
5.1.5.3	Observations	5-4
5.1.6	Technical and Financial Improvements/Benefits of Using MDO vs. Traditional Design Methods	5-6
5.1.7	References; Web Resources; Science Connect Link; and Validation Data Location	5-6
5.2	Benchmark Details	5-6
5.2.1	High-Level	5-6
5.2.2	Multidisciplinary Analysis (MDA)	5-6
5.2.2.1	Implementation Details of Analyses and Corresponding Responses Used to Formulate MDO Objective and Constraint Functions	5-6
5.2.2.2	Practical Concerns	5-9
5.2.3	MDO Problem Definition Details	5-9
5.2.4	MDO Algorithm	5-9
5.2.5	MDO Results	5-9
5.2.6	Technical and Financial Improvements/Benefits of Using MDO vs. Traditional Design Methods	5-10
5.2.7	References; Web Resources; Science Connect Link; and Validation Data Location	5-10
Chapter 6 – Benchmark: Goal Oriented Structural Design of the CRM Wing Box		6-1
6.1	Benchmark Executive Summary	6-1
6.1.1	Qualitative Optimization Problem Statement	6-1
6.1.1.1	Design Variables	6-2
6.1.1.2	Objective Function(s)	6-3
6.1.1.3	Constraint Function(s)	6-3
6.1.2	Description of Analyses/Disciplines/Theory/Fidelities Involved	6-3
6.1.3	MDO Approach (Algorithm/Architecture)	6-3
6.1.4	Implementation Details	6-3
6.1.4.1	Analysis Software	6-3
6.1.4.2	Optimization Software	6-3
6.1.4.3	Hardware	6-4
6.1.4.4	Human Effort	6-4
6.1.5	Results	6-4
6.1.5.1	Optimization Convergence History	6-4
6.1.5.2	Observations	6-5
6.1.6	Technical and Financial Improvements/Benefits of Using MDO vs. Traditional Design Methods	6-5

6.1.7	References; Web Resources; Science Connect Link; and Validation Data Location	6-6
6.2	Benchmark Details	6-6
6.2.1	High-Level	6-6
6.2.2	Multidisciplinary Analysis (MDA)	6-6
6.2.2.1	Implementation Details of Analyses and Corresponding Responses Used to Formulate MDO Objective and Constraint Functions	6-6
6.2.2.2	Practical Concerns	6-9
6.2.3	MDO Problem Definition Details	6-9
6.2.4	MDO Algorithm	6-10
6.2.5	MDO Results	6-10
6.2.6	Technical and Financial Improvements/Benefits of Using MDO vs. Traditional Design Methods	6-11
6.2.7	References; Web Resources; Science Connect Link; and Validation Data Location	6-11
 Chapter 7 – Benchmark: Multidisciplinary Robust Design Optimization of a Keel Fin of a Racing Sailboat		7-1
7.1	Benchmark Executive Summary	7-1
7.1.1	Qualitative Optimization Problem Statement	7-1
7.1.1.1	Design Variables	7-2
7.1.1.2	Objective Function(s)	7-2
7.1.1.3	Constraint Function(s)	7-2
7.1.2	Description of Analyses/Disciplines/Theory/Fidelities Involved	7-2
7.1.3	MDO Approach (Algorithm/Architecture)	7-3
7.1.4	Implementation Details	7-3
7.1.4.1	Analysis Software	7-3
7.1.4.2	Optimization Software	7-3
7.1.4.3	Hardware	7-3
7.1.4.4	Human Effort	7-3
7.1.5	Results	7-3
7.1.5.1	Initial Design (Design Variables, Objectives, Constraint Values)	7-3
7.1.5.2	Optimized Design (Design Variables, Objectives, Constraint Values)	7-3
7.1.5.3	Observations	7-4
7.1.6	Technical and Financial Improvements/Benefits of Using MDO vs. Traditional Design Methods	7-4
7.1.7	References; Web Resources; Science Connect Link; and Validation Data Location	7-4
7.2	Benchmark Details	7-5
7.2.1	High-Level	7-5
7.2.2	Multidisciplinary Analysis (MDA)	7-6
7.2.2.1	Implementation Details of Analyses and Corresponding Responses Used to Formulate MDO Objective and Constraint Functions	7-6
7.2.2.2	Practical Concerns	7-8
7.2.3	MDO Problem Definition Details	7-8
7.2.4	MDO Algorithm and Setup	7-9
7.2.5	MDO Results	7-14
7.2.6	Technical and Financial Improvements/Benefits of Using MDO vs. Traditional Design Methods	7-16
7.2.7	References; Web Resources; Science Connect Link; and Validation Data Location	7-16

Chapter 8 – Benchmark: Application of MDO for an Aircraft Wing Design		8-1
8.1	Benchmark Executive Summary	8-1
8.1.1	Qualitative Optimization Problem Statement	8-1
8.1.1.1	Design Variables	8-2
8.1.1.2	Objective Function(s)	8-2
8.1.1.3	Constraint Function(s)	8-2
8.1.2	Description of Analyses/Disciplines/Theory/Fidelities Involved	8-3
8.1.3	MDO Approach (Algorithm/Architecture)	8-4
8.1.4	Implementation Details	8-4
8.1.4.1	Analysis Software	8-4
8.1.4.2	Optimization Software	8-4
8.1.4.3	Hardware	8-4
8.1.4.4	Human Effort	8-4
8.1.5	Results	8-4
8.1.5.1	Initial Design (Design Variables, Objectives, Constraint Values)	8-4
8.1.5.2	Optimized Design (Design Variables, Objectives, Constraint Values)	8-5
8.1.5.3	Observations	8-6
8.1.6	Technical and Financial Improvements/Benefits of Using MDO vs. Traditional Design Methods	8-6
8.1.7	References; Web Resources; Science Connect Link; and Validation Data Location	8-6
8.2	Benchmark Details	8-6
8.2.1	High-Level	8-6
8.2.2	Multidisciplinary Analysis (MDA)	8-7
8.2.2.1	Implementation Details of Analyses and Corresponding Responses Used to Formulate MDO Objective and Constraint Functions	8-7
8.2.2.2	Practical Concerns	8-10
8.2.3	MDO Problem Definition Details	8-10
8.2.4	MDO Algorithm	8-12
8.2.5	MDO Results	8-12
8.2.5.1	Basic Test Case	8-12
8.2.5.2	Parametric Study 1: Structural Model	8-14
8.2.5.3	Parametric Study 2: Aerodynamic Model	8-14
8.2.5.4	Parametric Study 3: Pressure Control	8-15
8.2.5.5	Parametric Study 4: Bounds on Aerodynamic Variables	8-16
8.2.6	Technical and Financial Improvements/Benefits of Using MDO vs. Traditional Design Methods	8-16
8.2.6.1	Multidisciplinary vs. Single-Discipline Optimization	8-16
8.2.7	References; Web Resources; Science Connect Link; and Validation Data Location	8-17
Chapter 9 – Benchmark: Aerodynamics and Radar Cross Section Multiobjective and Multidisciplinary Optimization Study		9-1
9.1	Benchmark Executive Summary	9-1
9.1.1	Qualitative Optimization Problem Statement	9-1
9.1.1.1	Design Variables	9-1
9.1.1.2	Objective Function(s)	9-1
9.1.1.3	Constraint Function(s)	9-1
9.1.2	Description of Analyses/Disciplines/Theory/Fidelities Involved	9-1
9.1.3	MDO Approach (Algorithm/Architecture)	9-1

9.1.4	Implementation Details	9-2
9.1.4.1	Analysis Software	9-2
9.1.4.2	Optimization Software	9-2
9.1.4.3	Hardware	9-2
9.1.4.4	Human Effort	9-2
9.1.5	Results	9-2
9.1.5.1	Initial Design (Design Variables, Objectives, Constraint Values)	9-2
9.1.5.2	Optimized Design (Design Variables, Objectives, Constraint Values)	9-2
9.1.5.3	Observations	9-2
9.1.6	Technical and Financial Improvements/Benefits of Using MDO vs. Traditional Design Methods	9-3
9.1.7	References; Web Resources; Science Connect Link; and Validation Data Location	9-3
9.2	Benchmark Details	9-3
9.2.1	High-Level	9-3
9.2.2	Multidisciplinary Analysis (MDA)	9-3
9.2.2.1	Implementation Details of Analyses and Corresponding Responses Used to Formulate MDO Objective and Constraint Functions	9-3
9.2.2.2	Practical Concerns	9-6
9.2.3	MDO Problem Definition Details	9-6
9.2.4	MDO Algorithm	9-7
9.2.5	MDO Results	9-7
9.2.6	Technical and Financial Improvements/Benefits of Using MDO vs. Traditional Design Methods	9-7
9.2.7	References; Web Resources; Science Connect Link; and Validation Data Location	9-9
Chapter 10 – Benchmark: Efficient Supersonic Air Vehicle (ESAV)		10-1
10.1	Benchmark Executive Summary	10-1
10.1.1	Qualitative Optimization Problem Statement	10-1
10.1.1.1	Design Variables	10-1
10.1.1.2	Objective Function(s)	10-1
10.1.1.3	Constraint Function(s)	10-1
10.1.2	Description of Analyses/Disciplines/Theory/Fidelities Involved	10-1
10.1.3	MDO Approach (Algorithm/Architecture)	10-2
10.1.4	Implementation Details	10-3
10.1.4.1	Analysis Software	10-3
10.1.4.2	Optimization Software/Framework	10-3
10.1.4.3	Hardware	10-3
10.1.4.4	Human Effort	10-3
10.1.5	Results	10-4
10.1.5.1	Initial Design (Design Variables, Objectives, Constraint Values)	10-4
10.1.5.2	Optimized Design (Design Variables, Objectives, Constraint Values)	10-4
10.1.5.3	Observations	10-6
10.1.6	Technical and Financial Improvements/Benefits of Using MDO vs. Traditional Design Methods	10-6
10.1.7	References; Web Resources; Science Connect Link; and Validation Data Location	10-6
10.2	Benchmark Details	10-6
10.2.1	High-Level	10-7
10.2.2	Multidisciplinary Analysis (MDA)	10-9

10.2.2.1	Implementation Details of Analyses and Corresponding Responses Used to Formulate MDO Objective and Constraint Functions	10-9
10.2.2.2	Practical Concerns	10-12
10.2.3	MDO Problem Definition Details	10-13
10.2.4	MDO Algorithm	10-15
10.2.5	MDO Results	10-16
10.2.5.1	Design Variables: Initial, Final, and Optimization Iteration History	10-16
10.2.5.2	Objective and Constraint Values: Initial, Final, and Optimization Iteration History (Gradient Values if Applicable)	10-17
10.2.5.3	Pareto Fronts	10-18
10.2.5.4	Discussion of Physics of Initial and Final Designs	10-18
10.2.5.5	Resource Utilization and Cost	10-18
10.2.6	Technical and Financial Improvements/Benefits of Using MDO vs. Traditional Design Methods	10-19
10.2.7	References; Web Resources; Science Connect Link; and Validation Data Location	10-19
 Chapter 11 – Benchmark: Turbine Multidisciplinary Optimization at the Preliminary Design Phase		11-1
11.1	Benchmark Executive Summary	11-1
11.1.1	Qualitative Optimization Problem Statement	11-2
11.1.1.1	Design Variables	11-2
11.1.1.2	Objective Function(s)	11-2
11.1.1.3	Constraint Function(s)	11-2
11.1.2	Description of Analyses/Disciplines/Theory/Fidelities Involved	11-2
11.1.3	MDO Approach (Algorithm/Architecture)	11-3
11.1.4	Implementation Details	11-3
11.1.4.1	Analysis Software	11-6
11.1.4.2	Optimization Software	11-6
11.1.4.3	Hardware	11-6
11.1.4.4	Human Effort	11-6
11.1.5	Results	11-7
11.1.5.1	Initial Design (Design Variables, Objectives, Constraint Values)	11-7
11.1.5.2	Optimized Design (Design Variables, Objectives, Constraint Values)	11-8
11.1.5.3	Observations	11-8
11.1.6	Technical and Financial Improvements/Benefits of Using MDO vs. Traditional Design Methods	11-8
11.1.7	References; Web Resources; Science Connect Link; and Validation Data Location	11-8
 Chapter 12 – Benchmark: Assess the Ability to Optimize Hull Forms of Sea Vehicles for Best Performance in a Sea Environment		12-1
12.1	Benchmark Executive Summary	12-1
12.1.1	Qualitative Optimization Problem Statement	12-1
12.1.1.1	Design Variables	12-2
12.1.1.2	Objective Function(s)	12-2
12.1.1.3	Constraint Function(s)	12-3
12.1.2	Description of Analyses/Disciplines/Theory/Fidelities Involved	12-3
12.1.3	MDO Approach (Algorithm/Architecture)	12-3
12.1.4	Implementation Details	12-4

12.1.4.1	Analysis Software	12-4
12.1.4.2	Optimization Software	12-4
12.1.4.3	Hardware	12-4
12.1.4.4	Human Effort	12-4
12.1.5	Results	12-4
12.1.5.1	Propeller Optimization for Optimized Hull Form	12-7
12.1.5.2	Initial Design (Design Variables, Objectives, Constraint Values)	12-8
12.1.5.3	Optimized Design (Design Variables, Objectives, Constraint Values)	12-8
12.1.5.4	Observations	12-8
12.1.6	Technical and Financial Improvements/Benefits of Using MDO vs. Traditional Design Methods	12-9
12.1.7	References; Web Resources; Science Connect Link; and Validation Data Location	12-9

Chapter 13 – Benchmark: Reliability-Based Aeroelastic Optimization of the AGARD 445.6 Wing **13-1**

13.1	Benchmark Executive Summary	13-1
13.1.1	Qualitative Optimization Problem Statement	13-1
13.1.1.1	Design Variables	13-1
13.1.1.2	Objective Function(s)	13-2
13.1.1.3	Constraint Function(s)	13-2
13.1.2	Description of Analyses/Disciplines/Theory/Fidelities Involved	13-2
13.1.3	MDO Approach (Algorithm/Architecture)	13-3
13.1.4	Implementation Details	13-6
13.1.4.1	Analysis Software	13-6
13.1.4.2	Optimization Software	13-7
13.1.4.3	Hardware	13-7
13.1.4.4	Human Effort	13-8
13.1.5	Results	13-8
13.1.5.1	Initial Design (Design Variables, Objectives, Constraint Values)	13-8
13.1.5.2	Optimized Design (Design Variables, Objectives, Constraint Values)	13-8
13.1.5.3	Observations	13-9
13.1.6	Technical and Financial Improvements/Benefits of Using MDO vs. Traditional Design Methods	13-10
13.1.7	References; Web Resources; Science Connect Link; and Validation Data Location	13-10

Chapter 14 – Benchmark: The MALE UAV Case Studies at Airbus Military Aircraft **14-1**

14.1	Benchmark Executive Summary	14-2
14.1.1	Qualitative Optimization Problem Statement	14-2
14.1.1.1	Design Variables	14-7
14.1.1.2	Objective Function(s)	14-7
14.1.1.3	Constraint Function(s)	14-7
14.1.2	Description of Analyses/Disciplines/Theory/Fidelities Involved	14-7
14.1.3	MDO Approach (Algorithm/Architecture)	14-7
14.1.4	Implementation Details	14-8
14.1.4.1	Analysis Software	14-8
14.1.4.2	Optimization Software	14-10
14.1.4.3	Hardware	14-10

14.1.4.4	Human Effort	14-10
14.1.5	Results	14-12
14.1.5.1	Initial Design (Design Variables, Objectives, Constraint Values)	14-12
14.1.5.2	Optimized Design (Design Variables, Objectives, Constraint Values)	14-14
14.1.5.3	Observations	14-14
14.1.6	Technical and Financial Improvements/Benefits of Using MDO vs. Traditional Design Methods	14-16
14.1.7	References; Web Resources; Science Connect Link; and Validation Data Location	14-16

List of Figures

Figure		Page
Figure 3-1	The ESAV MDA N ² Diagram Includes Geometry Generation, an Aerodynamic Analysis, an Aeroelastic Analysis with Structural Sizing Optimization, and a Performance Analysis	3-4
Figure 3-2	The ESAV Optimization Result Half-Span Planforms: Baseline 1550 mi Range and 13125 lb Weight; 1500 mi Range and 13013 lb Weight; and 2500 mi Range and 14065 lb Weight	3-9
Figure 3-3	Results from ESAV Optimization Illustrate How the Design Variables, Objective and Constraint Functions are Manipulated by the SLP Technique (1500 mi Range Constraint; 2500 mi Range Constraint)	3-10
Figure 3-4	The ESAV Planform and Structural Design Thicknesses from the ASTROS Structural Sizing Sub-Optimization Problem are Shown Above for the 1550 mi Range Baseline Design, the 1500 mi Range Design and the 2500 mi Range Design Optimal Designs	3-11
Figure 4-1	Baseline CRM Structure Used for Tailoring Studies	4-6
Figure 4-2	CRM Aerodynamic DLM Box Pattern with Location of Structural Wing Box	4-9
Figure 4-3	CRM Structural Model Using Linear Solid Hexahedra Elements (150,300 Elements)	4-10
Figure 4-4	CRM Initial Design	4-12
Figure 4-5	Structural Topologies for $\eta = 0.75$, $\eta = 0.5$, $\eta = 0.25$	4-12
Figure 4-6	uCRM-9 Wingbox Optimized for Static Aerodynamic Loading	4-17
Figure 4-7	uCRM Meshes Used for Buckling Optimization	4-17
Figure 4-8	uCRM-13.5 Buckling and Stress Constraints Optimized Designs	4-18
Figure 5-1	Design Variables Used for the Optimization	5-2
Figure 5-2	Comparison of the Predicted and Measured Efficiency and Tip Bending Deformation as a Function of Lift Coefficient for Both the Aluminum NACA 0009 Baseline and the Optimized Aluminum Hydrofoils	5-5
Figure 5-3	Coupled Hydrostructural Optimization Procedure Flowchart	5-7
Figure 5-4	Dimensions and Boundary Conditions for the CFD and FEA Models of the Baseline NACA 0009 Hydrofoil	5-8
Figure 5-5	Comparisons of the Sectional Geometries of the NACA 0009 Baseline, the Multipoint Hydrodynamic-Only, and the Multipoint Hydrostructural Optimized Hydrofoil	5-10
Figure 6-1	Design Variables Definition	6-2
Figure 6-2	Initial and Target (Reference) Design Variable Values	6-2
Figure 6-3	Nested Structural Sizing Process with High Fidelity CFD/CSM Analysis and Derivatives	6-4

Figure 6-4	Design Variables Convergence History	6-5
Figure 6-5	Objective Function Convergence History	6-5
Figure 6-6	Finite Element Model Version v14 with Implicit Stiffeners	6-6
Figure 6-7	Initial Fluid Mesh in 1 G Cruise Flight Conditions and Corresponding Jig Shape	6-6
Figure 6-8	The Different Steps of the Steady Aeroelastic NLBGS (Non Linear Block Gauss Seidel) Solver	6-7
Figure 6-9	Steady Equilibrium in 1 G Cruise Flight Conditions	6-8
Figure 6-10	Pressure Coefficient Distributions for Steady Aeroelastic Configuration in 1 G Cruise Flight Conditions	6-8
Figure 6-11	Initial and Target Spanwise Twist Distributions	6-10
Figure 6-12	Initial and Final Design Variables Distribution	6-11
Figure 7-1	Keel Fin Optimization Examples	7-2
Figure 7-2	N ² Diagram Including Optimization, Uncertainty Quantification, and MDA	7-5
Figure 7-3	Pseudo-Code for MDO Algorithm	7-6
Figure 7-4	Pressure Coefficient for Original and Optimized Configurations – Starboard View and Port View (Yaw Angle, $\gamma = 5$ Deg)	7-8
Figure 7-5	Shape Modification Due to x_1	7-9
Figure 7-6	Shape Modification Due to x_2	7-9
Figure 7-7	Multidisciplinary Robust Design Optimization Using MDF Architecture	7-10
Figure 7-8	Metamodel-Based MRDO Using MDF Architecture	7-10
Figure 7-9	Variable-Accuracy MRDO Method Including Refinement for the Training Set DoE, Variable UQ Accuracy, and Variable MDA Coupling	7-11
Figure 7-10	Variable-Accuracy Global Metamodel-Based MRDO Algorithm	7-12
Figure 7-11	Deterministic Particle Swarm Optimization Algorithm Convergence	7-14
Figure 7-12	Original vs. MRDO Benchmark Solution	7-15
Figure 7-13	Parametric Analysis of the Hydrodynamic Efficiency vs. the Yaw Angle: Comparison of Original and Optimized Designs	7-15
Figure 8-1	Characteristics of Wing Geometry	8-1
Figure 8-2	Initial and Final Wing Section Shape	8-5
Figure 8-3	The N ² Diagram for the Wing Optimization Problem	8-7
Figure 8-4	Initial Root Wing Cross-Section Shape and Associated B-Spline Control Points	8-8
Figure 8-5	Wing Box Model	8-9
Figure 8-6	Optimization Problem Flowchart	8-11
Figure 8-7	Normalized Optimization Histories for the Basic Test Case	8-13
Figure 8-8	Initial and Final Cross-Sectional Shape for the Basic Test Case	8-13
Figure 8-9	Results for Pressure Control Parametric Study	8-15
Figure 8-10	Multidisciplinary vs. Sequential Single-Discipline Optimizations	8-17

Figure 9-1	The Design Variables and the Design Space	9-4
Figure 9-2	A Generated Grid Using Pointwise Scripting	9-5
Figure 9-3	Pareto Front Results	9-8
Figure 9-4	The Flow Pattern of the Final Design	9-8
Figure 10-1	Results	10-5
Figure 10-2	N ² Diagram	10-8
Figure 10-3	Optimization Results	10-17
Figure 11-1	Turbine System Optimizer Modules	11-2
Figure 11-2	Single Platform Integration Environment	11-3
Figure 11-3	Disc Design Charts	11-4
Figure 11-4	Tip Clearance Calculator (TCC)	11-5
Figure 11-5	Comparison of Final Design and RAF 3D Concept	11-7
Figure 12-1	Bio-Metric Methods are Used to Design Hull Forms	12-1
Figure 12-2	ISIS-CFD Computational Domain and Boundaries with a Computed Free Surface	12-5
Figure 12-3	Optimized and Original Hull Stations – INSEAN/UI (NK-WC); ITU; and NTUA	12-5
Figure 12-4	Optimized and Original Wave Elevations Distribution for Calm Water at Fr = 0.28 Stations – INSEAN/UI (NK-WC); ITU; and NTUA	12-6
Figure 12-5	Optimized and Original Wave Elevations Distribution for Calm Water at Fr = 0.41 Stations – INSEAN/UI (NK-WC); ITU; and NTUA	12-6
Figure 12-6	panMARE Computational Grid	12-7
Figure 12-7	Shape and Pressure Distribution on the Optimal Propeller	12-8
Figure 13-1	Wing Geometry	13-2
Figure 13-2	Staggered Algorithm for the Aeroelastic Coupling	13-3
Figure 13-3	Probability Density Function (PDF) for Limit-State Function g(.)	13-3
Figure 13-4	Transformation of Random Variables to Standard Normal Space	13-4
Figure 13-5	Reliability-Based Aeroelastic Optimization Workflow: AGARD 445.6 Wing	13-7
Figure 13-6	Mass vs. LD Ratio Space	13-9
Figure 14-1	The MALE UAV	14-1
Figure 14-2	MALE UAV Mock-Up (Airbus Talarion)	14-2
Figure 14-3	Excel-Based Creation of Wing Models with Different Tip Surfaces	14-3
Figure 14-4	Model Geometry and Zoning	14-4
Figure 14-5	Model Creation Process	14-9
Figure 14-6	Numbering Scheme for Structural and Aerodynamic Sub-Components	14-9
Figure 14-7	Structural Elements Numbering Scheme Within One Strip	14-10
Figure 14-8	Two Models Created by the Structural Analysis Department Method	14-11
Figure 14-9	Sets of Different Wing Tip Configurations	14-13

Figure 14-10	Model with Flexing Wing Tips	14-13
Figure 14-11	MALE Optimization Results with Different Optimization Methods	14-14
Figure 14-12	“Spider Web” Attachment for a Lumped Mass in the Forward Fuselage	14-15

List of Tables

Table		Page
Table 4-1	Summary of the Optimization Formulations	4-3
Table 4-2	Summary of the Optimization Studies: All Cases Satisfy $C_L = 5$, and All Optimizations Include the Wing Shape Variables as Well as the Geometric Constraints	4-3
Table 5-1	Problem Setup for the Coupled Hydrostructural Optimization of the 3-D Hydrofoil	5-4
Table 5-2	Assumed Probability of Operation at Each Lift Coefficient, and Comparison Between the Baseline and the Optimized Efficiency (C_L/C_D) for the Baseline and the Hydrostructural Optimized Hydrofoil	5-4
Table 7-1	MRDO Benchmark vs. Variable-Accuracy Results	7-4
Table 7-2	Variable-Accuracy MRDO Simulations	7-13
Table 7-3	MRDO Benchmark vs. Variable-Accuracy Results	7-14
Table 8-1	Aerodynamic Design Variable Details	8-8
Table 8-2	Wing Box Design Variables	8-9
Table 8-3	Wing Box Material Properties	8-9
Table 8-4	Structural Design Model Details	8-10
Table 8-5	Basic Test Case Initial and Final Design Performance Values	8-12
Table 8-6	Initial and Final Structural Designs for the Basic Test Case	8-13
Table 8-7	Results for the Structural Optimization Model Parametric Study	8-14
Table 8-8	Results for the Aerodynamic Optimization Model Parametric Study	8-14
Table 8-9	Optimal Results With and Without Pressure Control	8-15
Table 8-10	Results for the Aerodynamic Bounds Parametric Study	8-16
Table 9-1	The Sample Points (as Non-Dimensional) that are Selected by Latin Hypercube Sampling Method	9-4
Table 10-1	Design Variable Information	10-4
Table 10-2	Objective and Constraint Values	10-4
Table 10-3	Optimization Results	10-5
Table 10-4	Design Optimization Problem Statement	10-8
Table 10-5	Reference Aircraft Geometry Data	10-10
Table 10-6	Joined Wing Configuration Data	10-11
Table 10-7	Design Variables	10-13
Table 10-8	Optimization Objective Function Information	10-14
Table 10-9	Optimization Constraint Function Information	10-15
Table 10-10	Optimization Design Variable Results	10-16

Table 10-11	Optimization Objective and Constraint Function Results	10-18
Table 12-1	Optimization Results Summary – RANS Validation of PF-Based Optimal Solutions	12-7
Table 13-1	Pareto's of AGARD 445.6 Wing Aeroelastic Optimization with RBDO	13-8
Table 14-1	Main Geometry Data for the Reference Configuration	14-5
Table 14-2	Additional Design Data	14-5
Table 14-3	Airfoil Data	14-5
Table 14-4	Time Requirements for the MDO Process	14-7
Table 14-5	Computing Time Comparison for Different Sets of Design Variables	14-12

AVT-237 Membership List

CO-CHAIRS

Dr. Raymond KOLONAY
United States Air Force Research Lab
UNITED STATES
Email: Raymond.Kolonay@us.af.mil

Prof.Dr. Melike NIKBAY
Istanbul Technical University
TURKEY
Email: nikbay@itu.edu.tr

MEMBERS

Dr. W. Keith BELVIN
NASA Langley Research Center
UNITED STATES
Email: w.k.belvin@nasa.gov

Prof. Gregory GRIGOROPOULOS
National Technical University of Athens
GREECE
Email: gregory@central.ntua.gr

Mr. Christophe BLONDEAU
ONERA
FRANCE
Email: Christophe.blondeau@onera.fr

Dr. Jean-Pierre GRISVAL
ONERA
FRANCE
Email: jean-pierre.grisval@laposte.net

Dr. Scott BURTON
American Optimization LLC
UNITED STATES
Email: scottburton@amopti.com

Mr. Derya GURAK
TAI/TUSAS
TURKEY
Email: dgurak@tai.com.tr

Dr. Emilio CAMPANA
National Research Council of Italy –
CNR INSEAN
ITALY
Email: emiliofortunato.campana@cnr.it

Mr. Peter HOPGOOD
Dstl
UNITED KINGDOM
Email: pjhopgood@dstl.gov.uk

Dr. Fernass DAOUD
CASSIDIAN A/C Engineering COEAM4
GERMANY
Email: fernass.daoud@cassidian.com

Mr. Erdogan Tolga INSUYU
Turkish Aerospace Industry
TURKEY
Email: tinsuyu@tai.com.tr

Mr. Jakub GLOWKA
Industrial Research Institute for Automation &
Measurements PIAP
POLAND
Email: jglowka@piap.pl

Dr. Andrzej MAJKA
Rzeszow University of Technology
POLAND
Email: Andrzej.Majka@prz.edu.pl

Dr. Anant GREWAL
National Research Council – Aerospace Research
Centre
CANADA
Email: anant.grewal@nrc-cnrc.gc.ca

Dr. Hany MOUSTAPHA
Ecole de technologie supérieure
CANADA
Email: hany.moustapha@etsmtl.ca

Mr. Evren SAKARYA
TAI/TUSAS
TURKEY
Email: esakarya@tai.com.tr

Mr. Johannes SCHWEIGER
Self-Employed / Retired from EADS
GERMANY
Email: hschwe3449@aol.com

Miss Jessica SUMMERSBY
Dstl
UNITED KINGDOM
Email: jsummersby@dstl.gov.uk

Dipl.-Ing. Uwe VOGEL
MTU Aero Engines AG
GERMANY
Email: uwe.vogel@mtu.de

Dr.-Ing. Dirk ZIMPER
German Aerospace Center
GERMANY
Email: dirk.zimper@dlr.de

PANEL/GROUP MENTOR

Prof. Afzal SULEMAN
Instituto Superior Tecnico
PORTUGAL
Email: suleman@tecnico.ulisboa.pt

Benchmarks in Multidisciplinary Optimization and Design for Affordable Military Vehicles

(STO-TR-AVT-237)

Executive Summary

The primary purpose of this task group is to identify and collect enduring benchmark problems in Multidisciplinary Optimization and Design that represent a variety of multidisciplinary optimization and design issues for military vehicles. The purpose of the benchmark problems is to aid the development, assessment and promotion of multidisciplinary optimization and design methods. The availability of benchmark problems provide a means of verifying and validating new methods, define a process for multidisciplinary optimization and design, show the potential along with the limitations, and provide confidence in analytical results to anchor for certification.

The goal of the task group is to establish standards for multidisciplinary optimization and design benchmark problem descriptions for land, sea and air military vehicles and establish a repository of benchmark problems according to those standards.

The topics of interest to this working group fall into three categories: Optimization and design methods, analytical methods, and physical testing. Problems of interest in these categories address land, sea and air military vehicles.

Benchmarks for optimization and design methods address techniques such as multi-objective and multi-level optimization, the applicability of the methods, optimization and design for robustness, and the processes associated with each method.

Benchmarking analytical methods represent to some degree the degenerative case of optimization and design, where the design space has been reduced to a single point. However, it is still important to understand these problems, especially the applicability and limits of the analytical methods, for that defines the part of the design space in which reasonable results can be expected. Analytical methods issues of interest include analysis tool limits, tool fidelity interaction, virtual representation of manufacturing quality to address scale-up issues, and uncertainty quantification.

Physical benchmarks are used to validate point designs within the design space to increase confidence in the analytical results. Of primary interest with the physical benchmarks is to obtain as much information as possible regarding the test to increase reusability of test results.

Référentiels d'optimisation et de conception pluridisciplinaires pour des véhicules militaires abordables

(STO-TR-AVT-237)

Synthèse

L'objet principal de ce groupe de travail est d'identifier et de recenser les problèmes durables de référentiel en matière d'optimisation et de conception pluridisciplinaires, qui reflètent divers problèmes d'optimisation et de conception pluridisciplinaires des véhicules militaires. Cet inventariage vise à faciliter le développement, l'évaluation et la promotion de méthodes pluridisciplinaires d'optimisation et de conception. La mise à disposition des problèmes de référentiel permet de vérifier et valider de nouvelles méthodes, définir un processus d'optimisation et de conception pluridisciplinaires, démontrer le potentiel et les limites et donner confiance dans les résultats d'analyse pour qu'ils servent de base à la certification.

Le but du groupe de travail est d'établir des normes de description des problèmes de référentiel d'optimisation et de conception pluridisciplinaires pour les véhicules militaires terrestres, maritimes et aériens et d'établir un répertoire des problèmes de référentiel selon ces normes.

Les sujets intéressant ce groupe de travail entrent dans trois catégories : les méthodes d'optimisation et de conception, les méthodes d'analyse et les essais physiques. Les problèmes de ces catégories touchent aux véhicules militaires terrestres, maritimes et aériens.

Les référentiels des méthodes d'optimisation et de conception traitent de techniques telles que l'optimisation multiobjectif et multiniveau, l'applicabilité des méthodes, l'optimisation et la conception en vue de la robustesse et les processus associés à chaque méthode.

Les méthodes d'analyse de la référenciation représentent dans une certaine mesure la dégénérescence de l'optimisation et de la conception, puisque le champ de la conception est réduit à un seul point. Cependant, il demeure important de comprendre ces problèmes, en particulier l'applicabilité et les limites des méthodes d'analyse, qui définissent la part du champ de la conception dans laquelle on peut s'attendre à des résultats raisonnables. Les problèmes relatifs aux méthodes d'analyse sont notamment les limites des outils d'analyse, l'interaction entre les différentes fidélités des outils, la représentation virtuelle de la qualité de fabrication pour résoudre les problèmes de changement d'échelle et la quantification de l'incertitude.

Les référentiels physiques servent à valider des modèles à points dans le champ de conception, afin d'accroître la confiance dans les résultats d'analyse. Le premier intérêt des référentiels physiques est d'obtenir autant d'informations que possible à propos de l'essai, afin d'augmenter la possibilité de réutilisation des résultats d'essai.

Chapter 1 – INTRODUCTION

Raymond M. Kolonay
Air Force Research Laboratory
UNITED STATES

This AVT-237 final report is organized with the following sections:

- Introduction;
- Documentation Standards for Multidisciplinary Design Optimization Benchmarks;
- Multidisciplinary Design Optimization Benchmarks; and
- Conclusions and Closing Remarks.

1.1 BACKGROUND AND JUSTIFICATION

The political arena is rapidly changing. Military requirements differ significantly now than they did just a decade ago. To meet the new and ever-changing demands in a timely fashion, the time required and cost to develop new weapon systems needs to be significantly reduced. The need to bring new affordable and reliable weapons systems online rapidly requires a quick and thorough assessment of the design space. AVT recently completed assessments of this need from two different perspectives.

ET-054 explored the issue of affordable weapons systems and led to the formation of AVT-092, “Qualification by Analysis,” and AVT-093, “Integrated Tools and Processes for Affordable Weapons Systems.” AVT-093 focused on “the integration of tools and processes, not on the description of tools and processes.” AVT-093 also identified needs in multidisciplinary design optimization that could be addressed using the integration of tools and processes in a distributed parallel computing environment that would enable a feedback of information from detail to preliminary and preliminary to conceptual design. AVT-092 recognized that these capabilities described in AVT-093 are necessary to achieve the objective of rapid design and qualification of new vehicles. Both teams recognized that there is a gap between the current technology and the desired end state of rapidly developing affordable weapons systems and developments in multidisciplinary technologies are key capabilities for closing that gap. The recently completed AVT-173 demonstrated the current developments in MDO and Virtual Prototyping, but concluded that there is a great need to compare different approaches across a range of different benchmark applications.

Implementation of rapid analytical design development methodologies can lead to reduced technology risk, reduced occurrences of late defects (and hence reduce the need to correct or compensate for late defects), in addition to the reduced cycle time and reduced cost of development. An automated multidisciplinary approach also permits a more in depth consideration of operational and maintenance issues in the design process which in turn will reduce operational and maintenance costs. Verification and validation are key tools to developing successful rapid analytical design methodologies. The range of available methodologies and processes need evaluating.

1.2 OBJECTIVES

The primary purpose of this task group is to identify and collect enduring benchmark problems in Multidisciplinary Optimization and Design that represent a variety of multidisciplinary optimization and design

issues for military vehicles. The purpose of the benchmark problems is to aid the development, assessment and promotion of multidisciplinary optimization and design methods. The availability of benchmark problems provides a means of verifying and validating new methods, define a process for multidisciplinary optimization and design, show the potential along with the limitations, and provide confidence in analytical results to anchor for certification.

The goal of the task group is to establish standards for multidisciplinary optimization and design benchmark problem descriptions for land, sea and air military vehicles and establish a repository of benchmark problems according to those standards.

1.3 TOPICS COVERED

Of primary interest to this activity is establishing standards and a repository for multidisciplinary optimization and design for land, sea and air military vehicles. The standards for benchmark problems and resulting MDO design studies will define the information needed to sufficiently describe the benchmark and its area of applicability including its limits of applicability. Each problem in the repository of benchmark problems will adhere to the standards set forth by the group.

The topics of interest to this working group fall into three categories: optimization and design methods, analytical methods, and physical testing. Problems of interest in these categories address land, sea and air vehicles.

Benchmarks for optimization and design methods address techniques such as multi-objective and multi-level optimization, the applicability of the methods, optimization and design for robustness, and the processes associated with each method.

Benchmarking computational methods represent to some degree the degenerative case of optimization and design, where the design space has been reduced to a single point. However, it is still important to understand these problems, especially the applicability and limits of the methods for that defines the part of the design space in which reasonable results can be expected. Computational methods issues of interest include analysis tool limits, tool fidelity interaction, discipline coupling, virtual representation of manufacturing quality to address scale-up issues, and uncertainty quantification.

Physical benchmarks are used to validate point designs within the design space to increase confidence in the computational results. Of primary interest with the physical benchmarks is to obtain as much information as possible regarding the test to increase reusability of test results.

1.4 DELIVERABLES AND/OR END PRODUCT

This task group will deliver two products: a report giving a set of standards for multidisciplinary optimization and design benchmark definitions, and a repository of benchmarks.

1.5 TEAM AND RESOURCES

The Technical Team Leaders are Co-Chairs: Dr. Ray Kolonay (USA) and Prof. Melike Nikbay (TUR) and the Lead Nation is the United States. The panel mentor is Afzal Suleman (PRT). The following nations are participants: DEU, GBR, ITA, POL, PRT, TUR, USA.

The National and/or NATO resources required by the Exploratory Team are meeting space during AVT Panel Business Weeks. The meeting space is necessary to suitably prepare for and to coordinate the associated activities.



Chapter 2 – DOCUMENTATION STANDARDS FOR MDO BENCHMARKS

Scott A. Burton
American Optimization LLC
UNITED STATES

Raymond M. Kolonay
Air Force Research Laboratory
UNITED STATES

The first deliverable of the AVT-237 effort was to develop and codify documentation standards for Multidisciplinary Design Optimization (MDO) benchmark problems. The driving principal behind the standards was to develop standards that would provide a researcher the necessary information to understand and implement the vehicle optimization performed in a benchmark. Specifically, the goals of the standards were to:

- Describe pertinent aspects of MDO problem;
- Contain enough information to duplicate MDO results; and
- Document the technical and financial improvement by using MDO in design relative to a traditional design process.

The documentation standards were developed and refined over the course of the AVT-237 effort, edited and approved by the entire AVT-237 team, and used to document several MDO benchmark problems (covered in the next section of this document). The resulting documentation standards have two components: the Benchmark Executive Summary and the Benchmark Details.

2.1 DOCUMENTATION STANDARDS: BENCHMARK EXECUTIVE SUMMARY

The executive summary contains a brief description of the benchmark problem. An outline of the executive summary is as follows:

X.1.1 Qualitative Optimization Problem Statement

X.1.1.1 Design Variables

X.1.1.2 Objective Function(s)

X.1.1.3 Constraint Function(s)

X.1.2 Description of Analyses/Disciplines/Theory/Fidelities Involved

X.1.3 MDO Approach (Algorithm/Architecture)

X.1.4 Implementation Details

X.1.4.1 Analysis Software

X.1.4.2 Optimization Software

X.1.4.3 Hardware

X.1.4.4 Human Effort

X.1.5 Results

X.1.5.1 Initial Design (Design Variables, Objectives, Constraint Values)

X.1.5.2 Optimized Design (Design Variables, Objectives, Constraint Values)**X.1.5.3 Observations**

- Initial vs. final design physics;
- Comments on impact of MDO changes to initial design;
- Comments on computational cost;
- MDO setup time/ effort; and
- Comments on robustness of MDO method to MDA failures.

X.1.6 Technical and Financial Improvements/Benefits of Using MDO vs. Traditional Design Methods**X.1.7 References; Web Resources; Science Connect Link; and Validation Data Location****2.2 DOCUMENTATION STANDARDS: BENCHMARK DETAILS**

The Benchmark Details were developed to provide an in-depth description of the apparatus and results of the benchmark problem. The Benchmark Details are defined by the following outline:

X.2.1 High-Level

- Design phase: conceptual; preliminary; or detailed;
- Design scope: system-level; sub-system level; component-level discussion; and
- N² Diagram of responses required by objective and constraint functions (and analysis quality metrics).

X.2.2 MultiDisciplinary Analysis (MDA)**X.2.2.1 Implementation Details of Analyses and Corresponding Responses Used to Formulate MDO Objective and Constraint Functions**

- Analysis techniques/disciplines involved: deterministic; physics-based analysis details – FEM, CFD, etc.
- Probabilistic analysis details: random variable info – PDFs, etc.; and UQ method info – Monte Carlo, FORM, SORM, etc.
- Model details: input for each block in N²; mesh, boundary conditions, etc.; info. how to reconstruct input/models from scratch; and info. where to obtain/download model and input files required to execute analyses.
- Quality/fidelity/computational cost discussion: are there quality metrics that may be used as constraints or monitoring? Response quality metrics (coupled physics convergence criteria, sub-optimization convergence criteria, mesh criteria, etc.).
- Description of non-linear coupled physics approach (if present).
- Description of sub-optimizations (if present).
- Response gradients: implementation details – finite-difference; adjoint; automatic differentiation, etc.; quality discussion; computational cost discussion.

X.2.2.2 Practical Concerns

- Software description: commercial/in-house; software cost / license issues; operating system platforms supported (Windows, Linux, Macintosh, etc.); where/how to obtain/download software? Coarse-grain parallel compatibility / thread safety for multi-core machines.
- Hardware used/required: single PC specs (memory, CPU); grid computing specs; cluster computing specs; supercomputing specs; disc space required.
- Computational cost: CPU time; wall time.
- Human effort: MDA setup time; is MDA automatic?
- Reliability: if MDA fails, does it fail gracefully? How is MDA failure communicated to MDO algorithm? If MDA hangs, will there be a timeout and kill? Restartable?

X.2.3 MDO Problem Definition Details

- Design variables: integer; real; discrete; ordinal and non-ordinal.
- Objective function(s): multi- or single-objective; min/max; comments on function(s) quality (smooth, discontinuous, noisy w.r.t. design variables, etc.); computational cost.
- Objective function(s) gradient (if used): finite-difference; direct differentiation; adjoint, automatic differentiation; FD complex step, etc.; computational cost.
- Constraint functions: equality/inequality; bounds; comments on function(s) quality (smooth, discontinuous, noisy w.r.t. design variables, etc.); computational cost.
- Constraint functions gradients (if used): finite-difference; direct differentiation; adjoint, automatic differentiation; FD complex step, etc.; computational cost.
- Problem-specific constraint function formulation concerns: identification of critical load cases and appropriate # of loading conditions; Aeroelastic effects or rigid? Updated during MDO? Inertial effects? Is the air vehicle and engine trimmed?

X.2.4 MDO Algorithm/Approach

- Kind: deterministic, reliability-based, robust, etc. optimization.
- Type: shape, sizing, topology, other (geometric, performance such as aircraft engine or determining optimal trim parameters); monolithic MDA approaches (SLP, SQP, SAND, GA, etc.); MDO approaches (loosely coupled MDA); BLISS, CSSO, etc.).
- Surrogate models (if used): Kriging, RSM, neural nets, etc.; if sampling technique state type of sampling technique to train model surrogate models (DOE, Latin Hypercube, space filling designs, low discrepancy sequences) and number of samples to train surrogate model; state quality metrics? When to update during MDO?
- Reliability: is the algorithm tolerant of MDA (constraint and objective function failures)? Does the algorithm cache intermediate results to facilitate restart?
- Termination criteria/convergence criteria: consider running optimization a fixed computational budget; fixed number of function calls; fixed amount of wall time (schedule).

X.2.5 MDO Results

- Design variables: initial, final, and optimization iteration history.

- Objective and constraint values: initial, final, and optimization iteration history (gradient values if applicable).
- Pareto fronts.
- Discussion of physics of initial and final designs.
- Resource utilization and cost: computer hardware used; number of exact objective function calls (and gradient calls); number of exact constraint function calls (and gradient calls); CPU time, wall time, and time between problem definition and final first optimization. How well does the approach parallelize? How are license pools for software managed? How was the process affected by resource limitations (computational, software licenses, hardware, human)? Human effort.
- Optimization parameter settings.
- Number of optimization iterations; convergence criteria; number of generations.
- Comparison of results; compare to results without MDO; compare to results with other single-discipline/MDA/MDO methods; compare to experimental/validation data.
- Lessons learned.

X.2.6 Technical and Financial Improvements/Benefits of Using MDO vs. Traditional Design Methods

X.2.7 References; Web Resources; Science Connect Link; and Validation Data Location

2.3 DOCUMENTED BENCHMARKS

Several AVT-237 team members proposed, identified and created benchmark documentation for different vehicle design studies. The benchmarks included examples from land, sea, air and space applications. The benchmarks are:

- Scott Burton (AFRL): Efficient Supersonic Air Vehicle (ESAV);
- Johannes Schweiger (Air Bus Defence and Space, Military Aircraft): Medium Altitude Long Endurance (MALE) UAV;
- Melike Nikbay (Istanbul Technical University): Reliability-based Aeroelastic Optimization of the AGARD 445.6 Wing;
- Tolga Insuyu (Turkish Aerospace Industries): Evaluation of a Camber Morphing Concept Based on Controlled Flexibility;
- Afzal Suleman (University of Victoria): Joined wing optimization transport aircraft NOVEMOR Regional Jet;
- Anant Grewal (National Research Council): Application of MDO for an Aircraft Wing Design;
- Jean-Pierre Grisval (ONERA): M6 Wing Optimization, Aero-structural optimization of a high-fidelity wing-fuselage configuration;
- Emilio Campana, Italy: Naval MDO Benchmark;
- Hany Moustapha, Canada: Turbine Engine Benchmarks;
- Keith Belvin, United States: Space Systems Optimization; and
- Ray Kolonay, United States: NASA Common Research Model.

In addition to the documentation, some of the benchmarks have made available computer models and data via the Science Connect website to facilitate future research in MDO. Accessing the Science Connect website is done with the following steps:

- Login on this page: https://www.sto.nato.int/lm_auth_proxy?DoLMLogin?curl=L2f&curlid=3395279007-96106377.
- Select 'My Services' from 'MY PAGE' pull-down at top of page.
- Click 'Science Connect', then click LOWER (lower-right of page) 'Science Connect'.
- On left under 'Spaces', click 'AVT-237/RTG – Benchmarks_...'
- On left under 'Files' click 'Benchmarks'.



Chapter 3 – BENCHMARK: EFFICIENT SUPERSONIC AIR VEHICLE (ESAV)

Scott A. Burton

American Optimization LLC
UNITED STATES

The Air Force Research Lab's Multidisciplinary Science and Technology Center is investigating conceptual design processes and computing frameworks that could significantly impact the design of the next generation Efficient Supersonic Air Vehicle (ESAV). The ESAV conceptual design process must accommodate appropriate fidelity Multidisciplinary Engineering Analyses (MDAs) to assess the impact of new air vehicle technologies. These analyses may be coupled and computationally expensive, posing a challenge due to the large number of air vehicle configurations analyzed during conceptual design. In light of these observations, a design process using the Service-Oriented Computing Environment (SORCER) software is implemented to combine propulsion, structures, aerodynamics, aeroelasticity, and performance in an integrated MDA. The SORCER software provides the automation and tight integration to grid computing resources necessary to achieve the volume of appropriate fidelity analyses required. Two design studies are performed using a gradient-based optimization method to produce long and short range ESAV wing designs. The studies demonstrate the capability of the ESAV MDA, the optimization algorithm, and the computational scalability and reliability of the SORCER software.

3.1 BENCHMARK EXECUTIVE SUMMARY

3.1.1 Qualitative Optimization Problem Statement

The ESAV MDA is a blend of conceptual and preliminary analyses. The scope is system-level; design and analysis of an air vehicle.

3.1.1.1 Design Variables

The design variables are wing shape planform parameters: wing area, aspect ratio, and taper ratio.

3.1.1.2 Objective Function(s)

The single objective function is structural airframe weight of fuselage and wing.

3.1.1.3 Constraint Function(s)

There are two optimization problems solved in this benchmark:

- 1) A short-range design problem with a 1500 mile minimum range constraint; and
- 2) A long-range design problem with a 2500 mile minimum range constraint.

3.1.2 Description of Analyses/Disciplines/Theory/Fidelities Involved

The MDA is a blend of conceptual and preliminary analysis methods from geometry, propulsion, structures, aerodynamics, aeroelasticity, and performance disciplines. The process begins by parametrically generating

geometry, mesh, and input data suitable for several different analyses at varying fidelities. The geometry is used as input to compute several figures of merit of the air vehicle, which include the air vehicle drag polars, design mass, range, and aeroelastic performance. The different responses are evaluated for several flight conditions and manoeuvres. These responses are then used to construct the objective and constraints of the Multidisciplinary Optimization (MDO) problem.

3.1.3 MDO Approach (Algorithm/Architecture)

The optimization technique applied is an adaptation of the Frank-Wolf implementation of the Successive Linear Programming (SLP) method. It is a gradient-based method that uses a finite-difference approach to compute sensitivities. Issues of computational efficiency and robustness are addressed using parallel computations with SORCER and high-order/adaptive finite-differencing techniques.

3.1.4 Implementation Details

3.1.4.1 Analysis Software

Geometry generation and analysis input generation for AWAVE wave drag), ASTROS (aeroelastic structural sizing), FRICTION (viscous and profile drag), TORNADO (subsonic induced drag), WINGDES (supersonic induced drag), MSTCPERF (aircraft performance) are provided by a compiled MATLAB code called MSTCGEOM. AWAVE, FRICTION, and WINGDES are compiled FORTRAN; TORNADO and MSTCPERF are compiled MATLAB.

3.1.4.2 Optimization Software

The optimization software is a compiled MATLAB program developed at AFRL called MSTCOPT (“mystic-opt”). MSTCOPT is a robust Frank-Wolf SLP implementation adapted for parallel gradient and pseudo-line search calculations. The SORCER/MSTC-Engineering MDO framework is used to facilitate automatic MDA evaluations in parallel on multiple computers.

3.1.4.3 Hardware

Several desktop computers are used to implement a grid computing facilitating using SORCER and Java Space technology. A combination of four Macintosh and Linux PCs are used. The SORCER Space computing infrastructure allows the dynamic addition/removal of computer resources, so the number of computers used during the study is not fixed.

3.1.4.4 Human Effort

The human effort was not quantified.

3.1.5 Results

3.1.5.1 Initial Design (Design Variables, Objectives, Constraint Values)

Initial design variable values (wing area/aspect ratio/taper ratio): 400 ft²/0.85/0.28. Initial objective and constraint function values: weight = 13,125 lb; range = 1550 mi.

3.1.5.2 Optimized Design (Design Variables, Objectives, Constraint Values)

Short-range design: Design variable values (wing area/aspect ratio/taper ratio): 320 ft²/0.80/0.28; Objective and constraint function values: weight = 13,013 lb; range = 1500 mi. Long-range design: Design variable values (wing area/aspect ratio/taper ratio): 600 ft²/2.30/0.10; Objective and constraint function values: weight = 14,065 lb; range = 2500 mi.

3.1.5.3 Observations

Increasing aspect ratio and wing area increased range as expected. The limiting structural sizing sub-optimization was driven by the Mach 0.9/9 g pull in both cases, and additionally by the Mach 1.2/7.2 g pull in the short range case. The optimization algorithm used wing area and aspect ratio to both tune the weight and range. Gradient calculations were done in parallel on up to four machines. About seven hours for an optimization.

The MSTCOPT SLP implementation worked well; optimization converged as expected. SORCER enabled the addition of computers as they came available in the evening while the optimization was running.

The setup time and human effort were not recorded.

MSTCOPT is robust to failures; if errors occur, new points are generated and executed. SORCER will also regenerate requested runs if there is a failure in network or SORCER analysis provider.

3.1.6 Technical and Financial Improvements/Benefits of Using MDO vs. Traditional Design Methods

Unknown.

3.1.7 References; Web Resources; Science Connect Link; and Validation Data Location

Details on the benchmark may be found in:

Burton, S.A., Alyanak, E. and Kolonay, R.M. (2014). Efficient supersonic air vehicle design using the Service-Oriented Computer Environment (SORCER), *Int. J. Simul. Multisci. Des. Optim.*, 5, A25, DOI: 10.1051/smdo/2014005.

The Science Connect link is <https://scienceconnect.sto.nato.int/apps/10773>.

No validation data is available.

3.2 BENCHMARK DETAILS

3.2.1 High-Level

The ESAV MDA is a blend of conceptual and preliminary analyses. The scope is system-level; design and analysis of an air vehicle. See Figure 3-1 for ESAV N² diagram.

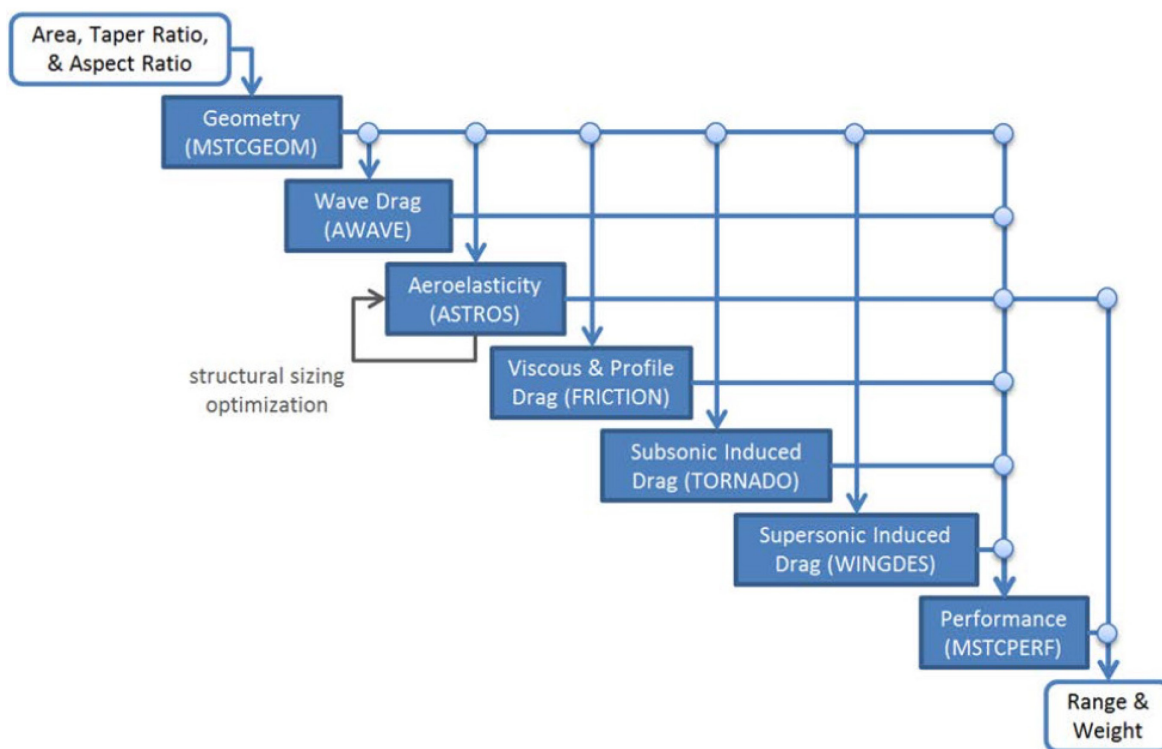


Figure 3-1: The ESAV MDA N^2 Diagram Includes Geometry Generation, an Aerodynamic Analysis, an Aeroelastic Analysis with Structural Sizing Optimization, and a Performance Analysis.

3.2.2 Multidisciplinary Analysis (MDA)

3.2.2.1 Implementation Details of Analyses and Corresponding Responses Used to Formulate MDO Objective and Constraint Functions

The MDA described herein is a blend of conceptual and preliminary analysis methods from geometry, propulsion, structures, aerodynamics, aeroelasticity, and performance disciplines.

The process begins by parametrically generating geometry, mesh, and input data suitable for several different analyses at varying fidelities. The geometry is used as input to compute several figures of merit of the air vehicle, which include the air vehicle drag polars, design mass, range, and aeroelastic performance. The different responses are evaluated for several flight conditions and manoeuvres. These responses are then used to construct the objective and constraints of the Multidisciplinary Optimization (MDO) problem.

The purpose of the airframe geometry application, MSTCGEOM, is to create geometry data for the physics-based analyses in the MDA. MSTCGEOM is compiled MATLAB™ code and is considered medium fidelity. The application does not replace or replicate the extensive functionality of a commercial CAD package (i.e., a high fidelity geometry application); however, it does go beyond the functionality of a typical conceptual design tool. MSTCGEOM parametrically creates mid-plane panel aerodynamic models and FEM analysis and design models. In the case of ASTROS or NASTRAN, these FEM models may include static and dynamic aeroelastic load cases. In addition, composite structural elements and distributed masses to represent sub-systems may be a part of the FEM models. The geometric features of the aircraft modelled include the fuselage and all of the

lifting aircraft components (wings, vertical stabilizer, and horizontal stabilizers). The physics-based analyses that use the MSTCGEOM output include ASTROS, FRICTION, TORNADO, AWAVE, WINGDES, and MSTCPERF.

MSTCGEOM is computationally inexpensive to execute and produces the required fidelity output for the ESAV analyses described herein. In this manner, MSTCGEOM is a bridge between conceptual and preliminary design fidelities. MSTCGEOM may be used to make both parametric and topological changes to the airframe wing during the MDO.

MSTCGEOM works by building up a series of major components such as cross sections, wing sections, point masses, and material definitions into assemblies such as wing components and a fuselage. Each of these components and assemblies are objects that contain methods that return information to support analysis model generation for a specific fidelity or type of model. For example, a cross section object may return mid-plane information to support the generation of a linear aerodynamic panel model. Likewise, the same cross section object can also return a completely discretized representation of itself for use in a FEM (i.e., the logic to produce both models exists in the same object). Any aerodynamic or structural mesh that is produced may be refined based on the user's requirements. The level of refinement used in the ESAV analyses is accurate enough to produce the correct physics-based global trends, but is not sufficient to identify stress concentrations that may be used in fatigue life prediction.

Stress analyses and aeroelastic sizing for the ESAV are performed for four static aeroelastic manoeuvre cases at an altitude of 10,000 ft. Specifically, they are the following:

- 1) A 9.0 g pull-up at Mach 0.9;
- 2) A 7.2 g pull-up at Mach 1.2;
- 3) A negative 3.0 g push-over at Mach 1.2; and
- 4) An anti-symmetric 100 deg·s⁻¹ aileron roll at Mach 1.2.

ASTROS is used to perform the aeroelastic analysis and structural sizing optimization that results in an optimized structural weight subject to stress constraints. The structural sizing optimization is considered a sub-optimization in regard to the overall optimization problem. To that end, the structural sizing optimization is an integral part of the MDA and is performed for each configuration analyzed. The structural sizing sub-optimization problem has fifty-seven design variables that are distributed over the wing and tail surface spar, rib, and skin thicknesses. The ESAV is modeled with aluminum and 70 ksi is used as the maximum allowable stress.

To assess the aero performance of a configuration, estimations of zero-lift drag and induced drag are required. The zero lift drag components estimated are viscous and profile drag. They are calculated using the FRICTION code. Solutions for zero lift drag are computed at a number of altitude and Mach numbers. Specifically, the altitudes are: 0; 10,000; 30,000 and 60,000 ft. The Mach numbers are: 0.0; 0.1; 0.5; 0.9; 1.0; 1.1; 1.5; and 2.0.

The induced drag is estimated using the vortex lattice code TORNADO. A TORNADO solution is computed over a range of angles of attack and Mach numbers and combined with the FRICTION results to develop a set of drag polars. The resulting set of drag polars are used in the mission performance calculations for each configuration.

BENCHMARK: EFFICIENT SUPERSONIC AIR VEHICLE (ESAV)

For the structural sizing problem, the aerodynamic analysis is internal to the ASTROS application. Specifically, USSAERO is the aerodynamic solver used in the version of ASTROS for the study herein. The USSAERO aerodynamic model contains all the lifting and control surfaces.

The aircraft engine performance is modeled using TERMAP (Turbine Engine Reverse Modeling Aid Program). TERMAP is an engine cycle performance program developed by Allison Engineering that uses a building block approach to predict both the steady state and transient performance of gas turbine engines. The program is FORTRAN-based and requires a user to define engine component characteristics. TERMAP uses this information to estimate flow path information at station numbers throughout the engine.

To improve the computational efficiency of the N^2 process in Figure 3-1, TERMAP is used to build an engine deck approximation of thrust and specific fuel consumption over all flight conditions of interest. The engine deck is used during the optimization to calculate range and optimal altitude trajectory for the flight leg of interest.

The mission performance assessment involves calculating the aircraft range for a given Mach number. This is accomplished by using the design weight from ASTROS. This FEM-based weight calculation is higher fidelity than an empirically-based calculation typically done in conceptual design. The design weight includes non-structural masses and internal fuel load, such that the design weight is the gross takeoff weight for the vehicle. (Since a half-span model is used, the weight from ASTROS is half the takeoff gross weight.) The design weight along with the drag polars and the propulsion system performance assessment are used to calculate the range for the vehicle.

The range calculation assumes that the air vehicle is flying at an optimal altitude for its weight. The altitude is allowed to increase as fuel is burned, thus returning a range equal to the distance travelled over the optimal altitude trajectory. For the ESAV studies herein, the range calculation is done for a 6000 lb fuel burn at Mach 0.8.

The ESAV benchmark is a deterministic MDO problem, therefore no UQ methods or random variables were defined.

Specific instructions to recreate the input/models are not available.

Computation data and models are available in the Science Connect website listed in the Executive Summary.

No MDA quality metrics were implemented as constraints.

No MDA quality metrics were implemented.

The MDA was uncoupled.

The sensitivity calculations for ESAV are obtained with a finite-difference approach. To ensure a sensitivity calculation is successful, four objective and constraint function evaluations are executed in parallel for each design variable at each SLP iteration. (The number of points used in the sensitivity calculation is based on the computational resources available and the experience of the designer.) The objective and constraint evaluations are used to calculate the highest-order finite-difference sensitivity possible given the number of successful function calls. If all of the function calls fail, the robust SLP algorithm attempts to adapt the step-size and recalculate the sensitivity. If this attempt fails, the user is prompted to take corrective action.

The computation cost to obtain the gradients of the objective function and constraint functions is $4 \cdot ndv + 1$ where ndv is the number of design variables.

3.2.2.2 Practical Concerns

All the software used was license-free (or unlimited license) which was necessary to do large numbers of MDAs in parallel. There were no issues with software cost or licenses. Windows, Linux and Macintosh platforms were supported and used. Online searches may be used to find several of the codes; ASTROS and the AFRL-developed codes (MSTCGEOM, MSTCPERF, MSTCOPT, etc.) may be obtained from AFRL.

All executables in the MDA supported coarse-grain parallel execution; multicore execution (of single MDA) was not supported.

Specific details on the computers used were not recorded; a mixture of desktop and cluster computers were used. A total of 4 – 5 computers were used and all major platforms were involved (Linux, Windows and Macintosh).

Information on the PC specs, the grid computing node used, disc space, and CPU time was not recorded.

A single MDA took approximately ten minutes on an average desktop.

The human effort required to implement the MDA was not documented. Since many of the individual applications involved in the MDA were custom, the human effort if the MDO involved implementing the individual analyses plus integrating them into an automated MDA.

The MDA is fully automated and contains exception handling for the reporting of analysis failures/errors.

In most cases, an MDA failure was graceful. Occasionally a process would hang (e.g., ASTROS) and would result in the process being killed. The MDA algorithm returned ‘nan’ for responses (objective or constraint functions) that failed. Timeouts were implemented in the MDA via the SORCER providers supporting the large-scale grid computing infrastructure.

The SLP algorithm is inherently restartable.

3.2.3 MDO Problem Definition Details

The design variables, \mathbf{x} , are the wing area, taper ratio, and aspect ratio (ndv equal to three). The lower and upper bounds on the design variables (x_{lb} and x_{ub}) are: 100 and 300 ft² for wing area, 0.6 and 5.0 for aspect ratio, and 0.1 and 1.0 for taper ratio, respectively.

The objective is to minimize the structural weight of the ESAV, which includes the fuselage and lifting surface weights. In this manner, the life cycle cost of the aircraft is kept down due to its correlation with takeoff gross weight. Each evaluation of the objective function, $f(\mathbf{x})$, involves a structural sizing sub-optimization of the wing and tail surface spar, rib, and skin thicknesses. This sub-optimization process is performed by ASTROS and is integral to the MDA.

Minimize structural weight.

A single MDA execution produces the objective and constraint function values in approximately 10 minutes on a desktop computer.

Gradient calculations of the objective and constraint functions were done using a finite-difference approach described previously in the MDA overview.

BENCHMARK: EFFICIENT SUPERSONIC AIR VEHICLE (ESAV)

Two optimization problems were solved with a single inequality range constraint ($ncon$ equal to one). In the first case, the cruise leg range, $g(x)$, is constrained to be above 1500 mi at Mach 0.8 for 6000 lb of fuel. In the second case, the range is increased to 2500 mi. Constraints and the objective are calculated by the same MDA; see previous discussion on computational cost.

Stress analyses and aeroelastic sizing for the ESAV are performed for four static aeroelastic manoeuvre cases at an altitude of 10,000 ft. Specifically, they are the following:

- 1) A 9.0 g pull-up at Mach 0.9;
- 2) A 7.2 g pull-up at Mach 1.2;
- 3) A negative 3.0 g push-over at Mach 1.2; and
- 4) An anti-symmetric 100 deg·s⁻¹ aileron roll at Mach 1.2.

ASTROS is used to perform the aeroelastic analysis and structural sizing optimization that results in an optimized structural weight subject to stress constraints. The structural sizing optimization is considered a sub-optimization in regard to the overall optimization problem discussed in Section 4.1 Optimization Problem Statement. To that end, the structural sizing optimization is an integral part of the MDA and is performed for each configuration analyzed. The structural sizing sub-optimization problem has fifty-seven design variables that are distributed over the wing and tail surface spar, rib, and skin thicknesses. The ESAV is modeled with aluminum and 70 ksi is used as the maximum allowable stress.

Aeroelastic and inertial effects were included by using ASTROS. The air vehicle was trimmed for different manoeuvres.

3.2.4 MDO Algorithm

The MDO algorithm was deterministic; specifically, it was an adaptation of the Frank-Wolf implementation of the Successive Linear Programming (SLP) method. It is a gradient-based method that uses a finite-difference approach to compute sensitivities. Issues of computational efficiency and robustness are addressed using parallel computations with SORCER and high-order/adaptive finite-differencing techniques.

Surrogate models were not used.

The MSTCOPT SLP implementation handles failures by oversampling the finite-difference calculations and using redundant points in its line search technique.

The SLP implementation does not require the caching of results for restarting. The MDA was run for approximately 6 – 7 hours in which time it was observed that the objective function improvements were small and the constraint was satisfied.

3.2.5 MDO Results

The initial design variables were [400 ft², 0.85, 0.28] for wing area, aspect ratio and taper ratio, respectively, with corresponding weight of 13,125 lb and range of 1550 mi. The short range (range minimum of 1500 mi) final design was [320 ft², 0.80, 0.28] resulting in a 13,125 lb weight and 1500 mi range. The long range (range minimum of 2500 mi) final design was [600 ft² 2.30, 0.10] resulting in a 14,065 lb weight and 2500 mi range.

Figure 3-2 shows the planforms for the baseline (approximately 1550 mi range and 13125 lb half-span weight), the 1500 mi range design (13013 lb half-span weight), and the 2500 mi range design (14065 lb half-span weight). The optimization iteration history is shown in Figure 3-3 for the design variables, constraint (range), and objective (weight). Figure 3-4 plots the results of the ASTROS structural sizing sub-optimization performed on the three ESAV designs. The figure shows the optimal thicknesses of the skins, ribs, and spars for the three configurations.

See Figure 3-3 for the objective and constraint value history.

In the first case with the 1500 mi range constraint, the wing area and taper ratio were reduced to minimize weight. Since the baseline range was slightly greater than 1500 mi, the optimizer had some design freedom to reduce the objective function in this manner. The overall reduction in weight from the baseline was approximately 0.9%. The structural sizing sub-optimization was driven in this case by two of the four manoeuvres: the 9.0 g pull-up at Mach 0.9; and the 7.2 g pull-up at Mach 1.2.

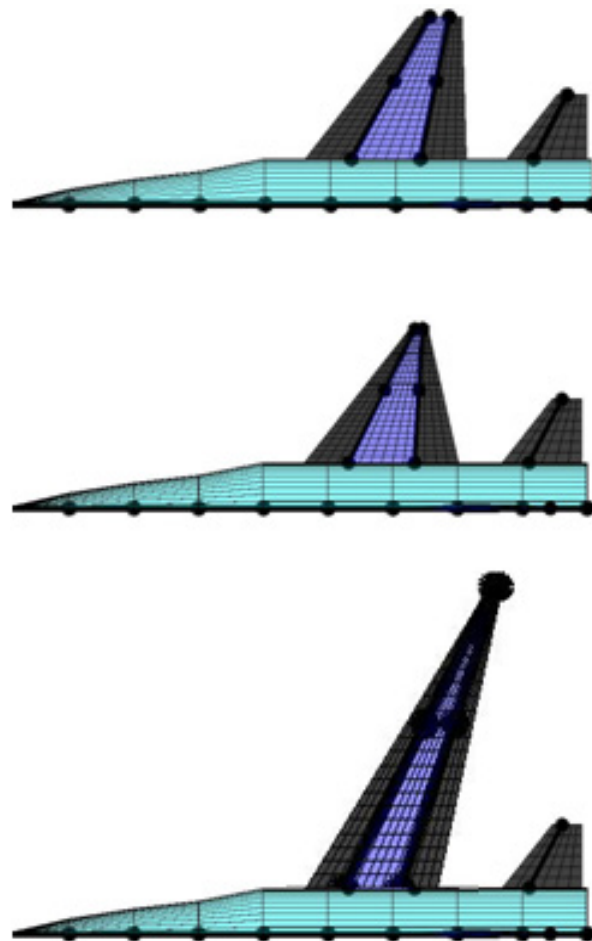


Figure 3-2: The ESAV Optimization Result Half-Span Planforms: Baseline 1550 mi Range and 13125 lb Weight (Top); 1500 mi Range and 13013 lb Weight (Middle); and 2500 mi Range and 14065 lb Weight (Bottom).

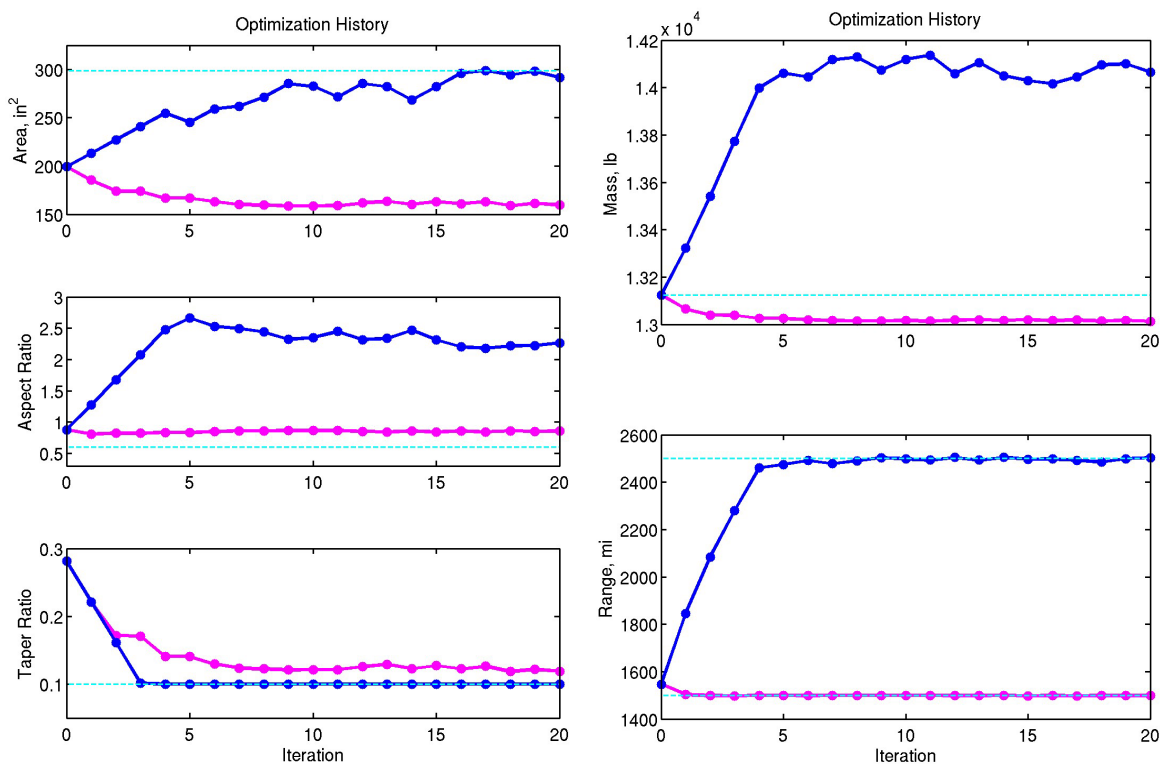


Figure 3-3: Results from ESAV Optimization Illustrate How the Design Variables, Objective and Constraint Functions are Manipulated by the SLP Technique (1500 mi Range Constraint, Magenta; 2500 mi Range Constraint, Blue).

The second optimization problem solved was for the 2500 mi range constraint. The planform of the wing in this case became long and slender with a high aspect ratio, high wing area, and low taper ratio. Since the initial design was infeasible, a considerable amount of weight was added via increases in wing area and aspect ratio to achieve the 2500 mi range. The weight was increased approximately 7.2% from the baseline design. The structural sizing sub-optimization was driven by the 9.0 g pull-up at Mach 0.9 manoeuvre.

The MDO used 4-5 computers; all were desktop varieties with one from a Linux cluster. See Figure 3-3 for objective call information. The wall time for the MDO execution was approximately 6 – 7 hours. Sensitivity calculations and line search operation parallelize well.

There were no licenses to manage.

Information on human effort, optimization parameter settings were not available.

See Figure 3-3 for the objective and constraint value history.

Results not using MDO or other optimization techniques were not available.

Experiment data were not available.

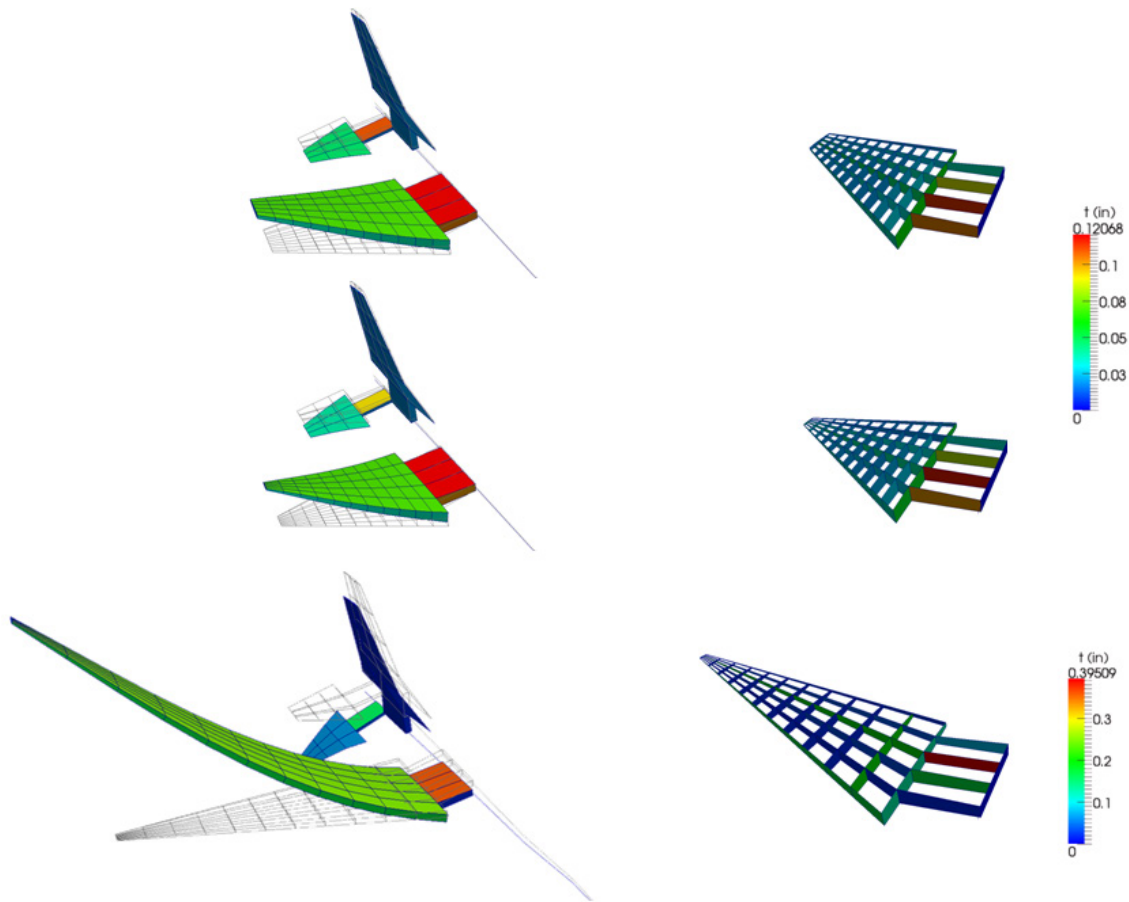


Figure 3-4: The ESAV Planform and Structural Design Thicknesses from the ASTROS Structural Sizing Sub-Optimization Problem are Shown Above for the 1550 mi Range Baseline Design (Top Row), the 1500 mi Range Design (Middle Row), and the 2500 mi Range Design (Bottom Row) Optimal Designs. (The left column shows the thicknesses for the wing skins and the right column shows the thicknesses of the ribs and spars.)

The SORCER engineering software was used successfully in the design of two prototype ESAVs. The results from both optimization cases exhibited the correct trends consistent with historical aircraft design. These results provide a degree of validation of the implementation of the MATLAB SLP code, the SORCER ESAV model, the SORCER providers, and the JavaSpaces technology.

The use of the JavaSpaces technology for parallel distributed computing proved reliable and efficient. It was a straightforward process to add computers to the SORCER grid as needed during the course of the two optimization studies. This flexibility proved valuable as the number of computers available varied from day-to-day.

Lastly, the application of a gradient-based SLP optimization technique capable of handling failed design points was demonstrated successfully. The robust nature of the SLP technique and its ability to perform gradient and line search functions in parallel made the ESAV optimization studies possible in a short period of time with minimal user intervention.

Although the SLP technique did not necessarily determine a global optimum, it did:

- 1) Find a feasible design when started from an infeasible one;
- 2) Improve the objective function when started from a feasible design; and
- 3) Operate autonomously while providing the user with feedback on the optimization process.

The results demonstrate the practical utility of the robust SLP approach. Furthermore, the algorithm was straightforward to implement, troubleshoot, and its successive nature (i.e., design improvements with each iteration) provided re-start capability. These qualities make it a sound approach for design optimization, especially when working with newly implemented MDAs where the univariate sweeps executed for the finite-difference sensitivities provide valuable feedback to the user.

3.2.6 Technical and Financial Improvements/Benefits of Using MDO vs. Traditional Design Methods

Information not available.

3.2.7 References; Web Resources; Science Connect Link; and Validation Data Location

Details on the benchmark may be found in:

Burton, S.A., Alyanak, E. and Kolonay, R.M. (2014). Efficient supersonic air vehicle design using the Service-Oriented Computer Environment (SORCER), *Int. J. Simul. Multisci. Des. Optim.*, 5, A25, DOI: 10.1051/smdo/2014005.

The Science Connect link is <https://scienceconnect.sto.nato.int/apps/10773>.

No validation data is available.

Chapter 4 – BENCHMARK: COMMON RESEARCH MODEL (CRM)

Raymond M. Kolonay
Air Force Research Laboratory
UNITED STATES

There are several different optimizations efforts that have been found in the literature on the NASA Common Research Model. Here, a summary of four of those efforts are covered. The NASA Common Research Model (CRM) was developed by Vassberg *et al.* [1] for the purpose of a test case for the AIAA CFD Drag Prediction Workshop. The model is a wing/body/nacelle/pylon/horizontal-tail configuration with a focus on the aerodynamic design of the wing. The wing has a contemporary transonic supercritical wing design with aerodynamic characteristics that are well behaved and of high performance for configurations with and without the nacelle/pylon group. The horizontal tail is robustly designed for dive Mach number conditions and is suitably sized for typical stability and control requirements. The fuselage is representative of a wide/body commercial transport aircraft; it includes a wing-body fairing, as well as a scrubbing seal for the horizontal tail. The nacelle is a single-cowl, high by-pass-ratio, flow-through design with an exit area sized to achieve a natural unforced mass-flow-ratio typical of commercial aircraft engines at cruise. The CRM is designed for a cruise Mach number of $M_\infty = 0.85$ and a corresponding design lift coefficient of $C_L = 0.5$. The aspect ratio is 9.0, the leading edge sweep angle is 35 deg, and at a Reynolds number of $Rn = 40$ million per reference chord. The full wing span of the model is 192.8 ft and has a reference chord of 22,98 ft. Although the model was originally developed for only aerodynamic calculations some structural models were developed at a later time [2]. Several full-scale semi-span wingbox structures were developed based on the original CRM outer mold line (OML) loft and contains combinations of explicitly modelled shell based structures. The CRM structural baseline FEMs are module-parametric CAE isotropic aluminum based primary and secondary structural models including two or more selectable spanwise zone-tailored main spars and skins, 50+ ribs, stringers, rib caps and stiffeners. A full description of all the available models (WT and computational) and many of the models them self can be found at <https://commonresearchmodel.larc.nasa.gov/> [1].

4.1 BENCHMARK EXECUTIVE SUMMARY: CRM EFFORT ONE

4.1.1 Qualitative Optimization Problem Statement

Uses 4th the Drag Prediction Workshop wing-body-tail configuration as the baseline and optimize the shape while maintaining lift and trim constraints using a RANS solver.

4.1.1.1 Design Variables

The design variables are wing and tail shape. Both the wing and the tail geometries are parameterized using the free-form deformation (FFD) volume approach. Hence the design variables are the z-coordinates of the free-form deformation points on both the wing and the horizontal tail. The wing regular grid with 17 spanwise by 24 chordwise points with two layers controlling the upper and lower surfaces separately (816 wing shape variables and 144 tail shape variables). Also, the trimmed angle of attack and the tail rotation required to balance the pitching moment are free during the optimization.

4.1.1.2 Objective Function(s)

The single objective function is vehicle drag (including trim drag).

4.1.1.3 Constraint Function(s)

A constraint on the lift coefficient ($CL = 0.5$) and a constraint on the pitching moment ($CM = 0$). Further the tail rotation is limited to ± 5 deg. and thickness constraints were placed on the wing and tail cross-sections.

4.1.2 Description of Analyses/Disciplines/Theory/Fidelities Involved

The analysis for computing the lift and drag required for the objective and constraints was a RANS code with a full turbulence model.

4.1.3 MDO Approach (Algorithm/Architecture)

The optimization algorithm was a sequential quadratic programming method with the gradients computed with an adjoint gradient technique.

4.1.4 Implementation Details

4.1.4.1 Analysis Software

The parametric geometry of the wing and tail outer mold line (OML) is created by employing a CAD-free geometry method using a free-from deformation volume approach [2].

For the CFD the Sumb flow solver, which is a finite volume, cell-centered multi-block solver for the RANS equations that also has a full turbulence model was used.

4.1.4.2 Optimization Software

The optimization algorithm SNOPT (sparse nonlinear optimizer) through the Python interface pyOpt was used within the University of Michigan multidisciplinary design optimization of aircraft configurations with high fidelity (MACH) environment. SNOPT is a gradient-based optimizer that implements a sequential quadratic programming method.

4.1.4.3 Hardware

FluxHigh-Performance Computing cluster at the University of Michigan Center of Advanced Computing. No other details available.

4.1.4.4 Human Effort

The human effort was not quantified.

4.1.5 Results

In this study six different cases we evaluated to determine the effect of including trim in aerodynamic shape optimization. The six cases are summarized in Table 4-1 (shown below) from Ref. [2].

Table 4-1: Summary of the Optimization Formulations.

Case	Configuration	Design variables	Constraints
1	Wing-body-tail	AoA, wing shape	Geometric $C_L = 0.5$
2	Wing-body-tail	AoA, wing shape tail rotation	Geometric $C_L = 0.5, C_M = 0$
3	Wing-body	AoA, wing shape	Geometric $C_L = 0.5,$ $C_M = 0$ (surrogate)
4	Wing-body	AoA, wing shape	Geometric $C_L = 0.5256,$ $C_M \geq -0.0996$
5	Wing-body-tail	AoA, wing shape, tail shape	Geometric $C_L = 0.5$
6	Wing-body-tail	AoA, wing shape, tail shape, tail rotation	Geometric $C_L = 0.5, C_M = 0$

4.1.5.1 Initial Design (Design Variables, Objectives, Constraint Values)

The initial configuration is the DPW-4 CRM, which is a wing-body-tail configuration, with the tail rotation set to zero. The development of the CRM is detailed by Vassberg *et al.* [1]. The reference area is 383.69 m², and the reference length (MAC) is 7.005 m. The nominal flight condition of the CRM is a cruise Mach number of 0.85 with a nominal lift coefficient of $C_L = 0.50$. The Reynolds number is five million.

4.1.5.2 Optimized Design (Design Variables, Objectives, Constraint Values)

Table 4-2 extracted from Ref. [3] summarizes the results for the six cases.

**Table 4-2: Summary of the Optimization Studies: All Cases Satisfy $C_L = 5$,
and All Optimizations Include the Wing Shape Variables
as Well as the Geometric Constraints.**

Case	C_D	C_{MY}	Tail shape	Tail rotation	$C_{MY} = 0$ constraint	Configuration
Baseline	0.02907	-0.0410				Wing-body-tail
Trimmed baseline	0.02947	0.0		•	•	Wing-body-tail
1	0.02804	-0.0780				Wing-body-tail
2	0.02826	0.0		•	•	Wing-body-tail
3	0.02838	0.0			•	Wing-body
4	0.02840	0.0			•	Wing-body
5	0.02796	-0.1326	•			Wing-body-tail
6	0.02823	0.0	•	•	•	Wing-body-tail

BENCHMARK: COMMON RESEARCH MODEL (CRM)

The optimal values for the geometric wing and tail parameters for each of the six cases are not given. They are presented as geometric shapes. The reader is referred to Ref. [3] for that information.

4.1.5.3 Observations

Nice process to perform drag minimization of a full aircraft configuration with shape and trim design variables. The technique utilized adjoint gradients and an SQP optimizer.

4.1.6 Technical and Financial Improvements/Benefits of Using MDO vs. Traditional Design Methods

Unknown.

4.1.7 References; Web Resources; Science Connect Link; and Validation Data Location

[1] Vassberg, J.C., DeHaan, M.A., Rivers, S.M., and Wahls, R.A. (2008). Development of a Common Research Model for Applied CFD Validation Studies. AIAA Paper 2008-6919. <https://commonresearchmodel.larc.nasa.gov/>.

[2] Kenway, G.K.W., Kennedy, G., and Martins, J.R.R.A. (2010). A CAD-Free Approach to High-Fidelity Aerostructural Optimization. 13th AIAA/ISSMO Multidisciplinary Analysis Optimization Conference, Multidisciplinary Analysis Optimization Conferences, AIAA 2010-9231. <https://doi-org.wrs.idm.oclc.org/10.2514/6.2010-9231>.

[3] Chen, S., Lyuy, Z., Kenway, G.K.W., and Martins, J.R.R.A. (2016). Aerodynamic Shape Optimization of the Common Research Model Wing-Body-Tail Configuration. Department of Aerospace Engineering, University of Michigan, Ann Arbor, MI Journal of Aircraft Vol. 53, No. 1, Jan. – Feb. 2016.

The Science Connect link is: none.

No validation data are available.

4.2 BENCHMARK EXECUTIVE SUMMARY: CMR EFFORT TWO

4.2.1 Qualitative Optimization Problem Statement

Using the CRM structural wing box perform aeroelastic tailoring considering various trade studies where the metrics of interest are weight, flutter and static aeroelastic stresses [1].

4.2.1.1 Design Variables

The design variables for the aeroelastic tailoring consisted of tow steered composite laminates, functionally graded metals, thickness distributions and curvilinear rib/spar, stringer topologies.

Tow steering composites variables – the study evaluated eight different combinations of stacking sequences and tow angle variations between the top and bottom skins. For all studies associated with the tow steering composite variables the topology of the system was held constant as the baseline configuration.

Material thickness and grading variables – thickness variables of the skins, spars and ribs were allowed to vary from .05 to .75 inches. The material gradient variables allowed the material to vary from an aluminum alloy to aluminum with silicon carbide particulates where the material fraction was specified everywhere along the wing (0 indicated 100% 2024-T3, 1 indicated AL_SiC). The density of both materials were very similar.

Structural Topology variables – variables to represent the number, location, orientation and curvilinearity of the ribs and spars. A few members were fixed, the front and rear spars, one rib at the wing break and one at the wing tip. The number of structural members along with their location-orientation, curvature were modified using 26 design parameters. An additional vector of eight parameters defined the spanwise members as spars or stringers.

4.2.1.2 Objective Function(s)

Several cases were run where the three merit functions were either free or held constant and pareto fronts were generated. The three objectives considered were weight, flutter and static aeroelastic stresses (using a KS function).

4.2.1.3 Constraint Function(s)

Depending on the study one of the three objectives may have been considered a constraint. In particular the weight was often constrained to the baseline value to identify the impact the design parameters on the other two objectives.

4.2.2 Description of Analyses/Disciplines/Theory/Fidelities Involved

CRM FEM model descriptions can be found at the NASA CRM web site. https://commonresearchmodel.larc.nasa.gov/files/2014/02/CRM_wingboxFEM_description_1.pdf.

A process was developed using MATLAB, PATRAN and NASTRAN to enable the generation of parametric models of the CRM. MATLAB was used to generate PATRAN session files to create the CRM outer mold line and the internal structural configuration. Further session files were generated to mesh the model (Structural model – CTRIA3 for ribs, spars, and skins. CBAR for stringers and rib stiffeners, Aerodynamic model – flat plate) and export the NASTRAN input files for the static and dynamic aeroelastic analysis and a structural buckling analysis. Linear flat plate panel methods were utilized for the steady and unsteady aeroelastic analyses. The model generation was easily accomplished for the tow steering, functionally gradient materials and sizing design variables but was a bit more complicated for the topology design variables (# of ribs and spars and their curvature) since this required a change in the internal geometry and re-meshing of the FEM. Once the analyses were executed by NASTRAN, MATLAB scripts were again used to parse the NASTRAN output files to obtain the necessary information for evaluating the performance metrics. Figure 4-1 shows the baseline structural model topology and thickness distribution. The baseline model was composed of aluminum alloy, 2024-T3 [1].

The static aeroelastic analysis was carried out at an altitude of 35000 feet, Mach 0.85 and angles of attack of -2, 0, 2, 4 degrees. The flutter analysis was performed with 20 structural modes, Mach 0.85 and a dynamic pressure ranging from 0.0 to 14.8.

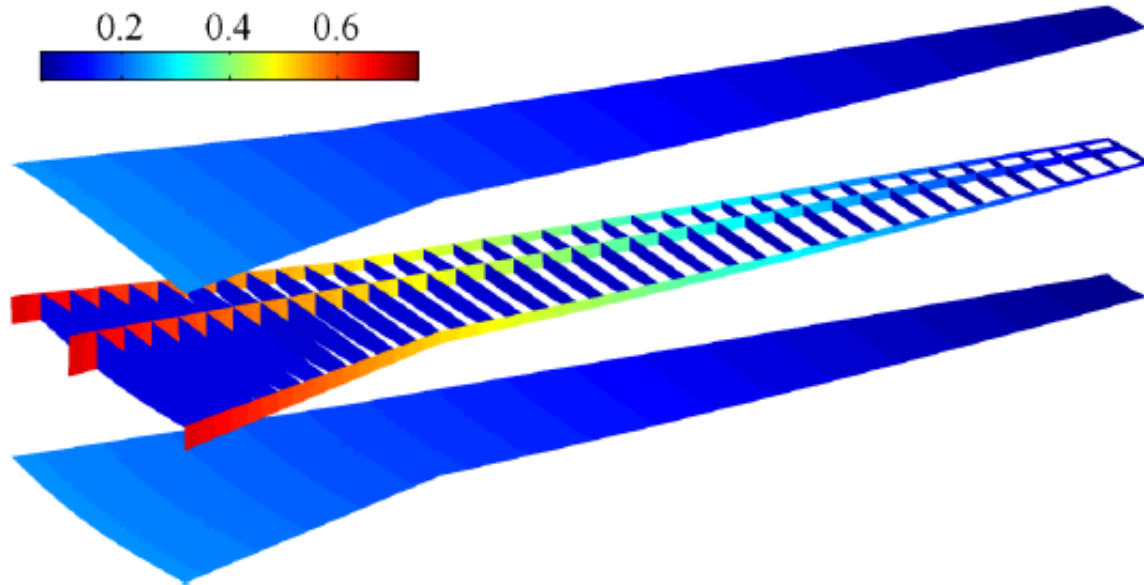


**Figure 4-1: Baseline CRM Structure Used for Tailoring Studies.
Contour indicates local shell thickness (inches).**

4.2.3 MDO Approach (Algorithm/Architecture)

No formal MDO algorithm was utilized. Depending on the study a genetic algorithm was used to identify Pareto front between two of the objectives. This was the case for the tow steering, sizing and functionally gradient material. But for the topology studies a full factorial design of experiments was carried out not a formal optimization.

4.2.4 Implementation Details

4.2.4.1 Analysis Software

A process was developed using MATLAB, PATRAN and NASTRAN to enable the generation of parametric models of the CRM. NASTRAN was used to perform all analysis. Linear static and dynamic aeroelastic along with a structural bucking analysis.

4.2.4.2 Optimization Software

A GA was used for some of the studies while a full-factorial DOE for others. No mention concerning which GA or what software was used. Since they mention the use of MATLAB and no other software it is assumed that a GA within MATLAB is employed.

For the studies associated with the tow steering, sizing and functionally graded materials a genetic algorithm was used to find Pareto fronts for the various objectives (weight, flutter speed, and static aeroelastic stress via the Kreisselmeier-Steinhauser – KS function). No mention of the GA used is given in the paper. It is assumed that it is one found within MATLAB. For the studies associated with the structural topology design variables a full-factorial design of experiments was performed to explore the design space and determine the impact of these parameters on the merit functions (weight, flutter speed and static aeroelastic stress).

4.2.4.3 Hardware

Not reported.

4.2.4.4 Human Effort

Not reported.

4.2.5 Results

Several different design studies were carried out in this effort. They were broken up into three separate areas; tow steering and composite laminate lay-up, material and thickness grading and structural topology (curvilinear rib and spar placement). For the tow steering studies designs that increased the flutter velocity by 100% and reduced weight by 3.5% were obtained. For the material and thickness studies it was found that many of the designs produced gravitated towards 100% of the Al-Sic since it has a higher stiffness and approximately the same density of the Al alone. A few exceptions to this was found with some of the flutter design since it was advantages to “soften” the structure in some areas to separate the frequencies that were coupling and producing flutter. Finally, the curvilinear spar/rib studies focused on the geometric effects on weight, flutter, and the static aeroelastic stress (KS function). These studies revealed that removing the inner spar resulted in significant weight reductions while the flutter and KS performance was maintained by shifting stringers forward and curving the ribs in the spanwise direction.

4.2.5.1 Initial Design (Design Variables, Objectives, Constraint Values)

N/A.

4.2.5.2 Optimized Design (Design Variables, Objectives, Constraint Values)

N/A.

4.2.5.3 Observations

N/A.

4.2.6 Technical and Financial Improvements/Benefits of Using MDO vs. Traditional Design Methods

Not reported.

4.2.7 References; Web Resources; Science Connect Link; and Validation Data Location

- [1] Jutte, C.V., Stanford, B.K., Wieseman, C.D., and Moore, J.B. (2014). Aeroelastic Tailoring of the NASA Common Research Model via Novel Material and Structural Configurations. AIAA SciTech 13 – 17 January 2014, National Harbor, Maryland 52nd Aerospace Sciences Meeting AIAA 2014-0598.

The Science Connect link is: none.

No validation data are available.

4.3 BENCHMARK EXECUTIVE SUMMARY: CMR EFFORT THREE

4.3.1 Qualitative Optimization Problem Statement

This is a summary of the work found in Dunning *et al.* [1]: “Aerostructural Level Set Topology Optimization for a Common Research Mode Wing”. It uses the CRM model to minimize the total compliance of the structure to define the internal structural topology of the wing under trimmed aeroelastic and ground loading conditions. The two load cases are considered simultaneously by a single weighted function that is composed of the compliance functions of each load case.

4.3.1.1 Design Variables

A conventional level set method is used with the design variables being a vector of the finite element densities. A value of 0 indicates a void and a value of 1 indicates solid material. For efficiency the finite element mesh remains fixed during the optimization. Thus, as the boundary moves during the optimization some elements can be cut leading to a discontinuity in the material properties within a single element. To address this issue a volume-fraction weighted approximation for the element stiffness is used. This is also referred to as the ersatz material approach. Also, the outer layer of elements are assumed fixed to remain part of the structure, thus the upper and lower layers of element act as the upper and lower skins of the wing. This ensures that holes do not develop in the upper and lower skins and that the outer mold-line remains continuous.

4.3.1.2 Objective Function(s)

The objective function is a weighted function constructed of the two compliance functions associated with the respective load cases. The first set of load cases are the trimmed aeroelastic loads for the specified flight conditions (1 g level flight, 2.5 g pull-up and a 1 g push-over) and the second is associated with a ground loading condition (2.5 g taxi bump).

$$\text{Minimize : } C(u) = f_i^T u \text{ or for multiple loading conditions Minimize : } C(u) = \eta C_a + (1 - \eta) C_g$$

where u is the deformation vector of the wing, $C(u)$ is the compliance of the wing and f_i^T is the load vector for the individual load cases and f_a^T - aerodynamic load, and f_g^T the ground load.

4.3.1.3 Constraint Function(s)

There are two constraints, the first enforces static equilibrium of the system and is posed as:

$$Ku = f_i = f_a(u) + N \bullet f_b$$

where K is the structural stiffness, N is the load factor and f_b are the body(inertial) forces. The second constraint is an enforcement of the aeroelastic trim conditions posed as:

$$L(u) = N \bullet (W_b + W_c)$$

where $L(u)$ is the total lift, including aeroelastic effects, and W_b is the weight of the wing box that participates in the design and W_c is the fixed weight within the system. The authors show that if $f_a(u)$ are trimmed aeroelastic

loads then the second constraint, $L(u) = N \bullet (W_b + W_c)$ can be eliminated. Further, since the displacements are required to compute the objective function, compliance, the solution to $Ku = f_t = f_a(u) + N \bullet f_b$ is satisfied by solving for u and can be eliminated from the optimization problem as a constraint. Hence the system can be solved as an unconstrained optimization problem. The authors do however state that it may be necessary to include an upper limit on the structural volume to obtain useful results.

4.3.2 Description of Analyses/Disciplines/Theory/Fidelities Involved

4.3.2.1 Analysis Model

For this study the CRM has an aspect ratio of 9, a taper ratio of 0.275, and a sweep angle of 35 degrees. For all flight conditions a dynamic pressure of 5,897 Pa is used. The structural wing box is located between 12% and 71% of the local airfoil chord and the fixed non-structural mass of the wing is set at 500 kn. The wing is assumed to be made from aluminium with $E = 68.95$ GPA, Poisson's ratio of 0.3 and a density of 2800 kg/m³.

The subsonic compressible aerodynamics are modelled using the Doublet Lattice Method (DLM) at zero frequency to obtain the steady aerodynamic loads [2]. The mesh pattern used for the DLM are 20 chord boxes and 100 spanwise boxes. Figure 4-2 shows the aerodynamic DLM model with the location of the structural wingbox outlined in red. The structure is modelled using linear finite elements (solid hexahedra) and the connection of the aerodynamic degrees of freedom to the structural degrees of freedom is achieved using the finite plate spline developed by Appa [3].

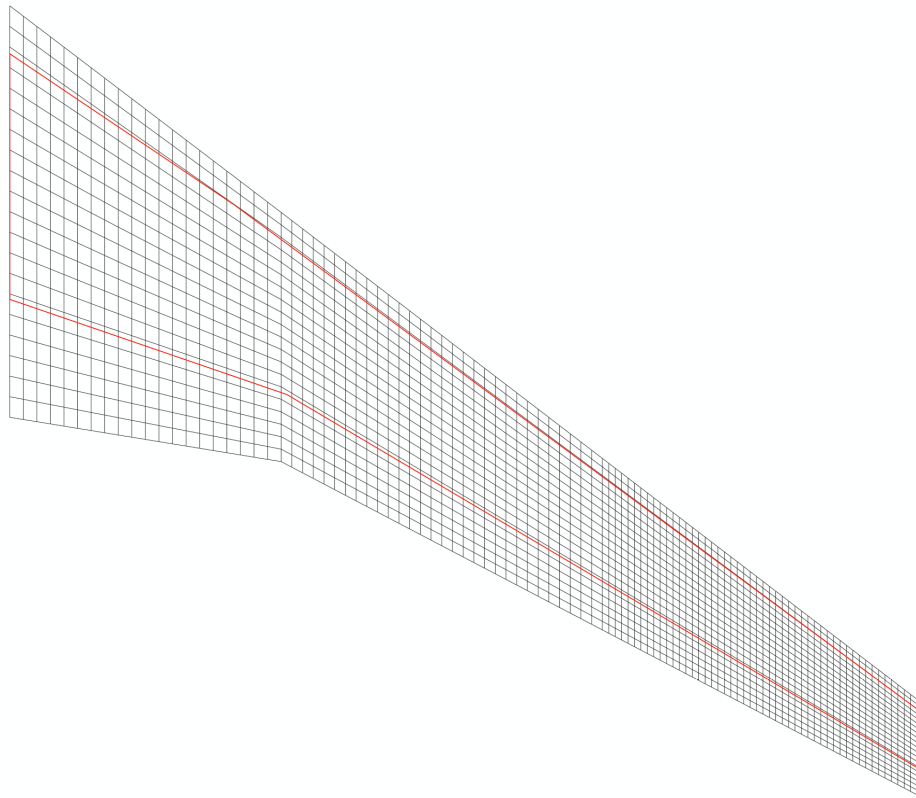


Figure 4-2: CRM Aerodynamic DLM Box Pattern with Location of Structural Wing Box.

Figure 4-3 shows the initial FEM for the CRM. The FEM consists of 150,300 solid hexahedral elements with 15 elements through the depth, 30 along the chord and 334 along the span. This mesh is used for the FEA and to discretize the implicit function used in the level set. Due to the fact that the hexahedra finite elements used to discretize the wing box cannot model thin, shell like structures typical of the conventional semi-monocoque wing construction the modulus and density of the material used during the optimization are 10% of the real values.

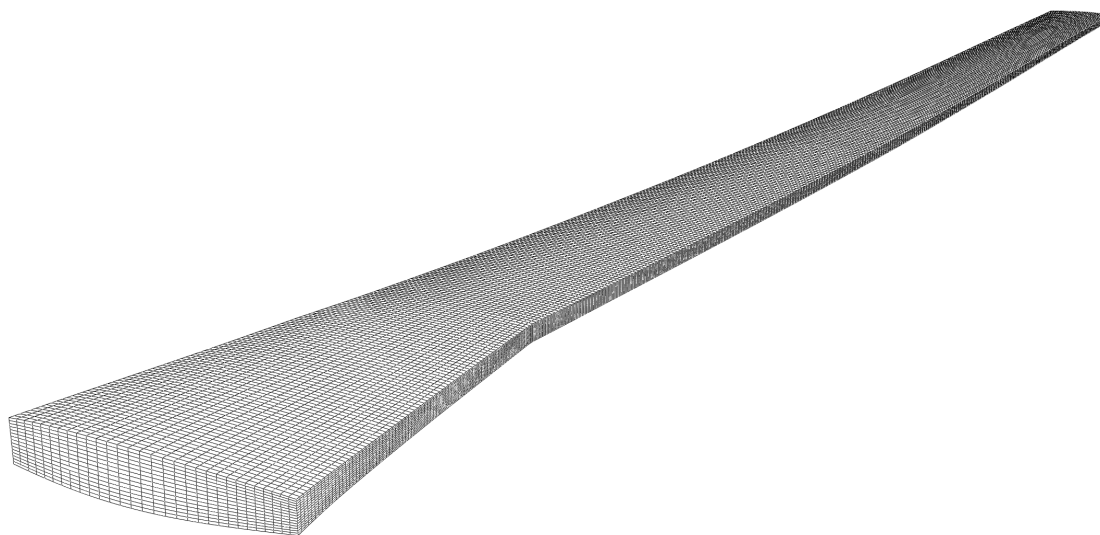


Figure 4-3: CRM Structural Model Using Linear Solid Hexahedra Elements (150,300 Elements).

Although the aeroelastic equations of motion, $Ku = f_t = f_a(u) + N \bullet f_b$, are linear with the aerodynamic and structural analysis theory chosen the authors choose to solve these equations iteratively stating that is more efficient due to the density of the aerodynamic matrix.

4.3.3 MDO Approach (Algorithm/Architecture)

A conventional three-dimensional level set method is employed to determine the wing box substructure. A new technique to handle unstructured grids within arbitrary domain shapes is developed and utilized.

4.3.4 Implementation Details

4.3.4.1 Optimization Algorithm

The optimization algorithm consists of the following steps:

- a) Assemble the global stiffness matrix from the volume ratio weighted element matrices using the following equation $K_e = (\beta_c / \beta_E) K_E$ where K_e is the approximated stiffness of the cut element, K_E is the stiffness of the same element without a cut, whose volume is β_E , and β_c is the volume of the cut element that lies inside the structure. The use of this “ersatz material” approach is required because a Cartesian mesh is used to represent the domain and the boundary of the structure will cut through elements leaving part of the element inside the structure and part of the element outside the structure.

- b) Solve for the primary state vector u and adjoint state vector p . The primary equation is the static aeroelastic trim equations $Ku = f_i = f_a(u) + N \bullet f_b$ and the associated adjoint equation is $K^T p = N \bullet f_b + [Q^T - (b \otimes f_\alpha) / L_\alpha](u + p), u = p = 0$ on Γ_D where Q is the aerodynamic stiffness matrix.
- c) Check for convergence of the problem using a criterion that checks the relative change in the objective from one iteration to the next. If not converged continue to d.
- d) Compute the span sensitivities at the boundary.
- e) Employ the velocity extension using the fast marching method.
- f) Compute the spatial gradients using an upwind scheme.
- g) Update the implicit function by $\phi_i^{k+1} = \phi_i^k - \Delta t |\nabla \phi_i^k| V_{n,i}$ where i is a discrete point within the domain (grid point in the mesh, the FEM mesh is used as the discretization of ϕ as well) and V_n is the velocity function defined normal to the boundary and Δt is the time step.

4.3.4.2 Analysis Software

None stated.

4.3.4.3 Optimization Software

None stated.

4.3.4.4 Hardware

None stated.

4.3.4.5 Human Effort

None stated.

4.3.5 Results

Topology optimization was carried out for various single load cases and combined/multiple load cases. The single load case examples were for the following load cases: steady level flight (1g lift trim condition), a 2 g pull-up lift trim condition, a 1 g push over lift trim condition and a ground load representing a taxi bump of -2.5 gs. For all trim cases on lift is balanced, there is no pitching moment trim included. For the multiple load case example the steady lift (1g lift trim) and the taxi ground loads are combined into a weighted objective function of the form $C(u) = \eta C_f + (1 - \eta) C_g$ where C_f is the compliance for the 1 g trim and C_g is the compliance for the ground load and η is the weighting function.

4.3.5.1 Initial Design (Design Variables, Objectives, Constraint Values)

The initial design for all cases is shown in Figure 4-4. It can be seen that the initial design is seeded with voids to address the issue associated with level set methods inability to create voids from just a solid domain.



Figure 4-4: CRM Initial Design.

4.3.5.2 Optimized Design (Design Variables, Objectives, Constraint Values)

Below are results for the multiple load case example of steady lift (1g lift trim) and the taxi ground load. The objective function is defined as $C(u) = \eta C_f + (1 - \eta)C_g$ where C_f is the compliance for the 1 g trim and C_g is the compliance for the ground load and η is the weighting function. Figure 4-5 illustrates structural topologies results for various η values.

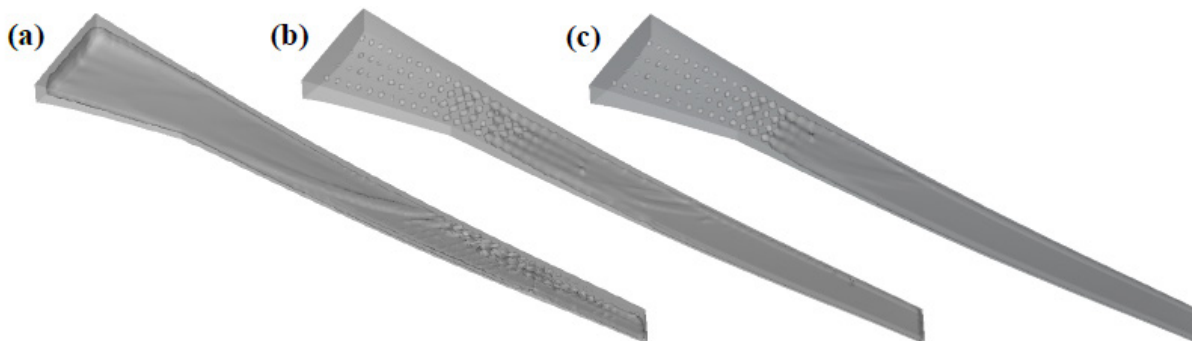


Figure 4-5: Structural Topologies for (a) $\eta = 0.75$, (b) $\eta = 0.5$, (c) $\eta = 0.25$.

4.3.5.3 Observations

The authors state that the hexahedra finite elements used to discretize the wing box cannot model thin, shell-like structures typical of traditional wing designs and construction. Hence, to obtain reasonable topologies the modulus and density of the material used during the optimization were set to 10% of their actual values. Finally, the three dimensional topology optimization technique presented produced structural designs that are significantly different from a traditional rib spar configuration. The topologies found by the optimization process consisted of large volumes that are either void or filled with material (see Figure 4-4).

4.3.6 Technical and Financial Improvements/Benefits of Using MDO vs. Traditional Design Methods

None stated.

4.3.7 References; Web Resources; Science Connect Link; and Validation Data Location

[1] Dunning, P.D., Stanford, B.K., and Kim, H.A. (2014). Aerostructural Level Set Topology Optimization for a Common Research Model Wing. AIAA SciTech 13 – 17 January 2014, National Harbor, Maryland, 10th AIAA Multidisciplinary Design Optimization Conference, AIAA 2014-0634.

[2] Rodden, W.P., Taylor, P.F., and McIntosh Jr., S.C. (1998). Further refinement of the subsonic doublet-lattice method. Journal of Aircraft, Vol. 35, No. 5, pp. 720-727.

[3] Appa, K. (1989). Finite-Surface Spline. Journal of Aircraft, Vol. 26, No. 5, pp. 495-496.

The Science Connect link is: none.

No validation data are available.

4.4 BENCHMARK EXECUTIVE SUMMARY: CRM EFFORT FOUR

4.4.1 Qualitative Optimization Problem Statement

This is a summary of work by Chin and Kennedy [1]: “Large-Scale Compliance-Minimization and Buckling Topology Optimization of the Undeformed Common Research Wing”. This work performs topology optimization of the undeformed CRM under point loads and fixed/rigid aerodynamic loads with two separate objective functions. The first is mass-constrained compliance minimization and the second is a mass-constrained buckling load maximization.

4.4.1.1 Design Variables

The design variables are defined as nearly discrete values representing either a solid or a void of each finite element (when solid elements are used). For the compliance-minimization problem the design variables are the density of the hexahedron solid elements. For the buckling minimization the design variables are the thicknesses of the shell finite elements.

4.4.1.2 Objective Function(s)

Two separate optimization problems are solved:

- a) **Mass constrained compliance minimization with the following formulation:**

$$\begin{aligned}
 &\text{minimize} && c(x) = \frac{1}{2} u^T f \\
 &&& \text{with respect to } x \\
 &\text{such that} && x_l \leq x \leq x_u \\
 &&& c(x) = m_{\text{fixed}} - m(x) \geq 0 \\
 &\text{governed by} && K(x)u = f
 \end{aligned}$$

BENCHMARK: COMMON RESEARCH MODEL (CRM)

where $c(x)$ is the compliance of the structure and u are the structural displacements and the design variables, x , represent the density of the solid elements with bounds of $x_l = 10^{-3}$ and $x_u = 1$.

b) Mass-constrained buckling maximization with compression forces, shear forces and stress constraints:

$$\begin{aligned}
 &\text{minimize} && c_{\text{KS}}(\lambda_j(x)) \quad j = 1, \dots, n \\
 &\text{with respect to} && x \\
 &\text{such that} && x_l \leq x \leq x_u \\
 &&& c_s(x) = m_{\text{fixed}} - m(x) \geq 0 \\
 &\text{governed by} && \mathbf{K}(x)\mathbf{u}_p = \mathbf{f} \\
 &&& [\mathbf{K}(x) + \lambda\mathbf{G}(x, \mathbf{u}_p)]\mathbf{u} = 0
 \end{aligned}$$

where c_{KS} is a Kreisselmeier-Steinhauser (KS) function that aggregates the lowest n eigenvalues with n a chosen parameter. The domain for the buckling problem is a shell model of the wing surface with two different geometries: a flat plate model and a segment of the upper skin. The design variables for this problem are the thicknesses of the skins. These variables take on either one of two values $t_o = 2.0$ mm and $t_l = 8.0$ mm.

4.4.1.3 Constraint Function(s)

a) Mass constrained compliance minimization with the following formulation

For the mass constrained compliance problem, the total mass is constrained by a fixed-mass constraint defined as $m_{\text{fixed}} = f_V V \rho_{\text{max}}$ where f_V is the volume fraction, fixed at 40%, and V is the volume occupied by the mesh.

b) Mass-constrained buckling maximization with compression forces, shear forces and stress constraints

For the buckling case the optimization problem is modified to account for multiple loading conditions (in-plane shear, and axial loading) and both stress and buckling constraints and results in the following formulation:

$$\begin{aligned}
 &\text{minimize} && -\beta \\
 &\text{with respect to} && x, \beta \\
 &\text{such that} && x_l \leq x \leq x_u \\
 &&& c_s(x) = m_{\text{fixed}} - m(x) \geq 0 \\
 &&& \beta \leq c_{\text{KS}}(\lambda_j^{\text{comp}}(x)) \\
 &&& \beta \leq c_{\text{KS}}(\lambda_j^{\text{shear}}(x)) \\
 &&& c_{\text{KS}}\left(\frac{\sigma(x_j)}{\sigma_{\text{VM}}}; u_f; \rho\right) \leq 1 \\
 &\text{governed by} && \mathbf{K}(x)\mathbf{u}_p = \mathbf{f} \\
 &&& [\mathbf{K}(x) + \lambda\mathbf{G}(x, \mathbf{u}_p)]\mathbf{u} = 0 \\
 &&& \mathbf{K}(x)\mathbf{u}_f = \mathbf{f}
 \end{aligned}$$

where $\sigma(x_j)$ is the stress at x_j , σ_{VM} is the von-Mises stress of the structure and β is the min-max bound variable on the criterion function c_{KS} . Further details on β can be found in Refs. [1] and [2].

4.4.2 Description of Analyses/Disciplines/Theory/Fidelities Involved

4.4.2.1 Analysis Model

The aerodynamic loads used for this work are computed using an unstructured three-dimensional panel method that solves the Prandtl-Glauert equation using constant source and doublet singularities on the lifting surface. This implementation can compute inviscid compressible flows. The original CRM outer mold-line model has a built-in 1g cruise shape included. This model is not well suited for aero-structural design studies. To address this, the authors used the undeformed Common Research Model (uCRM) developed in Ref. [4]. There are two variations to this model, the uCRM-9 and uCRM-13.5, the 9 and 13.5 referring to the respective aspect ratios of the wing. These two models are used within this work as the baseline configurations.

The finite element structural model for the mass constrained compliance minimization optimization consists of eight-noded hexahedral linear elements. The mesh consisted of 136 chord-wise, 312 span-wise and 8 elements through the thickness. For the mass-constrained buckling maximization two structural meshes were used a 33 x 97 quadrilateral mesh and a 49 x 49 quadrilateral mesh.

4.4.3 MDO Approach (Algorithm/Architecture)

Two separate approaches are used depending on the optimization problem being solved. For the mass-constrained compliance minimization a single material formulation is used and for the mass-constrained buckling maximization a two-thickness approach is applied.

For the compliance minimization problem, a solid void formulation is used with a Rationale Approximation of Material Properties (RAMP) interpolation. This can be expressed as:

$$C_j(x) = C w_j(x)$$

$$\rho_j = \rho x_j$$

Where

$$w_j(x) = \frac{x_j}{1 + p(1 - x_j)}$$

where p ($p = 3$ for this work) is the RAMP parameter and the design variable x_j are restricted in the range $x_j \in [\varepsilon, 1]$ with ε being a small finite value chosen here to be 10^{-3} .

For the mass-constrained buckling maximization the RAMP approach is modified to allow for a selection between two material thicknesses values given by t_0 and t_1 . This parametrization is written as:

$$t_j(x) = t_0 + (t_1 - t_0) \frac{x_j}{1 + p(1 - x_j)}$$

$$\rho_j = \rho x_j$$

where $x_j \approx \varepsilon$ corresponds to t_0 and $x_j \approx 1$ corresponds to t_1 . Once again $p = 3$ and $\varepsilon = 10^{-3}$.

The parametrization chosen has shown to suffer from mesh-dependence and checkerboard instabilities. To address this issue the authors utilized a spatial filter that distributes the stiffness contribution from one design variable spatially across several adjacent elements.

4.4.4 Implementation Details

4.4.4.1 Optimization Algorithm

An interior-point method, ParOpt [5], is used to solve the large optimization problem.

4.4.4.2 Analysis Software

Aerodynamics – TriPan [6].

4.4.4.3 Optimization Software

ParOpt [5], an interior-point method.

4.4.4.4 Hardware

No data supplied.

4.4.4.5 Human Effort

No data supplied.

4.4.5 Results

Results for the mass-constrained compliance minimization and the mass-constrained buckling optimization problems are presented. The initial design for the mass-constrained compliance minimization is the uCRM-9 model is the solid mesh consisting of eight-noded hexahedral linear elements. There are 136 chord-wise, 312 span-wise and 8 elements through the thickness of the initial domain. Below are the optimized results for the 1 g static aerodynamic loading.

Figure 4-6 illustrates that most of the mass is concentrated inboard and the through the thickness distribution exhibits a composite structure with stiffer face sheets.

The second case run was the mass-constrained buckling maximization of the wing skins of a segment of the uCRM-13.5. Figure 4-7 shows the mesh used for this example case.

Figure 4-8 are the results for the buckling and stress constrained optimization. For this case the ten lowest eigenvalues are retained for the buckling analysis. These results indicate a stiffening of the skins in a fashion to reduce the effective length to increase the buckling capability of the panel.

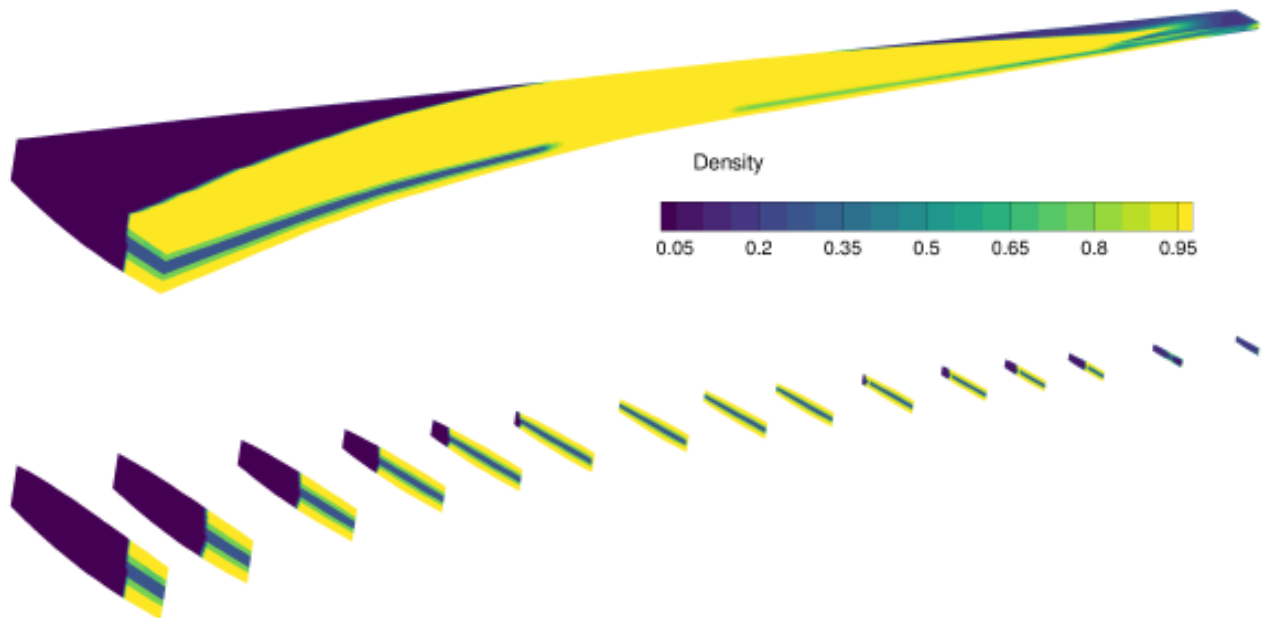


Figure 4-6: uCRM-9 Wingbox Optimized for Static Aerodynamic Loading.

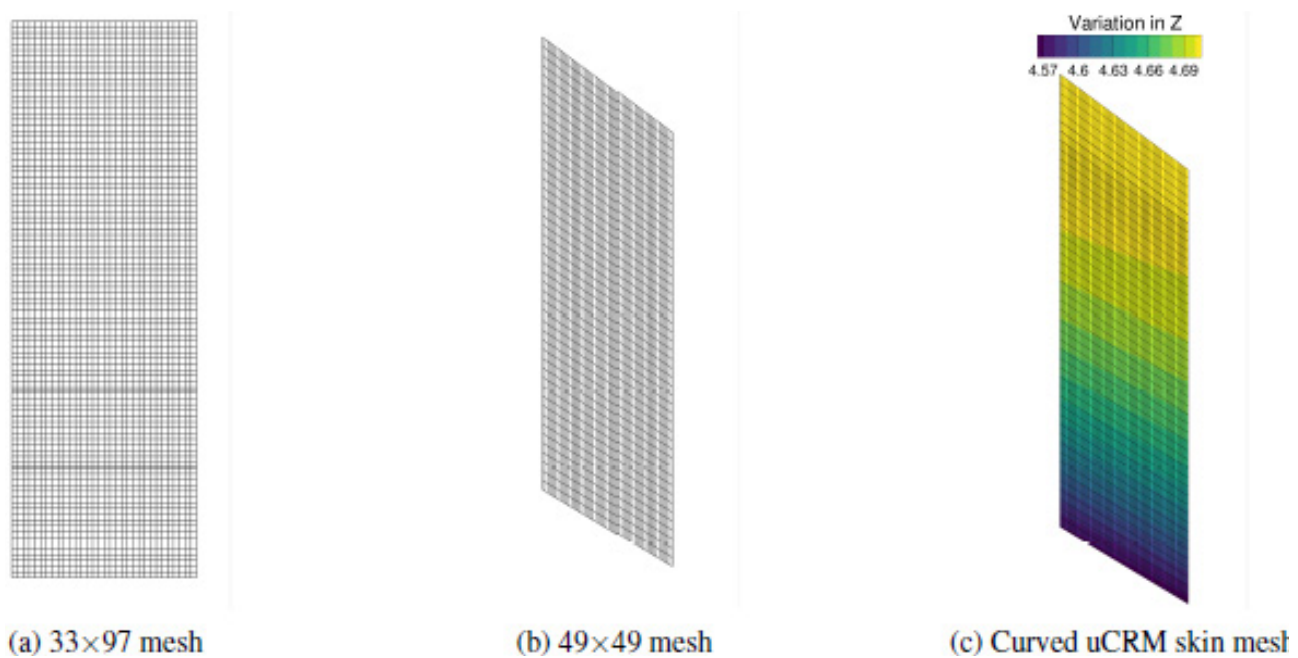


Figure 4-7: uCRM Meshes Used for Buckling Optimization.

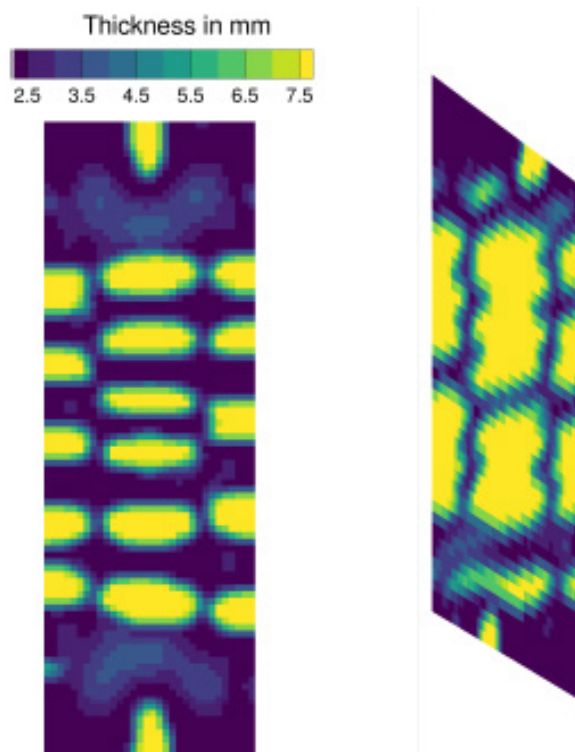


Figure 4-8: uCRM-13.5 Buckling and Stress Constraints Optimized Designs.

4.4.5.1 Initial Design

Not available.

4.4.5.2 Optimized Design

Not available.

4.4.5.3 Observations

This work presented a large-scale topology optimization technique to perform a mass-constrained compliance minimization and a mass-constrained buckling maximization of the un-deformed common research model (uCRM). The mass-constrained compliance minimization results exhibited through-thickness intermediate density material without clear resolution of a substructure. For the mass-constrained buckling maximization problem it was found that at least the lowest ten eigenvalues were required to obtain reasonable buckling designs. It was further observed that including the stress constraints with the buckling constraints smoothed out the stress concentrations resulting in more desirable designs.

4.4.6 Technical and Financial Improvements/Benefits of Using MDO vs. Traditional Design Methods

None given.

4.4.7 References; Web Resources; Science Connect Link; and Validation Data Location

- [1] Chin, T.W. and Kennedy, G.J. (2016). Large-Scale compliance-minimization and buckling topology optimization of the undeformed common research wing. AIAA SciTech Forum, 4 – 8 January 2016, San Diego, CA, 57th AIAA/ASCE/AHS/ASC Structures, Structural Dynamics, and Materials Conference. AIAA 2016-0939.
- [2] Olhoff, N. (1989). Multicriterion structural optimization via bound formulation and mathematical programming. *Structural and Multidisciplinary Optimization*, 1: pp.11-17. ISSN 1615-147X. doi:10.1007/BF01743805.
- [3] Taylor, J. and Bendsøe, M.P. (1984). An interpretation for min-max structural design problems including a method for relaxing constraints. *International Journal of Solids and Structures*, 20(4): pp. 301-314. ISSN 0020-7683. doi: [http://dx.doi.org/10.1016/0020-7683\(84\)90041-6](http://dx.doi.org/10.1016/0020-7683(84)90041-6). URL <http://www.sciencedirect.com/science/article/pii/0020768384900416>.
- [4] Kenway, G.K.W., Kennedy, G.J., and Martins, J.R.R.A. (2014). Aerostructural optimization of the Common Research Model configuration. In: 15th AIAA/ISSMO Multidisciplinary Analysis and Optimization Conference, Atlanta, GA. AIAA, 2014-3274.
- [5] Kennedy, G.J. (2015). Large-scale multimaterial topology optimization for additive manufacturing. In 56th AIAA/ASCE/AHS/ASC Structures, Structural Dynamics, and Materials Conference, Kissimmee, FL, 2015. URL http://gkennedy.gatech.edu/wp-content/uploads/2015/04/2015_SDM_paper.pdf.
- [6] Kennedy, G.J. and Martins, J.R.R.A. (2014). A parallel aerostructural optimization framework for aircraft design studies. *Structural and Multidisciplinary Optimization*, pp. 1-23. ISSN 1615-147X. URL http://gkennedy.gatech.edu/wp-content/uploads/2014/12/2013_tripan_paper.pdf.



Chapter 5 – BENCHMARK EXECUTIVE SUMMARY: COUPLED HYDROSTRUCTURAL OPTIMIZATION OF A 3-D HYDROFOIL

Yin Lu Young, Nitin Garg and Joaquim R.R.A. Martins
University of Michigan
UNITED STATES

5.1 BENCHMARK EXECUTIVE SUMMARY

5.1.1 Qualitative Optimization Problem Statement

We developed an efficient high-fidelity hydrostructural design optimization approach that can handle large numbers of design variables, multiple design points, as well as design constraints on cavitation, maximum von Mises stress, as well as manufacturing and handling tolerances. The motivation is to develop and validate an efficient MDO method to optimize the 3-D morphology and material composition of hydrodynamic lifting bodies such as hydrofoils, rudders, control surfaces, propellers, and turbines across a wide range of operating conditions. Compared to their aerospace counterparts, hydrodynamic lifting bodies typically have much lower aspect ratio, a thicker nose, and more complex 3-D geometry to withstand the high hydrodynamic loads caused by the higher fluid density, and to achieve maximum efficiency while avoiding cavitation. Cavitation occurs when the local pressure drops to at or below the saturated vapor pressure, and can cause undesirable effects such as dynamic load fluctuations, vibrations, noise, erosion, and performance decay. In addition to optimizing the morphology of the hydrodynamic lifting body, we are also interested in optimizing the material composition, as recent work [1] has shown that the anisotropic constitutive behavior of advanced composites can be used to improve overall efficiency and delay cavitation in addition to yielding a lighter structure that is resistant to marine growth and sea water corrosion.

Our hydrostructural solver couples a 3-D compressible Reynolds-Averaged Navier-Stokes (RANS) solver with a 3-D structural Finite Element Analysis (FEA) solver. A low-speed preconditioner is used to solve for nearly incompressible flows with Mach number as low as 0.01 [2]. The optimization method uses a gradient-based coupled adjoint approach. To validate the solver, a 3-D hydrofoil is used as a canonical proxy to more complex hydrodynamic lifting bodies. The baseline hydrofoil has an unswept trapezoidal planform with a loaded span of 300 mm, a base chord of 120 mm, and a tip chord of 60 mm. The baseline hydrofoil has symmetric NACA 0009 cross-sections and zero twist throughout the span. Both the baseline and the optimized hydrofoils are made of solid aluminum (6061-T6). The structural span is 320 mm because of the mounting setup. The optimized hydrofoil has the same planform as the baseline hydrofoil, but the camber, thickness, and twist distributions were allowed to change. The objective of the optimization is to maximize the overall efficiency of the hydrofoil across a wide range of lift conditions while satisfying cavitation, fatigue stress, and minimum trailing edge thickness constraints. Details of hydrodynamic-only optimization of a rigid hydrofoil are presented in Garg *et al.* [2], and hydrostructural optimization of a flexible aluminum hydrofoil is presented in Garg *et al.*[3]. Experimental validation studies of the baseline and the optimized hydrofoils are presented in Garg *et al.* [4]. Both hydrofoils are tested in the same variable pressure tunnel at the Cavitation Research Laboratory (CRL) of the Australian Maritime College. The manufacturing and testing of the hydrofoils were part of a collaborative project with the Defence Science and Technology Group and the Australian Maritime College. Good agreements were observed between predictions and measurements for the hydrodynamic load coefficients and tip deformations for both the baseline and the optimized hydrofoil across lift coefficients ranging from -0.15 to +0.75 at a chord-based

Reynolds number between 0.8 – 1.0 million. The experimental results show an increase in overall efficiency (or lift-to-drag ratio) of 29%, and a maximum increase in efficiency of 32% at a lift coefficient of 0.3. The results also show that the optimized hydrofoil could withstand much higher loading, yield much lower deformation, and has much higher resonance frequencies than the baseline hydrofoil because of the thicker cross-sections. Preliminary experimental results also confirmed that the optimized hydrofoil lead to significantly delayed cavitation inception compared to the baseline hydrofoil.

5.1.1.1 Design Variables

A total of 210 shape design variables were used, 200 to represent the thickness and camber distributions along the chord and span, and 10 to represent the twist distribution along the span. The shape design variables are shown in Figure 5-1.

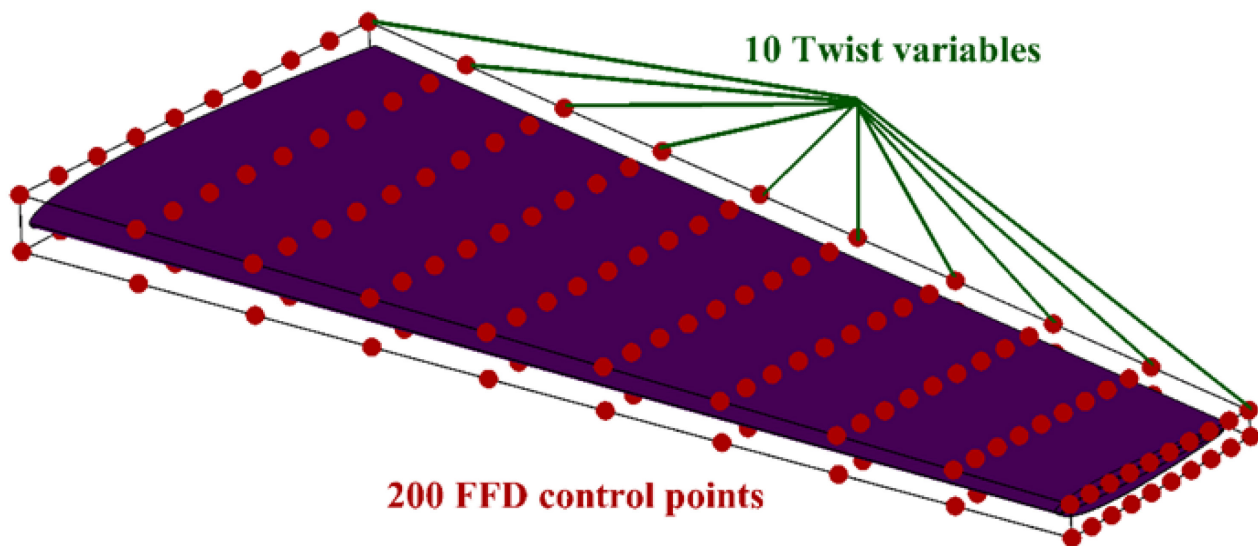


Figure 5-1: Design Variables Used for the Optimization.

5.1.1.2 Objective Function(s)

A single objective function was used to minimize the drag coefficient weighted by the probability of operation at lift coefficients ranging from -0.15 to +0.75.

5.1.1.3 Constraint Function(s)

The constraint functions include:

- Lift coefficient (5 in no.);
- Leading edge position (10 in no.);
- Cavitation constraint (5 in no.);
- Fatigue stress constraint (5 in no.); and
- Trailing edge thickness constraint (20 in no.).

5.1.2 Description of Analyses/Disciplines/Theory/Fidelities Involved

The 3-D hydrofoil was optimized using a coupled hydrostructural analysis with an adjoint-based gradient solver. The CFD (Computational Fluid Solver) solver is ADflow, a 3-D finite-volume, cell-centered multiblock solver for the compressible flow equations [5]. A low-speed preconditioner was used to solve nearly incompressible flows for Mach numbers as low as 0.01. The Jameson-Schmidt-Turkel [6] scheme augmented with artificial dissipation is used for spatial discretization. An explicit multi-stage Runge-Kutta method is used for the temporal discretization. The results presented used the RANS solver with the one-equation Spalart-Allmaras (SA) [7] turbulence model. ADflow includes a discrete adjoint solver that can efficiently compute the gradients. The cavitation constraint is implemented using an aggregated approach shown in Garg *et al.*[2]. Details and validation studies of the CFD solver can be found in Garg *et al.* [2], [3]. The structural solver is the Toolkit for the Analysis of Composite Structures (TACS) [8]. TACS is a parallel, general 3-D finite-element solver for structural analysis that can also efficiently compute the gradients using an adjoint method. The stress constraint is computed using the Kreisselmeier-Steinhauser constraint aggregation technique [9], [10].

For the hydrostructural optimization, the user needs to input the flow conditions, material properties, initial fluid and solid mesh, design variables, and constraints. To solve the coupled hydrostructural equations, the hydrodynamic analysis is first partially converged, and the forces are evaluated. These forces are then transferred to the structural analysis, and the corresponding displacements are computed. Thereafter, the displacements are transferred back to the hydrodynamic analysis, the geometry and the corresponding mesh is deformed, and a new CFD solution is found. This iterative loop continues until the coupled convergence criterion is satisfied, i.e., when the relative decrease in both the hydrodynamic and structural residuals is less than 10^{-5} . Details of the coupled hydrostructural formulation, algorithm, and validation studies can be found in Garg *et al.* [3].

5.1.3 MDO Approach (Algorithm/Architecture)

The optimization technique used herein is gradient-based optimization algorithm SNOPT (Sparse Nonlinear Optimizer) [11]. SNOPT utilizes a sequential quadratic programming algorithm, and is capable of efficiently solving large-scale nonlinear optimization problems with thousands of constraints and design variables.

5.1.4 Implementation Details

5.1.4.1 Analysis Software

Geometry for the analysis and optimization was developed using PyGeo. The fluid mesh and structural mesh for the optimization was developed using the commercial software, ICEMCFD [12].

5.1.4.2 Optimization Software

The optimization algorithm SNOPT was used via the Python interface pyOpt.

5.1.4.3 Hardware

The computations were performed on the Flux HPC cluster at the University of Michigan Center of Advanced Computing.

5.1.4.4 Human Effort

The human effort was not quantified.

5.1.5 Results

5.1.5.1 Initial Design (Design Variables, Objectives, Constraint Values)

The shape design variables are shown in Figure 5-1. The problem setup is shown in Table 5-1. The objective function is to minimize the weighted average of the drag coefficient at five loading conditions represented by the lift coefficient. The assumed probability of the five lift conditions along with the initial and optimized values are presented in Table 5-2. Note that the computed efficiencies presented in Table 5-2 are obtained using a CFD mesh with 515,520 cells and a FEA mesh with 44,800 elements.

Table 5-1: Problem Setup for the Coupled Hydrostructural Optimization of the 3-D Hydrofoil [3].

Objective function		Minimize C_D	
With respect to		FFD control points	200
		Twist design variables	10
Subject to	C_L^*	Lift coefficient constraint	1
		Fixed leading edge constraint	10
	$A_{cav} \leq 5 \times 10^{-4}$	Nondimensional cavitation constraint	1
	$KS_{ov} \leq 1$	Nondimensional stress Constraint	1
	$t_{TEI} \geq 1.1 t_{TEbase}$	Trailing edge thickness constraints	20

Table 5-2: Assumed Probability of Operation at Each Lift Coefficient, and Comparison Between the Baseline and the Optimized Efficiency (C_L/C_D) for the Baseline and the Hydrostructural Optimized Hydrofoil. Both results are based on numerical simulations with a CFD mesh with 515,520 cells and a FEA mesh with 44,800 elements.

Constraint (Lift Coefficient, C_L)	Probability	Baseline C_L/C_D	Optimized C_L/C_D	% Increase in C_L/C_D
-0.15	0.10	11.36	11.17	-1.70
0.30	0.15	17.34	18.67	7.70
0.50	0.25	19.01	20.93	10.10
0.65	0.45	20.18	22.00	9.02
0.75	0.05	19.13	21.68	13.32

5.1.5.2 Optimized Design (Design Variables, Objectives, Constraint Values)

Short-range design: Design variable values (wing area/aspect ratio/taper ratio): 320 ft²/0.80/0.28; Objective and constraint function values: weight = 13,013 lb; range = 1500 mi. Long-range design: Design variable values (wing area/aspect ratio/taper ratio): 600 ft²/2.30/0.10; Objective and constraint function values: weight = 14,065 lb; range = 2500 mi.

5.1.5.3 Observations

The high-fidelity hydrostructural design optimization of the 3-D hydrofoil show significant improvement in the hydroelastic performance of the hydrofoil, while meeting stress, cavitation, and manufacturing constraints.

As reported in Garg *et al.* [3], the numerical optimization results with a 515,520 cells CFD mesh and a 44,800 elements FEA mesh yielded a hydrofoil that had an 8.53% increase in overall efficiency and a 38% increase in cavitation inception speed compared to the NACA 0009 baseline. In addition, the multipoint hydrostructural optimized hydrofoil could satisfy the stress constraint up to the highest design lift coefficient of $CL = 0.75$, while the NACA 0009 baseline violates the stress constraint for $CL > 0.3$.

The studies in Garg *et al.* [3] also compared results from hydrodynamic-only optimization and coupled hydrostructural optimization. The results showed that hydrodynamic-only and hydrostructural optimization lead to completely different geometries, and that coupled hydrostructural optimization is needed, as the hydrodynamic-only optimized foil would violate the stress constraint for $CL > 0.3$. The computational time for the hydrostructural optimization is only 30% more than the hydrodynamic-only optimization, where the coupled hydrostructural optimization over 5 lift conditions took a total of 51 hrs on 192 processors. The studies suggest that it is possible to perform multipoint high-fidelity hydrostructural optimization of hydrodynamic lifting bodies with a large number of design variables overnight using 1000+ processors, which has the potential to revolutionize design of future marine and submarine vehicles and propulsors.

To validate the numerical optimization studies, we collaborated with the Defence Science and Technology Group (DSTG) and the Australian Maritime College (AMC) to manufacture and test the foils. Both foils were tested in the same variable pressure water tunnel at the Cavitation Research Laboratory (CRL) of the University of Tasmania. Details about the experimental setup and validation studies are shown in Garg *et al.* [4]. The optimization studies were conducted with a 515,520 cells CFD mesh and a 44,800 elements FEA mesh. However, grid convergence studies showed that a 4,124,160 cells CFD mesh and a 179,200 elements FEA is needed to achieve the drag convergence [3]. It should be noted that the coarser mesh was used for the optimization because of computational efficiency and because the different grids only affected the absolute values, but not the trends (derivatives), of the hydrodynamic load coefficients, and hence should not influence the shape optimization. For the experimental validation studies, however, the finer mesh with 4,124,160 cells CFD mesh and a 179,200 elements FEA was used for accuracy. As shown in Figure 5-2, good agreements were observed between predictions and measurements for the hydrodynamic load coefficients and tip bending deformations for both the baseline and the optimized hydrofoil across lift coefficients ranging from -0.15 to +0.75 at a chord-based Reynolds number between 0.8 – 1.0 million.

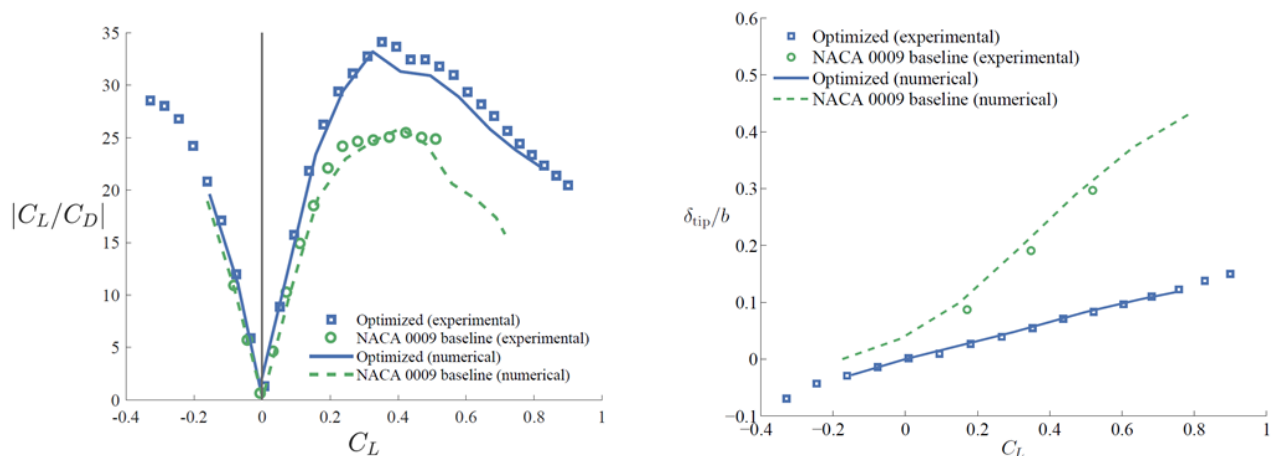


Figure 5-2: Comparison of the Predicted and Measured Efficiency (Left) and Tip Bending Deformation (Right) as a Function of Lift Coefficient for Both the Aluminum NACA 0009 Baseline and the Optimized Aluminum Hydrofoils [4]. The predictions were obtained using a 4,124,160 cells CFD mesh and a 179,200 elements FEA mesh.

The experimental results showed an increase in overall efficiency (or lift-to-drag ratio) of 29%, and a maximum increase in efficiency of 32% at $C_L \approx 0.3$. In addition, preliminary experimental results also confirmed that the optimized hydrofoil lead to significantly delayed cavitation compared to the baseline hydrofoil.

5.1.6 Technical and Financial Improvements/Benefits of Using MDO vs. Traditional Design Methods

Unknown.

5.1.7 References; Web Resources; Science Connect Link; and Validation Data Location

Details on the benchmark may be found in the following references. The complete list of references is provided at the end of this benchmark report.

Garg, N., Kenway, G.K.W., Martins, J.R.R.A., and Young, Y.L. (2015). High-fidelity hydrodynamic shape optimization of a 3-D hydrofoil. *Journal of Ship Research*, 59(4), pp. 209-226.

Garg, N., Kenway, G.K.W., Martins, J.R.R.A., and Young, Y.L. (2017). High-fidelity multipoint hydrostructural shape optimization of a 3-D hydrofoil. *Journal of Fluids and Structures*, 71: pp. 15-39.

Garg, N., Pearce, B.W., Brandner, P.A., Phillips, A.W., Martins, J.R.R.A., and Young, Y.L. (2019). Experimental investigation of a hydrofoil designed via hydrostructural optimization. *Journal of Fluids and Structures*, 84, pp. 243-262.

5.2 BENCHMARK DETAILS

5.2.1 High-Level

The multipoint hydrostructural optimization of a 3-D aluminum hydrofoil is a canonical representation of a detailed optimization of more complex marine propulsors or control surfaces, which are critical components of a marine vehicle.

5.2.2 Multidisciplinary Analysis (MDA)

5.2.2.1 Implementation Details of Analyses and Corresponding Responses Used to Formulate MDO Objective and Constraint Functions

The flowchart of the coupled hydrostructural optimization procedure is shown in Figure 5-3. The process begins with generation of the geometry and the mesh for the hydrodynamic (RANS) and structural (FEA) solvers. The CFD solver used herein is ADflow, which utilizes the one-equation Spalart-Allmaras (SA) turbulence model and computes the adjoint derivatives for the hydrodynamic components. In Garg *et al.* [2], a low-speed preconditioner was added to ADflow to solve nearly incompressible flows. The FEA solver used herein is TACS, which computes the adjoint derivatives for the structural components. In the coupled hydrostructural solver, the hydrodynamic loads (pressure and shear stresses) computed by ADflow are transferred to the structural solver, and the displacements from the structural solver in turn dictate the deformation of the CFD mesh. Iterations between the CFD and FEA solvers continue until the coupled convergence criterion is satisfied (when the relative decrease in both the hydrodynamic and structural residuals, R_H and R_S , compared to the free-stream values is less than 10^{-5}). The gradient-based optimization algorithm SNOPT is used to solve

the coupled adjoint equations, which calculates the gradients of the objective function and determines the perturbations to the geometry for the next step. The Free-Form Deformation (FFD) volume approach is used to efficiently parametrize the geometry, and the algebraic scheme is used to perturb the mesh in the shape optimization process [13]. The optimization flow loop continues until all the constraints are satisfied and that the objective is met. To avoid discontinuity when using a gradient-based approach, the cavitation constraint is implemented using a smooth Heaviside function representing the integral of the foil surface area where the pressure is at or below the vapor pressure [2], [3]. To efficiently implement the fatigue stress constraint, the Kreisselmeier-Steinhauser (KS) constraint aggregation technique is used to aggregate the difference between the von Mises stress and the fatigue stress for all the FEA elements representing the hydrofoil.

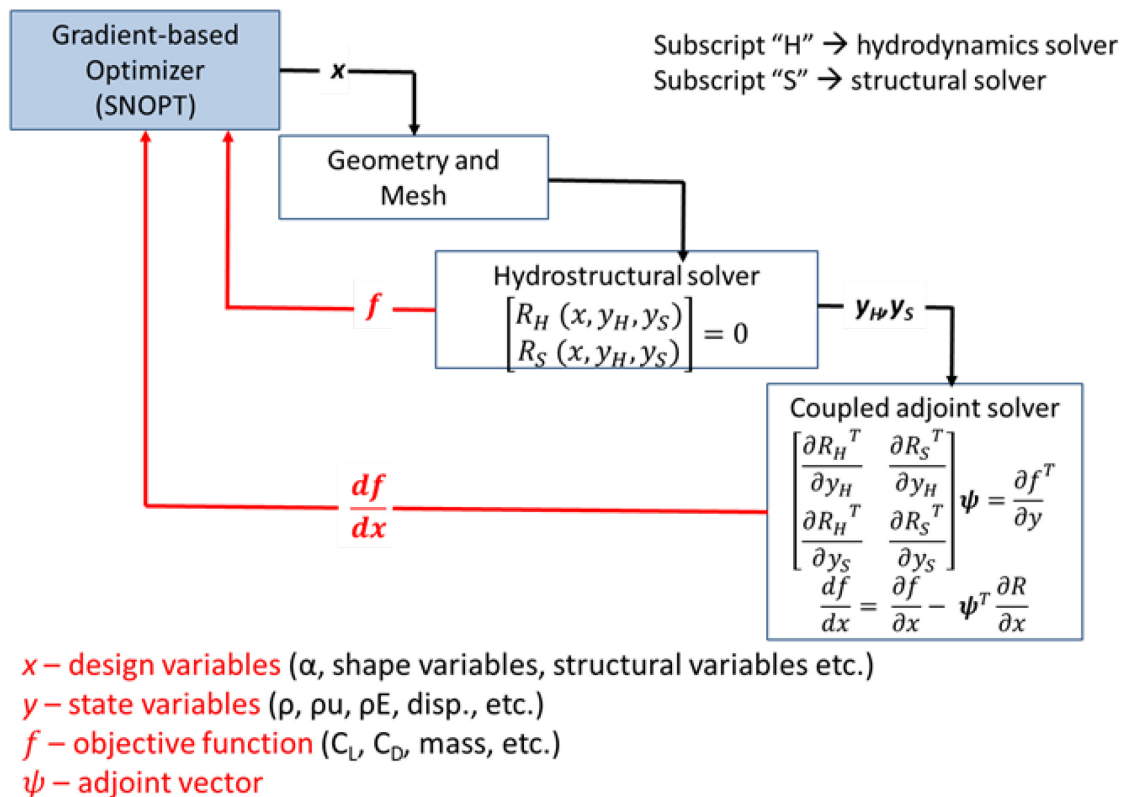


Figure 5-3: Coupled Hydrostructural Optimization Procedure Flowchart.

The problem setup is described in Section 5.1.1.1 – 5.1.1.3. The Initial and optimized design, including the assumed probability of operation at each lift condition, are described in Section 5.1.5. The CFD and FEA mesh, along with the respective boundary conditions, are shown in Figure 5-4. The hydrofoil is cantilevered from its root. Note that while the hydrodynamic loaded span was 300 mm, the structural span is 320 mm because the use of an acrylic fairing disk to seal the load cell and the associated mounting setup. In addition, to avoid zero thickness at the foil leading edge and trailing edge, less than 2% of chord is cut off at each end of the FEA model, which should have negligible influence on the structural stiffness and resulting response.

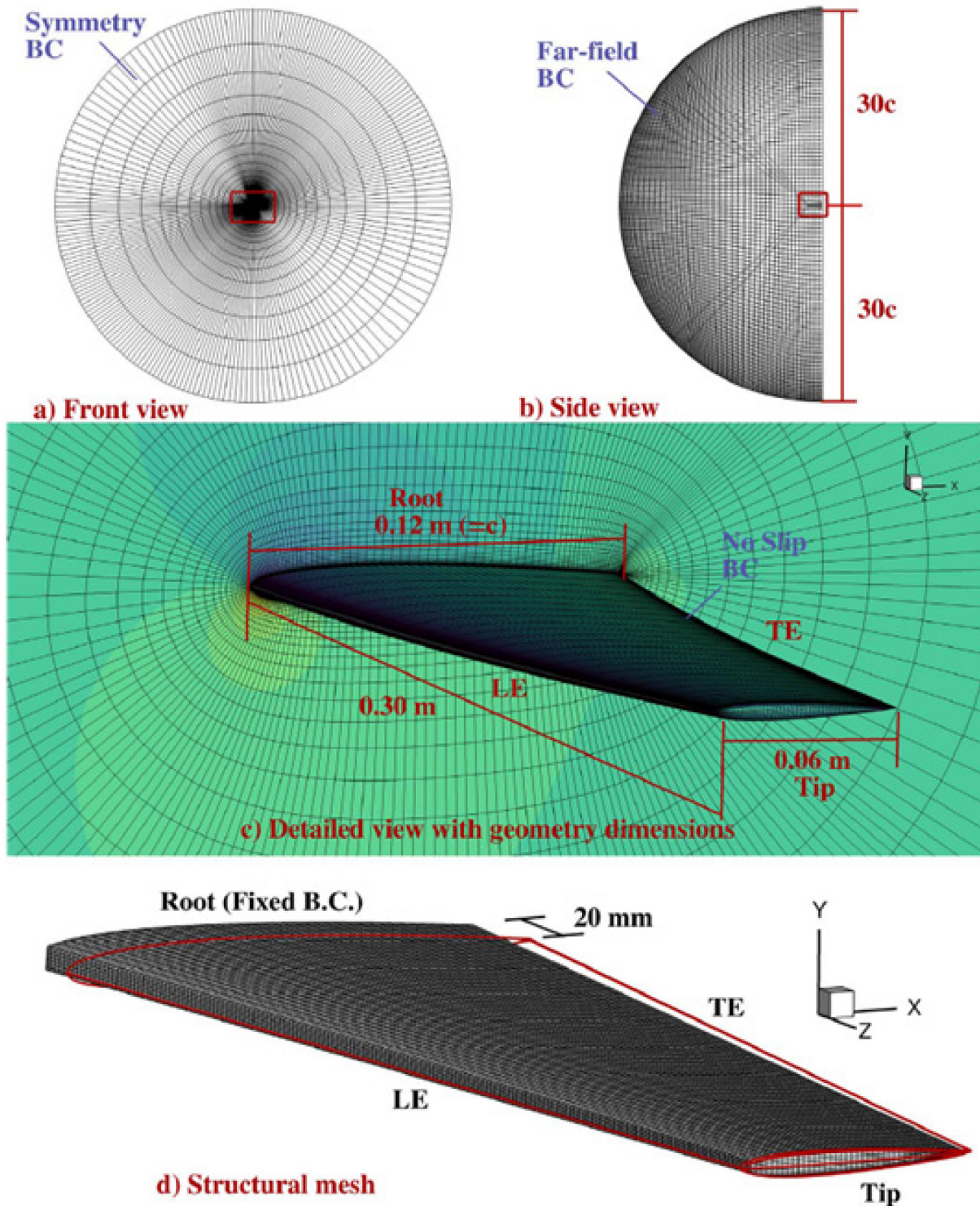


Figure 5-4: Dimensions and Boundary Conditions for the CFD and FEA Models of the Baseline NACA 0009 Hydrofoil [3].

Grid convergence study of the CFD and FEA solvers are shown in Garg *et al.* [3]. Convergence studies with the number of shape design variables can be found in Garg *et al.* [2]. They found that a minimum of 200+ shape design variables were needed to achieve an acceptable optimal solution because of the sensitivity of the pressure distributions to slight changes in geometry. Garg *et al.* [2] also compared results from Euler-based and RANS-based optimizations. They found that Euler-based and RANS-based optimization lead to different optimized geometry, and that the Euler-based geometry could not meet the actual lift constraints at high loading conditions. Garg *et al.* [2] also compared results from single point vs. multipoint hydrodynamic optimization. They found that a hydrofoil optimized for the highest lift condition will lead to inferior performance compared to the baseline at low lift conditions.

Garg *et al.* [3] compared the results of a hydrodynamic-only multipoint optimization vs. a hydrostructural multipoint optimization. They found that the hydrodynamic-only optimized hydrofoil lead to a very different geometry than the hydrostructural optimized foil, and that the hydrodynamic-only optimized hydrofoil would violate the fatigue stress constraint at lift coefficient at or greater than 0.3, instead of the maximum expected lift coefficient of 0.75 for the hydrostructural optimized hydrofoil. The computational cost for different number of design variables, number of design points, hydrodynamic-only and hydrostructural optimization can be found in Garg *et al.* [2] and Garg *et al.* [3]. The results show that the computational time for the hydrostructural optimization is only 30% more than the hydrodynamic optimization, and the computational time increases approximately linearly with the number of design lift conditions. For the coupled hydrostructural optimization over 5 lift conditions, the total required CPU time is 51 hrs on 192 processors [2.80 GHz Intel Xeon E5 to 2680 V2] [3].

5.2.2.2 Practical Concerns

All the software used was license-free, so there were no issues with software cost or license. The computations were conducted on Linux platform. The hardware used involves the standard Flux hardware on the Linux-based High-Performance Computing (HPC) cluster at the University of Michigan Center of Advanced Computing. Additional information is available via: <http://arc-ts.umich.edu/flux-configuration/>. The CPU wall time was reported above and in Garg *et al.* [2] and Garg *et al.* [3].

5.2.3 MDO Problem Definition Details

The MDO problem involved 210 shape design variables, which is shown in Figure 5-1. The optimization problem setup, including definition of objective and constraint functions, is shown in Table 5-1 and Table 5-2. The gradient-based optimization algorithm SNOPT is used to solve the coupled adjoint equations.

5.2.4 MDO Algorithm

Not available.

5.2.5 MDO Results

Comparisons of the sectional geometry of the NACA 0009 baseline, the multipoint hydrodynamic-only, and the multipoint hydrostructural optimized hydrofoils are shown in Figure 5-5. Detail comparisons of the pressure distributions, sectional lift distributions, maximum von Mises stress, tip deformations, and mode shapes of the baseline and the optimized hydrofoils are reported in Garg *et al.* [3]. The convergence history of the objective function, the cavitation and stress constraints are also shown in Garg *et al.* [3]. Results from the optimization study show that the hydrodynamic-only optimized hydrofoil has a slightly higher overall efficiency than the hydrostructural optimized hydrofoil, but it would not be able to meet the stress constraints. Hence, only the

multipoint hydrostructural optimized hydrofoil was selected as the final optimized geometry. Comparisons between the predicted (using a finer mesh than the optimization study) and measured hydrodynamic load coefficients and tip bending deformations of the baseline and the optimized aluminum hydrofoils are shown in Figure 5-2. The experimental results show an increase in overall efficiency of 29% based on the weighted average values for lift coefficients ranging from -0.15 to +0.75, and a maximum increase in efficiency of 32% at a lift coefficient of 0.3. The optimized hydrofoil is thicker, particularly near the root, than the baseline, and hence is heavier (with a mass of 0.58 kg compared to the baseline of 0.41 kg) than the baseline. It is important to note that weight is not as a critical driver for marine applications compare to aerospace applications due to the high buoyant force provided by the high density of water. The generally thicker sections and rounder nose allowed the optimized hydrofoil to achieve much higher cavitation inception speed, as well as yield much lower deformation, higher resonance frequencies, and allowed the foil to withstand much higher loads, compared to the baseline. It is important to note the impressive increase in efficiency considering that:

- 1) The NACA 0009 baseline is a very efficiency hydrofoil to begin with; and
- 2) The optimized hydrofoil is thicker and heavier than the baseline hydrofoil.

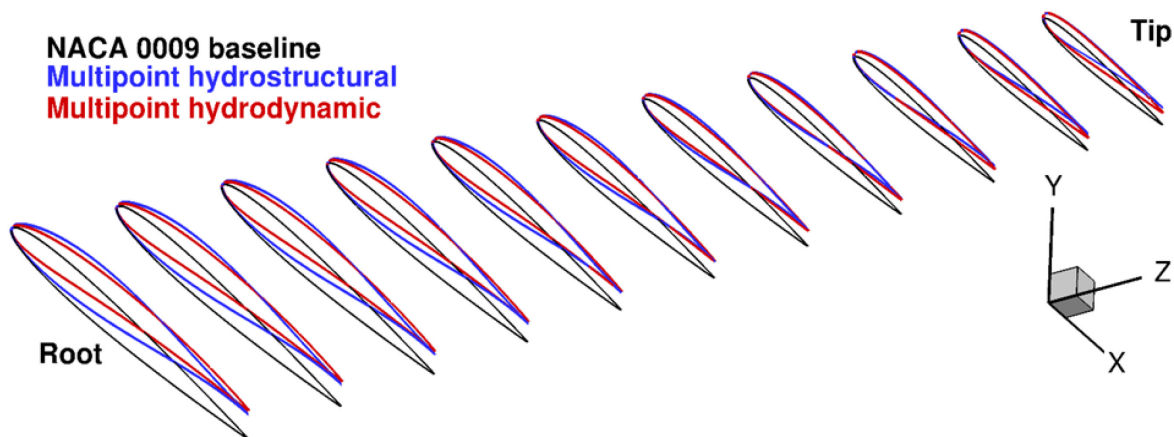


Figure 5-5: Comparisons of the Sectional Geometries of the NACA 0009 Baseline, the Multipoint Hydrodynamic-Only, and the Multipoint Hydrostructural Optimized Hydrofoil [3].

5.2.6 Technical and Financial Improvements/Benefits of Using MDO vs. Traditional Design Methods

Information not available.

5.2.7 References; Web Resources; Science Connect Link; and Validation Data Location

- [1] Young, Y.L., Motley, M.R., Barber, R., Chae, E.J., and Garg, N. (2016). Adaptive composite marine propulsors and turbines: Progress and challenges. *Appl. Mech. Rev.* 68(6), 060803.
- [2] Garg, N., Kenway, G.K.W., Martins, J.R.R.A., and Young, Y.L. (2015). High-fidelity hydrodynamic shape optimization of a 3-D hydrofoil. *Journal of Ship Research*, 59(4), pp. 209-226.
- [3] Garg, N., Kenway, G.K.W., Martins, J.R.R.A., and Young, Y.L. (2017). High-fidelity multipoint hydrostructural shape optimization of a 3-D hydrofoil. *Journal of Fluids and Structures*, 71, pp. 15-39.

- [4] Garg, N., Pearce, B.W., Brandner, P.A., Phillips, A.W., Martins, J.R.R.A., and Young, Y.L. (2019). Experimental investigation of a hydrofoil designed via hydrostructural optimization. *Journal of Fluids and Structures*, 84, pp. 243-262.
- [5] van der Weide, E., Kalitzin, G., Schluter, J., and Alonso, J.J. (2006). Unsteady turbomachinery computations using massively parallel platforms. In: *Proceedings of the 44th AIAA Aerospace Sciences Meeting and Exhibit*, Reno, NV, AIAA 2006-0421.
- [6] Jameson, A., Schmidt, W., and Turkel, E. (1981). Numerical solutions of the Euler equations by finite volume methods using Runge-Kutta time-stepping schemes. *AIAA Paper*, p. 1259.
- [7] Spalart, P. and Allmaras, S. (1992). A one-equation turbulence model for aerodynamic flows. In: *30th Aerospace Sciences Meeting and Exhibit*, 1992. doi:10.2514/6.1992-439. URL <http://dx.doi.org/10.2514/6.1992-439>.
- [8] Kennedy, G.J. and Martins, J.R.R.A. (2014). A parallel finite-element framework for large-scale gradient-based design optimization of high-performance structures. *Finite Elem. Anal. Des.* 87, pp. 56-73.
- [9] Wrenn, G.A. (1989). An indirect method for numerical optimization using the Kreisselmeier-Steinhauser function. *Technical Report CR-4220*. NASA.
- [10] Lambe, A.B., Kennedy, G.J., and Martins, J.R.R.A. (2017). An evaluation of constraint aggregation strategies for wing box mass minimization. *Structural and Multidisciplinary Optimization*, 55(1), pp. 257-277.
- [11] Gill, P.E., Murray, W., and Saunders, M.A. (2002). SNOPT: An SQP algorithm for large-scale constrained optimization. *SIAM J. Optim.*, 12 (4), pp. 979-1006.
- [12] Ansys, I.C.E.M. (2015). *CFD. ICEM CFD theory guide*, Ansys, Inc., Canonsburg, PA.
- [13] Kenway, G.K.W., Kennedy, G.J., and Martins, J.R.R.A. (2014). Scalable parallel approach for high-fidelity steady-state aeroelastic analysis and derivative computations. *AIAA J.* 52(5), pp. 935-951. <http://dx.doi.org/10.2514/1.J052255>.

No validation data are available.



Chapter 6 – BENCHMARK: GOAL ORIENTED STRUCTURAL DESIGN OF THE CRM WING BOX

Christophe Blondeau and Timothée Achard

ONERA
FRANCE

6.1 BENCHMARK EXECUTIVE SUMMARY

6.1.1 Qualitative Optimization Problem Statement

The structural design of a primary wing box in industry traditionally considers corrected DLM (Doublet Lattice Method) aeroelastic loads (with wind tunnel data, high-fidelity CFD pressure distribution). Although this approach is mature and allows the loads to be sufficiently accurately modeled when high angles of attack and strong non-linearities occur, it is difficult to extend in the context of a gradient-based optimization process when additionally loads sensitivities are required.

Rather, we propose a multi-fidelity integrated approach where aeroelastic loads can be computed either through high-fidelity aeroelastic analyses coupling 3D CFD (Euler/RANS) and CSM solvers or through traditional DLM linear aerodynamics corrected with a CFD rigid database (built offline). In the following, the latter approach will be called the Hybrid Static Approach [1].

In order to demonstrate the added value of high-fidelity aeroelastic loads in the sizing process, it is necessary to compute the corresponding load sensitivities using an efficient coupled aero-structure gradient capability based on the tangent or the adjoint formulation.

The proposed benchmark is a simple inverse design problem of the Common Research Model wing box in order to match a target twist distribution in nominal 1 G cruise flight conditions. The objective function is formulated as a sum of squared errors between target and computed displacements. The first step consists in deriving an unloaded jig shape for the fluid and the structure grids. This process is iterative and starts from the in-flight shape position of the fluid and structure meshes. A simple procedure for obtaining the jig shape has been proposed in Ref. [2]. In order to set up the inverse design problem, the wing skin thickness distribution is modified for the FEM aligned with the jig position. Then, at each iteration of the sizing process, a new steady aeroelastic equilibrium is computed along with the corresponding structural load and displacement sensitivities. As long as the computed twist distribution doesn't match the target reference one, the process iterates by changing the thickness distribution.

The CFD grid is multi-block structured and corresponds to the Wing-Body-HTP (WBH) configuration which has been downloaded from the 4th Drag prediction Workshop site ftp://cmb24.larc.nasa.gov/outgoing/DPW4/multiblock_Boeing/CGNS/ and the FEM from the NASA web site at the following location: <http://commonresearchmodel.larc.nasa.gov/fem-file/wingbox-fem-files/>. A full description can be found in Refs. [3] and [4]. In order to use standard SI units, the fluid and structure models have been converted in a pre-processing step.

6.1.1.1 Design Variables

The design variables control the upper and lower skin thickness distribution. Eight areas have been defined. The upper and lower skin parameterizations are linked together. The design variable definition is given in Figure 6-1.

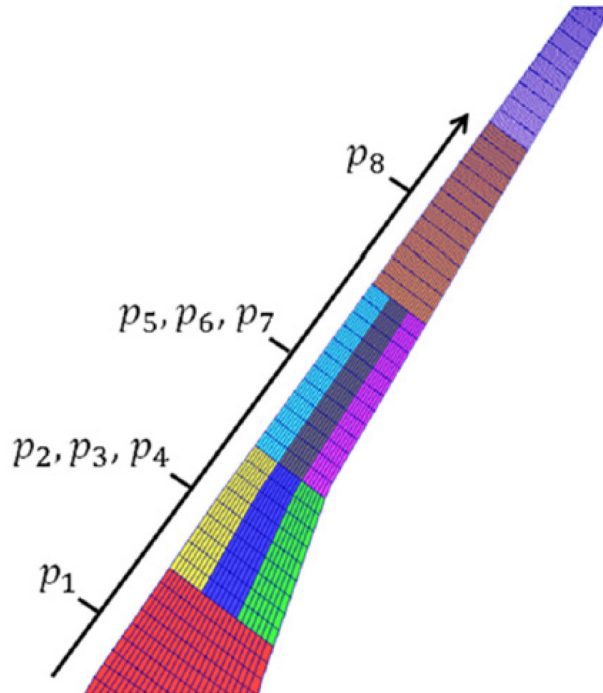


Figure 6-1: Design Variables Definition.

Also, in Figure 6-2 the initial design variable values distribution and the target one are depicted. The reference thickness distribution is uniform and corresponds to a value of 8.89 mm. All design variable values have been normalized by the reference value of 8.89 mm. We can see in Figure 6-2 that up to 45% of deviation has been applied for the definition of the initial design model.

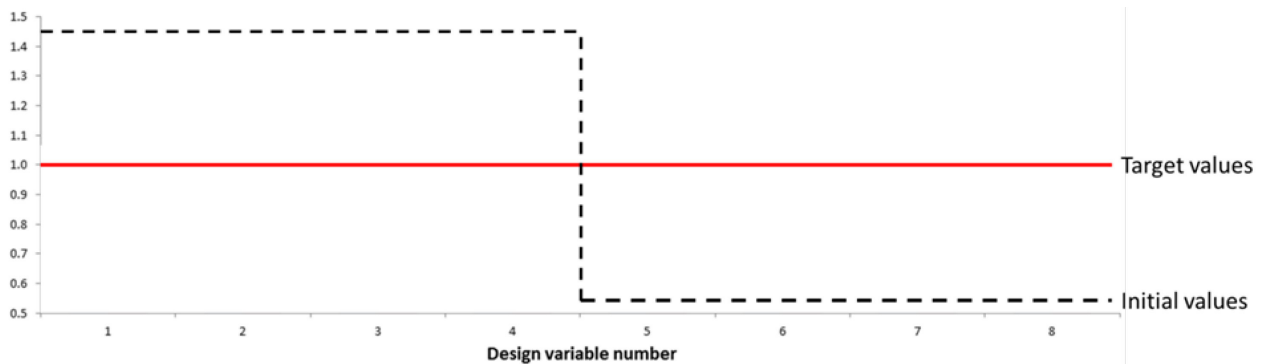


Figure 6-2: Initial and Target (Reference) Design Variable Values. The values have been normalized with the reference thickness value of 8.89 mm.

6.1.1.2 Objective Function(s)

The objective function is formulated as a sum of squared errors between target and computed displacements. The displacements correspond to vertical deflections at nodes belonging to the front and rear spars.

6.1.1.3 Constraint Function(s)

A total of 2664 maximum strain design constraints are defined in each finite element of the upper and lower skin. There are used to emulate an equivalent critical load case at a 2.5 g load factor. Additional upper and lower bound constraints are associated to the design variables and a minimum gauge is defined for the skin thickness.

6.1.2 Description of Analyses/Disciplines/Theory/Fidelities Involved

On the DPW4 website several levels of grids are available. In order to limit the computation time, the coarse model of 5.4 million cells, split into 26 blocks, has been selected (cgns file “vgrd_WBH0_cRe5M.splt.cgns”). A fluid RANS model is used with an upwind Roe scheme and a MUSCL interpolation associated to a Van Albada limiting function. The Spalart-Allmaras one-equation turbulence model is selected. However, for this demonstration and also for simplicity the high-fidelity coupled derivatives are computed using a frozen eddy viscosity assumption. For this particular prospective work, the grid has been further coarsened by a factor 2 in each direction, ending up with a number of about 700×103 cells.

The version v14 of the CRM FEM has been selected. The CRM model description can be found at the NASA web site https://commonresearchmodel.larc.nasa.gov/files/2014/02/CRM_wingboxFEM_description_1.pdf.

6.1.3 MDO Approach (Algorithm/Architecture)

The design process consists of two nested loops (see Figure 6-3). The outer loop controls the high-fidelity loads and loads sensitivity computation, and the inner loop corresponds to the internal design process controlled by the MSC/NASTRAN SOL200. Hence there are two levels of convergence, one at the outer level on loads and one at the inner level inside the structure sizing process. At the end of each structural sizing process, the finite element model is updated according to the new set of optimum sizing parameters for the subsequent high-fidelity computations.

The orchestration of the inner and outer loops is performed through dedicated Python and shell scripts.

6.1.4 Implementation Details

6.1.4.1 Analysis Software

The aeroelastic steady analysis is computed with the multi-block structured elsA CFD software [5]. The FEA package is MSC/NASTRAN. It is used in a pre-processing step to prepare structure input data required for the aeroelastic and coupled sensitivities computation by elsA.

6.1.4.2 Optimization Software

The optimization is performed with the MSC/NASTRAN SOL200 which has been slightly altered with some DMAP (Direct Matrix Abstraction Programming) in order to use the high-fidelity load sensitivities computed externally by the CFD package. The Modified Method of Feasible Direction (MMFD) algorithm has been selected in conjunction with a classical constraint screening approach.

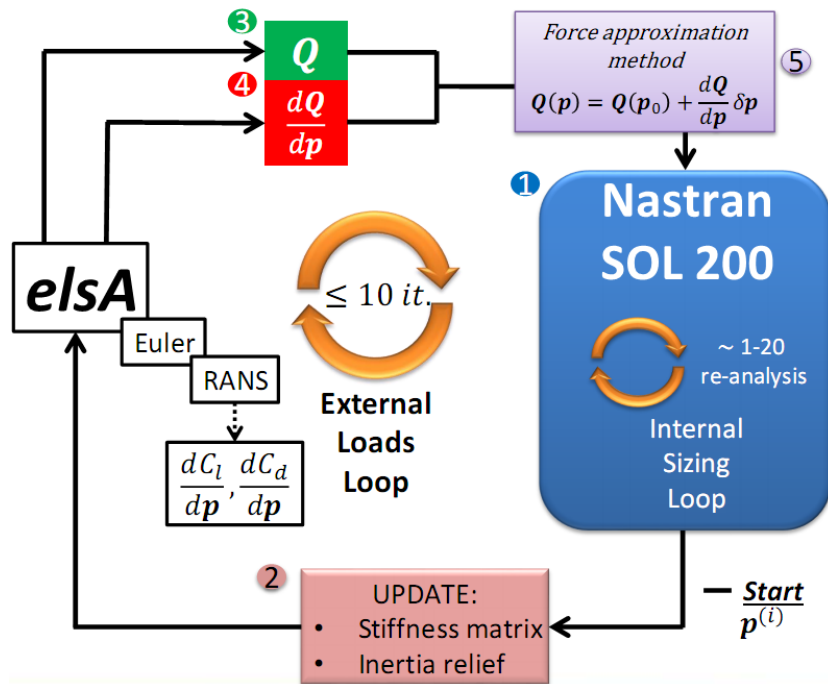


Figure 6-3: Nested Structural Sizing Process with High Fidelity CFD/CSM Analysis and Derivatives.

6.1.4.3 Hardware

Local HP cluster comprising 10 nodes with 2 quad-cores each (X5550, 2.67 GHz).

The current benchmark 26 fluid domains were distributed on 16 cores.

6.1.4.4 Human Effort

The human effort was not quantified.

6.1.5 Results

Results are presented in the following sections.

6.1.5.1 Optimization Convergence History

The convergence history for the 8 design variables and for the objective function is presented in Figure 6-4 and Figure 6-5. The convergence is typically achieved in about ten high-fidelity re-analyses and gradient computations. The quantities referred to as design variables are scaled by the reference value of 8.89 mm. This allows a quick check of the final values that should consequently match a unit value.

It is also interesting to observe that in case of a zeroth order updating strategy for the high-fidelity CFD loads, the convergence exhibits some peaks because of the inconsistency between the fluid and structure blocks. When a first order gradient-based predictor is introduced, the convergence is much more regular and also faster.

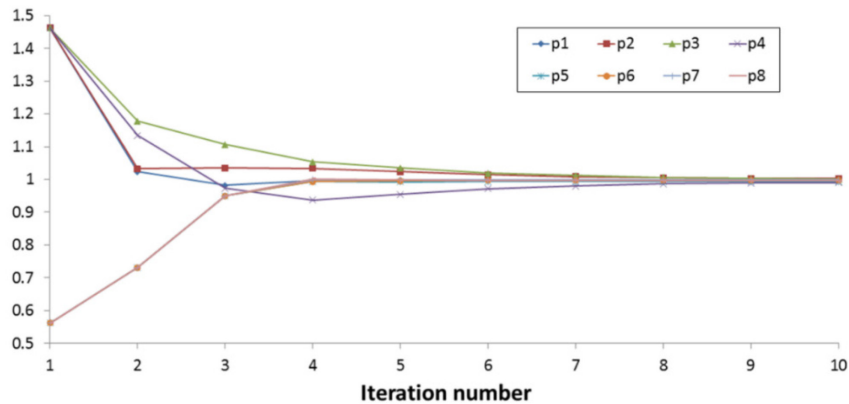


Figure 6-4: Design Variables Convergence History.

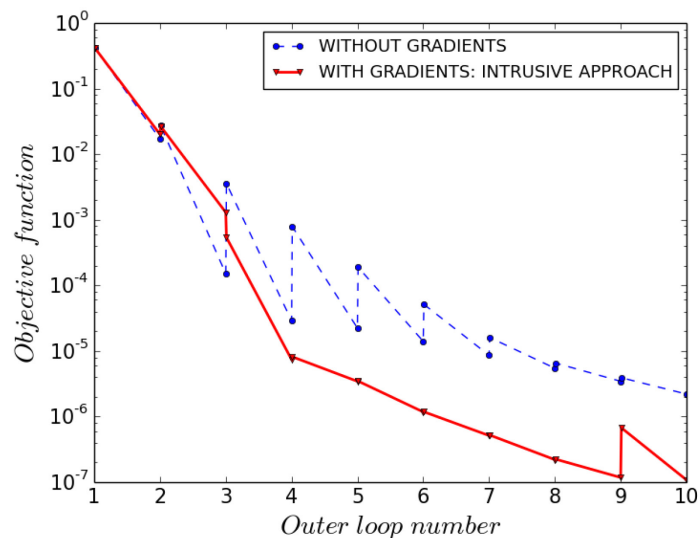


Figure 6-5: Objective Function Convergence History. Effect of the first-order load predictor based on the high-fidelity total load derivative computation.

6.1.5.2 Observations

The accuracy of the iterative numerical procedure for solving the coupled sensitivity equations can be greatly affected by the condition number of the fluid Jacobian matrix. This is why efficient preconditioners have to be applied. Also, of great importance is the level of convergence (i.e., residual decrease) of the mean flow solution around which the aeroelastic system is linearized. Practically speaking, this means that a great care should be taken when generated CFD grids dedicated to sensitivity analysis.

6.1.6 Technical and Financial Improvements/Benefits of Using MDO vs. Traditional Design Methods

None documented.

6.1.7 References; Web Resources; Science Connect Link; and Validation Data Location

The CFD database (CGNS files) and the FEM model in jig configuration and in SI units can be obtained from the author by sending an email (Christophe.Blondeau@onera.fr).

6.2 BENCHMARK DETAILS

6.2.1 High-Level

This design study is typical of what can be envisaged at the preliminary design phase in aircraft industry. The current trend of bringing high-fidelity earlier in the design process requires adequate numerical models able to tackle complex physic phenomena but at an affordable computational cost. This is why we put the right level of model at the right place by considering light RANS CFD meshes and GFEM with lumped mass distribution.

6.2.2 Multidisciplinary Analysis (MDA)

6.2.2.1 Implementation Details of Analyses and Corresponding Responses Used to Formulate MDO Objective and Constraint Functions

The version v14 of the CRM FEM is depicted in Figure 6-6 and Figure 6-7. The corresponding number of degrees of freedom is 28092.

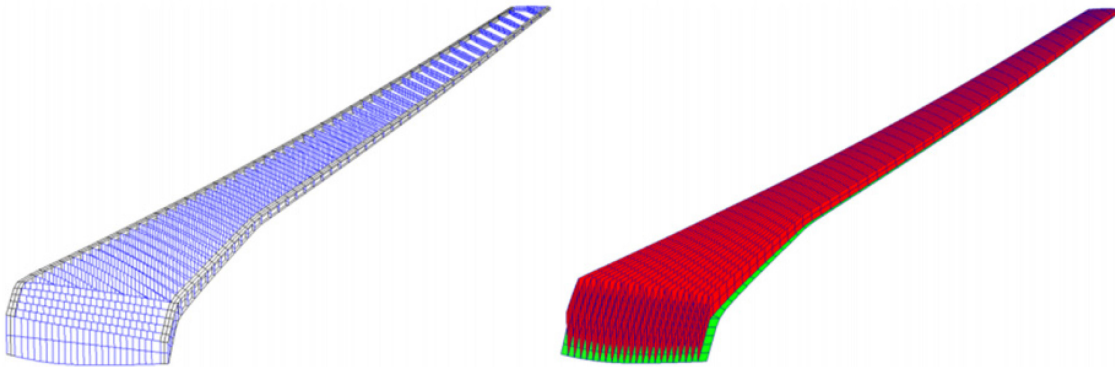


Figure 6-6: Finite Element Model Version v14 with Implicit Stiffeners.



Figure 6-7: Initial Fluid Mesh in 1 G Cruise Flight Conditions and Corresponding Jig Shape.

Before computing the gradient, we need to obtain the aeroelastic equilibrium configuration. There are numerous algorithms for solving the coupled nonlinear problem, among which the Non-Linear Block Gauss-Seidel (NLBGS) method is arguably the most popular and easiest to implement. Figure 6-8 presents the typical flowchart of the steady aeroelastic solution process. After converging the fluid equations, the loads are transferred on the structure skin and the structural displacements are then splined on the aerodynamic skin. In a second step, these surface displacements are transferred to the interior of the fluid domain using a mesh deformation technique. The process is then iterated starting from the jig shape until convergence at the flight shape position. It is worth mentioning that the aeroelastic solution has been obtained using a “one-shot” mesh deformation formulation in which the deformation operators only depend on the reference grid coordinates and allow the full amplitude of the structural displacements field to be applied to the jig CFD grid in one step.

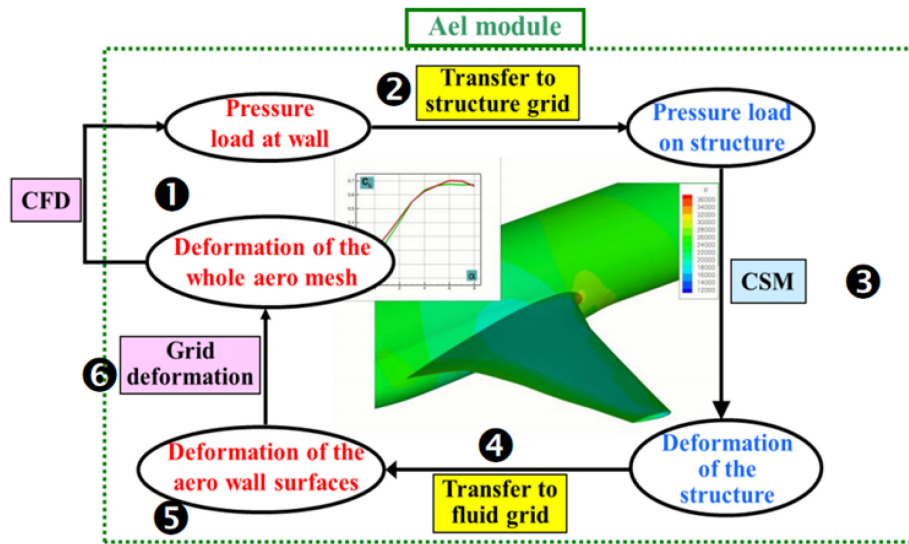


Figure 6-8: The Different Steps of the Steady Aeroelastic NLBGS (Non-Linear Block Gauss Seidel) Solver.

The equilibrium configuration in 1 G cruise flight conditions is shown in Figure 6-9. The skin is colored with the contours of the pressure coefficient distribution. Detailed C_p distributions for different sections are provided in Figure 6-10. These distributions fairly compare with results presented in Ref. [3].

In order to solve the inverse design problem, we need to compute the total derivatives of the structural displacements field dU/dp , and also of the aerodynamic forces on the skin dQ_a/dp . In this case, the linearized approach is best suited as they are much design responses than design parameters.

Let the discrete steady-state nonlinear flow problem be expressed in residual form as $R_a(W, X_a) = 0$ where W are the flow variables and X_a the aerodynamic grid coordinates. Moreover, let $R_s(U, X_s) = KU - Q_s = 0$ be the linear structural discrete problem where K is the global stiffness matrix, X_s the structural grid coordinates, U the structural displacement field and Q_s the aerodynamic loads interpolated on the structural skin. At the aeroelastic equilibrium, the state variables and the meshes satisfy the coupled discretized equations simultaneously:

$$\begin{cases} R_a(W, X_a, U) = 0 \\ R_s(U, X_s, W) = 0 \end{cases}$$

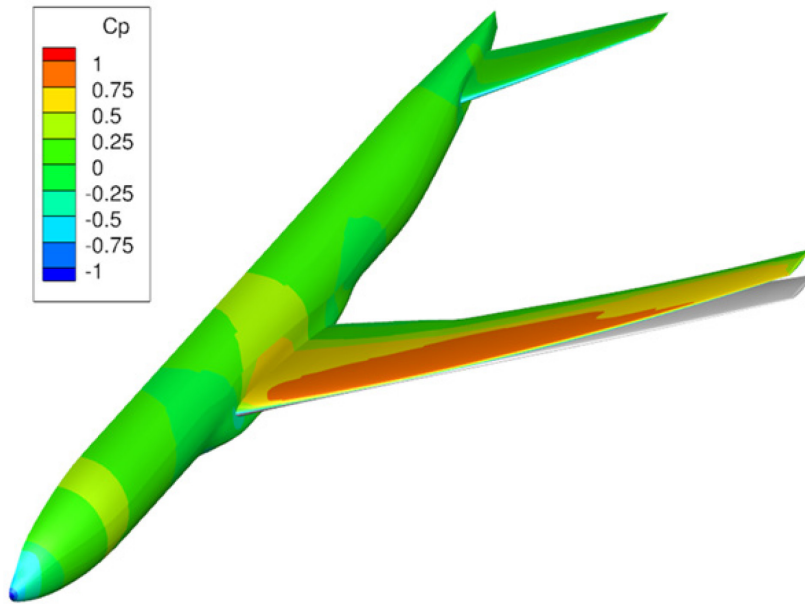


**Figure 6-9: Steady Equilibrium in 1 G Cruise Flight Conditions.
The jig shape is plotted in shaded grey.**

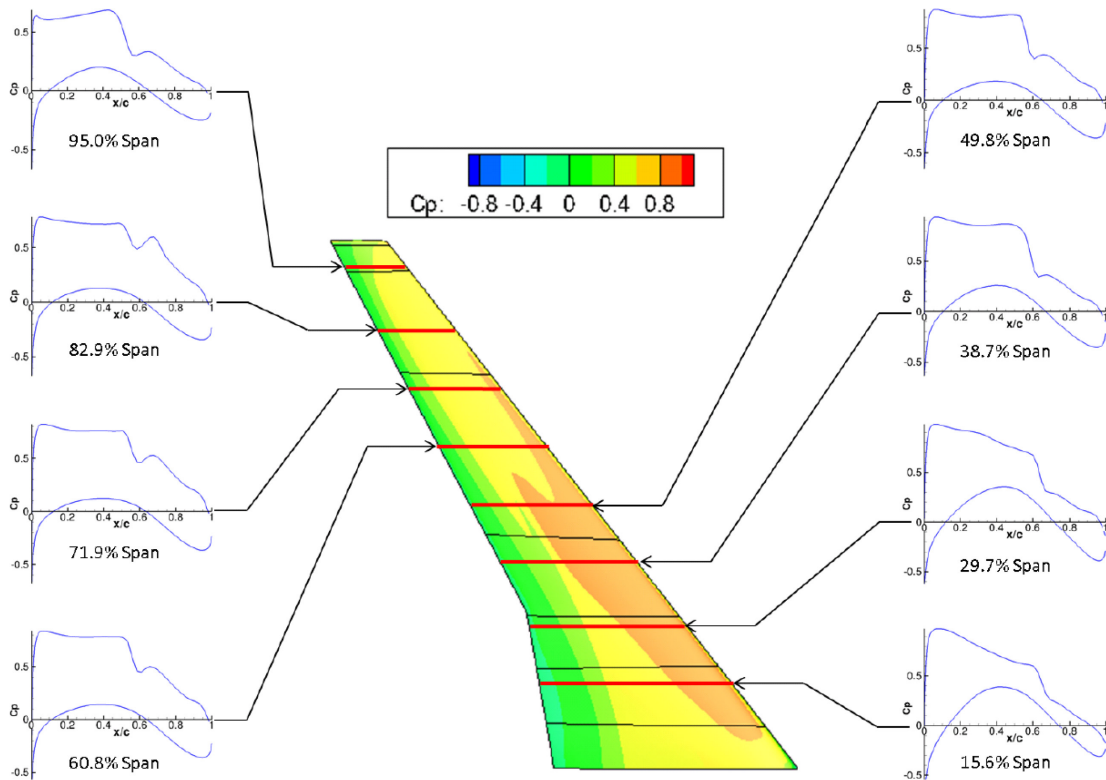


Figure 6-10: Pressure Coefficient Distributions for Steady Aeroelastic Configuration in 1 G Cruise Flight Conditions.

The system of discrete equations for coupled sensitivity computation is derived by direct differentiation of this coupled system of equations with respect to a given sizing parameter p :

$$\begin{bmatrix} \frac{\partial R_a}{\partial W} & \frac{\partial R_a}{\partial X_a} [A] \\ -[B] \frac{dU}{dp} & K - [C] \end{bmatrix} \begin{bmatrix} \frac{dW}{dp} \\ \frac{dU}{dp} \end{bmatrix} = \begin{bmatrix} 0 \frac{dU}{dp} \\ -\frac{\partial K}{\partial p} U \end{bmatrix}$$

Constant matrices $[A]$, $[B]$ and $[C]$ are defined analytically with the following formulas:

$$[A] = T_{vol} T_{surf}^U, [B] = T_{surf}^Q \frac{\partial Q_a}{\partial W}, [C] = T_{surf}^Q \frac{\partial Q_a}{\partial X_a} T_{surf}^U$$

The linear operator T_{surf}^U is used to smooth displacements from structure to aerodynamic skin and similarly T_{surf}^Q transfers the aerodynamic loads Q_a onto the structure wetted surface. The linear mesh deformation volume operator T_{vol} propagates the aeroelastic interface motion inside the interior of the fluid domain. The partial derivative of the aerodynamic loads with respect to the fluid conservative variables at the boundary is denoted $\partial Q_a / \partial W$ and its geometric counterpart is denoted $\partial Q_a / \partial X_a$. In the above equation we have also assumed that $\partial X_a / \partial p = \partial X_s / \partial p = 0$, because the meshes are not affected by design parameters changes.

6.2.2.2 Practical Concerns

The methodology presented in this chapter is fully automated with respect to the aeroelastic analysis (MDA) and the coupled sensitivity analysis. The elsA/AEL (Aeroelastic module) and elsA/AOC (Coupled sensitivities) standard capabilities and problem set up have been used as is.

6.2.3 MDO Problem Definition Details

The inverse design problem is formulated as:

$$\text{Minimize } J(\mathbf{p}) \text{ such that: } \begin{cases} J(\mathbf{p}) = \sum_{i=1}^N \left(1 - \frac{U_i(\mathbf{p})}{U_i^T} \right)^2 \\ \varepsilon(\mathbf{p}) \leq \varepsilon_{max} \\ \mathbf{p}_{min} \leq \mathbf{p} \leq \mathbf{p}_{max} \end{cases}$$

As previously mentioned, 8 design variables have been defined. A minimum value of 20% and a maximum value of 200% of the initial guess are defined.

The upper and lower strain bounds are identical and have been set at $-1254 \mu\epsilon$ and $+1254 \mu\epsilon$ respectively. They have been derived from a Von Mises yield stress of 324 Mpa with a safety factor of 1.50.

A minimum technological thickness has been imposed at 2 mm everywhere.

6.2.4 MDO Algorithm

The design process consists in two nested loops. The outer loop controls the high-fidelity loads and loads sensitivity computation, and the inner loop corresponds to the internal design process controlled by the MSC/NASTRAN SOL200, see Figure 6-3. Hence there are two levels of convergence, one at the outer level on loads and one at the inner level inside the structure sizing process. At the end of each structural sizing process, the finite element model is updated according to the new set of optimum sizing parameters for the subsequent high-fidelity computations. The aeroelastic steady analysis is computed with the multi-block structured elsA CFD software. The FEA package is used in a pre-processing step to prepare structure input data required for the aeroelastic and coupled sensitivities computation by elsA.

The optimization solution SOL200 has been slightly altered with some DMAP (Direct Matrix Abstraction Programming) in order to use the high-fidelity load sensitivities computed externally by the CFD package. The Modified Method of Feasible Direction (MMFD, [6] algorithm has been selected in conjunction with a classical constraint screening approach. The maximum design cycle number in the structural sizing sub-process has been set at 1. This means that a true strong coupling between CFD and CSM solvers is performed.

6.2.5 MDO Results

Figure 6-11 compares the initial and target twist distributions. Although the difference between the two twist laws seems small, it is the consequence of large stiffness variations. Specifically, it is very difficult to modify the displacements of the inboard wing which is inherently very stiff.

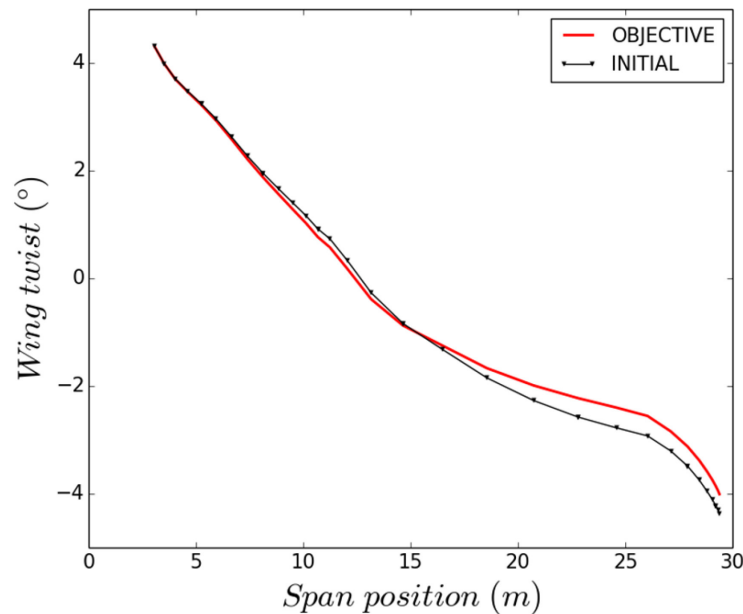


Figure 6-11: Initial and Target Spanwise Twist Distributions.

In this prospective work two approaches have been considered for the structural loads update at the outer loop level. The first approach only updates the loads value in order to emulate a fixed-point strategy and subsequently assess the benefit of introducing a first-order approximation for the loads in the structural sizing process. The loads total derivatives have been obtained by the coupled tangent method. The design variable distribution

for the initial and the final configurations are reproduced in Figure 6-12. It can be seen that the optimum design obtained by the gradient-based process is very close to the target values. For the zeroth order loads update approach, the final values are slightly less accurate but as can be seen in Figure 6-4, this process requires additional iterations to achieve the same level of convergence.

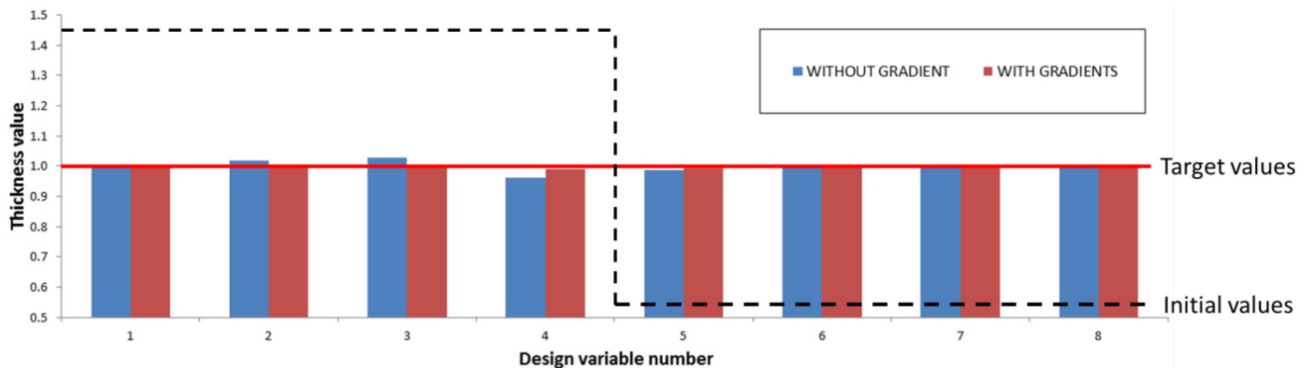


Figure 6-12: Initial and Final Design Variables Distribution.

The objective function convergence history is depicted in Figure 6-5. The gradient-based formulation exhibits a very fast convergence rate and a limited number of iterations is required to achieve seven orders of magnitude of residual decrease. It is also worth mentioning that the first order predictor for the structural loads almost suppresses all peaks in the convergence behavior.

6.2.6 Technical and Financial Improvements/Benefits of Using MDO vs. Traditional Design Methods

N/A.

6.2.7 References; Web Resources; Science Connect Link; and Validation Data Location

- [1] Vincenzo, F.G.D. (2012). Hybrid Static Aeroelasticity New Capabilities – CFD Data Management. http://pages.mscsoftware.com/rs/mscsoftware/images/trim-cfd_marseille_24mai2012.pdf.
- [2] Achard, T., Blondeau, C., and Ohayon, R. (2016). An Uncoupled Approach to Compute Aero-Structure Gradients Using High-Fidelity CFD-CSM. 17th AIAA/ISSMO Multidisciplinary Analysis and Optimization Conference, AIAA Paper 2016-4121.
- [3] Vassberg, J.C. (2011). A Unified Baseline Grid about the Common Research Model Wing-Body for the Fifth AIAA CFD Drag Prediction Workshop. 29th Applied Aerodynamics Conference, Honolulu, Hawaii, AIAA Paper 2011-3508.
- [4] Vassberg, J.C., DeHann, M.A., Rivers, S.M., and Wahls, R.A. (2008). Development of a Common Research Model for Applied CFD Validation Studies. AIAA Paper 2008-6919.
- [5] Cambier, L., Gazaix, M., Heib, S., Plot, S., Pointot, M., Veillot, J.P., Boussuge, J.F., and Montagnac, M. (2011). An Overview of the Multi-Purpose elsA Flow Solver. Aerospace Lab Journal, Issue 2, March, 2011.

- [6] Vanderplaats, G. and Salajegheh, E. (1989). New Approximation Method for Stress Constraints in Structural Synthesis. *AIAA Journal* 27(3), pp. 352-358.

Chapter 7 – BENCHMARK: MULTIDISCIPLINARY ROBUST DESIGN OPTIMIZATION OF A KEEL FIN OF A RACING SAILBOAT

Cecilia Leotardi, Emilio F. Campana and Matteo Diez
National Research Council
ITALY

The multidisciplinary robust design optimization of a keel fin of a racing sailboat is presented subject to stochastic operating conditions (yaw angle). The optimized design is identified by a variable-accuracy global metamodel-based optimization method, based on the extension of the Multidisciplinary Feasible (MDF) architecture. The approach encompasses a variable:

- a) Density of the design of experiments for the metamodel training;
- b) Accuracy of the Uncertainty Quantification (UQ); and
- c) Discipline coupling in the Multidisciplinary Analysis (MDA, introducing a variable tolerance for the multidisciplinary consistency).

Specifically, a two-way steady fluid-structure interaction problem is investigated using partitioned solvers for fluid and structure. The results provided by the current architecture are compared to a benchmark solution, given by a standard MDF procedure with fully coupled MDA, fully convergent UQ, and optimization without metamodels. For the sake of simplicity and replicability as a benchmark problem, analysis and optimization pertain to the isolated fin, though earlier research for deterministic and stochastic multidisciplinary optimization included the effects of the hull and the free-surface.

7.1 BENCHMARK EXECUTIVE SUMMARY

7.1.1 Qualitative Optimization Problem Statement

A Multidisciplinary Robust Design Optimization (MRDO) of a keel fin of a racing sailboat (see Figure 7-1) is presented, subject to stochastic operating conditions (yaw angle) [1], [2], [3], [4]. The geometric dimensions of the fin are:

- Root chord $c_R = 0.90$ m;
- Tip chord $c_T = 0.76$ m; and
- Span $s = 2.82$ m.

The fin is made of stainless steel and sustains a 22,000 kg ballast bulb that equilibrates the roll moment due to the sail pressure distribution. For the sake of simplicity and replicability as a benchmark problem, the isolated fin is considered hereafter, though earlier research for deterministic and stochastic Multidisciplinary Design Optimization (MDO) included the effects of the hull and the free-surface. The fin is clamped at root and free at tip (cantilever). In the current benchmark problem, the bulb is modelled as a concentrated mass at the tip mid-chord.

7.1.1.1 Design Variables

Two design variables (x_1, x_2) control the thickness of the root and the tip sections, based on Bézier surfaces. A linear interpolation of the thickness variation is applied span wise.

7.1.1.2 Objective Function(s)

The objective function is the expected value of the hydrodynamic efficiency, $\mu(f)$, with $f = C_Y/C_X$ (lift and drag coefficients), evaluated considering:

- The yaw angle as stochastic parameter varying from 1 to 9 deg. and following a uniform distribution;
- A fixed sailing speed equal to 10 knots; and
- A fixed heel angle equal to 30 deg.

A separate analysis and/or optimization of C_Y and C_X is not pursued in the current test case.

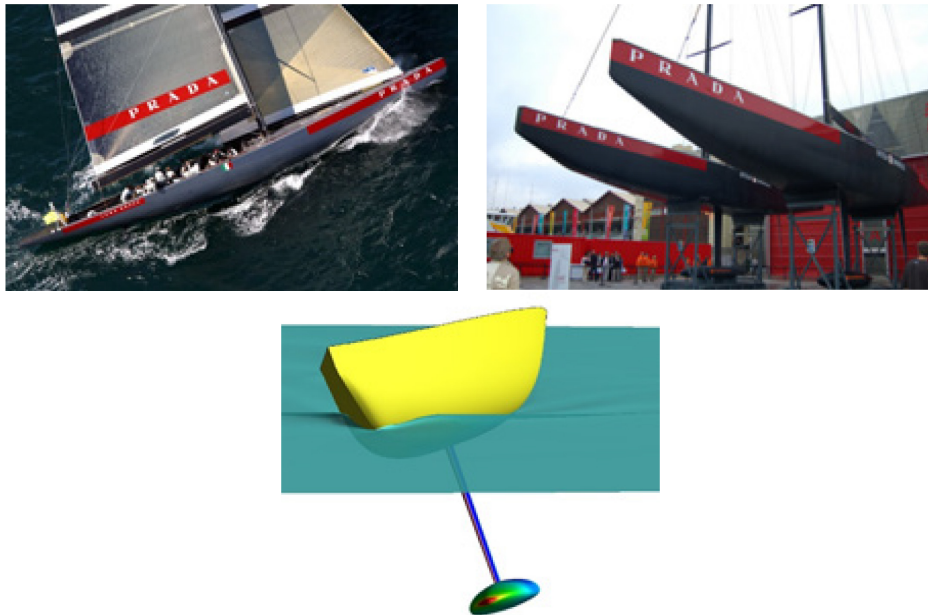


Figure 7-1: Keel Fin Optimization Examples.

7.1.1.3 Constraint Function(s)

Box constraints are imposed to the design variables x_1 and x_2 . Specifically, $-0.1 \leq x_1 \leq 0.1$ and $-0.05 \leq x_2 \leq 0.05$. No functional constraints are considered for the current test case.

7.1.2 Description of Analyses/Disciplines/Theory/Fidelities Involved

Two disciplines are evaluated in the Multidisciplinary Analysis (MDA): hydrodynamics and structural mechanics.

7.1.3 MDO Approach (Algorithm/Architecture)

The optimized design is achieved by a variable-accuracy metamodel-based architecture, including subsequent optimization stages with:

- a) Increasing accuracy in metamodel training;
- b) Increasing accuracy in the Uncertainty Quantification (UQ) analysis; and
- c) Increasing coupling between disciplines in MDA, performed by partitioned solvers for hydrodynamics and structure.

Fully accurate UQ and fully converged MDA are achieved at the final optimization stage [4].

7.1.4 Implementation Details

7.1.4.1 Analysis Software

The hydrodynamic loads are computed using a non-linear Boundary Element Method (BEM) solver, developed in-house at CNR-INSEAN, namely WARP (Wave Resistance Program) [5]. The elastic displacement of the structure is evaluated by an open source Finite Element Method (FEM) solver, namely CALCULIX [6]. The steady fluid-structure interaction equilibrium is achieved by a two-way coupled system (exchanging loads and displacements). The UQ analysis is performed by a quasi-Monte Carlo (MC) approach, based on a deterministic variant of the Latin Hypercube Sampling (LHS). Finally, a Thin Plate Spline (TPS) metamodel trained by Hammersley Sequence Sampling (HSS) [7] is used for the metamodel-based optimization.

7.1.4.2 Optimization Software

A deterministic version of the global, Derivative-free Particle Swarm Optimization Algorithm (DPSO) [8] is used as optimization algorithm.

7.1.4.3 Hardware

Both benchmark MRDO and variable-accuracy metamodel-based MRDO procedures are performed on a 16 GB RAM Intel Xeon E5-1620 v2@370GHz eight-core workstation.

7.1.4.4 Human Effort

The human effort due to non-automatic processes has not been evaluated.

7.1.5 Results

7.1.5.1 Initial Design (Design Variables, Objectives, Constraint Values)

The design variable values for the original configuration are $x_1 = x_2 = 0$. The objective function evaluated for the original configuration is $\mu(f) = 11.91$.

7.1.5.2 Optimized Design (Design Variables, Objectives, Constraint Values)

Solutions are shown in Table 7-1, obtained using a standard Multidisciplinary Feasible (MDF) approach for the MRDO and the metamodel-based approach [4]. Design variable benchmark values are $x_1 = -0.0578$

and $x_2 = -0.0302$. The corresponding objective function value is $\mu(f) = 27.32$. The number of function evaluations (budget of simulations) used to achieve the optimized design is also shown in Table 7-1.

Table 7-1: MRDO Benchmark vs. Variable-Accuracy Results.

Strategy	Design Var. 1	Design Var. 2	Obj. Function	abs(ϵ) %	Budget %	N_s/N_{DV}
MRDO Benchmark	-5.78E-02	3.02E-02	27.32	–	100%	2,631,680
Metamodel-Based MRDO	-5.51E-02	2.57E-02	25.91	5.16	10%	265,356
	-5.53E-02	2.61E-02	26.12	4.39	20%	530,712
	-5.48E-02	2.73E-02	26.43	3.25	30%	769,068
	-5.61E-02	2.81E-02	26.57	2.74	40%	1,061,424
	-5.65E-02	2.88E-02	26.68	2.34	50%	1,326,780

7.1.5.3 Observations

The optimized fin is thinner at root and thicker at tip and shows a quite remarkable improvement of the hydrodynamic efficiency, $\mu(f) = 27.32$, compared to the original, $\mu(f) = 11.91$.

The metamodel-based optimization method converged to the benchmark (or at least to the proximity of the benchmark) achieving satisfactory results in terms of identification of the optimum. Specifically, the penalty associated to the identification of the optimum using fractions of the overall (benchmark) computational cost ranges from 5.16 to 2.34 %, using 10 to 50 % of the benchmark cost, respectively.

Following the approach proposed, which is an adaptation of the multidisciplinary feasible architecture, the MDO results are robust since the multidisciplinary consistency is guaranteed/enforced at the final stage of the variable-accuracy metamodel-based optimization.

7.1.6 Technical and Financial Improvements/Benefits of Using MDO vs. Traditional Design Methods

This information is not available.

7.1.7 References; Web Resources; Science Connect Link; and Validation Data Location

Details on the benchmark problem may be found in:

Leotardi, C., Serani, A., Iemma, U., Campana, E.F., and Diez, M. (2016). A variable-accuracy metamodel-based architecture for global MDO under uncertainty. *Structural Multidisciplinary Optimization* 54(3), pp. 573-593. DOI 10.1007/s00158-016-1423-4. Available at: <https://link.springer.com/article/10.1007/s00158-016-1423-4>.

Additional background information may be found in:

Diez, M., Peri, D., Fasano, G., and Campana, E.F. (2012). Hydroelastic optimization of a keel fin of a sailing boat: a multidisciplinary robust formulation for ship design. *Structural and Multidisciplinary Optimization* 46(4), pp. 613-625. DOI 10.1007/s00158-012-0783-7. Available at: <https://link.springer.com/article/10.1007/s00158-012-0783-7>.

Campana, E.F., Fasano, G., and Peri, D. (2006). Issues on nonlinear programming for Multidisciplinary Design Optimization (MDO), in ship design frameworks. In: Mota Soares C.A. et al. (Eds.) III European Conference on Computational Mechanics for Solids, Structures and Coupled Problems in Engineering, Lisbon, Portugal. Available at: <http://citeseerx.ist.psu.edu/viewdoc/download?doi=10.1.1.583.6046&rep=rep1&type=pdf>.

Related papers and computational (surface) grids are available at: <https://scienceconnect.sto.nato.int/apps/23964>. A complete reference list may be found in Section 7.2.7.

7.2 BENCHMARK DETAILS

7.2.1 High-Level

The current application addresses a preliminary design phase, concerning a component-level optimization for marine vehicles, namely the MRDO of a keel fin of a racing sailboat, subject to stochastic operating conditions (yaw angle).

The N^2 diagram is shown in Figure 7-2 and the corresponding pseudo-code in Figure 7-3. Specifically, the optimization process is initialized at step 0 using the design variables $x^{(0)}$, starts at 1 and ends at 8. At step 1 the UQ loop is initialized using the initial value of the uncertain parameter y , the loop starts at 2 and is repeated until step 7 when convergence is achieved. The MDA loop is initialized at step 2 with the actual value of the uncertain parameter and the initial value of the variables shared among the two disciplines involved in the process (Analysis 1 block provides for the hydrodynamic analysis and Analysis 2 for the structural analysis). The MDA loop starts at 3, is repeated till convergence, and ends at step 5. The MDA output function is provided at step 6, the objective function μ corresponding to the optimized design variables values x is provided at step 8.

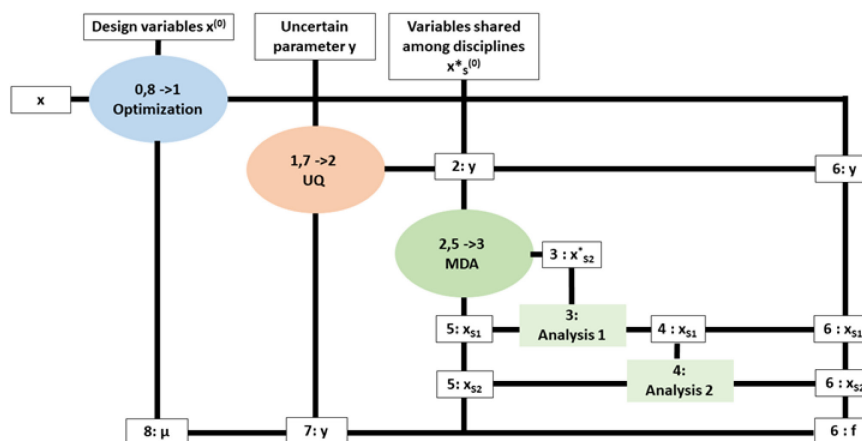


Figure 7-2: N^2 Diagram Including Optimization, Uncertainty Quantification, and MDA.

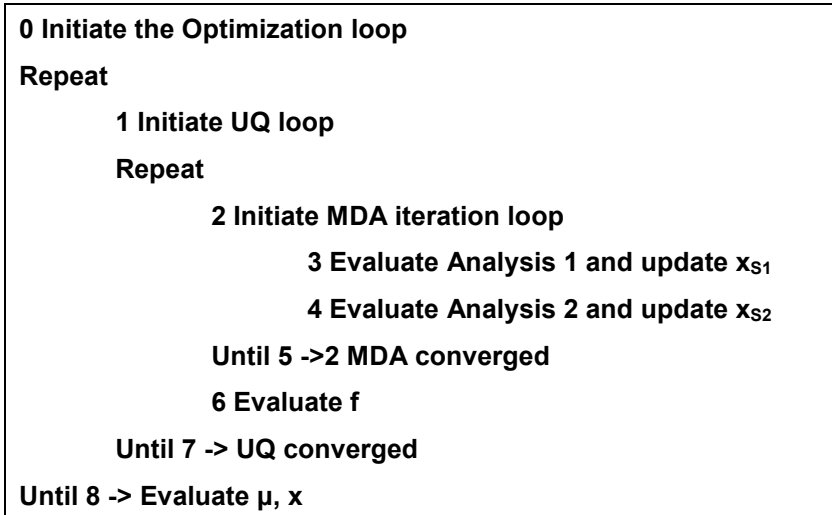


Figure 7-3: Pseudo-Code for MDO Algorithm.

7.2.2 Multidisciplinary Analysis (MDA)

7.2.2.1 Implementation Details of Analyses and Corresponding Responses Used to Formulate MDO Objective and Constraint Functions

The two disciplines involved in the MDA are hydrodynamics and structural mechanics and are solved using physics-based solvers.

Specifically, the hydrodynamic loads are evaluated via a non-linear quasi-potential flow solver [5], based on the Laplace equation $\nabla^2 \phi = 0$, where ϕ is the velocity scalar potential, satisfying $u = \nabla\phi$ and u is the flow velocity. The corresponding boundary integral representation reads:

$$\phi(\mathbf{z}) = \int_{S_B \cup S_F \cup S_W} \left[G(\mathbf{z}, \mathbf{z}') \frac{\partial \phi}{\partial n} - \phi(\mathbf{z}') \frac{\partial G(\mathbf{z}, \mathbf{z}')}{\partial n} \right] dS(\mathbf{z}, \mathbf{z}') \quad (7-1)$$

where $\mathbf{z}, \mathbf{z}' \in \mathbb{R}^3$ are the spatial coordinate, S_B , S_F , and S_W are respectively the body surface, the free surface and the wake surface, $G = -1/4\pi(|z-z'|)$ is the Green function, $\|\cdot\|$ is the Euclidean norm and $\partial/\partial n = \nabla \cdot \mathbf{n}$, with \mathbf{n} normal to the boundary surface (out of the body). The integral equation is solved applying the following boundary conditions for steady problem:

$$\left\{ \begin{array}{l} \frac{\partial \phi}{\partial n} = \mathbf{u}_B \cdot \mathbf{n} \text{ on } S_B \\ \mathbf{u}_W \cdot \nabla(\Delta\phi) = 0 \text{ on } S_W \\ \frac{\partial \phi}{\partial x} \frac{\partial \eta}{\partial x} = \frac{\partial \phi}{\partial z} \text{ and } \frac{p_\infty}{\rho} + \frac{(\nabla\phi)^2}{2} - g\eta = \text{const on } S_F \end{array} \right. \quad (7-2)$$

where \mathbf{u}_B is the velocity of the body, \mathbf{u}_W is the velocity of the wake, $\Delta\phi$ is the potential jump across the wake, η is the wave elevation, x and z are the cartesian spatial coordinates parallel to the flow and orthogonal to the unperturbed free surface (downwards), respectively, p_∞ is the atmospheric pressure, and ρ is the water density.

The hydrodynamic forces \mathbf{f} are estimated using the pressure distribution obtained through the Bernoulli theorem:

$$\frac{p}{\rho} + \frac{(\nabla\phi)^2}{2} - gz = \text{const} \quad (7-3)$$

The proposed benchmark includes the evaluation of the hydrodynamic loads on the keel fin imposing the following simplifying assumptions: the effects of the hull, bulb, and free-surface are neglected. The structural analysis is solved considering the equilibrium equation, the stress/strain constitutive law, and the strain/displacement constitutive law:

$$\begin{cases} \nabla \cdot \mathbf{T} + \rho \mathbf{f} = 0 \\ \mathbf{T} = \mathbf{C} : \mathbf{E} \\ \mathbf{E} = \frac{1}{2}(\nabla \mathbf{u} + \nabla \mathbf{u}^T) \end{cases} \quad (7-4)$$

where \mathbf{T} , \mathbf{C} , and \mathbf{E} are respectively the Cauchy stress tensor, the isothermal elastic stiffness tensor, and the strain tensor; \mathbf{u} and \mathbf{f} are the elastic displacement and the body forces.

The boundary conditions are given in terms of \mathbf{u} and \mathbf{T} , as:

$$\begin{cases} \mathbf{u}(\mathbf{x}) = \mathbf{u}^*(\mathbf{x}) \\ \mathbf{t}(\mathbf{x}) = \mathbf{t}^*(\mathbf{x}) \end{cases} \quad (7-5)$$

with $\mathbf{t} = \mathbf{T} \cdot \mathbf{n}$. The boundary value problem, reformulated in the weak form, is numerically solved by FEM providing $\mathbf{K}\mathbf{u} = \mathbf{f}$, where \mathbf{K} is the stiffness matrix.

The steady equilibrium is achieved by Gauss-Seidel iterations. C_Y and C_X are evaluated by integration of the hydrodynamic loads over the fin surface.

The objective function (expected value of the hydrodynamic efficiency) is approximated using a quasi-MC method:

$$\mu(f) \approx \frac{1}{N_{UQ}} \sum_{i=1}^{N_{UQ}} f(\mathbf{x}, \mathbf{y}_i) \quad (7-6)$$

where the uncertain parameter domain is sampled by a deterministic version of the LHS method, using a number of points $N_{UQ} = 2^h + 1$, $h \in \mathbb{N}$. Evenly spaced items are used.

The problem is solved using the following setup. The fin is made in stainless steel and has geometric dimensions equal to: root chord $c_R = 0.90$ m, tip chord $c_T = 0.76$ m, and span $s = 2.82$ m. The fin sustains a ballast bulb, which is modelled as a concentrated mass of 22,000 kg at the tip mid chord. The fin is clamped at root and free at tip (cantilever). The material properties are: Young modulus $E = 210$ GPa, Poisson ratio $\nu = 0.3$, density $\rho_M = 7800$ kg/m³.

The optimization problem is solved using a quite coarse 20 x 10 panel grid for the evaluation of the hydrodynamic loads (surface grids are provided as supplemental material in the NATO Science Connect website), whereas for the structural FEM analysis a 9 x 9 x 1 brick-element grid is applied. In the current test case, the MDA provides in output the value of the hydrodynamic efficiency. A separate analysis of C_Y and C_X is not pursued in the current study.

Figure 7-4 shows the pressure distribution for the original and optimized keel fin configurations.

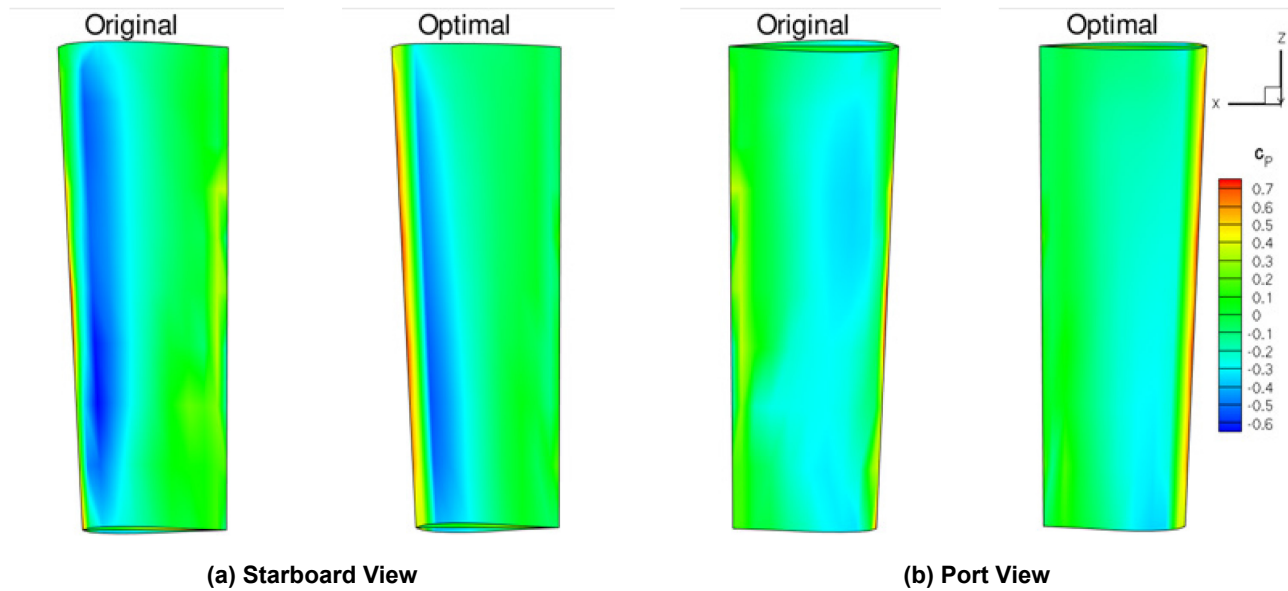


Figure 7-4: Pressure Coefficient for Original and Optimized Configurations, (a) Starboard View and (b) Port View (Yaw Angle, $\gamma = 5$ Deg.).

7.2.2.2 Practical Concerns

The non-linear BEM solver, developed in-house at CNR-INSEAN, namely WARP (WAVE Resistance Program) [5] runs on Linux operating system platforms. The open source FEM solver CALCULIX [6] runs on multiple operating system platforms, such as Linux, Macintosh and Windows. The optimization problem runs in parallel, whereas hydrodynamic and structural simulations are serial. The hydrodynamic solver can run using multi-threading.

The MDA is performed as an automatic process and stopped if multidisciplinary equilibrium is achieved within a given tolerance (for solution changes), or a prescribed maximum number of iterations is reached. Both benchmark and variable-accuracy metamodel-based problems are solved on a 16 GB RAM Intel Xeon E5-1620 v2@370GHz eight-core workstation. The total CPU-time associated to the benchmark solution is about 1.58×10^6 s (0.6 s per single evaluation), whereas the metamodel-based total CPU times, corresponding to 10 to 50 % of the benchmark budget are respectively 1.59×10^5 s, 3.2×10^5 s, 4.61×10^5 s, 6.36×10^5 s, and 7.96×10^5 s.

Information on disk space required is not available.

7.2.3 MDO Problem Definition Details

The optimization problem is stated as:

$$\begin{aligned}
 &\text{maximize } \mu(f) = \int_Y f(x_1, x_2, y)p(y)dy \\
 &\text{with } (x_1, x_2) \in X \subset \mathbb{R}^2 \\
 &\text{and } p(y) \text{ uniform distribution, } y \in [1, 9] \text{ deg.} \\
 &\text{subject to } -0.1 \leq x_1 \leq 0.1 \\
 &\quad \quad -0.05 \leq x_2 \leq 0.05
 \end{aligned} \tag{7-7}$$

The two deterministic (real) design variables (x_1 , x_2) control the thickness of the root and tip sections, based on Bézier surfaces (Figure 7-5 and Figure 7-6). Specifically, two control points, one at root (x_1) and one at tip (x_2), control a linear modification of the sections along the fin span.

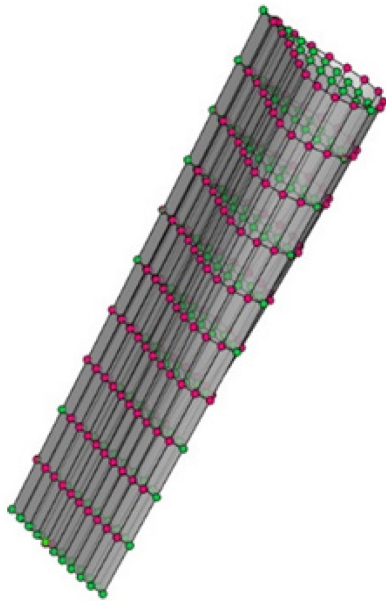


Figure 7-5: Shape Modification Due to x_1 .

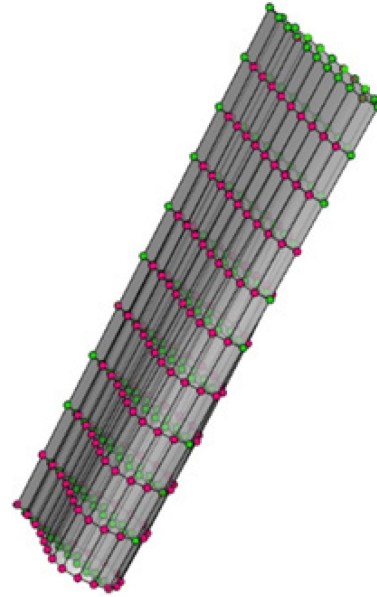


Figure 7-6: Shape Modification Due to x_2 .

The objective function is the expected value of the hydrodynamic efficiency $\mu(f)$, where $f = C_Y / C_X$, where $C_Y = 2F_Y / \rho u_B^2 S$, $C_X = 2F_X / \rho u_B^2 S$; F_Y and F_X are the Y and X force (lift and drag); ρ is the fluid density (the water is considered incompressible); u_B is the modulus of the velocity vector of the body in the fluid; and $p(y)$ is the probability density function associated to the yaw angle, here indicated by 'y'. Operating conditions are defined in terms of speed (equal to 10 knots) and heel angle (equal to 30 deg.), whereas a uniform probability density function between 1 and 9 deg. is assumed for the yaw angle. Box constraints are imposed on both design variables with $-0.1 \leq x_1 \leq 0.1$ and $-0.05 \leq x_2 \leq 0.05$. Functional constraints are not used.

7.2.4 MDO Algorithm and Setup

The optimization problem is solved using a monolithic approach based on an extension of the MDF architecture with partitioned solvers for hydrodynamics and structural mechanics. The proposed variable-accuracy metamodel-based optimization is compared to a benchmark MRDO solved using a standard MDF procedure to solve the fully coupled MDA, fully convergent UQ, and optimization without metamodels (Figure 7-7). Each element of the architecture presented in Figure 7-8 (optimizer/metamodel, UQ, MDA) provides a solution with a certain level of accuracy depending on the density of the training points, the UQ sample size, and the MDA tolerance. The variable-accuracy procedure aims at bringing MDA, UQ and the metamodel training to convergence in the neighbourhood of the global optimum when also optimization is close to convergence.

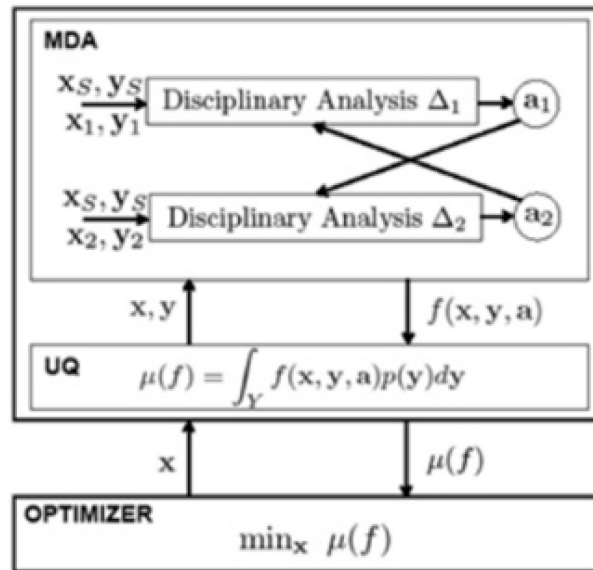


Figure 7-7: Multidisciplinary Robust Design Optimization Using MDF Architecture.

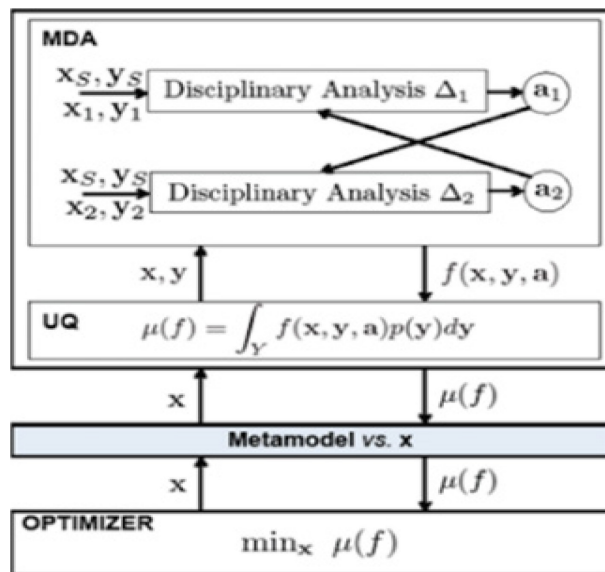


Figure 7-8: Metamodel-Based MRDO Using MDF Architecture.

The method includes subsequent optimization stages characterized by variable:

- Density (training set size and domain) of the DoE for the metamodel-training;
- Accuracy (sample size) of the UQ analysis (through a tolerance parameter, namely τ_2); and
- Coupling between disciplines in the MDA (through a tolerance parameter for the multidisciplinary consistency, namely τ_1).

Figure 7-9 shows two subsequent DoE refinements obtained varying the design variable domain and the training point density. At the first stage, the training points are distributed in the whole domain and the corresponding objective function is evaluated considering both a low level of accuracy in UQ and a weak coupling between disciplines. After the first optimization stage, a refined subdomain centered in the current optimum is defined as well as a new training set, with the corresponding objective function values obtained increasing both the UQ accuracy and the MDA coupling. The procedure is iterated for an appropriate number of stages. A deterministic version of the PSO optimization algorithm [8] is used as a minimizer.

The pseudo-code of the method is shown in Figure 7-10, where N_OS is the number of the optimization stages, N_TP is the number of the training points (metamodel) for each design domain, N_UQ is the number of items used for the UQ (based on the value of τ_2), and N_MDA is the number of iterations used to achieve the convergence of the MDA (based on the value of τ_1). Fully converged MDA and fully accurate UQ values are achieved at the final optimization stage.

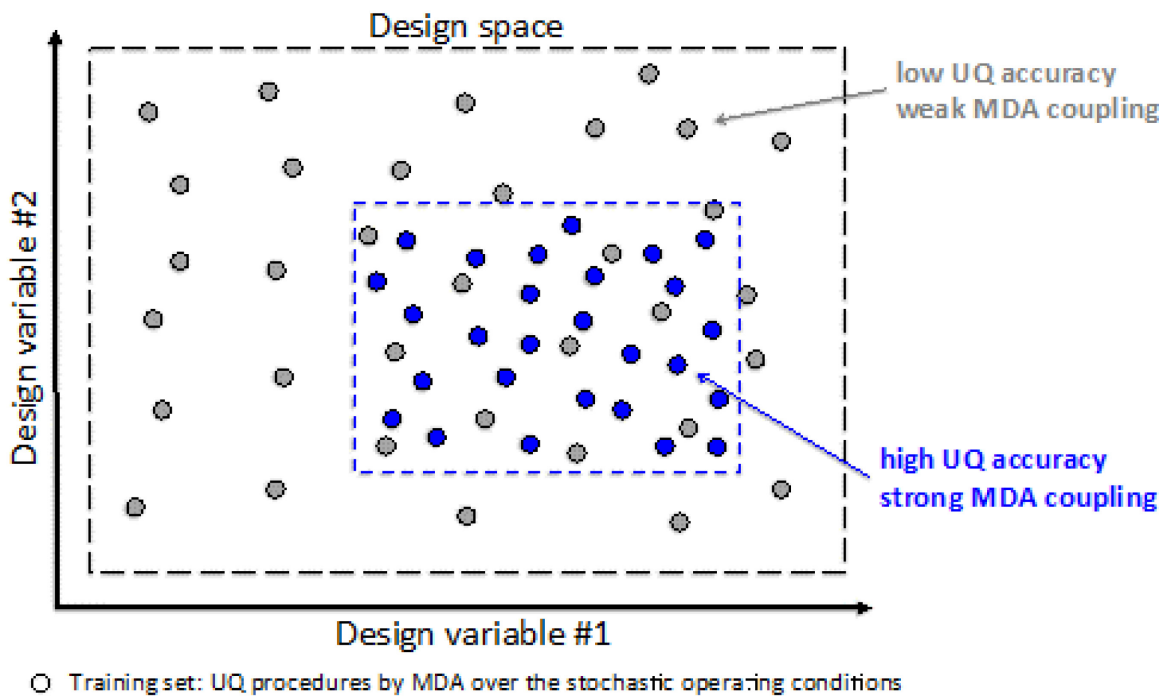


Figure 7-9: Variable-Accuracy MRDO Method Including Refinement for the Training Set DoE, Variable UQ Accuracy, and Variable MDA Coupling.

The numerical setup for the benchmark problem (MRDO with fully accurate UQ, fully coupled MDA, and optimization without metamodel) is summarized herein. A preliminary convergence analysis of MDA is performed for design variables and stochastic parameter at center domain values ($x_1 = x_2 = 0$ and $y = 5$ deg.). This reveals that for a tolerance $\tau_1 = [10]^{-5}$ the number of iterations required is $N_MDA = 10$. The convergence of UQ is investigated as solution change vs. the number of items $N_UQ = 2^{h+1}, h \in \mathbb{N}$, for $x_1 = x_2 = 0$ and $N_MDA = 10$. A number of items $N_UQ = 257$ provides a tolerance $\tau_2 = 3 \cdot [10]^{-4}$. The number of PSO function evaluation is set equal to $N_PSO = 1024 \cdot N_DV$ (where N_DV is the number of design variables). Finally, the (benchmark) number of simulation for each discipline is $N_S = N_PSO \cdot N_UQ \cdot N_MDA$.

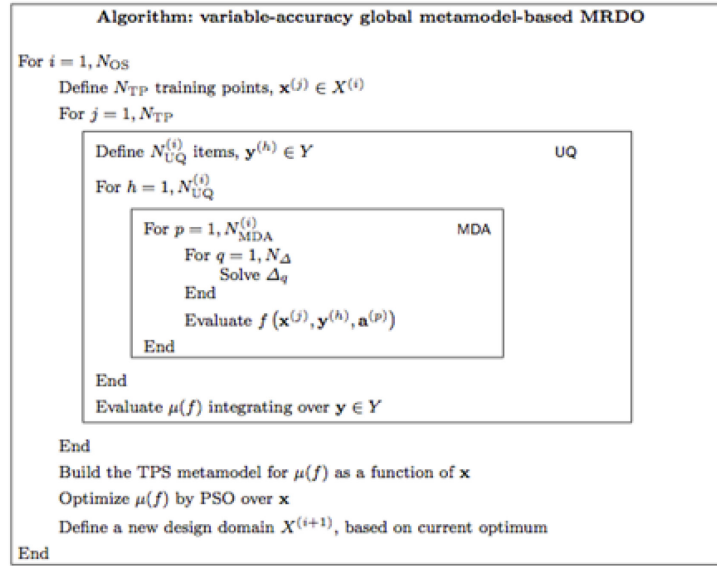


Figure 7-10: Variable-Accuracy Global Metamodel-Based MRDO Algorithm.

The numerical setup for the variable-accuracy metamodel-based optimization is summarized herein. The number of the optimization stages N_{OS} is set equal 3. At each optimization stage the sampling region is halved along each variable and centered at the current optimum. The number of the UQ items is doubled at each optimization stage, finally achieving $N_{UQ} = 257$. Similarly, the number of MDA is doubled at each stage, finally achieving the target benchmark value of $N_{MDA} = 10$.

The number of function evaluation for each discipline N_S associated to each optimization stage is:

$$\begin{aligned}
 N_S^1 &= N_{TP} \cdot \frac{N_{UQ}}{4} \cdot \frac{N_{MDA}}{4} \\
 N_S^2 &= N_{TP} \cdot \frac{N_{UQ}}{2} \cdot \frac{N_{MDA}}{2} \\
 N_S^3 &= N_{TP} \cdot N_{UQ} \cdot N_{MDA}
 \end{aligned} \tag{7-8}$$

with a total number of simulations:

$$N_S^T = N_S^1 + N_S^2 + N_S^3 = N_{TP} \cdot N_{UQ} \cdot N_{MDA} \cdot \frac{21}{16} \tag{7-9}$$

where N_{TP} is the metamodel training set size. Specifically, a TPS metamodel (special case of the radial basis function) is used for the optimization. Given the set of training points (herein provided by HSS [7]) $\{\{\mathbf{x}\}_i, i = 1, \dots, N_{TP}\}$ and the corresponding objective function values $f(\mathbf{x}_i)$, the objective function $f(\mathbf{x})$ is approximated by $\hat{f}(\mathbf{x})$ using RBF as per:

$$\hat{f}(\mathbf{x}) = \sum_{i=1}^{N_{TP}} d_i \phi[r(\mathbf{x}, \mathbf{x}_i)] \tag{7-10}$$

where $\phi(r) = r^2 \log r$ is the RBF kernel, with $r = \|\mathbf{x} - \mathbf{x}_i\|$. The coefficients d_i are the solutions of $\{\phi(\mathbf{x}_i, \mathbf{x}_j)\}\{d_j\} = \{f(\mathbf{x}_i)\}$.

When setting up benchmark tolerances, MDA is terminated if the multidisciplinary equilibrium is not achieved within a prescribed maximum number of iterations; intermediate results are stored in order to check the MDA convergence and allow for restarting, if needed. The termination criterion for the overall optimization (both for the MRDO benchmark and variable-accuracy metamodel-based MRDO) is set by the total number of discipline calls. The efficiency and effectiveness of the method is evaluated by imposing a target reduction in the number of discipline analyses from 50 to 90 %, as summarized in Table 7-2.

Table 7-2: Variable-Accuracy MRDO Simulations.

Strategy	ID	Stage 1	Stage 2	Stage 3	N_s	Budget %
Metamodel- Based MRDO	N_{TP}	78	78	78		
	N_{UQ}	64	128	257		
	N_{MDA}	3	5	10		
	$N_s^{(i)}$	14,976	49,920	200,460	265,356	10%
	N_{TP}	155	155	155		
	N_{UQ}	64	128	257		
	N_{MDA}	3	5	10		
	$N_s^{(i)}$	29,952	99,840	400,920	530,712	20%
	N_{TP}	234	234	234		
	N_{UQ}	64	128	257		
	N_{MDA}	3	5	10		
	$N_s^{(i)}$	44,928	149,760	610,380	769,068	30%
	N_{TP}	312	312	312		
	N_{UQ}	64	128	257		
	N_{MDA}	3	5	10		
	$N_s^{(i)}$	59,904	199,680	801,840	1,061,424	40%
	N_{TP}	390	390	390		
	N_{UQ}	64	128	257		
N_{MDA}	3	5	10			
$N_s^{(i)}$	74,880	249,600	1,002,300	1,326,780	50%	

Finally, the parameter settings of the optimization algorithm (in the strict sense) are chosen following [8]. Specifically, the swarm size is set to $4 \cdot N_{DV}$ (N_{DV} indicates the number of design variables), the swarm is initialized using HSS [7] over the design variables domain and its boundaries with non-null velocity and the PSO coefficients are defined as $\chi = 0.721$, $c_1 = c_2 = 1.625$. Finally, the number of function evaluations is set to $N_{PSO} = 1024 \cdot N_{DV}$.

7.2.5 MDO Results

The results of the optimization procedures are summarized in Table 7-3, whereas the optimization algorithm convergence history is shown in Figure 7-11.

Table 7-3: MRDO Benchmark vs. Variable-Accuracy Results.

Strategy	Design Var. 1	Design Var. 2	Obj. Function	abs(ϵ) %	Budget %	N _s /N _{DV}
MRDO Benchmark	-5.78E-02	3.02E-02	27.32	–	100%	2,631,680
Metamodel-Based MRDO	-5.51E-02	2.57E-02	25.91	5.16	10%	265,356
	-5.53E-02	2.61E-02	26.12	4.39	20%	530,712
	-5.48E-02	2.73E-02	26.43	3.25	30%	769,068
	-5.61E-02	2.81E-02	26.57	2.74	40%	1,061,424
	-5.65E-02	2.88E-02	26.68	2.34	50%	1,326,780

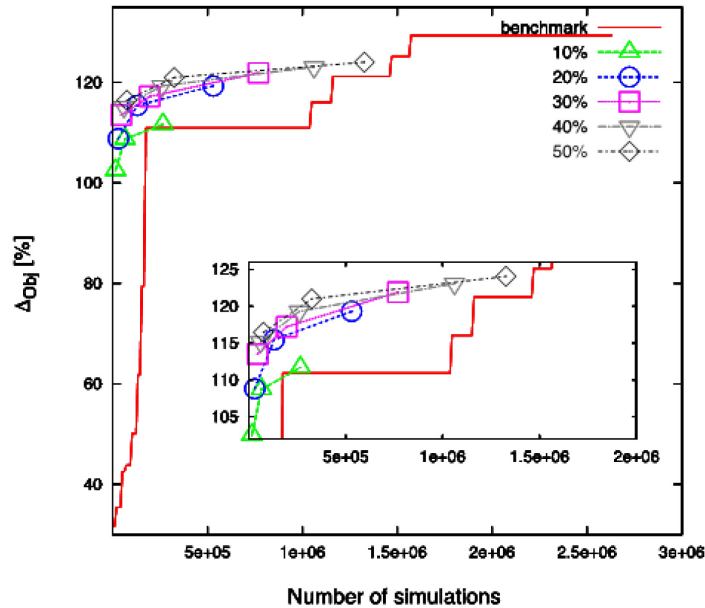


Figure 7-11: Deterministic Particle Swarm Optimization Algorithm Convergence.

The optimized fin is thinner at root and thicker at tip and shows a quite remarkable improvement of the hydrodynamic efficiency, $\mu(f) = 27.32$, compared to the original, $\mu(f) = 11.91$ (see Figure 7-12). The metamodel-based optimization method converged to the benchmark (or at least to the proximity of the benchmark) achieving satisfactory results in terms of the identification of the optimum.

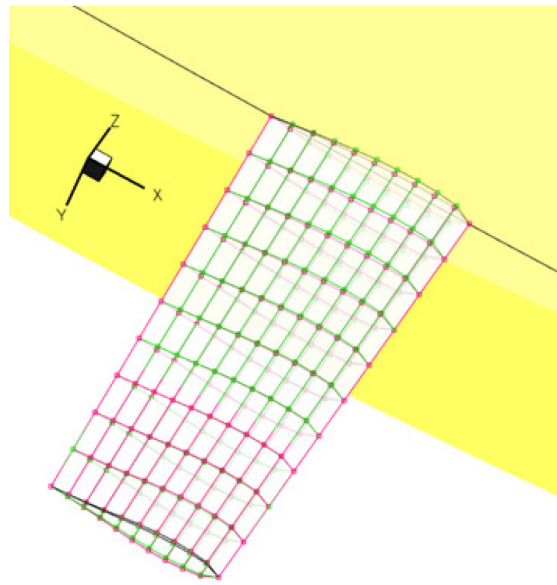


Figure 7-12: Original vs. MRDO Benchmark Solution.

The hydrodynamic efficiency vs. the yaw angle of the original and optimized designs is compared in Figure 7-13. The latter presents the best overall behaviour, showing a remarkable improvement over the whole yaw angle range. The designs obtained using the metamodel-based approach give an overall performance very close to the benchmark solution at one tenth to half of the computational cost.

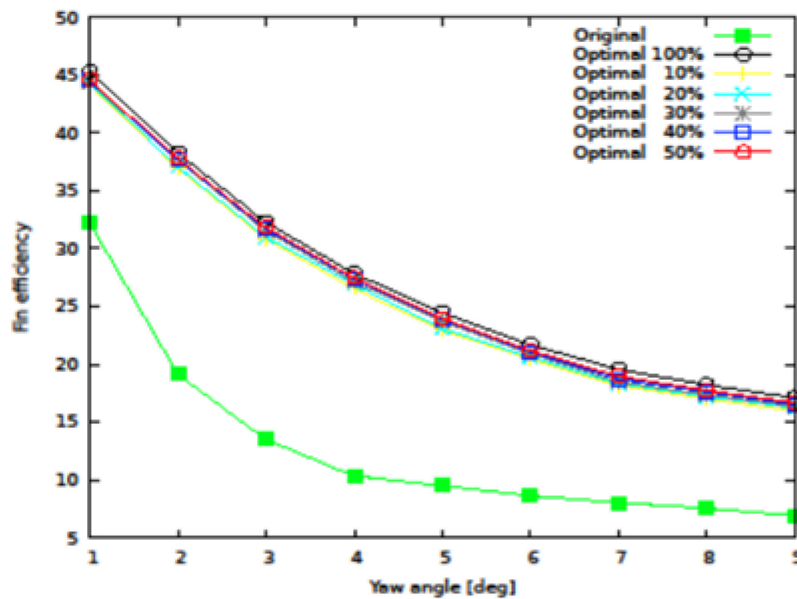


Figure 7-13: Parametric Analysis of the Hydrodynamic Efficiency vs. the Yaw Angle: Comparison of Original and Optimized Designs.

Both benchmark and variable-accuracy metamodel-based problems are solved on a 16 GB RAM Intel Xeon E5-1620 v2@370GHz eight-core workstation. The total CPU-time associated to the benchmark solution is about 1.58×10^6 s (0.6 s per single evaluation), whereas the metamodel-based total CPU times, corresponding to 10 to 50 % of the benchmark budget are respectively 1.59×10^5 s, 3.2×10^5 s, 4.61×10^5 s, 6.36×10^5 s, and 7.96×10^5 s.

The human effort due to non-automatic processes has not been evaluated.

No experimental data are publicly available for the current problem.

In conclusion, the solution of the MRDO problem is still a theoretical, algorithmic, and computational challenge, since MDA, UQ and optimization processes are high-cost tasks. When MDF architectures are used to solve the MDA, the computational cost of the process is extremely high, since the multidisciplinary equilibrium is achieved for each design variable and stochastic parameter values. The proposed variable-accuracy metamodel-based MRDO architecture combines concurrent elements aiming at reducing the computational cost of the MRDO process, including subsequent optimization using metamodels built on refined domains/training sets using increasing accuracy in the UQ evaluation and MDA coupling. The method provides for an extension of the classic MDF procedure. Similarly to MDF, the multidisciplinary consistency is achieved to some extent at each optimization iteration, requiring the solution of the MDA at each design point. The variable tolerance for the multidisciplinary consistency provides for some of the advantages of the All-At-Once (AAO), Individual Discipline Feasible (IDF) and Simultaneous Analysis and Design (SAND) procedures, in which the optimizer handles the multidisciplinary consistency during the optimization process. Similarly to AAO, IDF and SAND, full multidisciplinary consistency (strong coupling) is achieved only at the end of the optimization process.

In summary, the optimized fin shows a quite remarkable improvement of the hydrodynamic efficiency, $\mu(f) = 27.32$, compared to the original, $\mu(f) = 11.91$. For current application the metamodel-based optimization converged to the benchmark (or at least to the proximity of the benchmark), achieving satisfactory results in terms of the identification of the optimum. The penalty associated to the identification of the optimum (compared to the benchmark solution) ranges from 5.16 to 2.34 %, whereas the computational cost ranges from 10 to 50 % of the original computational cost spent to achieve the benchmark solution.

7.2.6 Technical and Financial Improvements/Benefits of Using MDO vs. Traditional Design Methods

Information not available.

7.2.7 References; Web Resources; Science Connect Link; and Validation Data Location

Details on the benchmark problem may be found in Ref. [4]. Additional background information may be found in Refs. [1] and [3].

Related papers and computational (surface) grids are available at: <https://scienceconnect.sto.nato.int/apps/23964>.

- [1] Campana, E.F., Fasano, G., and Peri, D. (2006). Issues on nonlinear programming for Multidisciplinary Design Optimization (MDO), in ship design frameworks. In: Mota Soares C.A. et al. (Eds.) III European Conference on Computational Mechanics for Solids, Structures and Coupled Problems in Engineering, Lisbon, Portugal. Available at: <http://citeseerx.ist.psu.edu/viewdoc/download?doi=10.1.1.583.6046&rep=rep1&type=pdf>.

- [2] Diez, M., Peri, D., Fasano, G., and Campana, E.F. (2010). Multidisciplinary Robust Optimization for Ship Design, In: Proceedings of 28th Symposium on Naval Hydrodynamics, Pasadena, California, 12 – 17 September 2010.
- [3] Diez, M., Peri, D., Fasano, G., and Campana, E.F. (2012). Hydroelastic optimization of a keel fin of a sailing boat: a multidisciplinary robust formulation for ship design. *Structural and Multidisciplinary Optimization* 46(4), pp. 613-625. DOI 10.1007/s00158-012-0783-7. Available at: <https://link.springer.com/article/10.1007/s00158-012-0783-7>.
- [4] Leotardi, C., Serani, A., Iemma, U., Campana, E.F., and Diez, M. (2016). A variable-accuracy metamodel-based architecture for global MDO under uncertainty. *Structural Multidisciplinary Optimization* 54(3), pp. 573-593. DOI 10.1007/s00158-016-1423-4. Available at: <https://link.springer.com/article/10.1007/s00158-016-1423-4>.
- [5] Landrini, M. and Campana, E.F. (1996). Steady weaves and forces about a yawing flat plate. *Journal of Ship Research* 40(3), pp.179-192.
- [6] CALCULIX (1998). Free Software Three-Dimensional Structural Finite Element Program. Available from <http://www.calculix.de/>.
- [7] Wong T.T., Luk, W.S, and Heng P.A. (1997). Sampling with Hammersley and Halton points. *J Graph Tools* 2(2), pp.9-24.
- [8] Serani, A., Leotardi, C., Iemma, U., Campana, E.F., Fasano G., and Diez, M. (2016). Parameter selection in synchronous and asynchronous deterministic particle swarm for ship hydrodynamic problems. *Applied Soft Computing*, 49, pp. 313-334.



Chapter 8 – BENCHMARK: APPLICATION OF MDO FOR AN AIRCRAFT WING DESIGN

Anant Grewal and Guillaume Renaud
National Research Council
CANADA

An application of Multidisciplinary Design Optimization (MDO) on a wing model including the disciplines of structures, aerodynamics and aeroelasticity is presented. The problem, using the Multidisciplinary Feasible (MDF) formulation, was defined as a single-level optimization where all design variables and constraints were treated simultaneously at the system level. The objective was to maximize the range of an aircraft by optimizing the structural and aerodynamic design of the wings, given constraints on the allowable stress and displacement, wing shape and flutter speed. Several tests were performed to evaluate the effects of the complexity of the disciplinary optimization models. In all cases, MDF performed well and demonstrated the need of a multidisciplinary formulation to solve the presented problem.

8.1 BENCHMARK EXECUTIVE SUMMARY

8.1.1 Qualitative Optimization Problem Statement

The objective of this multidisciplinary problem was to maximize the range of an aircraft by optimizing the structural and aerodynamic design (i.e., wing cross-section shape) of the wings, given constraints on the allowable stress and displacement, wing shape and flutter speed. The ONERA M6 wing, scaled up 10 times to obtain dimensions comparable to that for a regional aircraft, was selected as the initial aerodynamic design. The wing geometry and flight parameters are presented in Figure 8-1.

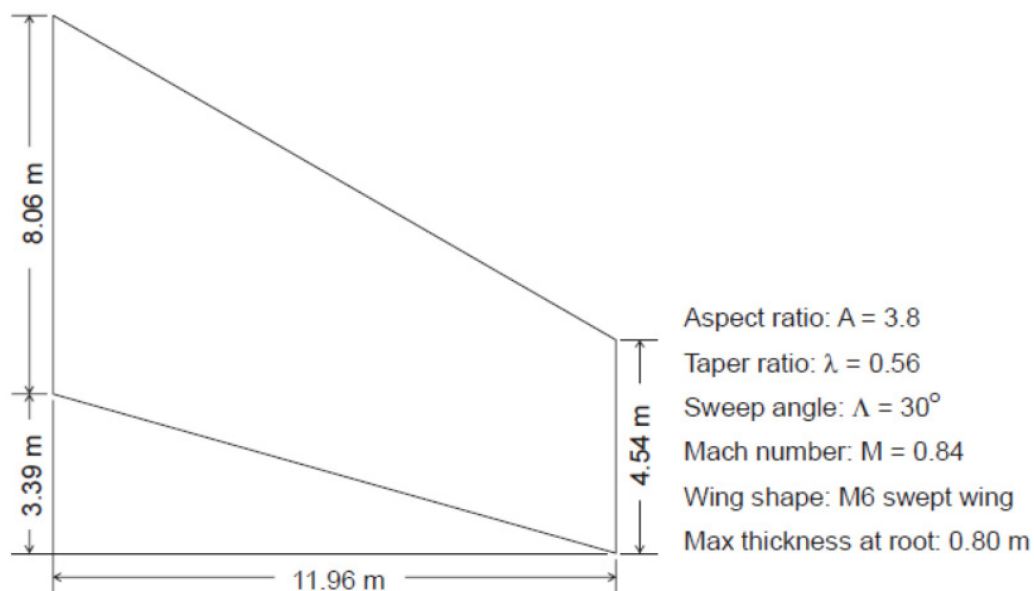


Figure 8-1: Characteristics of Wing Geometry.

8.1.1.1 Design Variables

The design variables are the B-spline control points that define the shape of the wing cross-section, the angle of attack, and the sizes of various structural elements of the wing (i.e., the thickness of the wing skin, spar webs, rib webs, post areas, and the stringer and spar beam dimensions).

Aerodynamics:

- Airfoil Shape via B-spline control points (cross-sectional shape). Upper/lower bounds of +/- 3% of control point coordinates.
- Angle of attack.
- 3 cases with varying order of B-splines, and control points per curve resulting in 19, 23 and 27 aerodynamic design variables.
- Wing planform is fixed (Scaled ONERA M6 with 11.96 m. half-span).
- Mach Number is fixed at 0.84.

Structures:

- Thickness of skins, spars webs and rib webs (min. = 0.635 cm, max. = 2.54 cm).
- Area of posts (min. = 0.645 cm², max. = 1.29 cm²).
- Dimensions of stringers and spar beams (min. width and height = 0.254 cm, max. width and height = 2.54 cm).
- 5 cases with varying number of design variables (7, 14, 17, 24, 35). i.e.:
 - i) Uniform thickness for each class of component, resulting in 7 structural design variables;
 - ii) Linear distribution for skins and spars, unique for all ribs, resulting in 14 structural design variables;
 - iii) Uniform for each individual component, resulting in 17 structural design variables;
 - iv) Linear distribution for skins and spars, uniform for each individual rib, resulting in 24 structural design variables; and
 - v) Linear distribution for skins, spars and ribs, resulting in 35 structural variables.

8.1.1.2 Objective Function(s)

The single objective function is the range of aircraft estimated using the simplified Breguet formula.

8.1.1.3 Constraint Function(s)

The constraints for the problem are a defined range for the Trailing Edge Angle (TEA), maximum wing thickness maximum wing deflection maximum allowable stress, and a flutter speed greater than the design speed ($M = 0.84$).

Aircraft:

- Lift > Aircraft Weight.
- Total Aircraft weight = 63,503 kg (note: the mass of the fuel is automatically determined by the difference between the fixed total aircraft weight and the sum of the fixed fuselage mass and wing mass).

Aerodynamics:

- Trailing edge angle ($5^\circ < \text{TEA} < 20^\circ$).
- Maximum wing thickness ($t < 0.08c$, where c is the chord length).

Structures:

- Maximum wing deflection ($\delta < 0.05b$, where b is the wingspan).
- Allowable stresses (below yield strength).

Aeroelasticity:

- Flutter speed $>$ flight speed.

8.1.2 Description of Analyses/Disciplines/Theory/Fidelities Involved

The geometry of the wing, including all structural elements was generated using MSC.PATRAN. The structural and aeroelastic analyses were performed using MSC.NASTRAN. The aerodynamic analysis was performed using KTRAN, which uses a modified Transonic Small Disturbance (TSD) code for pressure distribution along with a mixture of semi-empirical and CFD-based routines for drag prediction to within engineering accuracy. KTRAN also employs automatic Cartesian grid embedding, which makes it suitable for shape optimization problems. KTRAN is capable of analyzing full aircraft configuration (i.e., including engines, winglets, H-tail and nacelles).

The structural analysis was conducted using MSC.PATRAN and MSC.NASTRAN. The following element types were used in the structural analysis:

- Skin of the wing was modelled using Shell elements;
- Rib and Spar webs modelled as Shear Panel (CSHEAR) elements;
- Rib posts modelled as CROD elements; and
- Spar beams and Stringers modelled as CBAR elements.

For the flutter analysis, the Aeroelasticity I module in MSC.NASTRAN was employed. This analysis uses the Doublet Lattice Method (DLM) for representing the Unsteady Aerodynamics of the wing. Ten structural modes were used in the analysis and the P-K Method was employed.

The MDA process begins by an initial definition of the airfoil shape and wing structural parameters. The KTRAN CFD code computes the aerodynamic loads which are then applied to the structure. The resulting stresses, displacements and weight are computed using MSC.PATRAN and MSC.NASTRAN. The MSC.NASTRAN Aeroelasticity module (using DLM and structural modes computed using MSC.NASTRAN) is also used to determine the flutter speed of the wing for the given structural design and flight conditions.

The calculated lift, drag and wing weight were used to evaluate the range of the aircraft, which is the objective function to be maximized. Similarly, the stresses, displacements, wing shape and flutter speed are used to formulate a set of optimization constraints. The objective and constraint values were transferred to the top level multidisciplinary optimization algorithm to generate the next design.

The constraints on stresses, deflections, wing shape and flutter speed are verified. The objective function is then calculated from the simplified Breguet Range equation.

8.1.3 MDO Approach (Algorithm/Architecture)

For this problem, the Multidisciplinary Feasible Formulation (MDF) was employed, wherein the disciplines are directly coupled, and all design variables are optimized at the top level. The Sequentially Quadratic Programming (SQP) gradient-based algorithm of the MATLAB Optimization Toolbox was used.

8.1.4 Implementation Details

8.1.4.1 Analysis Software

KTRAN, a CFD code developed by Bombardier Aerospace was used in this analysis. KTRAN uses the modified Transonic Small Disturbance equation (TSD) to compute the pressure distribution over full aircraft configurations. It also employs a mixture of semi-empirical and CFD for drag prediction to within engineering accuracy. Another feature of KTRAN is the embedded Cartesian grid generation which makes it suitable for shape optimization problems. Structural and flutter analysis is conducted with MSC.NATRAN. MATLAB was used as the platform for controlling the overall process and calling the various disciplinary programs. The coupling among the disciplines was done with automated in-house MATLAB and MSC.PATRAN Command Language (PLC) programs. This automatic coupling included the transformation of the aerodynamic pressure distribution to structural nodal forces, and wing shape to nodal coordinates.

MATLAB was used as the platform controlling the overall process and calling the various disciplinary programs. The coupling among the disciplines was done with automated in-house MATLAB and PATRAN Command Language (PLC) programs. This automatic coupling included the transformation of the aerodynamic pressure distribution to structural nodal forces, and wing shape to nodal coordinates.

8.1.4.2 Optimization Software

The MATLAB Optimization Toolbox implementation of the Sequential Quadratic Programming (SQP) optimization algorithm (*fmincon*) was employed in this analysis.

8.1.4.3 Hardware

An SGI Origin 2000 Computer with 32 CPUs and 32 GB RAM running the IRIX operating system was the hardware platform used.

8.1.4.4 Human Effort

The human effort was not quantified or reported.

8.1.5 Results

8.1.5.1 Initial Design (Design Variables, Objectives, Constraint Values)

Initial design variable values:

- i) Wing section shape – ONERA M6.
- ii) Angle-of-attack = 3°.
- iii) Upper and lower skin, rib web, spar web thickness = 1.905 cm.

- iv) Post area = 0.968 cm².
- v) Spar web and stringer width = 1.27 cm.
- vi) Spar web and stringer height = 1.27 cm.

Initial objective and constraint function values:

- i) Initial range = 3,689 km.
- ii) Initial wing mass = 8,228 kg.
- iii) Initial C_L/C_d = 14.38.

8.1.5.2 Optimized Design (Design Variables, Objectives, Constraint Values)

Final design variable values:

- i) Wing section shape (See Figure 8-2).
- ii) Upper skin thickness = 0.965 cm.
- iii) Lower skin thickness = 0.991 cm.
- iv) Rib web thickness = 0.635 cm.
- v) Spar web thickness = 1.118 cm.
- vi) Post area = 0.775 cm².
- vii) Spar web and stringer width = 2.54 cm.
- viii) Spar web and stringer height = 2.54 cm.

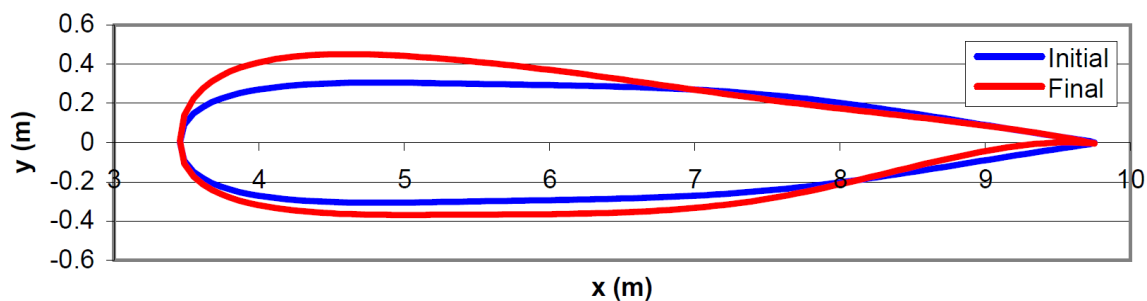


Figure 8-2: Initial and Final Wing Section Shape.

Final objective and constraint function values:

- i) Final range = 11,681 km.
- ii) Final wing mass = 4,093 kg.
- iii) Final C_L/C_d = 24.84.

8.1.5.3 Observations

The final wing sectional shape was thicker over most of the chord length. This strategy allowed for the reduction of the thickness of the wing box structural components while maintaining an appropriate overall wing bending stiffness. In addition, the lower surface of the trailing edge became more tapered, thus improving the aerodynamics properties of the wing. Spar beam and stringers dimensions converged to their upper bounds, whereas rib web thickness converged to their lower bound values.

Parametric studies showed that increasing the number of wing shape (aerodynamic) design variables (i.e., more B-spline control points leading to increased more control over airfoil shape) resulted in a significant improvement of the objective function, whereas increasing the number of structural design variables (i.e., more control over structural member geometry) produced a relatively minor improvement of the objective function.

The analysis required approximately 15 minutes per iteration on the SGI Origin 2000 system (single processor), and approximately 20 iterations were required for convergence. The optimization scheme was found to be stable and robust.

8.1.6 Technical and Financial Improvements/Benefits of Using MDO vs. Traditional Design Methods

The study demonstrated the advantage of MDO over traditional design approaches using sequential single-disciplinary design approaches. With the MDF approach, the range converged to 11,681 km. With a scheme where structural optimization was performed, followed by aerodynamic optimization, the range converged to just over 9,000 km. When aerodynamic optimization was performed first, followed by structural optimization, the converged range was slightly below 9,000 km.

No experimental validation data was available.

8.1.7 References; Web Resources; Science Connect Link; and Validation Data Location

None.

8.2 BENCHMARK DETAILS

8.2.1 High-Level

This benchmark problem involves a preliminary design of the wing for a regional aircraft. The planform of the wing is fixed. The shape of the wing section and the structural design of the wing, including skin thickness and wingbox sizing parameters are the primary design variables. The N^2 for the current optimization problem is shown in Figure 8-3.

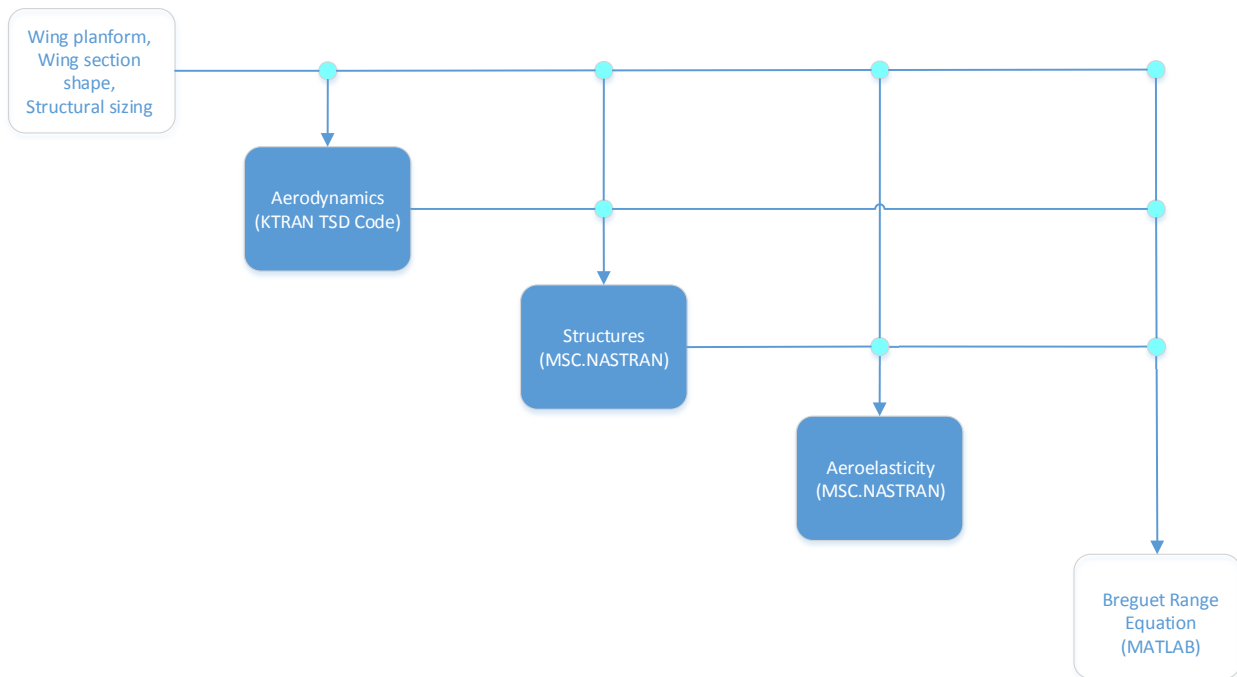


Figure 8-3: The N² Diagram for the Wing Optimization Problem.

8.2.2 Multidisciplinary Analysis (MDA)

8.2.2.1 Implementation Details of Analyses and Corresponding Responses Used to Formulate MDO Objective and Constraint Functions

The multidisciplinary analysis that was applied for this problem can be described as a preliminary aerostructural analysis of a wing for a regional aircraft. The planform of the wing was fixed and was taken to be a scaled (10 times) of the ONERA M6. The design variables were the sectional shape of the wing as well as the structural design of the wing. The aerodynamic analysis was performed using KTRAN, a Transonic Small Disturbance (TSD) CFD code that also includes drag prediction using a combination of computational and empirical methods. The structural analysis was performed using the MSC.NASTRAN FEA code. Aeroelastic analysis using the Doublet-Lattice Method was performed using MSC.NASTRAN.

The inputs to the aerodynamic analysis were the geometry and cross-sectional shape of the wing, the angle of attack of the wing, the number of surface mesh nodes, and the flow conditions. The output of the aerodynamic analysis was the pressure distribution, which was subsequently applied as a distributed load for the structural analysis.

For simplicity, it was assumed that the wing cross-sectional shape is uniform in the span-wise direction and that the wing planform was fixed. The wing cross-section was parameterized using two B-spline curves corresponding to the upper and lower wing surfaces. A FORTRAN code was used to transform the B-spline control points to CFD mesh nodes on a smooth surface. Several B-spline formulations were used to represent the wing cross-section. Table 8-1 lists the aerodynamic models that were used for the results presented in this chapter. The number of design variables includes the angle of attack and the x- and y-coordinates of the moveable control points, taking into account the fixed wing planform and the continuity of slope at the leading edge.

Table 8-1: Aerodynamic Design Variable Details.

Model	Order of B-Spline Curves	Number of Control Points per Curve	Number of Design Variables
Aero-1	4	6	19
Aero-2	6	7	23
Aero-3	6	8	27

The initial aerodynamic design corresponded to the shape that is the closest to the ONERA M6 wing in a least-square sense, with an angle of attack of 3 degrees. Further, the maximum allowed changes in the shape design variables corresponded to an x-and y-direction movement of the control points of 3% of the local chord length. The initial root cross-sectional wing shape and corresponding B-spline control points for model Aero-1 are shown in Figure 8-4.

The lift and drag coefficients resulting from the CFD analysis were used in the range calculation. The aerodynamic constraints specified that the trailing edge angle should remain between 5 and 20 degrees and that the maximum wing thickness should be lower than or equal to 8% of the local chord length.

The inputs to the structural analysis were the aerodynamic loading of the wing, after appropriate interpolation and transformation from the aerodynamic to structural mesh and coordinate system. The outputs of the structural analysis were the wing weight, wing deflection and stresses. The structural design variables consisted of the sizing of the wing box components. The wing box finite element model was automatically generated, using the PATRAN Command Language (PCL) programming interface, and taking into consideration changes in the aerodynamic shape and pressure distribution [1]. The structural model is shown in Figure 8-5.

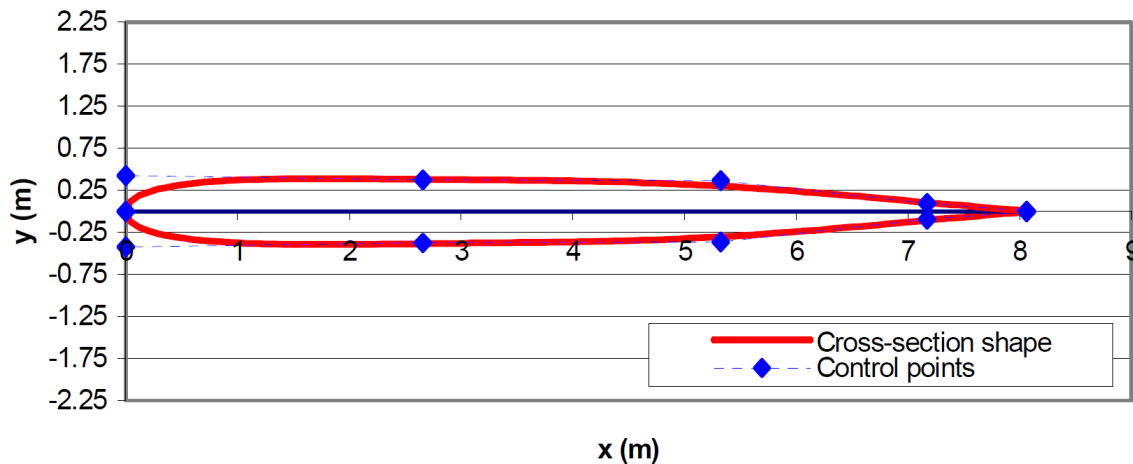


Figure 8-4: Initial Root Wing Cross-Section Shape and Associated B-Spline Control Points.

In addition to the wing box, weightless components were used to simulate the effects of the leading and trailing edges on the structural elements. These components acted as rigid links that transfer the edge pressure loading to the wing box.

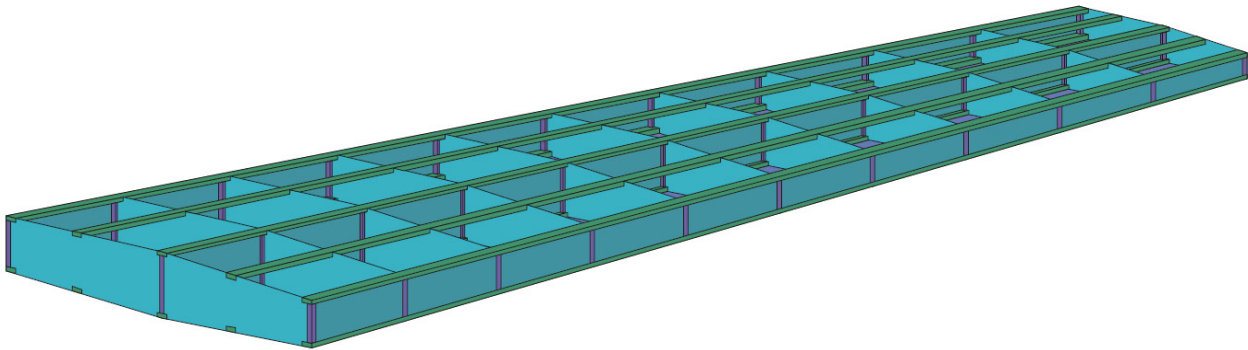


Figure 8-5: Wing Box Model (Note that the upper skin is not shown).

Supplementing a set of fixed parameters, including the material properties, planform, et cetera, the wing box design was represented by a vector of variables bounded by the maximum and minimum allowable values. Table 8-2 lists the wing box components and their associated materials, design variables, initial values and bounds. The material properties are described in Table 8-3. These properties are, in order, the Young’s modulus, the Poisson’s ratio, and the tensile, compressive, and shear yield stresses.

Table 8-2: Wing Box Design Variables.

Component	Material	Variable	Min	Initial	Max
Upper skin	Aluminum	Thickness	0.635 cm	1.905 cm	2.54 cm
Lower skin	Aluminum	Thickness	0.635 cm	1.905 cm	2.54 cm
Rib webs	Aluminum	Thickness	0.635 cm	1.905 cm	2.54 cm
Spar webs	Aluminum	Thickness	0.635 cm	1.905 cm	2.54 cm
Posts	Steel	Area	0.645 cm ²	0.968 cm ²	1.290 cm ²
Spar beams and stringers	Steel	Width	0.254 cm	1.270 cm	2.54 cm
Spar beams and stringers	Steel	Height	0.254 cm	1.270 cm	2.54 cm

Table 8-3: Wing Box Material Properties.

Material	E (MPa)	ν	$\sigma_{y,t}$ (MPa)	$\sigma_{y,c}$ (MPa)	$\sigma_{y,s}$ (MPa)
Aluminum	72395	0.3	296	269	159
Steel	206843	0.3	517	414	310

Several optimization models can be built from the defined set of variables by assuming the form of the thickness distributions of the wing box components. Table 8-4 lists the various structural models that were used for the results presented in this chapter. It can be seen that the number of design variables is different for each model. In all cases, the dimensions of the posts and beams are assumed identical for all individual components.

Table 8-4: Structural Design Model Details.

Model	Thickness Characteristics	Number of Design Variables
Struct-1	Uniform for each class of component	7
Struct-2	Linear distribution for skins and spars, unique for all ribs	14
Struct-3	Uniform for each individual component	17
Struct-4	Linear distribution for skins and spars, uniform for each individual rib	24
Struct-5	Linear distribution for skins, spars and ribs	35

The global optimization process formulated constraints by comparing the stresses obtained from the finite element analysis to the allowable values. An additional constraint specified that the maximum deflection of the wing must be less than 5% of the wingspan. Furthermore, the wing weight, evaluated from the model's geometry and thickness distribution, is used for the range calculation.

The aeroelasticity model combined the structural model and some aerodynamic parameters such as the angle of attack and the free stream Mach number. Aeroelastic calculations resulted in evaluating the system constraint specifying that the flutter speed must be higher than the flight speed. More details concerning the aeroelastic model are given in Ref. [2].

8.2.2.2 Practical Concerns

The aerodynamic analysis code, KTRAN, is an in-house TSD CFD code was employed in this study developed by Bombardier Aerospace (BA). BA permitted NRC to use the code for this non-commercial project. The embedded Cartesian grid meshing capability of KTRAN facilitates the re-meshing of the computational domain when the wing shape is altered. Boundary layer calculations on the lifting surfaces are used to estimate the drag, typically to within 2 – 3 % of measured data [3]. The CFD analysis was performed on a single processor of an SGI Origin 2000 workstation running the IRIX operating system. The MSC.NASTRAN code was also executed on the same computational environment.

The MDA was automated using MATLAB scripting which performed the executive functions, including the execution of PATRAN Command Language (PCL) to read the current value of the structural design variables, and the material properties to generate the MSC.NASTRAN *.bdf deck to perform the FEA and Aeroelastic analysis. Similarly, the MATLAB script also prepared the KTRAN input files from the aerodynamic design variables and the flow parameters, executed KTRAN and post-processed and interpolated the aerodynamic loads to the structural mesh.

Each iteration of the required MDA was executed in approximately 15 minutes on a single processor of the SGI Origin 2000 system. Approximately 20 iterations were required for convergence of the MDO problem, and the optimization scheme was found to be stable and robust.

8.2.3 MDO Problem Definition Details

The Multidisciplinary Feasible (MDF) formulation was applied for the current optimization problem. The MDF formulation implies that the coupled problem was fully solved at each optimization step and that all variables

and constraints were treated at the global level. A flowchart for the MDF-formulated wing design problem is shown in Figure 8-6.

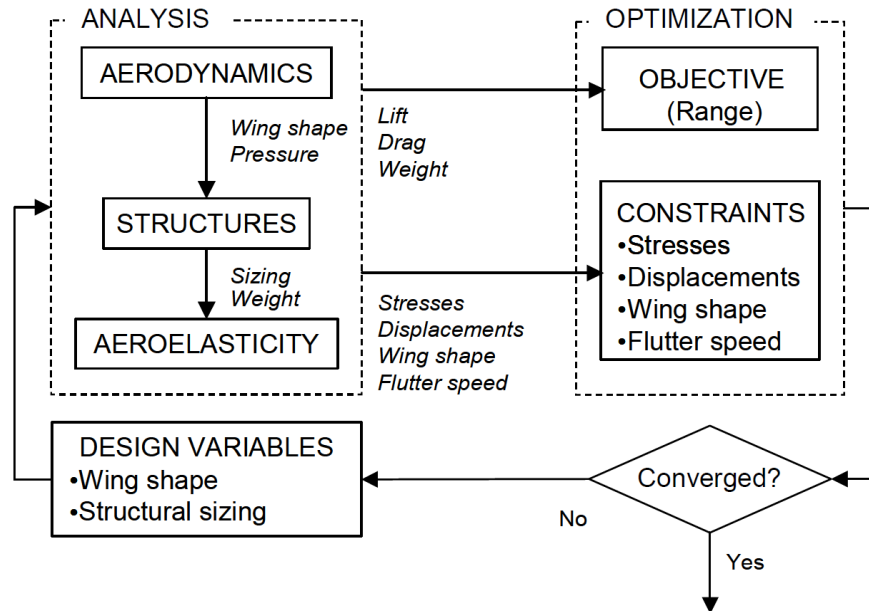


Figure 8-6: Optimization Problem Flowchart.

The MDF formulation can be seen as a cycle of full multidisciplinary analyses followed by design updates. In the present problem, the multidisciplinary analysis process consisted of a sequence of three steps. First, the aerodynamic properties of the wing, such as the pressure distribution, lift and drag were calculated for the given wing shape and flight conditions. Second, the wing box structural stresses, deformations and weight, corresponding to the given wing shape, structural sizing and calculated pressure distributions were found. Third, the flutter speed was evaluated for the given structural design and flight conditions. Since there was no feedback to aerodynamics, the analysis process was not iterative. A more accurate analysis would have applied the structural deformation computed by the FEA step to the CFD mesh and recomputed the aerodynamic loading. This step would be repeated until convergence of the aerodynamic loads, wing stresses and wing deflections.

The calculated lift, drag and wing weight were used to evaluate the range R of the aircraft, which is the single objective function to be maximized. Similarly, the stresses, displacements, wing shape and flutter speed were used to formulate a set of optimization constraints. These constraints will be defined in the next sections. The objective and constraint values were transferred to an optimization algorithm to generate the next design.

The simplified Breguet formula [4] was used to relate the lift-to-drag ratio and wing weight to an estimation of the range as:

$$R = k \frac{C_L}{C_D} \ln \left(\frac{W_T}{W_0 + W_W} \right) \quad (8-1)$$

where C_L and C_D are the coefficients of lift and drag and W_T , W_0 and W_W are the total, base and wing weights, respectively. The coefficient k , related to the engine efficiency, was arbitrarily chosen to be equal to 2897 km in

order to have an initial range of about 3500 km. This parameter was assumed fixed because the engine was not considered in the present system analysis.

The parameters W_T and W_0 were fixed to be 63,503 kg and 49,895 kg, respectively. The total weight can be decomposed as:

$$W_T = W_0 + W_W + W_F \quad (8-2)$$

where W_F is the fuel weight. Because the total and base weights were assumed constant, the fuel weight varied automatically when the wing weight was changed.

Equation (8-1) and Equation (8-2) demonstrate that the best way to increase the aircraft range is to increase the lift-to-drag ratio and decrease the wing weight. Thus, both the aerodynamic and structural designs can therefore be modified to form a joint design that is multidisciplinary optimal.

8.2.4 MDO Algorithm

The MultiDisciplinary Feasible (MDF), which is a monolithic MDO architecture, is employed, whereby the multidisciplinary problem is fully solved as a single optimization problem by conventional iterative methods at each optimization step resulting in a system that is always multidisciplinary feasible. It is not a decomposition method and does not exploit the modularity of the problem. Therefore, all variables and constraints are treated at the global level.

In this problem, surrogate modelling was not employed, and the overall problem is treated as a deterministic one. The Sequential Quadratic Programming (SQP) method as implemented within the *fmincon* routine in the MATLAB Optimization Toolbox is employed. Details of SQP can be found in many references in the literature [5]. A salient feature of the method is the nonlinear optimization problem is modeled by a subproblem which approximates the objective function by a quadratic function.

8.2.5 MDO Results

Several optimization runs were carried out to evaluate the use of the MDF approach on the wing system design. The test case described next was selected as the basis for a comparison from which other runs were developed to perform the parametric studies.

8.2.5.1 Basic Test Case

The basic test case corresponded to the use of the Aero-1 and Struct-1 models with all the default values mentioned in the previous sections. The optimization histories of the range, weight, and lift-to-drag ratio, normalized with respect to their initial values are illustrated in Figure 8-7. The actual initial and final values are listed in Table 8-5.

Table 8-5: Basic Test Case Initial and Final Design Performance Values.

	R	C_L/C_D	W_W
Initial	3689 km	14.38	8228 kg
Final	11681 km	24.84	4093 kg

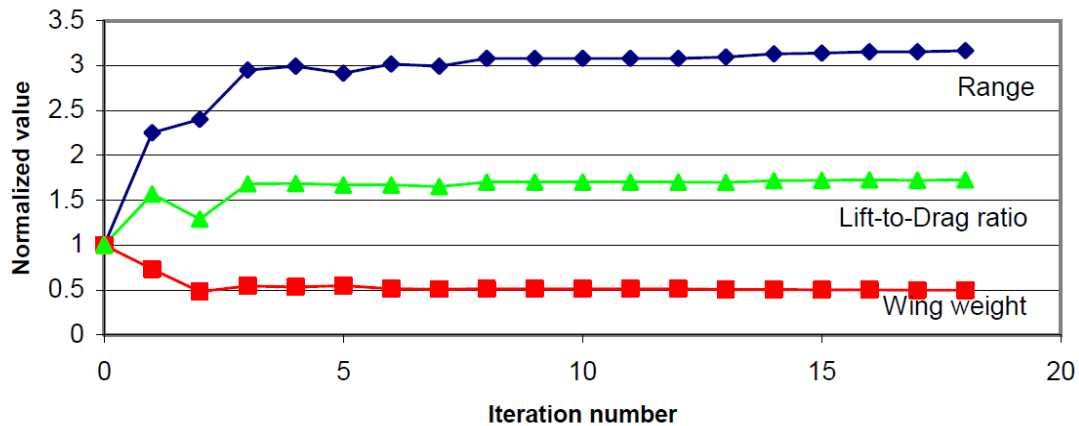


Figure 8-7: Normalized Optimization Histories for the Basic Test Case.

The aircraft range was increased by 217% after the design optimization. This performance improvement came from the combined effect of a 50% weight reduction and a 73% lift-to-drag ratio increase.

The initial and final cross-sectional shapes are shown in Figure 8-8. The final wing was thicker over most of the chord length. This strategy allowed for the reduction of the thickness of the wing box components while keeping an appropriate overall wing bending stiffness. In addition, the lower surface of the trailing edge became more tapered, thus improving the aerodynamics properties of the wing.

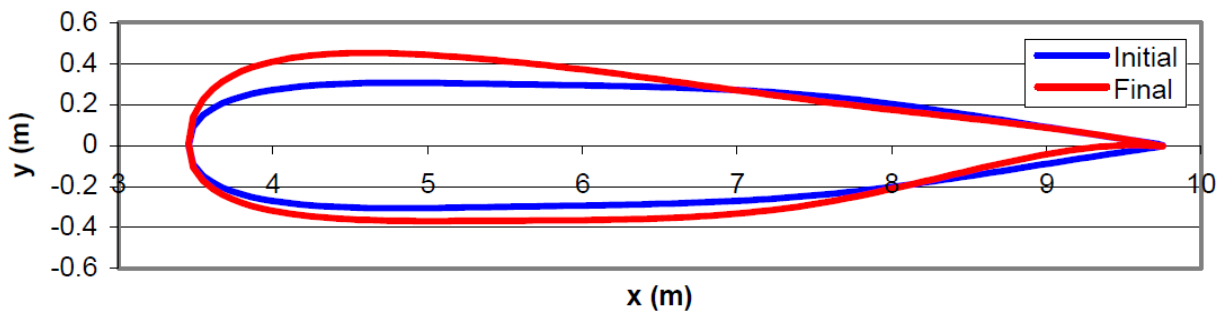


Figure 8-8: Initial and Final Cross-Sectional Shape for the Basic Test Case.

The differences between the initial and final structural designs are listed in Table 8-6. On one hand, the thickness of all two-dimensional components were reduced, especially that of the ribs, which converged to its lowest possible value. On the other hand, the beams and stringers dimensions were increased to the upper bounds.

Table 8-6: Initial and Final Structural Designs for the Basic Test Case.

	Upper Skin	Lower Skin	Rib Webs	Spar Webs	Posts	Spar Beams and Stringers	
	Thickness	Thickness	Thickness	Thickness	Area	Width	Height
Initial	1.905 cm	1.905 cm	1.905 cm	1.905 cm	0.968 cm ²	1.27 cm	1.27 cm
Final	0.965 cm	0.991 cm	0.635 cm	1.118 cm	0.775 cm ²	2.54 cm	2.54 cm

8.2.5.2 Parametric Study 1: Structural Model

A parametric study was performed to compare the various structural optimization models with respect to the optimization process and final system performance. The final values of range, wing weight and lift-to-drag ratio are shown in Table 8-7. The number of system analyses is also noted, as it directly relates to the computational effort required to solve the problem. The shaded row corresponds to the basic test case.

Table 8-7: Results for the Structural Optimization Model Parametric Study.

Models	R	W_w	C_L/C_D	Number of Analyses
Aero-1; Struct-1	11681 km	4093 kg	24.84	477
Aero-1; Struct-2	11722 km	3997 kg	24.66	789
Aero-1; Struct-3	11961 km	3876 kg	24.82	794
Aero-1; Struct-4	11684 km	3976 kg	24.52	1191
Aero-1; Struct-5	11632 km	4074 kg	24.65	1098

A comparison of Table 8-4 and Table 8-7 shows that that the number of required system analyses was directly related to the number of design variables. However, the improvement in system performance was relatively small for the increased computational price when more complex models were used. Furthermore, it was seen that at least one local optimum existed in the objective function because the best solution was obtained with Struct-3, a model that can be defined in the design spaces of the more complex models Struct-4 and Struct-5. Consequently, it does not seem appropriate for this particular problem to include a linear tapering of the wing box components.

Most of the optimized designs adopted similar configurations. The ribs converged to their minimum allowable thickness and the spar thickness increased from the front spar to the rear spar. Furthermore, when possible, most span-wise components were tapered to the minimum allowable thickness at the wing tip. It should be mentioned that other tests on other problems showed that the linear tapering strategy was highly beneficial when the lower bounds on the components thickness are reduced. In these cases, the wing was greatly reduced.

8.2.5.3 Parametric Study 2: Aerodynamic Model

A similar parametric study was carried out to evaluate the effects of the aerodynamic model complexity. The information of Table 8-4 when the Struct-1 model is associated to various aerodynamics models is repeated in Table 8-8. The shaded row corresponds to the basic test case.

Table 8-8: Results for the Aerodynamic Optimization Model Parametric Study.

Models	R	W_w	C_L/C_D	Number of Analyses
Aero-1; Struct-1	11681 km	4093 kg	24.87	477
Aero-2; Struct-1	12067 km	3756 kg	24.70	593
Aero-3; Struct-1	12746 km	3209 kg	24.60	1196

It is seen that the complexity of the aerodynamics model had a greater influence on the aircraft range than that for the structural model. However, the increase in the aerodynamic shape design flexibility did not improve system performance by improving the aerodynamic behavior of the wing. Indeed, the lift-to-drag ratio remained practically the same from one model to the other. Actually, the more complex aerodynamic shapes increased the aircraft range by allowing greater reduction in the wing box weight.

8.2.5.4 Parametric Study 3: Pressure Control

A crossing of the upper and lower surface pressure curves was observed for most of the optimal designs presented previously. Since this feature can be undesirable, an additional set of constraints was defined to avoid it.

The inclusion of the pressure control constraints resulted in reduced system performance. This is shown in Table 8-9, where the results from the basic test case (without pressure control) are compared to the ones obtained with pressure control. It is therefore up to the designer to decide if the use of this strategy is desirable or not.

Table 8-9: Optimal Results With and Without Pressure Control.

Models	<i>R</i>	<i>W_w</i>	<i>C_L/C_D</i>	Number of Analyses
Without pressure control	11681 km	4093 kg	24.87	477
With pressure control	10488 km	4889 kg	24.52	407

The chord-wise coefficient of the pressure distributions at half the wing-span for the initial, optimal design for the basic test case, and optimal designs with pressure control are shown in Figure 8-9.

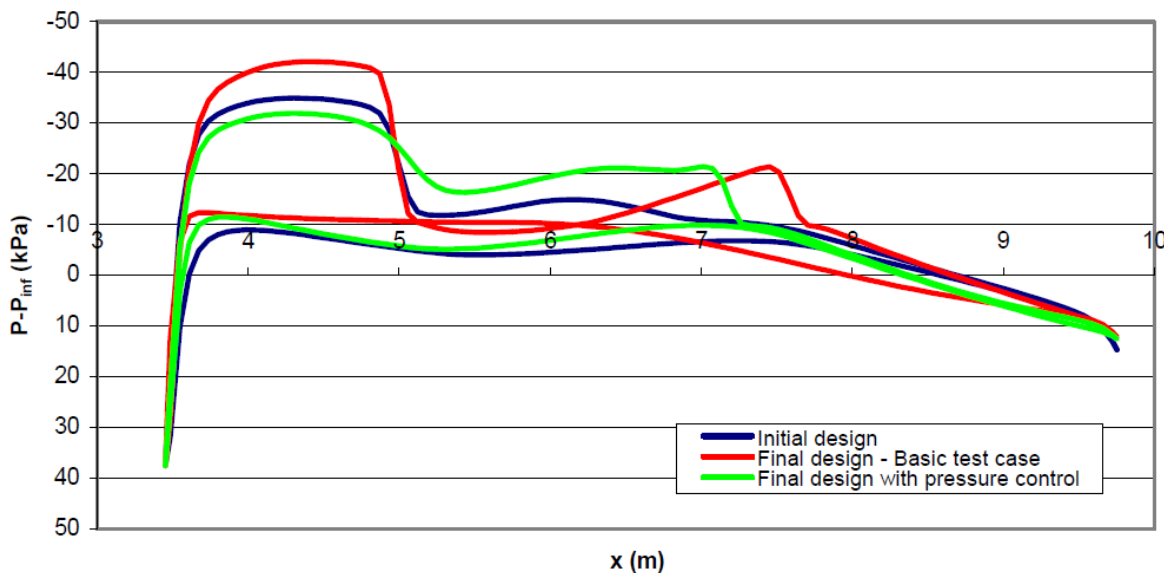


Figure 8-9: Results for Pressure Control Parametric Study.

8.2.5.5 Parametric Study 4: Bounds on Aerodynamic Variables

The last parametric study concerned the bounds of the aerodynamic variables. The results from different bounds to the basic test case 3% bounds are compared in Table 8-10.

Table 8-10: Results for the Aerodynamic Bounds Parametric Study.

Aerodynamics Bounds	<i>R</i>	<i>WW</i>	<i>C_L/C_D</i>	Number of Analyses
±1%	10398 km	4999 kg	24.64	230
±2%	11454 km	4199 kg	24.66	366
±3%	11681 km	4093 kg	24.84	477
±4%	11597 km	4087 kg	24.65	491
±5%	11803 km	3955 kg	24.71	709

Increasing the bounds of the aerodynamic variables had a similar effect to increasing the complexity of the aerodynamic optimization model. Indeed, higher bounds resulted in similar aerodynamic performances but in a lighter wing box. However, care should be taken as it appears that the use of large bounds increase the risk of convergence to a local optimum, as for the 4% case.

An MDF-formulated wing optimization capability, simultaneously linking structural, aerodynamic, and aeroelastic models, was successfully developed and tested. The formulation was found to be stable, efficient and easy to use and implement. However, because a gradient-based optimization technique was used, the process converged to local optima in at least two cases.

A series of studies was performed to evaluate the influence of various system and disciplinary parameters on the optimization process and on the final design. Some general observations were outlined from these studies. For example, for the set of parameters considered it was more appropriate to increase the aerodynamic design flexibility than the structural design flexibility. Indeed, an improvement in the aerodynamic optimization model was beneficial from a system point of view because it permitted wing weight reduction. This observation reflects the true multidisciplinary nature of the problem considered and the usefulness of multidisciplinary optimization instead of a sequential approach. However, it should be stressed that an increase in the structural design flexibility was not found to be beneficial because of the high restriction in the allowed component thicknesses.

8.2.6 Technical and Financial Improvements/Benefits of Using MDO vs. Traditional Design Methods

8.2.6.1 Multidisciplinary vs. Single-Discipline Optimization

A study was carried out to illustrate the benefits of multidisciplinary optimization for solving the present problem. The behaviour of the multidisciplinary optimization compared to two sequential processes where one discipline is optimized after the other is shown in Figure 8-10. The basic test case was used for these runs.

Each point on this chart corresponds to a multidisciplinary feasible design initiating a new iteration. It is easily noticeable that the multidisciplinary approach was superior to the design cycles where only one discipline was

optimized at a time. Indeed, for a given number of system analyses, the range resulting from MDO was greater than that from the single-discipline optimizations. Furthermore, although the cycles of single-discipline optimization could have been repeated, the absence of a global system optimization involved the risks of getting trapped in a loop oscillating among various single-discipline optimal designs.

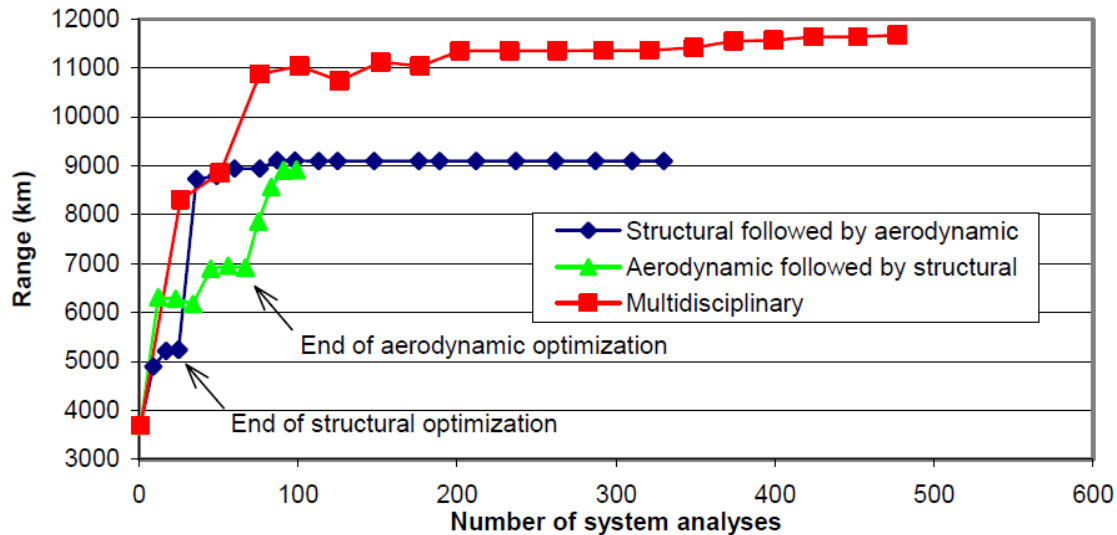


Figure 8-10: Multidisciplinary vs. Sequential Single-Discipline Optimizations.

8.2.7 References; Web Resources; Science Connect Link; and Validation Data Location

- [1] Shi, G., Renaud, G., Yang, X., Zhang, F., and Chen, S. (2002). Integrated Wing Design with Three Disciplines. In: Proceedings of 9th AIAA/ISSMO Symposium on Multidisciplinary Analysis and Optimization, AIAA-2002-5405, Atlanta, GA, USA, 2002.
- [2] Chen, S., Zhang, F., Renaud, G., Shi, G., and Yang, X. (2002). A Preliminary Study of Wing Aerodynamic, Structure and Aeroelastic Design and Optimization. In: Proceedings of the 9th AIAA/ISSMO Symposium on Multidisciplinary Analysis and Optimization, AIAA-2002-5656, Atlanta, GA, USA, 2002.
- [3] Deblois, A. and Abdo, M. (2010). Multi-Fidelity Multidisciplinary Design Optimization of Metallic and Composite Regional and Business Jets. In: Proceedings of the 13th AIAA/ISSMO Multidisciplinary Analysis Optimization Conference, AIAA-2010-9191, Fort Worth, Texas, 2010.
- [4] Garcelon, J.H., Balabanov, V. and Sobieski, J. (1999). Multidisciplinary Optimization of a Transport Aircraft Wing using VisualDOC. In: Proceedings of 40th AIAA/ASME/ASCE/AHS/ASC Structures, Structural Dynamics, and Materials Conference and Exhibit, St. Louis, MO, USA, April 12 – 15, 1999.
- [5] Nodet, J. and Wright, S. (2006). Numerical Optimization, New York: Springer Verlag.



Chapter 9 – BENCHMARK: AERODYNAMICS AND RADAR CROSS SECTION MULTIOBJECTIVE AND MULTIDISCIPLINARY OPTIMIZATION STUDY

Ali Karakoç

Defence Industries Research and Development Institute of The
Scientific and Technological Research Council of Turkey
TURKEY

Halil Kaya and Evren Sakarya

Turkish Aerospace Industries Inc.
TURKEY

The present study aims to suggest an aerodynamics and RCS signature optimization for NATO AVT-251 Task Group's UCAV configuration MULDICON. The methodology incorporates design of experiment, the concept of surrogate models and multi-objective genetic algorithm. In the present study, MULDICON configuration was optimized to increase CL max (usable), which is defined as CL value where large local gradient changes of static stability appears, at take-off condition by keeping RCS signature value constant.

9.1 BENCHMARK EXECUTIVE SUMMARY

9.1.1 Qualitative Optimization Problem Statement

9.1.1.1 Design Variables

The design variables are leading edge radii and twist angles of wing profiles.

9.1.1.2 Objective Function(s)

The objective is to maximize CL value of UCAV, where large a local gradient change of static stability as a function of angle of attack firstly occurs providing the same target RCS signature value.

9.1.1.3 Constraint Function(s)

As a constraint function RCS signature value is defined. The aim is not to increase RCS signature value.

9.1.2 Description of Analyses/Disciplines/Theory/Fidelities Involved

The MDA consists of a high fidelity RANS solver as aerodynamic solver and low fidelity physical optics approximation as RCS solver. The process employs openVSP to parametrically generate geometries and surface mesh required for RCS analyses. The mesh that is required for aerodynamic analyses are created using pointwise scripting. The selection of sampling points is performed using Latin Hypercube Sampling method. After the analyses completed for the selected design points, meta-models for aerodynamics and RCS signature are created using kriging approximation.

9.1.3 MDO Approach (Algorithm/Architecture)

As an optimization algorithm, MDO employs Multi Objective Genetic Algorithm. The algorithm takes advantage of surrogate models created using analyses results with kriging approximation technique.

9.1.4 Implementation Details

9.1.4.1 Analysis Software

Aerodynamics analyses are conducted by using SU2 (open source software). The turbulence model is the Spalart-Allmaras turbulence model. RCS signature analyses are performed by employing SAGE-R RCS analysis tool (an implementation of physical optics approximation).

9.1.4.2 Optimization Software

The optimization software that is employed to create surrogate models and to get pareto frontier is modeFRONTIER.

9.1.4.3 Hardware

Aerodynamics analyses are conducted on a RedHat Linux cluster. 4 nodes are employed to conduct the analyses; each node has 24 Intel Xeon 2.5 Ghz cores and 256 Gb memory. Furthermore, the system has infiniband switch. The RCS signature analyses are conducted on a Notebook with 2.5 GHz Intel i5 processor.

9.1.4.4 Human Effort

The required human effort is around 4 days.

9.1.5 Results

9.1.5.1 Initial Design (Design Variables, Objectives, Constraint Values)

Design variables are twist and leading edge radius of the airfoils. Initial design variable values (twist1, LERA1, twist2, LERA2): -1.40, 8.57 cm, -5.00, 1.57 cm. Initial objective function values: CL max usable = 0.728, f_RCS: Ratio of total angles to angles which have RCS value of greater than 1 m²: 13.27%.

9.1.5.2 Optimized Design (Design Variables, Objectives, Constraint Values)

Optimized design variables (twist1, LERA1, twist2, LERA2): -1.30, 17.10 cm, -6.00, 2.70 cm. Optimized objective function values: CL max usable = 0.809, f_RCS: Ratio of total angles to angles which have RCS signature value of greater than 1 m²: 13.27%. (from pareto frontier the design with max CL max usable is selected for the same RCS value with initial design).

9.1.5.3 Observations

- Vortex breakdown is delayed in the final design by decreasing the twist angle of the outer profiles.
- MDO increased leading edge radii of the profiles and decreased the twist angle of the outer profile.
- To create meta-models aerodynamic analyses and RCS signature analyses were conducted. Aerodynamic analyses took time around 15 days and RCS analyses took just 6 hours, since it employed a low fidelity solver which is an implementation of physical optics approximation.

- Since surrogate models are employed, to setup and post processing effort don't take much time. Whole MDO execution time was around 3 hours.
- Since MDO take advantage of surrogate models, robustness do not affect from MDA failures.

9.1.6 Technical and Financial Improvements/Benefits of Using MDO vs. Traditional Design Methods

Unknown.

9.1.7 References; Web Resources; Science Connect Link; and Validation Data Location

None.

9.2 BENCHMARK DETAILS

9.2.1 High-Level

The MDA presented involves a detailed analysis method of aerodynamics and a preliminary analysis method of radar cross section signature.

9.2.2 Multidisciplinary Analysis (MDA)

9.2.2.1 Implementation Details of Analyses and Corresponding Responses Used to Formulate MDO Objective and Constraint Functions

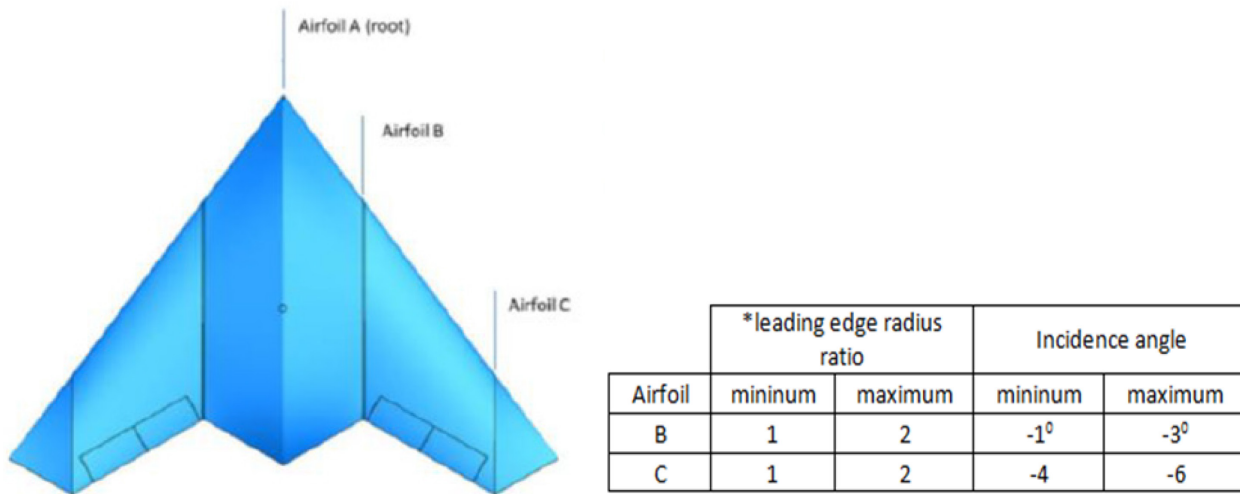
The implementation incorporates design of experiment, the concept of surrogate models and multi-objective genetic algorithm.

“For optimization problems, surrogate models can be regarded as approximation models for the cost function(s) and state function(s), which are built from sampled data obtained by randomly probing the design space (called sampling via Design of Experiment (DoE)). Once the surrogate models are built, an optimization algorithm such as Genetic Algorithms (GA) can be used to search the new design (based on the surrogate models) that is most likely to be the optimum. Since the prediction with a surrogate model is generally much more efficient than that with a numerical analysis code, the computational cost associated with the search based on the surrogate models is generally negligible.” [1]

Since it is needed to generate the surrogate models over which the optimization will be conducted, both for aerodynamics and radar cross section signature values, firstly, the design space and the design of experiment should be established.

The design variables are leading edge radii and twist angles of the airfoil B and airfoil C that is illustrated in the Figure 9-1. According to the study [2], leading edge radii and twist angles of the profiles have significant importance on vortex breakdown. The design space is also given in Figure 9-1.

The selection of sampling points is performed using Latin Hypercube Sampling method. Due to limitation in time and computational resources, only 15 sampling points are selected within the design space. The sample points are shared below in Table 9-1.



*Leading edge radius ratio: leading edge radius of generated profile/initial leading edge radius

Figure 9-1: The Design Variables and the Design Space.

Table 9-1: The Sample Points (as Non-Dimensional) that are Selected by Latin Hypercube Sampling Method.

Design ID	variable_1_LE	variable_2_LE	variable 3_TW	variable 4_TW
0	0,02777	0,47222	0,13889	0,52778
1	0,47222	0,02778	0,41667	0,08333
2	0,91666	0,13889	0,75000	0,25000
3	0,36111	0,97222	0,69444	0,30500
4	0,08333	0,69444	0,63888	0,69444
5	0,63888	0,63889	0,25000	0,63888
6	0,75000	0,08333	0,58333	0,75000
7	0,97222	0,52777	0,36111	0,41666
8	0,19444	0,86111	0,19444	0,97222
9	0,41666	0,25000	0,02778	0,47222
10	0,86111	0,80556	0,80556	0,58333
11	0,30555	0,75000	0,30555	0,02777
12	0,52777	0,41667	0,91666	0,86111
13	0,13888	0,30556	0,86111	0,36111
14	0,58333	0,58333	0,97222	0,19444

After selection of sample points, it is needed to generate the geometries that should be formed regarding the selected design variables. To generate the geometries parametrically, Xfoil and OpenVSP scripting are

employed. The profiles with the selected leading edge radii are generated by employing Xfoil. Then by using the generated airfoils, constant span, chord lengths and finally the selected incidence angles of profiles at predetermined stations, OpenVSP scripting creates the required geometries and exports them in .iges and .stl file format.

To get aerodynamics coefficient of each design point in the design of experiment, SU2 a suite of open-source software tools written in C++ for the numerical solution of partial differential equations is employed as a flow solver. Its main application is on computational fluid dynamics and its suite includes compressible Reynolds Average Navier-Stokes solver. Thus, it is a high fidelity analysis tool.

Since a finite volume solver is employed to get aerodynamics coefficients, for each sample point, flow solver requires a suitable grid. To generate required grids, Pointwise scripting is operated. Firstly, a surface and a volume grid is generated on MULDICON UCAV geometry, manually. Then whole process is written as a Pointwise script in a file. After that, by using this file as a template, the required grids are generated automatically. The generated grids have around 190K surfaces elements. The volume grid includes around 7 M tetrahedral and 4.5 M prism elements (Figure 9-2).

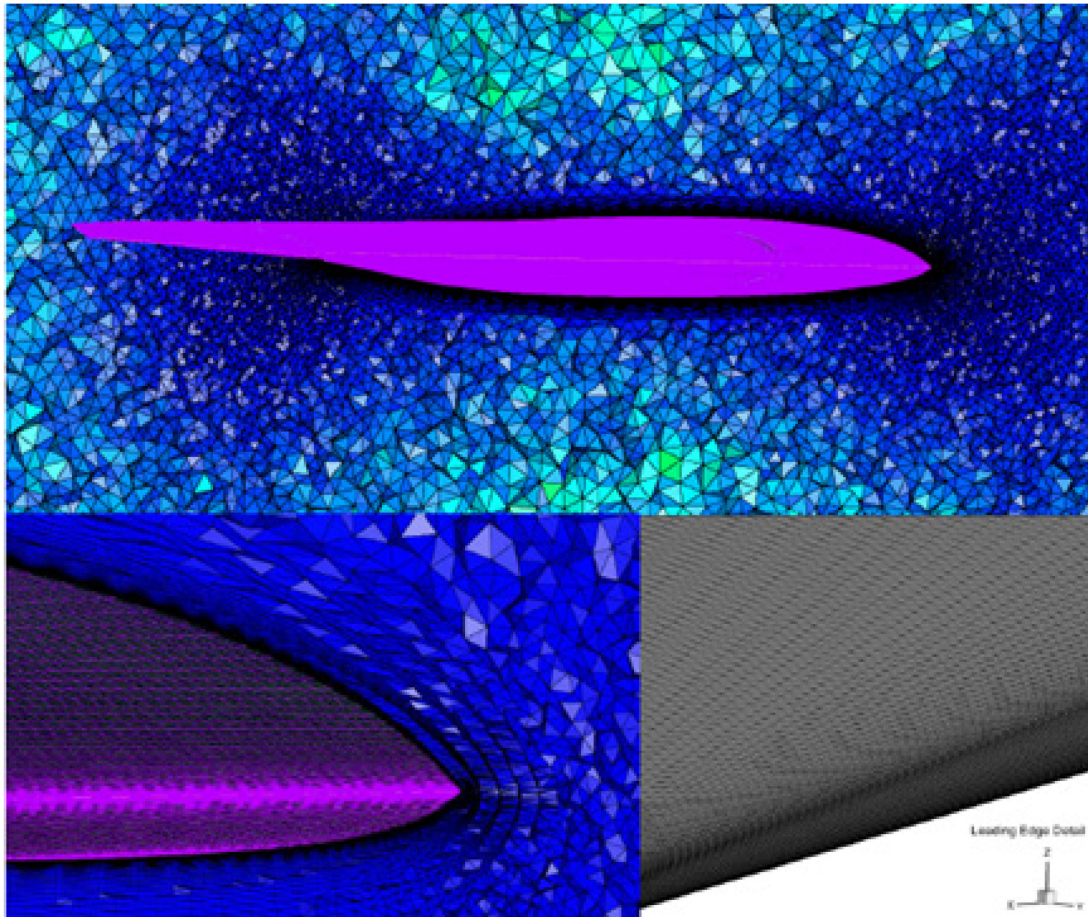


Figure 9-2: A Generated Grid Using Pointwise Scripting.

As a turbulence model, Spalart-Allmaras one equation turbulence model is utilized. As a linear system solver, GMRES is selected. The convective terms are calculated by using second order Roe Scheme (with entropy fix). As boundary condition, far-field and no slip wall boundary conditions are used.

To create a surrogate model for RCS signature, the sample geometries are analyzed by employing SAGE-R RCS analysis tool (an implementation of physical optics approximation). It is an in-house code developed by Defence Industries Research and Development Institute of the Scientific and Technological Research Council of Turkey. To estimate better RCS signature values, physical optics method which was driven for the main solutions is coupled with geometrical optics for multi bounces at 9 GHz frequency, vertical polarization, for up to 3 ray bounces is used. The software requires the geometry in .stl format. That is produced by OpenVSP scripting.

Finally, the geometry, mesh, configuration file of flow solver generation processes is driven by a python script.

In the present study, no MDA quality metrics are implemented as constraints. Moreover, no MDA quality metrics are implemented and MDA is uncoupled.

9.2.2.2 Practical Concerns

In the present study, python, OpenVSP, Xfoil, SU2, SAGE-R and Pointwise software are employed. Python, OpenVSP, Xfoil, SU2 are all open-source software. All this software can be downloaded from related web sources. Windows and Linux platforms are supported.

SAGE-R RCS analysis software is an in-house code developed by Defence Industries Research and Development Institute of the Scientific and Technological Research Council of Turkey. It works on Windows platform. It is not available to get a license.

Pointwise and ModeFRONTIER are licensed software. Windows and Linux platforms are supported.

Aerodynamics analyses were conducted on a Red Hat Linux cluster. Four nodes were employed to conduct the analyses; each node has 24 Intel Xeon 2.5 GHz cores and 256 GB memory. Furthermore, the system has Infini-band switch. The RCS signature analyses were conducted on a Notebook with 2.5GHz Intel i5 processor. Disc space requirements are not recorded.

To get required aerodynamics coefficients, each sample point is analyzed at 5 different angles of attack. Hence, including the base geometry 80 different high fidelity aerodynamics analyses are conducted. The total required wall time is around 360 hours.

The required human effort to setup MDA is around 4 days. It includes generating the template geometry, the template mesh, the template configuration file and the driven script that allows conducting MDA analyses, automatically.

An MDA fail case has not been occurred. Even if it failed it would not affect the MDO algorithm, because MDA analyses are conducted to feed the surrogate model over which the optimization will be conducted.

9.2.3 MDO Problem Definition Details

The design variables are the leading edge radii ratio and incidence angles. The variables are real numbers.

The objective function is to maximize CL value of UCAV, where large a local gradient change of static stability as a function of angle of attack firstly occurs, whereas RCS signature value does not increase. Since the aim is to maximize CL value of UCAV by keeping RCS signature values constant, it is a single objective, multi-disciplinary optimization. However, by employing MOGA algorithm, a Pareto front is obtained, the method can also be used for multi-objective optimization.

Since the optimization algorithm, which is multi objective genetic algorithm, is a gradient-free algorithm, there is not any gradient calculation.

9.2.4 MDO Algorithm

The utilized MDO algorithm is the multi-objective genetic algorithm. It is a stochastic optimization algorithm.

A Surrogate model is used to shorten the computational cost of optimization process. The construction of surrogate models is performed using Kriging approximation technique. The sampling points are selected using latin hypercube sampling method. Due to limitation in time and computational resources, only 15 sampling points are selected within the design space.

The optimization software that is employed to create surrogate models and to get pareto frontier is modeFRONTIER.

9.2.5 MDO Results

Design variables were twist and leading edge radius of the airfoils. Initial design variable values (twist1, LERA1, twist2, LERA2): -1.40, 8.57 cm, -5.00, 1.57 cm. Initial objective function values: CL max usable = 0.728, f_RCS: Ratio of total angles to angles which have RCS value of greater than 1 m²: 13.27%.

Optimized design variables (twist1, LERA1, twist2, LERA2): -1.30, 17.10 cm, -6.00, 2.70 cm. Optimized objective function values: CL max usable = 0.809, f_RCS: Ratio of total angles to angles which have RCS signature value of greater than 1 m²: 13.27%. (From pareto frontier the design with max CL max usable is selected for the same RCS value with initial design).

The pareto front that is obtained is given in Figure 9-3. As it is seen from pareto front, whereas CL max usable increases, RCS signature value also increases. So, the design with the maximum CL max usable value that provides the same target RCS signature value has selected as an optimum design. After the validation of estimated value by repeating analyses at the optimum design point, the final values are obtained. The estimated value for RCS signature is 13.25, the analyzed value is 13.27. The estimated value for CL max usable is 0.826, the analyzed value is 0.809. At the final design, by decreasing twist angle of outer profiles vortex breakdown is delayed. The flow pattern of final design is illustrated in Figure 9-4.

9.2.6 Technical and Financial Improvements/Benefits of Using MDO vs. Traditional Design Methods

Unknown.

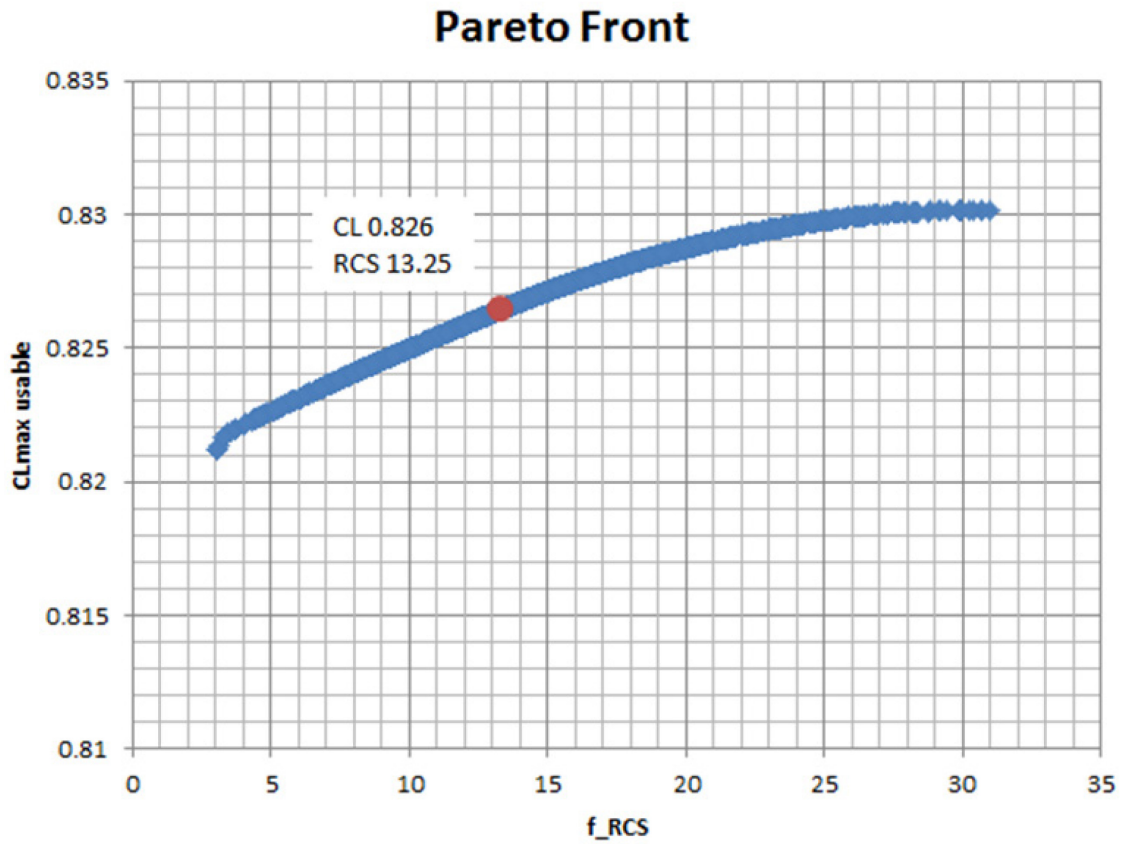


Figure 9-3: Pareto Front Results.

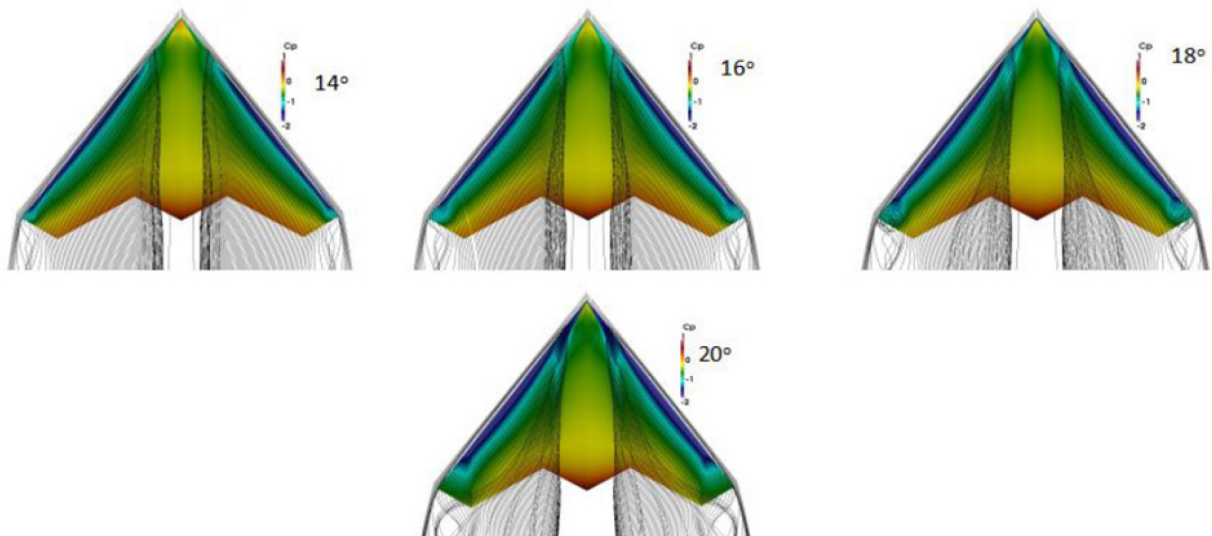


Figure 9-4: The Flow Pattern of the Final Design.

9.2.7 References; Web Resources; Science Connect Link; and Validation Data Location

- [1] Han, Z.-H. and Zhang, K.-S. (2012). Surrogate-Based Optimization, Real-World Applications of Genetic Algorithms. Ed. O. Roeva. ISBN: 978-953-51-0146-8, InTech. Available from: <http://www.intechopen.com/books/real-world-applications-of-genetic-algorithms/surrogate-based-optimization>.

- [2] Schütte, A. (2017). Numerical Investigations of Vortical Flow on Swept Wings with Round Leading Edge. Journal of Aircraft, Vol. 54, No. 2, pp. 572-601.



Chapter 10 – BENCHMARK: EFFICIENT SUPERSONIC AIR VEHICLE (ESAV)

F. Afonso, J. Vale and F. Lau
Instituto Superior Tecnico
PORTUGAL

A. Suleman
University of Victoria
CANADA

10.1 BENCHMARK EXECUTIVE SUMMARY

10.1.1 Qualitative Optimization Problem Statement

10.1.1.1 Design Variables

Two sets of design variables were defined, one for each optimization level: configuration design variables (in the upper optimization level); and control design variables (in the lower optimization level). The configuration design variables are the wing-box internal thicknesses (webs and caps) for both reference and joined-wing models and two wing factors just for the joined-wing model (front wing area factor; and aft wing control factor). The control design variables are the angle of attack, engine throttle and horizontal tail incidence (for the reference model) or elevator (for the joined-wing model).

10.1.1.2 Objective Function(s)

For each point in a typical regional jet mission profile an optimization problem was set in the lower level of optimization for a given configuration (set of configuration design variables). The achieved results were used to compute the objective function of the upper optimization level. Objective functions set for both reference and joined-wing models were the same.

10.1.1.3 Constraint Function(s)

As constraints, trimmed conditions were defined in the lower optimization level; and maximum stress level for two critical maneuvers (2.5 g pull-up and -1.5 g pull-down) was set to be lower than the material yield stress in the upper optimization level. As for the objective function, the constraints were set the same in both reference and joined-wing models.

10.1.2 Description of Analyses/Disciplines/Theory/Fidelities Involved

An MDO framework was implemented in C++ for preliminary aircraft design, with a unified aircraft multidisciplinary optimization environment in mind. This framework was designed to be versatile and modular, allowing for the integration of customized models to replace the existing ones: geometry; aerodynamics; structures; propulsion; fuel; payload; performance; and optimization. All of these modules were developed or adapted for this framework. Another relevant feature is the option to import databases that can be used to generate surrogate models (which are built using a code adapted from DACE software tool) of disciplines and reduce the computational effort of the optimization and/or improve the fidelity of the optimization results.

An aircraft can be easily sketch in the geometry module, where the user defines the aircraft configuration to be optimized. Items like fuselage, lifting surfaces, fuel tanks, structural layout, payload and systems placement,

and engines are parameterized in the geometry module along with other relevant information. The data collected in this module feeds all others.

The aerodynamics module is a panel method code that includes includes compressibility corrections for the pressure coefficient (Prandtl-Glauert) and flat plate zero pressure gradient friction drag based calculation (based on FRICTION correction). From the geometry parameterized in the geometry module it automatically generates an aerodynamic mesh, which can be changed in this module. Both steady and unsteady calculations are allowed. In replacement of this module, a previously generated aerodynamic database was employment. This database was computed using this aerodynamic model, so the fidelity was not changed.

A condensed 3D equivalent beam model based on the finite element method formulation is generated on the structural module from the parameterized structural layout. The cross-section properties of the equivalent beam model are computed based on the wing-box layout for lifting surfaces and fuselage frames for the fuselage. Non-structural weights, including payload, systems, passengers, engines and fuel, are accounted for as lumped mass points rigidly linked to the beam model as in NeoCASS. This module performs linear and nonlinear static and dynamic analyses as well as modal analyses. As for the aerodynamic module, a surrogate model of the structural module was used in the optimization instead of running this module. No aeroelastic effects were considered in the analyses carried out in this work, instead the aircraft was assumed rigid.

The propulsion model consists of ideal aircraft turbofan or turbojet engines. The engine modeling assumes the airflow as isentropic in every engine component (inlet, compressor, burner, turbine and nozzle) and does not account for choking of the nozzle. The engine models were based on a formulation described by Hill and Peterson. For this test case, a higher fidelity database provided by Embraer was used instead of this module.

Fuel and payload modules are used to distribute the loads through the aircraft structure and provide the performance module with the fuel and payload configurations (mass, center of mass and inertia moments). Before setting the entire optimization problem, a surrogate model of this module was computed and used in the optimization.

In the performance module one can set the lower level of optimization, where the available controls in the aircraft (set of control design variables, which includes morphing controls) can be used to minimize or maximize a given set of performance goals for an aircraft configuration (set of configuration design variables) at the same time that respects some prescribed constraints (e.g., trim conditions). This module is directly associated with the optimization module, which provides the aircraft configuration and receives the outcomes from the performance module to compute the global objective function and constraints. All optimization in both modules are carried out using the Feasible Sequential Quadratic Programming (FSQP) algorithm.

10.1.3 MDO Approach (Algorithm/Architecture)

An MDO strategy was especially designed to allow studying, at a preliminary level, the two main goals of the EU FP7 project NOVEMOR: analyze novel configurations; and explore morphing solutions. For this task, a performance based MDO framework that aims at flight operation optimization and aircraft configuration optimization was developed. One optimization level was defined for each one of the above-mentioned optimization goals.

At the lower optimization level, several MDO problems are set for a given aircraft configuration, the outcome of these MDO problems will feed the upper optimization level objective function and constraints with performance results (in this example fuel burned and maximum stress levels for critical maneuvers, respectively). The multidisciplinary at this level consists solely on the fact that different disciplines are involved in the

computation of the objective function and constraints; there is no coupling between disciplines. Therefore, one might say that the optimization problems at this level consist only in determining the best control layout (control design variables) that minimize or maximize a given objective function while respecting the prescribed constraints. A FSQP algorithm is used to conduct the optimizations.

The main geometric parameters, those not allowed to change during flight (configuration design variables), are optimized at the upper optimization level. For each optimization iteration at this level, a different aircraft configuration (set of configuration design variables) is sent to the lower optimization level to determine the best control layout that minimizes or maximizes a given lower level objective function. From the outcomes of the lower optimization level, the upper level objective function and constraints is formulated. The upper level optimization problem is solved using the FSQP algorithm.

This framework allows the usage of databases to build surrogate models aiming at reducing the computational effort of optimizing a complete aircraft. Two different kinds of surrogate models may be defined: one for replacing an aircraft discipline (e.g., aerodynamics and structures); and another for replacing the lower level of optimizing (render in a performance map of a given aircraft configuration).

10.1.4 Implementation Details

10.1.4.1 Analysis Software

All the modules were especially developed or adapted in C++ for this performance based MDO framework, which includes: geometry module (parameterizes the aircraft geometry); aerodynamic module (panel method with compressibility and friction drag corrections); structural module (equivalent beam model); propulsion module (ideal turbofan model replaced by a high fidelity turbofan databank); fuel and payload modules (responsible for computing the payload and fuel inertial properties); performance (lower optimization level, where the aircraft control layouts are optimized for a given set of performance goals) and optimization (upper optimization level, responsible for optimizing the aircraft configuration based on the performance target selected) modules.

10.1.4.2 Optimization Software/Framework

All the optimizations were carried out using the FSQP (Feasible Sequential Quadratic Programming). No parallel computing was employed. In order to improve the numerical efficiency of the optimizer, the design variables, constraints and objective functions were normalized to have approximately the same dimension: the design variables are normalized in respect to the span between their lower and upper values; the stress constraints were normalized to the material yield strength; the fuel burned was normalized to an equivalent fuel burned value calculated for the reference aircraft with a similar Take-Off Weight (TOW).

10.1.4.3 Hardware

The developed framework was implemented in C++ for Windows. Several computers were used to generate the databases, although only one computer was required to solve the MDO problem.

10.1.4.4 Human Effort

The human effort was not quantified.

10.1.5 Results

10.1.5.1 Initial Design (Design Variables, Objectives, Constraint Values)

Table 10-1 and Table 10-2 present the design variables, objective function and constraint values for the reference (B) and joined-wing (JW) models. Note that the constraints and objective function are normalized and presented only for the upper optimization level.

Table 10-1: Design Variable Information.

	Design Variables	Lower Boundary	Upper Boundary	Initial Guess	Model	Optimization Level
Config	t_w/c	0.0010	0.0100	0.0086	B, JW	Upper
	t_s/t_{max}	0.0010	0.0100	0.0086	B, JW	Upper
	F_{FW}	0.500	0.800	0.755	JW	Upper
	F_{AW}	0.275	0.925	0.827	JW	Upper
Control	Throttle	0.0	1.0	0.1	B, JW	Lower
	α	-10.0°	10.0°	0°	B, JW	Lower
	I_{HT}	-8.0°	8.0°	0°	B	Lower
	δ_e	-30.0°	30.0°	0°	JW	Lower

Table 10-2: Objective and Constraint Values.

	Model	Initial Guess
Objective Function: Normalized Fuel Burned	B	1.0017
	JW	0.8688
Constraint: Normalized Maximum Stress	B	-0.3884
	JW	1.1185

10.1.5.2 Optimized Design (Design Variables, Objectives, Constraint Values)

Only the design variables, objective function and constraint for the upper optimization level are shown in Table 10-3. The design variables and objective function results for the lower optimization level are solely shown for the final aircraft configuration (final set of upper level design variables) in the form of graphs in Figure 10-1. Trim conditions were achieved for all the optimization problems at the lower optimization level.

Table 10-3: Optimization Results.

Design Variables	Parameter	Final Results (B)	Final Results (JW)	Level
	t_w/c	0.0010	0.0100	Upper
	t_s/t_{max}	0.0054	0.0100	Upper
	F_{FW}		0.500	Upper
	F_{AW}		0.925	Upper
Objective Function	Fuel Burned	0.9288	0.7976	Upper
Constraint	Maximum Stress	-0.0498	-0.0023	Upper

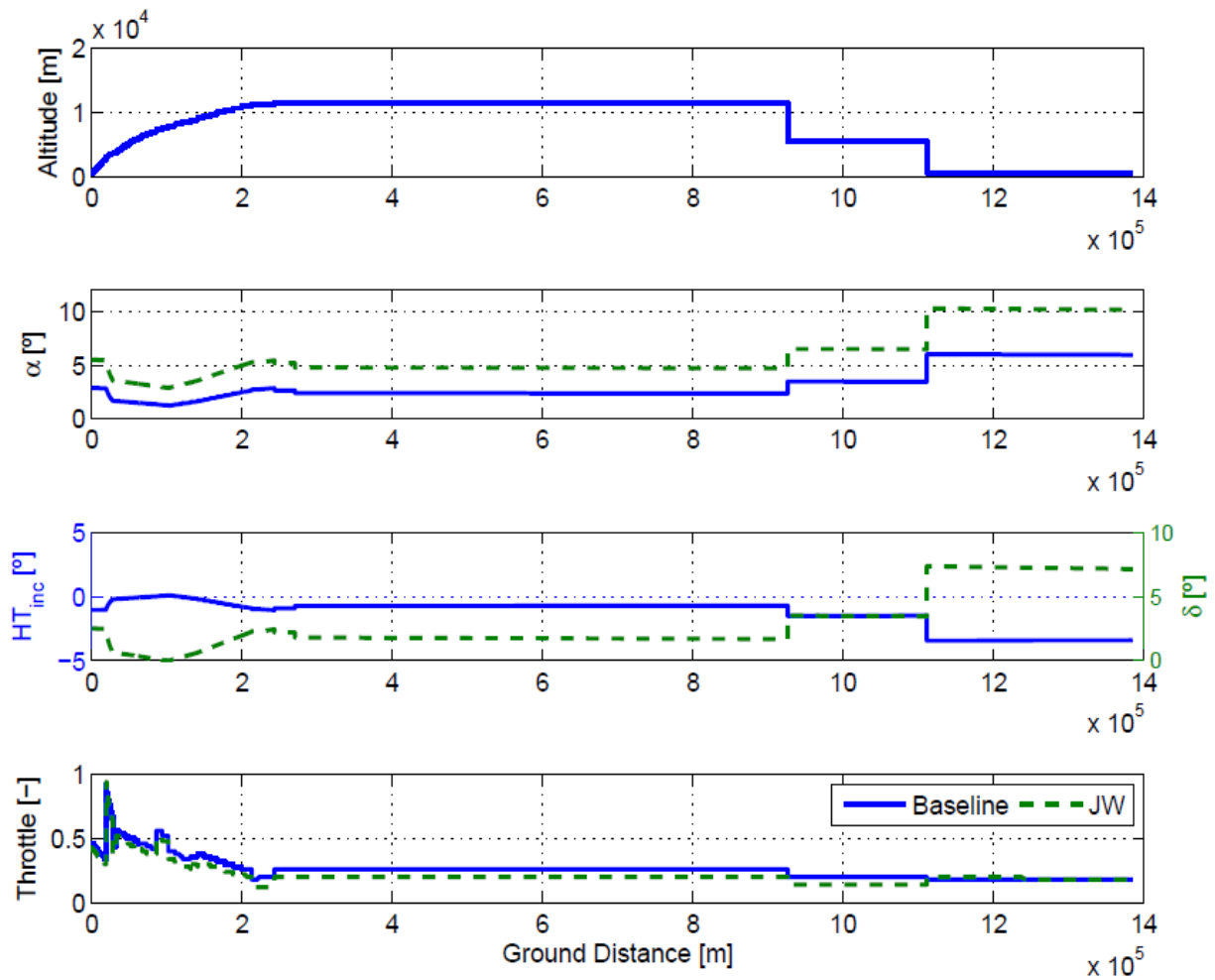


Figure 10-1: Results.

10.1.5.3 Observations

Initial vs. final design physics: For the reference model, only the structural layout of the lifting surfaces was optimized to improve the comparison between conventional and joined-wing configurations. In this first problem, the optimizer was able to reduce both the structural weight and the fuel burned while fulfilling the maximum stress constraint applied to the critical pull-up and pull-down maneuvers. Unlike in the reference model case, the initial guess is not a feasible solution for the joined-wing case. Despite the fact that the wingbox thicknesses were increased to fulfill the maximum stress constraint, the fuel burned was reduced due to the geometric changes in the aircraft planform. These planform changes were expected results considering the aerodynamic model employed: the aspect-ratio of the front wing increase to the double to reduce the aerodynamic induced drag; and the elevator actuation area in the rear wing was increased to reduce the aerodynamic trim drag.

Comments on impact of MDO changes to initial design: In what concerns the reference model, small changes were introduced using the MDO since only the structural layout of the wings was optimized. However, for the joined-wing considerable changes in planform were observed aiming at aerodynamic drag reduction.

Comments/metrics on computational cost: Despite not quantified, the database generation (for both disciplines and performance optimization problems) was noted to take the highest computational cost in the overall optimization process.

MDO execution: All optimization analyses converged with feasible solutions.

Setup time/effort; post processing effort: Not quantified.

Robustness to MDA failures, etc.: Since the design space was mapped when the databases were generated to build the surrogate models, no failures were found in the analysis modules and thus the framework for this application was considered robust.

10.1.6 Technical and Financial Improvements/Benefits of Using MDO vs. Traditional Design Methods

The developed framework allows designing an aircraft at a preliminary level using a performed based MDO strategy, which simplifies the definition of the objective function of the problem. Since performance metrics are used, other classic objective functions (for instance, L/D, minimum weight, range or endurance) are implicit in the performance parameters, particularly if the aircraft's purpose is to perform a mission or a set of missions. The problems solved here demonstrate how a solution with higher weight can reduce the overall fuel consumption, for instance. Other points in favour of using databases for different models are the possibility of parallelizing the work and use expert groups for the different fields. Also, the optimization can be performed for different sets of missions without needing to rerun the different disciplines analysis.

10.1.7 References; Web Resources; Science Connect Link; and Validation Data Location

No validation data are available.

10.2 BENCHMARK DETAILS

This document reports the details about the MDO benchmark problem for both conventional and joined-wing regional jet models.

10.2.1 High-Level

One of the MDO problems addressed is the preliminary design of the wingbox structure of the lifting surfaces of a transport Reference Aircraft (RA) model with a fixed exterior geometry for minimum fuel consumption in a mission profile. The other MDO problem addressed is the front and rear wing and internal structure of the lifting surfaces design for a Joined-Wing (JW) transport aircraft configuration, minimizing the fuel consumption in the same mission profile as the reference aircraft.

The overall problem solutions are obtained at the system-level, with total mission fuel consumption as the metric for the objective function. Nevertheless, the MDO procedure includes several sub-system level MDO procedures for optimal control determination. Details can be found in the next section.

Design phase (conceptual, preliminary, or detailed): Preliminary.

Design scope (system-level, sub-system level, component-level discussion): System-level.

Figure 10-2 shows the N² Diagram of responses required by objective and constraint functions (and analysis quality metrics).

Figure 10-2 depicts the data flow of the optimization methodology applied to the design problems described. The system level (or upper level) optimization is a simple procedure which calculates the objective function and constraints based on the mission performance metrics (total mission fuel consumption for the objective function and maximum absolute values of stress in pull up and down maneuvers for the constraints) as function of the configuration variables (structural thicknesses in the RA case and additionally geometrical parameters in the JW case).

The sub-system level (or lower level) optimization is used to calculate the optimal control for a user defined objective function minimization (in the analyzed cases is fuel flow) in all relevant flight conditions. It should be noted that while in a conventional aircraft the control calculation is deterministic since there are no redundancies in the control variables, for the case of multiple control surfaces or morphing wings with geometric adaptation capability, the lower level optimization provides the optimal control or morphing strategy for a given flight condition.

Once these results are available, the mission /and stress calculator can use the data available (control strategy and fuel flow) to integrate the fuel flow along the mission profile and eventually other quantities of interest that could be estimated from the control strategy, as total actuation energy. The control determined for the maneuver loads can also be used for a one-way Aero-Structural analysis for stress calculations.

Both upper and lower levels of optimization are based on database (or sample) generation and use surrogate models for the calculation of the necessary output quantities. The lower level uses databases of the different disciplines as functions of the relevant configuration and control variables, while the upper level uses databases of the performance metrics as functions of the configuration variables only.

A summary of the optimization levels for the RA and JW cases is presented in Table 10-4, which includes the design variables, state variable, objective functions, constraints and prescribed values. The nomenclature employed here can found in Vale *et al.* [1].

BENCHMARK: EFFICIENT SUPERSONIC AIR VEHICLE (ESAV)

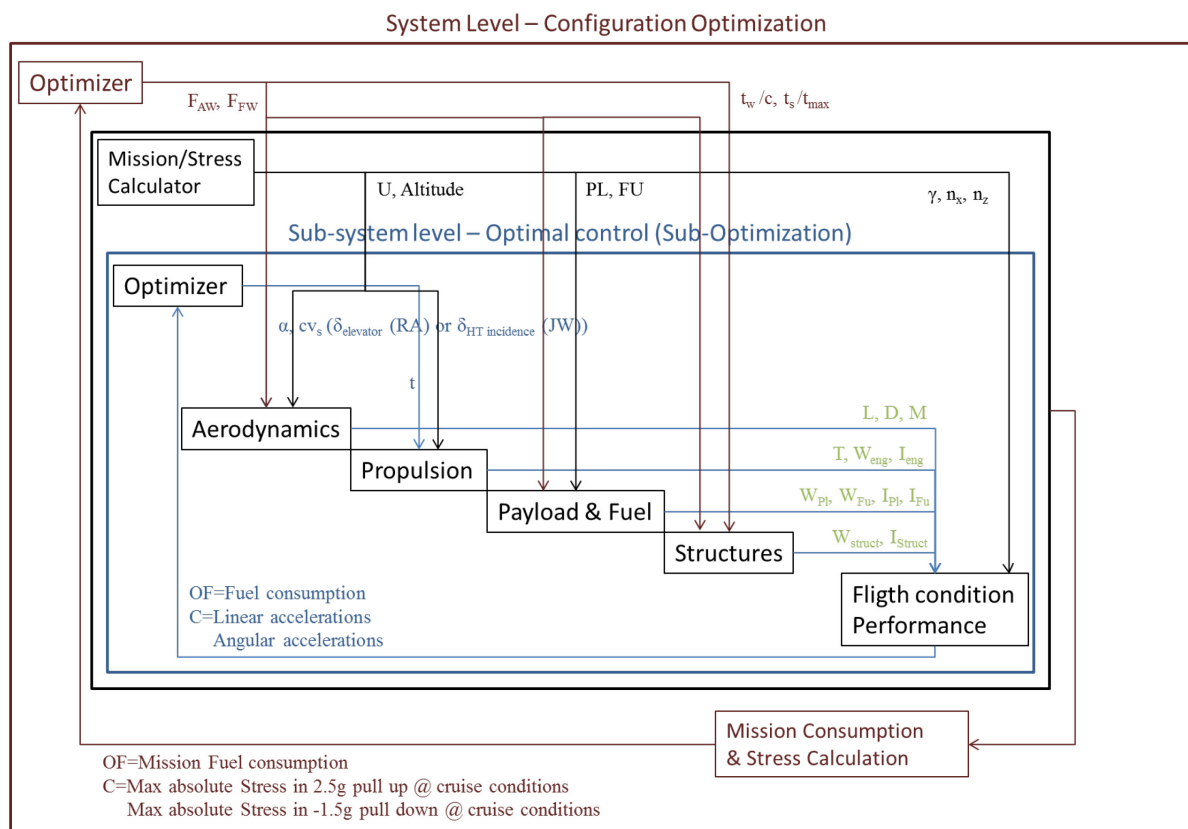


Figure 10-2: N² Diagram.

Table 10-4: Design Optimization Problem Statement.

	Model	System Level (Upper Optimization Level)	Sub-system Level (Lower Optimization Level)
Design Variables	RA	$t_w/c, t_s/t_{max}$	α, HT_{inc}, t
	JW	$t_w/c, t_s/t_{max}, F_{AW}, F_{FW}$	α, δ_e, t
State Variables	RA		$L, D, M, T, W_{eng}, I_{eng}, W_{Pl}, I_{Pl}, W_{Fu}, I_{Fu}, W_{struct}, I_{struct}$
	JW		
Objective Functions	RA	Minimize Mission Fuel Consumption	Minimize Fuel Consumption
	JW		
Constraints	RA	Max Stress for a 2.5 g pull-up and for a - 1.5 g pull-down	Linear accelerations Angular accelerations
	JW		
Prescribed Values	RA		$U, Altitude, Pl, Fu, \gamma, n_x, n_z$
	JW		

10.2.2 Multidisciplinary Analysis (MDA)

10.2.2.1 Implementation Details of Analyses and Corresponding Responses Used to Formulate MDO Objective and Constraint Functions

Deterministic analyses were used in the optimization:

- Aerodynamics were calculated using an in-house first order panel method code with compressibility corrections for the pressure coefficient (Prandtl-Glauert) and flat plate zero pressure gradient friction drag based calculation (based on FRICTION correction). The accuracy of such models in drag prediction is not good and it does not include wave drag components. Nevertheless, in a comparative analysis it should point out the best designs.
- A condensed 3D Equivalent Beam model was used to calculate the stiffness and mass properties of the wingbox structures and FE analysis used to obtain displacements and bending and twist components of stress of the structure under the prescribed loading.
- Propulsive force and fuel consumption is predicted using the ideal turbofan and turbojet models. As for the aerodynamics approach, the fidelity of such model is not good in fuel consumption prediction, but it should provide correct trends in consumption calculations. For these MDO problems, a higher fidelity database provided by Embraer was used instead of this module.
- Payload and Fuel mass distributions contribute to the mass and inertia properties of the aircraft. Payload is composed of user prescribed mass points with inertial properties. Fuel tanks are discretized and the mass and inertia properties of the fuel elements are also calculated.
- Aircraft performance, in particular fuel consumption, is calculated using surrogate models based in database samples generated by the previous models. Each discipline/model is analyzed sweeping the appropriate model variables within regions of interest, in order to create surrogate models of each discipline. For instance, the aerodynamics model is analyzed for altitude, speed, angle of attack, sideslip angle, control surfaces deflections or incidences in the range of interest given a specific mission profile. Surrogate models are then used together with the flight conditions for attitude and control optimization for user defined objective functions and constraints. The user can prescribe trim conditions or load factors as constraints for the control optimization while keeping the fuel consumption minimization as the objective function. In a conventional aircraft, this optimization procedure consists in solving the linear or non-linear 6 (or 3 if the longitudinal movement only is being considered) degree of freedom dynamic equations, but for a multiple control surface aircraft or a morphing aircraft this procedure is intended to determine the optimal control according to the user's criteria.

The two different models are used with some common parts of geometry:

- Both aircraft use the same airfoils geometry in the main wing.
- The main wing airfoils of both aircraft are kept in the same spanwise relative position.
- The reference aircraft Horizontal Tail (HT) airfoil is the same as the JW rear wing.
- The wingbox chordwise relative positions in the main wing are the same for both aircraft.
- The Vertical Tail geometry is the same for both aircraft.
- The fuselage geometry is the same for both aircraft.
- The payload distribution is the same for both aircraft.

Additional information on the optimization parameters can be found in Vale *et al.* [1]

Table 10-5 and Table 10-6 present the geometrical parameters for the two models optimized. The lifting surfaces are defined by a piecewise linear leading edge line and airfoils at different spanwise stations. Airfoil evolution in the spanwise direction is made by interpolation of between the airfoils defined in the lifting surface segment. The fuselage is defined with a nose, central and end segments. The central segment is a cylinder of prescribed radius. The nose and end segments are parabolic surfaces of revolution. The reference frame has the x axis pointing towards the flight direction and the z axis pointing upwards.

Table 10-5: Reference Aircraft Geometry Data.

LE Position (m)			Chord (m)	Airfoil File	Spars Chordwise Position (%)	
x	y	z			Front	Rear
Main Wing						
6.6949	0.0000	-0.5770	7.573	EMB1	10.4	55.0
3.9655	6.1810	-0.0370	3.995	EMB2	17.2	61.0
0.3684	12.110	0.4820	2.588	EMB3	23.9	68.3
-1.5219	15.7270	0.7990	1.727	EMB4	33.3	68.3
Horizontal Tail						
-12.8741	0.0000	0.5000	3.543	EMB HT	20.0	70.0
-13.831	1.5000	0.6840	2.987	EMB HT	20.0	70.0
-16.8302	5.8330	1.2160	1.382	EMB HT	20.0	70.0
Vertical Tail						
-10.2812	0.0000	1.0000	5.630	EMB VT	13.0	69.0
-11.9420	0.0000	1.9200	5.050	EMB VT	13.0	69.0
-13.0232	0.0000	4.4950	3.426	EMB VT	13.0	69.0
-15.4048	0.0000	7.3700	1.614	EMB VT	13.0	69.0
Fuselage						
		x (m)	y (m)	z (m)	Radius (m)	
Nose		18.4300	0.0000	-0.9302	0.0000	
Central Section	Begin	14.6990	0.0000	0.0000	1.7500	
	End	-4.4255	0.0000	0.0000	1.7500	
End		-18.430	0.0000	1.1520	0.0000	

Table 10-6: Joined Wing Configuration Data.

LE Position (m)			Chord (m)	Airfoil File	Spars Chordwise Position (%)	
x	y	z			Front	Rear
Main Wing						
6.6949	0.0000	-0.5770	7.573	EMB1	10.4	55.0
3.9655	6.1810	-0.0370	3.995	EMB2	17.2	61.0
1.9281	9.1455	0.2230	3.329	EMBJW3	20.5	62.4
0.3684	12.1100	0.4820	2.588	EMB3	23.9	68.3
-1.5219	15.7270	0.7990	1.727	EMB4	33.3	68.3
Rear Wing						
1.9281	9.1455	0.2230	3.329	EMBJW3	20.5	62.4
0.0580	8.6882	0.5000	3.543	EMB HT JW	20.0	70.0
-13.7230	1.5	0.6840	2.987	EMB HT JW	20.0	70.0
-15.4048	5.833	1.2160	1.382	EMB VT	13.0	69.0
Vertical Tail						
-10.2812	0.0000	1.0000	5.630	EMB VT	13.0	69.0
-11.9420	0.0000	1.9200	5.050	EMB VT	13.0	69.0
-13.0232	0.0000	4.4950	3.426	EMB VT	13.0	69.0
-15.4048	0.0000	7.3700	1.614	EMB VT	13.0	69.0

The geometry of the used airfoils can be obtained by request. The files with nodes and elements of the RA used for the panel method formulation can be obtained by request. The files with the FE model used for the initial design and optimal structure designs are available upon request. The files with mission final results for the initial RA, optimal RA and JW aircraft mission are available upon request.

There are fuel consumption estimates made with a different framework and with the same framework with a different propulsion database. In general, the fidelity of the used models is low and therefore the results cannot be used except for a comparative analysis between configurations using the same models. Major deficiencies are in drag calculations in the aerodynamic model and in fuel consumption calculations with the propulsion module.

The computational cost of the models for a single analysis is low but the amount of analysis required for a mission fuel consumption calculation is high. The advantage of such an approach is that once the necessary databases are available, several mission profiles can be analyzed with reduced cost, and the outputs from mission analysis already assist in optimal control determination. Multi-mission analysis based objective functions can also be implemented.

There is no coupled physics in this problem. Each surrogate model is assessed using a sample larger than the database size. The surrogate model results with this new sample are compared with the computed results by

determining the root mean square error. This process is carried out before starting the optimization, if the surrogate model quality is not good, more points are added to the model to improve its quality.

Sub-optimizations are used in the lower level of optimization, when the aircraft configuration is frozen and optimal control is being determined for that configuration in several flight conditions described by the following parameters:

- Speed;
- Altitude;
- Angle of Climb/Rate of Climb;
- Load factor components (nx, ny, nz);
- Payload distribution; and
- Fuel distribution.

These parameters (with exception for the fuel distribution) are determined by the mission profile used in the fuel consumption calculation. Only longitudinal movement was considered in the optimization. Therefore, only the x, z translations and pitch rotation degrees of freedom are used in the sub-optimization.

For the flight conditions specified, the control parameters (throttle, aerodynamic controls and angle of attack) are determined for fuel consumption minimization as the objective function, which is directly related to the throttle control variable.

The constraints depend upon the flight condition desired, namely the angle of climb/rate of climb and the load factor components. For cruise trimmed conditions, for instance, the constraints require the usual Lift = Weight, Drag = Thrust and Pitch Moment = 0.

The sub-optimizations are performed using the FSQP (Feasible Sequential Quadratic Programming) algorithm embedded within the performance model code. They are used for database generation of Consumption and Control Variables vs. Flight conditions, for subsequent surrogate model generation.

Gradients used are finite-difference gradients. Their quality is as good as the quality of the surrogate models of the various disciplines used. Highly nonlinear and noisy databases will decrease the gradient quality.

Linear interpolation of the databases was used as surrogate model for the various disciplines. The finite-difference gradients computed in such way are discontinuous introducing also discontinuities in the objective function and constraints gradients. The objective function minimum tends to be at a point of the sample with gradient discontinuity if the constraints are not active.

The number of runs of the several models used is related to the desired size of the samples. Again, once the databases are computed, the computational time of the sub-optimization is low, but the amount of sub optimizations performed depends on the level of detail desired for the control strategy optimization and fuel consumption determination.

10.2.2.2 Practical Concerns

All software was In-house, non-commercial on the Windows 7, DirectX10.0 platforms. The software can be obtained by request, although it is not easy to use without prior knowledge of the code. The hardware used for this benchmark was Intel(R) Xeon(R) CPU E5620 @ 2.4 GHZ x2, 16 core, 32 GB RAM, 64 bit operating system.

MDA setup time: The user is required to generate the different required databases (aerodynamics, structural, payload, fuel, propulsion). Besides this, the user is required to know the convenient sample for flight conditions to be generated. Once this is done, setting up the MDA takes about 5 min. After the Consumption and Control Variables vs. Flight conditions database is available, the user is required to define the mission(s) segments to be calculated. The setup procedure for this once the mission(s) is defined is about 5 min. If the user uses the existing framework for the disciplines databases generation of all models, it require about 10 min setup time.

The MDA is automatic in the sense that, after the disciplines databases are generated, no intervention is required by the user except in setting up mission calculations analysis. If the MDA fails, a flag is recorded in the databases generation. Subsequent use of the databases excludes the failed analysis.

10.2.3 MDO Problem Definition Details

Design Variables: Design variables are shown in Table 10-7. All the employed design variables in both optimization levels were set continuous (real).

Table 10-7: Design Variables.

Design Variables	Lower Boundary	Upper Boundary	Model	Optimization Level	Type
t_w/c	0.0010	0.0100	B, JW	Upper	Real
t_s/t_{max}	0.0010	0.0100	B, JW	Upper	Real
F_{FW}	0.500	0.800	JW	Upper	Real
F_{AW}	0.275	0.925	JW	Upper	Real
t (throttle)	0.0	1.0	B, JW	Lower	Real
α	-10.0°	10.0°	B, JW	Lower	Real
I_{HT}	-8.0°	8.0°	B	Lower	Real
δ_e	-30.0°	30.0°	JW	Lower	Real

Objective function(s): The lower optimization level objective functions have a single-objective, while the upper level objective function consists in summing all the lower optimization level objective functions without introducing any weights since they are based on the same metric. All objective functions are of minimization type.

- **Multi- or single-objective** – Single-objective (for both upper and lower optimization levels).
- **Min/Max** – Min (for all the objective functions).
- **Comments on function(s) quality: smooth, discontinuous, noisy w.r.t. design variables, etc.** – Linear interpolation of the databases was used as surrogate model for the various disciplines. The finite-difference gradients computed in such way are discontinuous introducing also discontinuities in the objective function gradients. The objective function minimum tends to be at a point of the sample with gradient discontinuity if the constraints are not active.

BENCHMARK: EFFICIENT SUPERSONIC AIR VEHICLE (ESAV)

- **Computational cost** – Not quantified, although one may say that the major computational cost is in the database generation and not in the optimization *per se*.
- **Gradient computation (if used)** – All optimization problems were solved using a gradient based algorithm, the FSQP (Feasible Sequential Quadratic Programming).
 - **Implementation: finite-difference, direct differentiation, adjoint, automatic differentiation, FD complex step, etc.** – Finite-difference were employed.
- **Computational Cost** – Not observed to be very time consuming, however it should be noted that surrogate models were used instead of the discipline models.

See Table 10-8 for optimization information (objective function).

Table 10-8: Optimization Objective Function Information.

Optimization Level	Model	Objective Function	Type
Upper	B, JW	Min Fuel Burned	Single-objective
Lower	B, JW	Min Fuel Burn Rate	Single-objective

Constraints:

- **Equality/inequality** – All constraints were set as inequality constraints in both optimization levels, even for the trim conditions in the lower optimization level inequality constraints were selected using small tolerances.
- **Bounds** – A tolerance of 1e-6 was defined.
- **Comments on function(s) quality: smooth, discontinuous, noisy w.r.t. design variables, etc.** Linear interpolation of the databases was used as surrogate model for the various disciplines. The finite-difference gradients computed in such way are discontinuous introducing also discontinuities in the constraints gradients.
- **Computational cost** – Not quantified, as for the objective function the major contribution to the overall optimization cost was the database generation.
- **Gradient computation (if used)** – The FSQP algorithm was used, which is a gradient based algorithm.
 - **Implementation: finite-difference, direct differentiation, adjoint, automatic differentiation, FD complex step, etc.?** – Finite-difference.
 - **Computational Cost** – Not observed to be very time consuming, although the cost was perceived to be higher than for the objective function as expected since the number of constraints is also higher.

Problem-specific constraint function formulation concerns:

- **Identification of critical load cases and appropriate # of loading conditions** – Two critical maneuvers were set to define the structural layout: 1) 2.5 g pull-up maneuver; 2) -1.5 g pull-down maneuver.
- **Aeroelastic effects or rigid? Updated during MDO? Inertial effects?** – No aeroelastic effects were considered in the calculations, the aircraft was assumed rigid. In the structural analysis, the structure

self-weight was considered. Furthermore, besides the aerodynamic and propulsive loadings, also the engine, payload and fuel weights were accounted for in the calculations by modeling them as lumped masses rigidly linked to the aircraft structure.

- **Is the air vehicle and engine trimmed?** – Trim conditions are set as constraints in the lower optimization level.

See Table 10-9 for optimization information (constraint function).

Table 10-9: Optimization Constraint Function Information.

Optimization Level	Model	Constraint	Type	Tolerance
Upper	B, JW	Max Stress for a 2.5 g pull-up and for a -1.5 g pull-down	Inequality	1e-6
Lower	B, JW	Trim Conditions	Inequality	1e-6

10.2.4 MDO Algorithm

- **Kind: deterministic, reliability-based, robust, etc. optimization** – All the optimizations were set deterministic.
- **Type: shape, sizing, topology, other (geometric, performance such as aircraft engine or determining optimal trim parameters)** – As before mentioned an MDO strategy was especially developed to allow the study of novel configurations and morphing solutions in an optimization environmental at a preliminary level. For this task, a two-level performance based MDO architecture was defined that aims at: flight operation optimization at the lower level (where the control design variables are determined to minimize the fuel burn rate while trimming the aircraft); and aircraft configuration optimization at the upper level (configuration design variables are optimized to achieve the lowest block of fuel burned at the same time that structural integrity is ensured for a 2.5 g pull-up and -1.5 g pull-down maneuvers).
- **Monolithic MDA approaches** – The MDAs were set sequentially for the lower optimization level.
- **MDO approaches** – A partially different MDO architecture, early described, was employed instead of the using an existing one.

Surrogate models (if used):

- **Type: Kriging, RSM, neural nets, etc.** – Linear interpolation.
- **If Sampling technique state type of sampling technique to train model surrogate models: DOE, Latin Hypercube, space filling designs, low discrepancy sequences. Number of samples to train surrogate model.** – A full factorial sampling was employed sweeping the design space coarsely. After some prior runs of the procedure and gaining insight of the optimality design variables regions, the samples where refined in those regions. This way a manageable sample size was maintained. This was the procedure used for the aerodynamics database, which was the largest. For all other disciplines the refined sample size was manageable and the surrogate quality good. Prior knowledge of the level of non-linearity of the database parameters also aids in the sample size decision.

- **Quality metrics? When to update during MDO?** – Root mean square error. Prior to the optimization starts, the quality of the surrogate model was assessed using a larger sample. No updates during the MDO are required using the selected sampling technique, since the entire design space is already swept using the full factorial sampling.

Reliability:

- **Is the algorithm tolerant of MDA (constraint and objective function failures)?** – When the optimization algorithm fails, an error flag becomes active and the framework developed reads this flag. Whenever this flag is active the optimization results in the lower optimization level are discarded in order not to contaminate the results.
- **Does the algorithm cache intermediate results to facilitate restart?** No.

Termination criteria over convergence criteria?

- Consider running optimization a fixed computational budget; or
- Fixed number of function calls; or
- Fixed amount of wall time (schedule).

The stopping criteria prevail over the convergence criteria. Two stopping criteria were used in the optimizations conducted: maximum number of iterations; and maximum number of function calls. The convergence criteria are the tolerances for the objective function and constraints.

10.2.5 MDO Results

10.2.5.1 Design Variables: Initial, Final, and Optimization Iteration History

In Table 10-10 the design variables are divided in 2 categories, upper and lower, which correspond to the design variables of the upper and lower optimization levels. In the next table are summarized the design variables’ boundaries, initial guess and final results for the reference (B) and joined-wing (JW) models. The final results of the lower optimization level design variables are not shown in Table 10-10, due to the very high number of MDO problems in the lower optimization level (2550), instead they are depicted in a series of graphs in Figure 10-3.

Table 10-10: Optimization Design Variable Results.

Design Variables	Lower Boundary	Upper Boundary	Initial Guess	Final Results (B)	Final Results (JW)	Model	Optimization Level
t_w/c	0.0010	0.0100	0.0086	0.0010	0.0100	B, JW	Upper
t_s/t_{max}	0.0010	0.0100	0.0086	0.0054	0.0100	B, JW	Upper
F_{FW}	0.500	0.800	0.755		0.500	JW	Upper
F_{AW}	0.275	0.925	0.827		0.925	JW	Upper

Design Variables	Lower Boundary	Upper Boundary	Initial Guess	Final Results (B)	Final Results (JW)	Model	Optimization Level
t (throttle)	0.0	1.0	0.1			B, JW	Lower
α	-10.0°	10.0°	0°			B, JW	Lower
I_{HT}	-8.0°	8.0°	0°			B	Lower
δ_e	-30.0°	30.0°	0°			JW	Lower

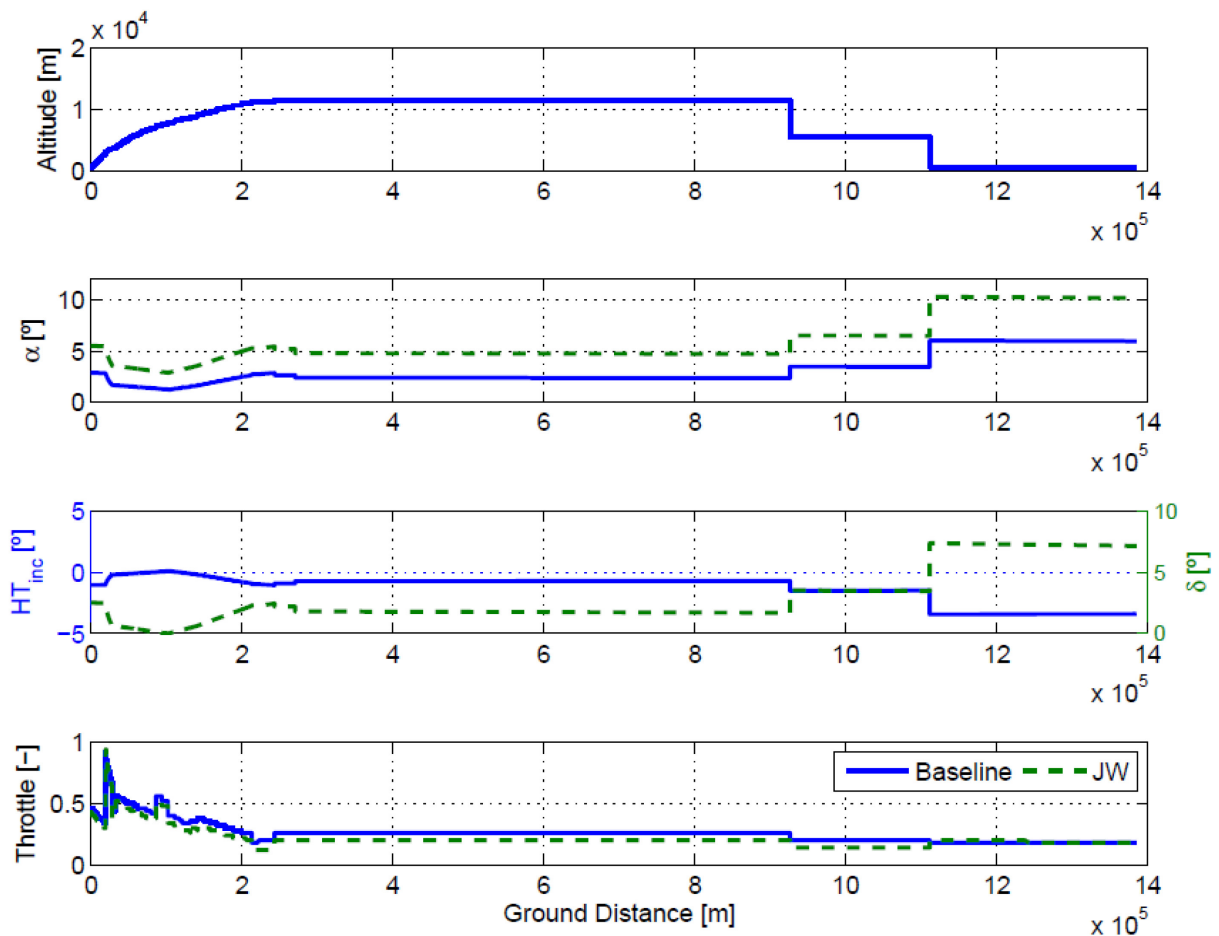


Figure 10-3: Optimization Results.

10.2.5.2 Objective and Constraint Values: Initial, Final, and Optimization Iteration History (Gradient Values if Applicable)

All the constraints (trim conditions) in the lower optimization level were respected and the objective functions were to minimize the fuel burn rate which variation can be observed in the throttle variation (in Figure 10-3).

The objective function and constraint values for the upper optimization level are shown in the Table 10-11 for the reference (B) and joined-wing (JW) models.

Table 10-11: Optimization Objective and Constraint Function Results.

		Initial Guess (B)	Final Results (B)	Initial Guess (JW)	Final Results (JW)
Objective Function	Fuel Burned	1.0017	0.9288	0.8688	0.7976
Constraint	Maximum Stress	-0.3884	-0.0498	1.1185	-0.0023

10.2.5.3 Pareto Fronts

Since the objective functions were of single-objective type, no Pareto front was drawn.

10.2.5.4 Discussion of Physics of Initial and Final Designs

For the reference model, only the structural layout of the lifting surfaces was optimized to improve the comparison between conventional and joined-wing configurations. In this first problem, the optimizer was able to reduce both the structural weight and the fuel burned while fulfilling the maximum stress constraint applied to the critical pull-up and pull-down maneuvers. Unlike in the reference model case, the initial guess is not a feasible solution for the joined-wing case. Despite the fact that the wingbox thicknesses were increased to fulfill the maximum stress constraint, the fuel burned was reduced due to the geometric changes in the aircraft planform. These planform changes were expected results considering the aerodynamic model employed: the aspect-ratio of the front wing increase to the double to reduce the aerodynamic induced drag; and the elevator actuation area in the rear wing was increased to reduce the aerodynamic trim drag.

10.2.5.5 Resource Utilization and Cost

- **Computer hardware used** – Intel (R) Xeon (R) CPU e5620 @ 2.40 Ghz 2.40 Ghz (2 processors); RAM 32.0 GB; 64 bits.
- **Number of exact objective function calls (and gradient calls)** – Not quantified.
- **Number of exact constraint function calls (and gradient calls)** – Not quantified.
- **CPU time, wall time, and time between problem definition and final first optimization** – Despite not quantified, the database generation (for both disciplines and performance optimization problems) was noted to take the highest computational cost in the overall optimization process.
- **How well does the approach parallelize?** – No parallelization was applied in the optimizations conducted, although one can parallelize the several optimizers in the lower optimization level.
- **How are license pools for software managed? How was the process affected by resource limitations (computational, software licenses, hardware, human)?** – Not applicable.
- **Human effort** – Not quantified.

- **Optimization parameter settings** – Finite-differences computed with a step of $1e-6$; a tolerance of $1e-6$ was set for the objective functions and constraints; a maximum of 300 iterations was allowed.
- **Number of optimization iterations; convergence criteria; number of generations** – Not quantified.
- **Comparison of results:**
 - **Compare to results without MDO** – Not performed.
 - **Compare to results with other single-discipline/MDA/MDO methods** – Not performed.
 - **Compare to experimental/validation data** – Not performed.
- **Lessons learned:**
 - Extreme care in the use of Kriging methods for surrogate model generation, due to poor quality of the results when the sampling is not well structured, as in the case of the propulsive databases provided for this work.
 - Kriging methods were found computationally heavy in surrogate generation for high dimension samples.
 - The low fidelity aerodynamic model can easily provide unrealistic results due to the deficient drag prediction. Results need to be carefully analyzed or the problem setup should be made in order to prevent evaluations outside the domain of applicability of the models.
 - Nevertheless, the optimization strategy seems to be adequate for performance based optimization, since the optimization results agree with the modeled physics.
 - The fidelity of the results is directly related to the fidelity of the models generating the databases.

10.2.6 Technical and Financial Improvements/Benefits of Using MDO vs. Traditional Design Methods

The developed framework allows designing an aircraft at a preliminary level using a performance based MDO strategy, which simplifies the definition of the objective function of the problem. Since performance metrics are used, other classic objective functions (for instance, L/D , minimum weight, range or endurance) are implicit in the performance parameters, particularly if the aircraft's purpose is to perform a mission or a set of missions. The problems solved here demonstrate how a solution with higher weight can reduce the overall fuel consumption, for instance. Other points in favor of using databases for different models are the possibility of parallelizing the work and use expert groups for the different fields. Also, the optimization can be performed for different sets of missions without needing to rerun the different disciplines analysis.

10.2.7 References; Web Resources; Science Connect Link; and Validation Data Location

- [1] Vale, J., Afonso, F., Lau, F., and Suleman, A. (2015). Performance Based MDO of a Joined Wing Regional Transport Aircraft. In: Proceedings of the 56th AIAA/ASCE/AHS/ASC Structures, Structural dynamics, and Material conference (SciTech 2015), Kissimmee, Florida, USA. <http://dx.doi.org/10.2514/6.2015-0696>.



Chapter 11 – BENCHMARK: TURBINE MULTIDISCIPLINARY OPTIMIZATION AT THE PRELIMINARY DESIGN PHASE

Hany Moustapha

Ecole de technologie Supérieure
CANADA

11.1 BENCHMARK EXECUTIVE SUMMARY

Traditionally, the design of a gas turbine engine follows two major phases: Preliminary (Conceptual) Design and Detailed Design. At the Preliminary Design (also called Pre-Detailed Design PDD) stage of an engine, the aim is to develop a concept far enough to be able to estimate with reasonable accuracy the performance, weight and cost of the engine. This information is used directly in formulating a proposal to the aircraft manufacturer. The PDD phase is normally characterized by the use of low fidelity tools (correlations and one-dimensional tools) and speed. On the contrary, high fidelity tools are used in the detailed design phase with lots of MDO and iterations between the various disciplines and components.

A number of excellent MDO techniques and design integration initiatives started to show big impact on the way today's gas turbines are being designed. Great emphasis has been placed on MDO in the detailed design phase including system integration, cross disciplines leveraging of tools, and interaction between the various components of the engine as well as between the propulsion system and the aircraft. This was presented in two NATO technology reports [1], [2], which highlighted the following main recommendations:

- Computing codes should be developed with MDO in mind;
- Intelligent or adding guided instructions to MDO;
- Probabilistic optimization and its impact on computing architecture;
- Intelligent computing architecture; and
- Integration with system engineering processes.

However, very little work has been done on the application of MDO in the PDD phase (Preliminary MDO or PMDO) as indicated by Panchenko *et al.* [3] and Brophy *et al.* [4]. Although the use of MDO methodology is indisputably beneficial at every stage of the design process, employing it at the conceptual phase of the design is crucial, since it is at this stage that the largest influence on the final product is realized. During this PDD stage, the successful selection of the final engine concept greatly depends upon the availability of an “Integrated Engine Design System” providing seamless integration and communication between tools, processes and data. Although the integration of tools and processes is not an end in itself, it is the foundation for achieving the ultimate goal of designing an optimum engine system. Key barriers to the development and implementation of such a system include incompatibility of software and hardware, ineffective management of data and a prolific number of analytical tools that do not link easily with other tools (low interoperability).

The focus will be on the “Turbine” part of the engine, being a critical component due to its high temperatures and stresses, cooling, material and coating requirements. The following benchmarking details will first address the overall system architecture and then several turbine modules such as: disc, blade, platform, housing, etc.

11.1.1 Qualitative Optimization Problem Statement

11.1.1.1 Design Variables

Not available.

11.1.1.2 Objective Function(s)

Not available.

11.1.1.3 Constraint Function(s)

Not available.

11.1.2 Description of Analyses/Disciplines/Theory/Fidelities Involved

The overall system architecture, interface and data structure (Figure 11-1), is vital in order to ensure one common data base for all turbine disciplines and later on for all engine components.

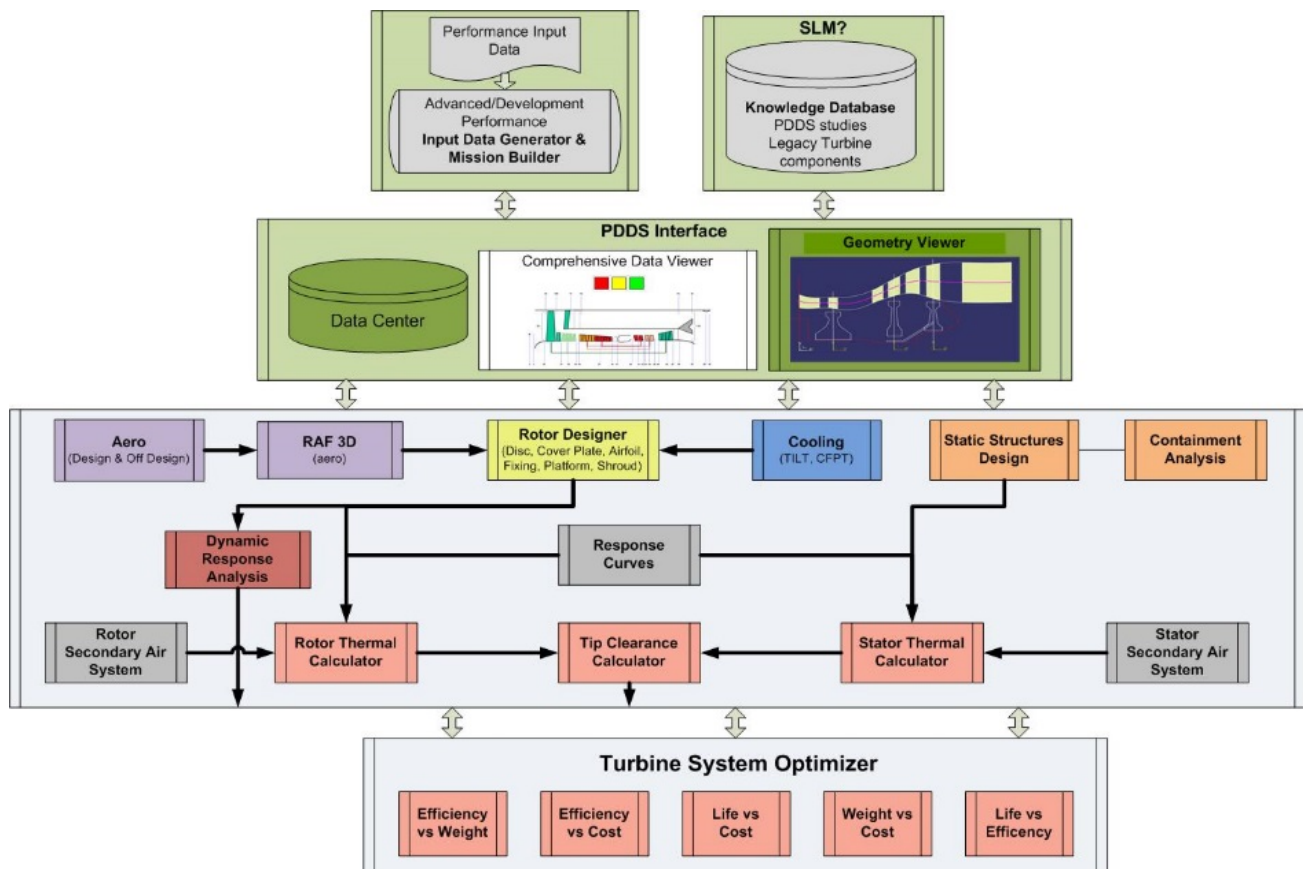


Figure 11-1: Turbine System Optimizer Modules.

Investigation was done on the state of the art software interoperability technical solutions and the development of the first module of a new single platform D&A (Design and Analysis) tool for simulation and prediction of stress and burst behavior at preliminary design stage [5]. This platform singularity requires integration of multiple CAD (Computer Aided Design) and FEA (Finite Element Analysis) tools processing in batch mode and driven from a SPIE (Single Platform Integration Environment, Figure 11-2). The single platform concept has proven to be feasible and a real improvement compared to the present D&A tool, enabling a cohesive single integrated simulation environment that offers reduction on user manipulation and execution time of 30 to 40 %, through an automated and secured system.

11.1.3 MDO Approach (Algorithm/Architecture)

Not available.

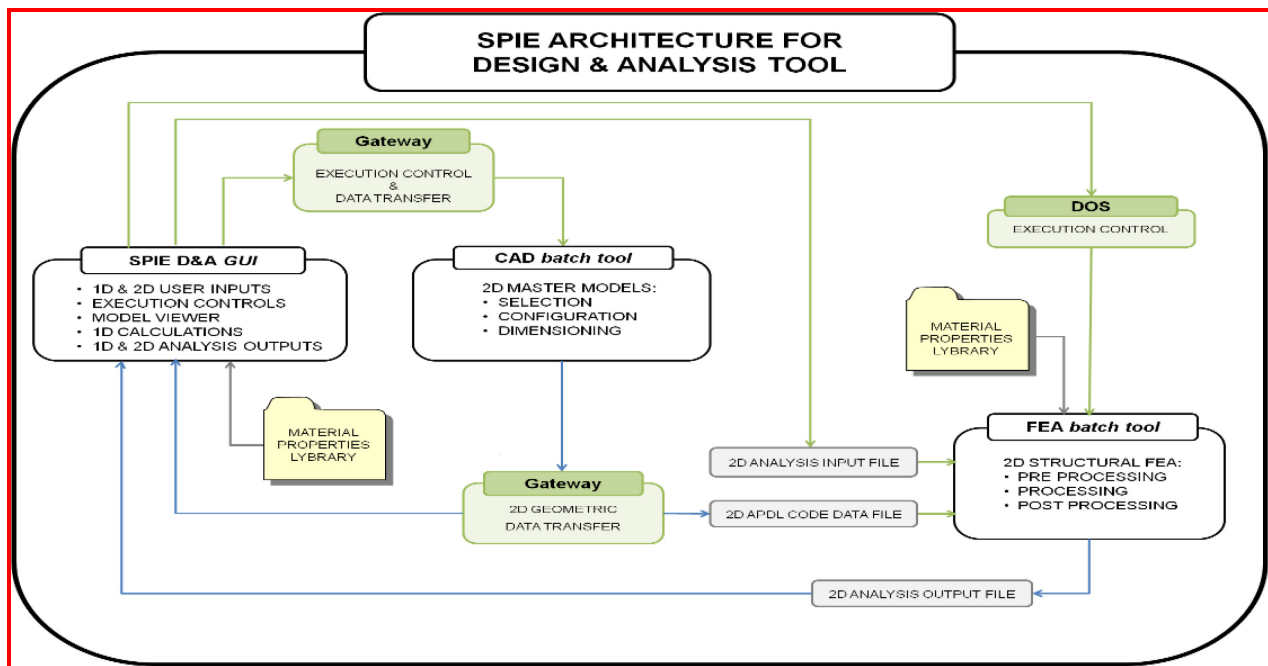


Figure 11-2: Single Platform Integration Environment.

11.1.4 Implementation Details

An optimization of disc geometry was performed by using different optimization algorithms and configurations for a given disc parameterized model. The results showed potential improvement over the current preliminary rotor discs for life and burst limited design [6]. Optimal curves obtained by developing HPT (High Pressure Turbine) disc reference charts (Figure 11-3), indicated how to get the minimum weight for given mechanical performance without running any structural analysis. Those design charts allow engineers to better understand the design space for HPT disc.

Turbine Fixing: Similar to the disc a single platform SPIE was used to create a fully parameterized fixing that is able to model legacy, current designs and provides flexibility to design fixings not yet conceived. Using the automated use of FEA software through a secure and reliable gateway, stress analysis can be performed and the

results displayed back to the user through a GUI. This tool provided a significant increase in quality and time savings of 10 fold to design a fixing when compared to the previous design methodologies [7].

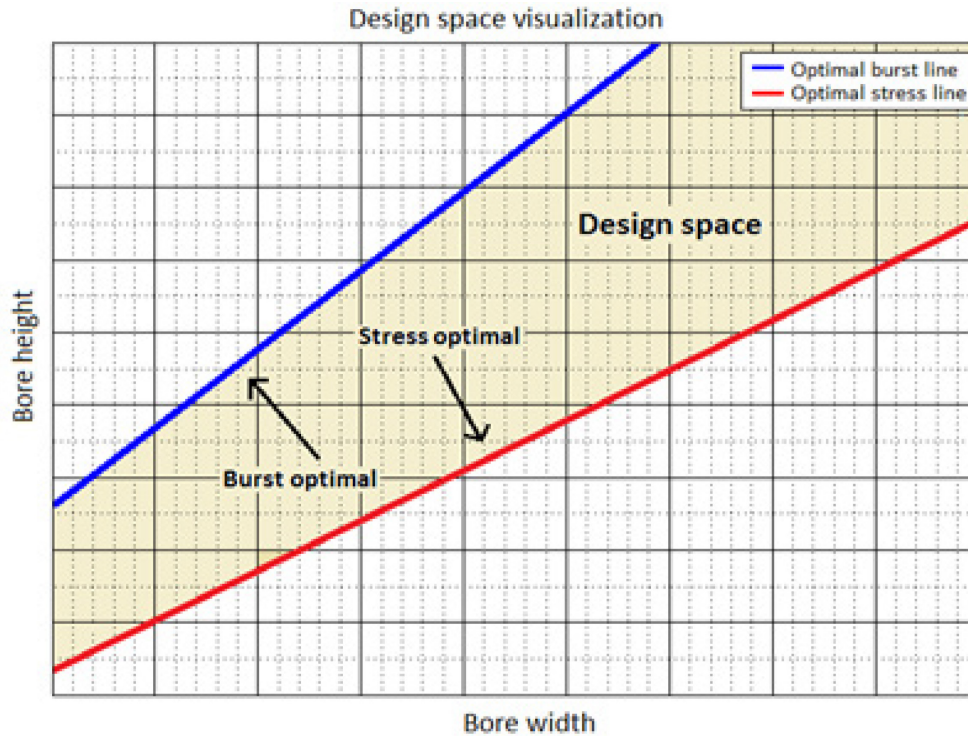


Figure 11-3: Disc Design Charts.

Turbine Cover Plate: Parameterization modeling of the turbine cover plate was achieved by using commercial CAD (computer aided design) software processing. Two main approaches were done: the outer face and the skeleton models. These models were integrated into an iterative process for designing optimal shapes. Both models are capable of reproducing existing cover plate with reasonable accuracy in relatively shorter time periods. However, the skeleton approach provided probably the best results in terms of flexibility and accuracy, but increases programming complexity and requires greater run times [8].

Platform: The platform designing tool is based on a parameterized platform model with a high level of robustness. It is intimately linked with the fixing and provides the location of the fixing starting point definition, a crucial point in a rotor geometry definition. This point location greatly affects all components below the platform as it radially places all of them, thus defining the size of the turbine rotor. The module allows the same kind of analysis performed currently and includes more detailed features while designing. With that amount of features, the model is now able to reproduce almost all existing detailed design currently used in engines on the market.

Housing and Shroud Segments: The concept of PMDO was used for the creation of a new design process for high pressure gas turbine housing and shroud segments. The new design process consists of parametric models and geometry and cooling flow correlations. Dedicated parametric models were created because of their reusability and versatility. Their ease of use compared to non-parameterized models allows more design

iterations and reduces set up and design time. The parametric models, the geometric correlations and the user interface, the new design process was found to be 7 times faster and almost 3 times more flexible than the current design process that used a single non-parameterized model. On the other hand, with the cooling flow correlations, the number of engine parameters was reduced by a factor of 6. A simplified prediction model was created with the remaining parameters to improve the design time with fewer engine parameters and a simplified shroud segment selection process [9]

Rotor Thermal Calculator: In order to develop the Tip Clearance Calculator TCC (Figure 11-4), a Rotor and Stator Thermal Calculator (RTC and STC) as well as an air system generator needs to be developed for the rotor and the stator. The RTC project was divided into three phases. The first phase is the implementation methodology of the thermal Boundary Conditions (BCs) calculator. The second phase describes the analyses set up: importing the conception tools geometry as well as the air system network and the mission conditions, automatic meshing of the turbine components, and application of the thermal BCs. The third phase is the results' numerical validation. Great improvements were obtained when comparing this work's analysis results with regular pre-detailed level tools. It was also found to be faster than the detailed design tools used as a target. By requiring fewer user inputs, this system decreases the risk of human errors while entirely leaving the important decisions to the user [10].

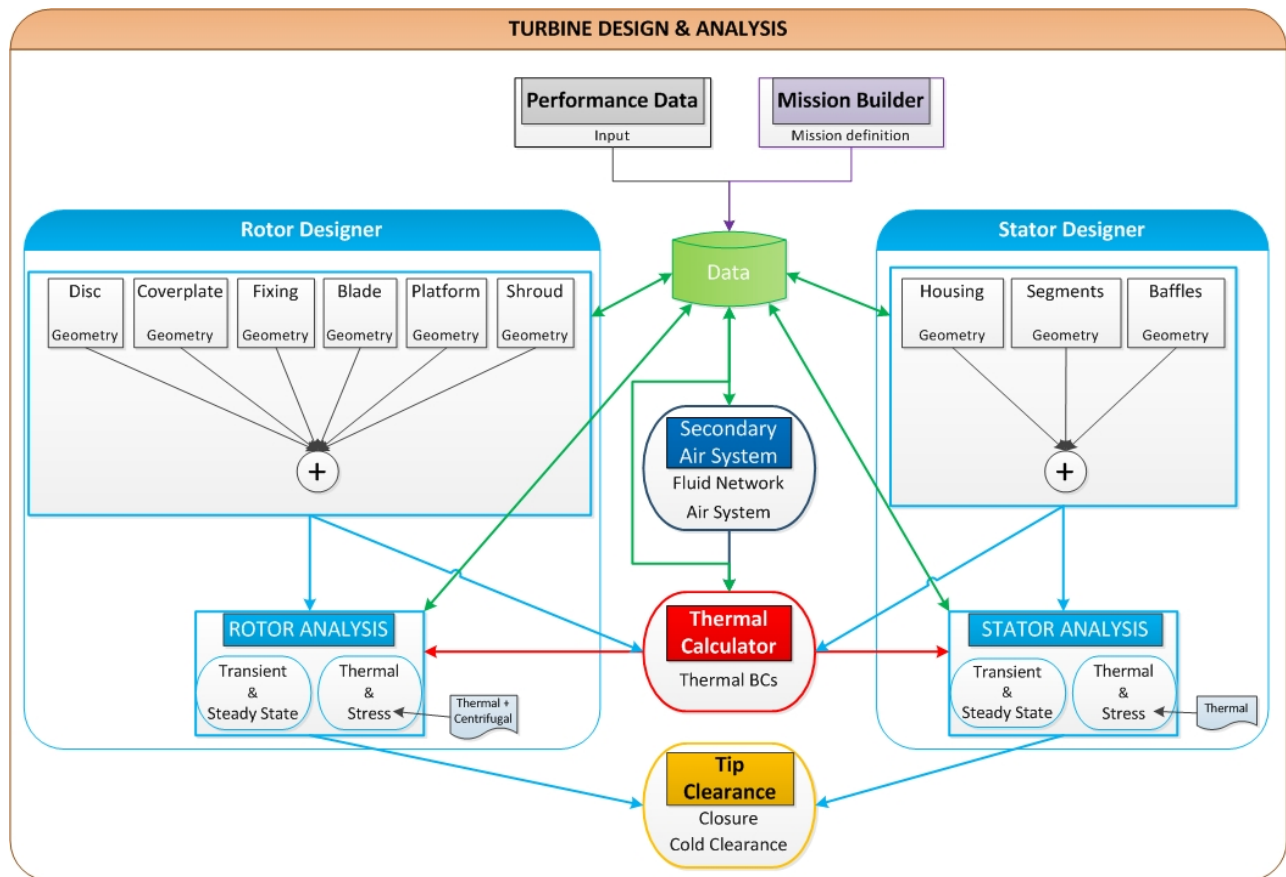


Figure 11-4: Tip Clearance Calculator (TCC).

Rapid Airfoil Generator: The objective is to automate the first pass airfoil generation process, referred to as Rapid Airfoil 3D (RAF 3D) for an uncooled high pressure turbine blades. Using turbine aero mean-line program, in parallel with a database of previously designed airfoils, in-house design rules and best practices, a pre-detailed airfoil shape is defined which can be fed back to other analytical groups for pre-detail analyses, such as for structures and vibrations. Resulting airfoil shapes are aerodynamically validated using an in-house 3D CFD code (Figure 11-5). Based on preliminary results for uncooled airfoils, RAF 3D shortened the turnaround time for turbine aerodynamics group to provide a preliminary 3D airfoil shape to turbine structures group by up to a factor of ten [11]. Additionally, the preliminary assessments of stress and vibration specialists are more accurate as their assessments will be based on a first pass airfoil that has had inputs from all functional groups.

Integrated Rotor System Optimizer: By applying the concepts of PMDO to the design of an uncooled [12], cooled and shrouded turbine rotor, a design system will be created to integrate the design of the platform, fixing, disc and cover plate based on the thermal and mechanical stresses as well as the airfoil based on aerodynamic, thermal and mechanical stresses, and cooling requirements. The system will allow more knowledge to be injected into the design process at the early stage of design, allowing the designer to rapidly synthesize a complete rotor and evaluate its attributes over a range of alternative designs. Starting from a set of design conditions, the system will be able to explore more turbine blade designs that meet or exceed the performance objectives at a higher fidelity. This design system will allow an engineer to explore many more designs than were previously possible, ensuring that a larger design space can be investigated at the early stages of development with a higher degree of fidelity in all disciplines. A highly flexible and robust parametrized model of the shroud will be built as a starting point for the shroud module. The analysis part includes stress calculations (1D and ultimately 3D) as well as creep life. Once those calculations are done, the results will be displayed in a GUI, in relation with the rotor interface. Eventually, the module will include an option to generate a parametric stress location map on the rotor shroud. A turbine airfoil will be developed taking the airfoil geometry generated by RAF-3D as an input. The cooling requirements from CFPT and TILT will be injected in the case of a cooled airfoil and the stress and metal area distribution will be calculated. The Airfoil module will also run CFD to check the aerodynamic performance of the altered geometry before the full 3D airfoil passed on to other modules.

11.1.4.1 Analysis Software

Not available.

11.1.4.2 Optimization Software

Not available.

11.1.4.3 Hardware

Not available.

11.1.4.4 Human Effort

Not available.

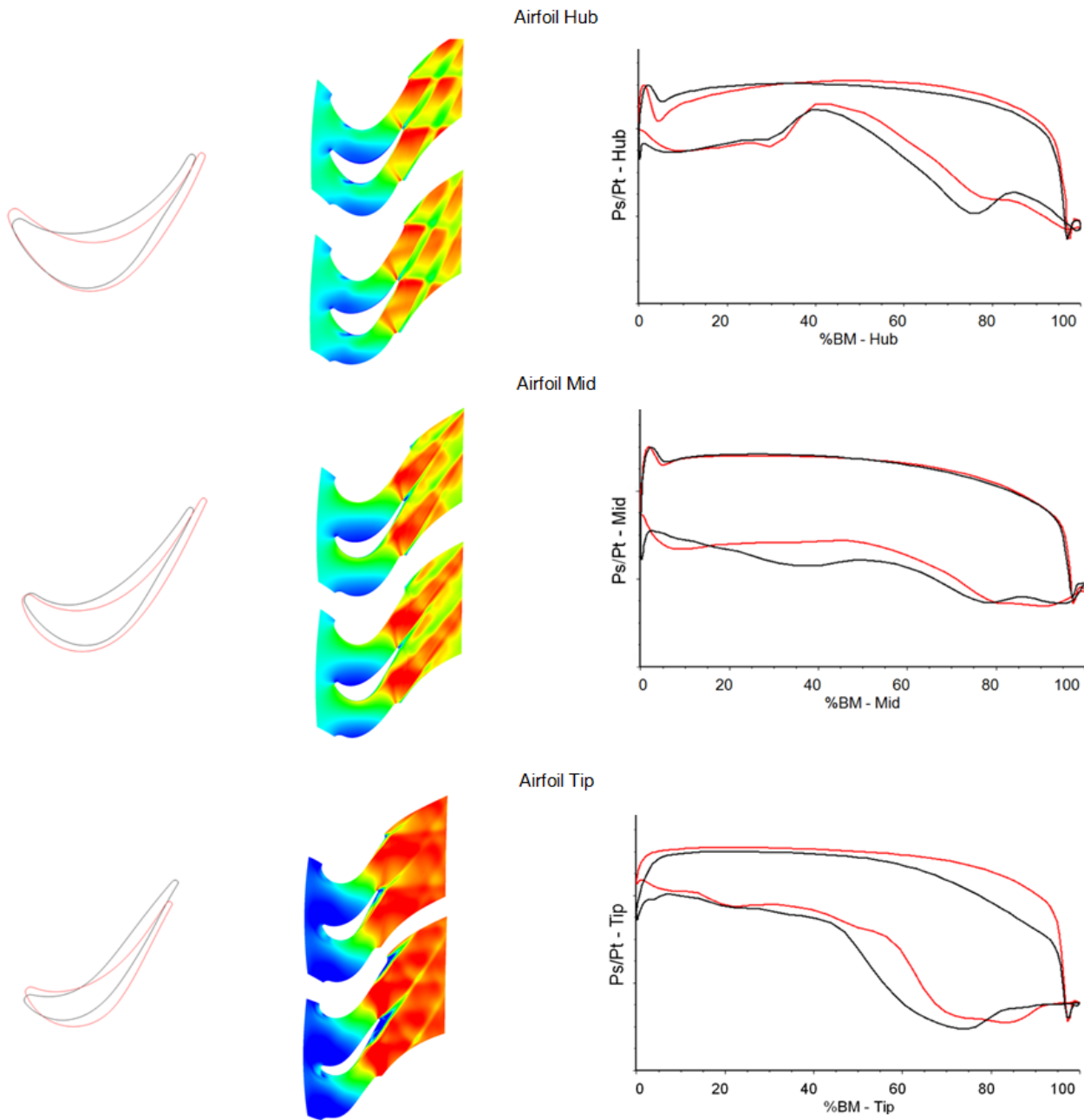


Figure 11-5: Comparison of Final Design (Red) and RAF 3D Concept (Black).

11.1.5 Results

11.1.5.1 Initial Design (Design Variables, Objectives, Constraint Values)

Not available.

11.1.5.2 Optimized Design (Design Variables, Objectives, Constraint Values)

Not available.

11.1.5.3 Observations

- Initial vs. final design physics.
- Comments on impact of MDO changes to initial design.
- Comments on computational cost.
- MDO setup time/effort.
- Comments on robustness of MDO method to MDA failures.

11.1.6 Technical and Financial Improvements/Benefits of Using MDO vs. Traditional Design Methods

Not available.

11.1.7 References; Web Resources; Science Connect Link; and Validation Data Location

- [1] NATO STO (2010). Strategies for Optimization and Automated Design of Gas Turbine Engines, NATO AVT-167 Lecture Series, April 2010.
- [2] NATO STO (2006). Integration of Tools and Processes for Affordable Vehicles, NATO AVT-093 Report.
- [3] Panchenko, Y., Patel, K.V., Moustapha, S.H., Dowhan, M., Mah, S. and Hall, D. (2002). Preliminary Multi-Disciplinary Design Optimization in Turbomachinery Design, NATO-AVT Symposium, Paris, April 2002.
- [4] Brophy, F., Mah, S., and Turcotte, J. (2010). Preliminary Multi-Disciplinary Optimization (PMDO) an Example at Engine Level – Paper 12, AVT-167 Lecture series on strategies for optimization and automated design of gas turbine engine, p. 14. Berlin, Germany: NATO Science and Technology Organization.
- [5] Lagloire, F., Ouellet, Y., Blondin, B., Garnier, F. and Moustapha, S.H. (2014). Single Platform Integration Environment for Turbine Rotor Design and Analysis, Journal of Energy and Power Engineering 8, pp. 1600-1608.
- [6] Ouellet, Y., Savaria, C., Roy, F., Moustapha, S.H. and Garnier, F. (2016). A Preliminary Design System for Turbine Discs, International Journal of Turbo and Jet Engines, DOI: <https://doi.org/10.1515/tjj-2016-0067>, June 2016.
- [7] Twahir, A., Roy, F., Attia, M. and Moustapha (2014). S.H. Preliminary Design and Analysis Tool for Aeroengine Turbine Fixings, IMECE2014, Montreal, November 2014.
- [8] Mesbah, N., Seifert, S., Chatelois, B., Garnier, F. and Moustapha, S.H. (2014). Parameterization Modeling of a Gas Turbine Coverplate, Journal of Energy and Power Engineering 8, August 2014.

- [9] Savaria, C., Garnier, F., Phutthavong, P., and Moustapha, S.H. (2017). Preliminary Design of Turbine Housing and Shroud Segments, *Aeronautical Journal*, 122(1248): pp. 1-23, June 2017.
- [10] Moret, M., Delecourt, A., Moustapha, H., Abenhaimb, A-I. and Garnier, F. (2017). Automated Thermal and Stress Preliminary Analyses Applied to a Turbine Rotor, *Journal of Aerospace Science and Technology*, Vol. 63, pp. 123-131.
- [11] Moradi N. and Moustapha, S.H. (2015). Rapid Airfoil Design for Uncooled High Pressure Turbine Blades, *ASME Turbo Expo*, Montreal, June 2015.
- [12] Twahir, A., Roy, F., Doré S. and Moustapha, S.H. (2017). A Framework for an Integrated Turbine Rotor, *GPPF*, Zurich, January 2017.



Chapter 12 – BENCHMARK: ASSESS THE ABILITY TO OPTIMIZE HULL FORMS OF SEA VEHICLES FOR BEST PERFORMANCE IN A SEA ENVIRONMENT

Gregory Grigoropoulos
National Technical University of Athens
GREECE

Within the overall design process, the optimization of hull forms, for best performance in a sea environment was analyzed. For a range of missions, the applicable warship performance, efficiency and safety criteria were identified. Numerical methods to generate and assess hull form variants, as well as, multi-objective selection methods to identify best candidate hull form variants are recommended.

12.1 BENCHMARK EXECUTIVE SUMMARY

12.1.1 Qualitative Optimization Problem Statement

Within the overall design process, the optimization of hull forms, for best performance in a sea environment was analyzed. For a range of missions, the applicable warship performance, efficiency and safety criteria were identified. Numerical methods to generate and assess hull form variants, as well as, multi-objective selection methods to identify best candidate hull form variants are recommended.

The bio-memetic methods introduced in optimization, supported by the parametric representation of hull lines, opened a new era in the ship design process (Figure 12-1). The geometry of the hull forms can now be correlated to the operational characteristics of the vessels. The application of these new ideas in the optimization of a naval combatant hull form for its hydrodynamic performance is aimed by AVT-204 RTG. Multi objectives are imposed by the missions assigned to the naval ship.

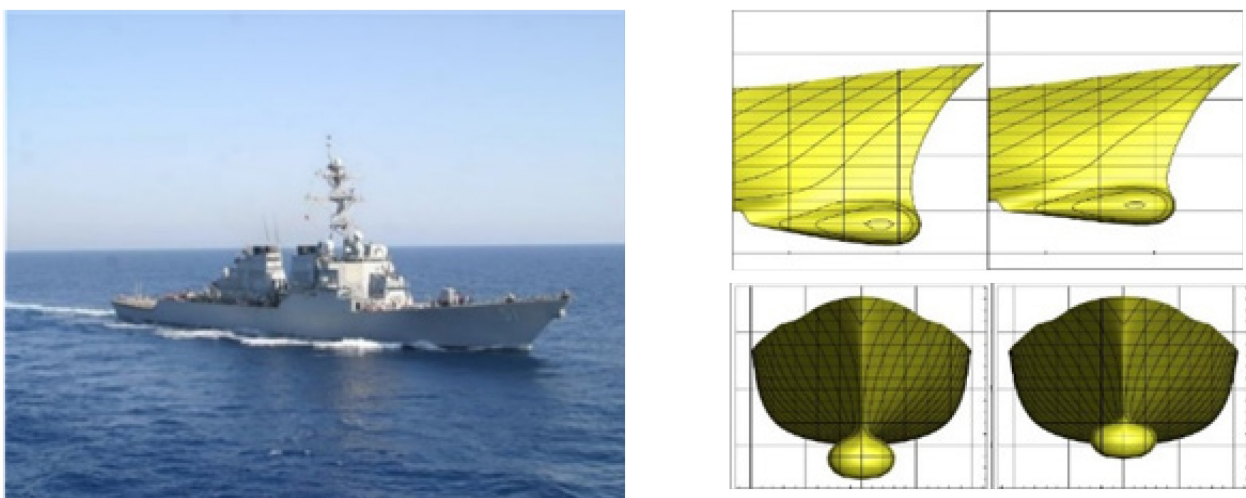


Figure 12-1: Bio-Metric Methods are Used to Design Hull Forms.

12.1.1.1 Design Variables

Not available.

12.1.1.2 Objective Function(s)

The objectives of this RTG were:

- Minimization of calm water resistance at 18 and 30 knots without specifying any lower limit. The best of the hull variants is selected.
- Minimization of vertical acceleration at bridge at 30 knots and head waves, for safe transit operation (TP, HS).
- Minimization of roll motion when the ship sails at 15 knots, in 30-deg. stern waves at 18 knots ship speed, for safe helicopter operation.

In addition, to evaluate and recommend numerical methods to generate and to assess hull form variants, and multi-objective selection methods to identify best candidate hull form variants.

To be more specific the MDO is formulated as follows:

$$\begin{aligned} & \text{Minimize } \{f_1(x), f_2(x)\} \\ & \text{subject to } g_k(x) = 0, k = 1, \dots, K \\ & \text{and to } h_l(x) \leq 0, l = 1, \dots, L \end{aligned} \quad (12-1)$$

where x is the design variable vector, the first objective f_1 is the weighted sum of the normalized total resistance in calm water at 18 kn ($Fr = 0.25$) and 30 kn ($Fr = 0.41$), respectively:

$$f_1(x) = 0.85 (RT/RT_0)^{18kn} + 0.15(RT/RT_0)^{30kn} \quad (12-2)$$

with RT_0 the total resistance of the parent hull. This formulation is based on the expertise of the members and some statistical data from US Navy, that destroyers operate most of their time at the fleet speed (close to 18 kn) and only 15% at the maximum speed (around 30 kn). The second objective f_2 is a seakeeping merit factor, defined as:

$$f_2(x) = 0.5 [RMS(az) / RMS(az_0)]^{30kn, 180 \text{ deg.}} + 0.5 [RMS(\phi) / RMS(\phi_0)]^{18kn, 30 \text{ deg.}} \quad (12-3)$$

where RMS represents the root mean square, az is the vertical acceleration at the bridge (located 27 m forward amidships and 24.75 m above keel) at 30 kn in head long-crested waves (180 deg.), and ϕ is the roll angle at 18 kn in stern long-crested waves (30 deg.). The wave conditions correspond to sea state 5, using the Bretschneider spectrum with a significant wave height of 3.25 m and modal period of 9.7 s. Subscript '0' refers to parent-hull values.

The selected dynamic responses are critical at completely different operating conditions (speed, heading, location along the vessel). However, we assume that similar sea conditions prevail in both cases, which form the seakeeping objective. The contribution of each operating condition in the objective is the same (50%).

12.1.1.3 Constraint Function(s)

Geometrical equality constraints, $g_k(x)$, include fixed length between perpendicular and displacement, whereas geometrical inequality constraints, $h_l(x)$, include limited variation of beam and draught, $\pm 5\%$, and reserved volume for the sonar in the dome, corresponding to 4.9 m diameter and 1.7 m length (cylinder).

12.1.2 Description of Analyses/Disciplines/Theory/Fidelities Involved

Not available.

12.1.3 MDO Approach (Algorithm/Architecture)

INSEAN (Italy) / Univ. of Iowa (USA): The SBDO framework used for the first optimization phase by INSEAN/UI integrates low fidelity solvers of calm-water resistance and seakeeping prediction, a design modification method based on linear expansion of orthogonal basis function, and single/multi-objective optimization algorithm based on the particle swarm metaheuristic [2], [3]. The WAVE Resistance Program (WARP), a linear potential flow code (in-house developed at INSEAN) is used for the calm-water prediction. The Standard Ship Motion program (SMP), developed at the David Taylor Naval Ship Research and Development Center, a potential flow solver based on linearized strip theory, is used for the seakeeping prediction.

The comparison of WARP and SMP with EFD data for the original DTMB 5415 has shown a reasonable agreement. Grid studies have been also performed. Six design spaces are investigated varying the space dimension (with dimensionality ranging from two to six) and the associated design variables bounds. The design space is defined using orthogonal modification functions.

Sensitivity analyses are performed for resistance and motions, showing a significant variability of the performance. The same design spaces are used for single-objective optimization for separate f_1 and f_2 , achieving an improvement by nearly 12% and 13.3% respectively. Multi-objective optimization combining f_1 and f_2 is finally performed. The most promising design produces an improvement of nearly 7% for both, f_1 and f_2 and is selected for further investigation by RANS.

ITU (Turkey): ITU uses a relatively simpler approach in obtaining design modifications (experimental space). The hull form variation is based on a limited number of control points, laying on specific (two in the demo case) waterlines and stations (six in the demo case) along the hull. On these control points relaxation coefficients 1 ± 0.05 are applied to deform the hull form and to generate variants. Each variant is then faired using Akima's method. On the basis of the generated data base of 250 modified hull forms a static Artificial Neural Network (ANN) is trained and the combined (or aggregate) objective function is expressed as:

$$FWC_{combined} = wf_1 + (1 - w)f_2 \quad (12-4)$$

where $w = \{0, 0.1, \dots, 0.9, 1.0\}$ is employed as a weighting factor. The selected optimization algorithm is based on sequential quadratic programming (SQP) within MATLAB optimization toolbox, suitable for constraint optimization problems whose design variables include upper and lower bounds. The optimal forms, for each weighting factor w , are investigated by considering in the ANN training process. The SQP application on the meta-model provided by $FWC_{combined}$ the ANN gives an optimal point, which is expected to be part of the overall Pareto front. Using the above methodology and numerical analysis by low-fidelity solvers (ITU-Dawson and ITU-SHIPMO for calm-water and seakeeping, respectively) point out 7% and 13.5% improvements in resistance and seakeeping performances, respectively, attained by the selected optimal hull.

NTUA (Greece): The optimization is based on the parametric representation of the hull form using CAESES/FRIENDSHIP-Framework. The design is split into a set of surfaces and a total number of ten design variables were selected for hull variation. Five of them refer to the main hull and the rest to the sonar dome. For the hydrodynamic evaluation of the parent and the variant hull forms SWAN2 and SPP-86 potential flow codes are used. The multi-objective optimization with respect to Equation (12-1) is carried out by employing the Non-dominating Sorting Genetic Algorithm-II (NSGA-II, [4]). Parametric modeling using B- and F-Splines, variation and optimization is integrated in CAESES/FFW environment. The hydrodynamic evaluation of the variant hull forms was carried out via the aforementioned codes called within the same environment. The methodology after the generation and the evaluation of 400 faired variants concludes with a Pareto front offering optimized hull forms with varying improvements in resistance and seakeeping. In this case, the improvement in the former results in deterioration of the latter. The selected optimized hull form constitutes a compromise over the two selection criteria, which takes into consideration the magnitude of the improvement in each criterion and its significance on the overall performance of the vessel. The finally proposed optimum hull form offers resistance index reduced by 17% and seakeeping index reduced by 6% over the parent one.

12.1.4 Implementation Details

12.1.4.1 Analysis Software

Not available.

12.1.4.2 Optimization Software

Not available.

12.1.4.3 Hardware

Not available.

12.1.4.4 Human Effort

The human effort was not quantified.

12.1.5 Results

The objective of the work by ECN-CNRS is to validate the optimized geometries (full scale) with their in-house ISIS-CFD code. The flow solver, available as a part of the FINETM/Marine computing suite, is an incompressible unsteady Reynolds-averaged Navier-Stokes (URANS) method mainly devoted to marine hydrodynamics (a typical domain is shown in Figure 12-2).

ECN-CNRS evaluated two designs proposed by INSEAN, the NK-WC (obtained by Neumann-Kelvin linearization with the transverse Wave Cut method and DM-PI (obtained by Double-Model Pressure Integral method), and the designs proposed by ITU and NTUA (Figure 12-3). The latest was found significantly better than the other three with respect to the present rating criteria. Furthermore, the calm water resistance reduction of the optimized over the parent hull form as predicted by SWAN2 2002 software, a potential flow method incorporated in NTUAs methodology, is quite similar to the one derived using the URANS method. The other three potential flow methods overestimate the performance improvement of

the optimized hull. The NTUA geometry offers a 6.1% reduction for f_1 , and specifically an 8.8% reduction of total resistance at $Fr = 0.25$, with a 3% increment at $Fr = 0.41$.

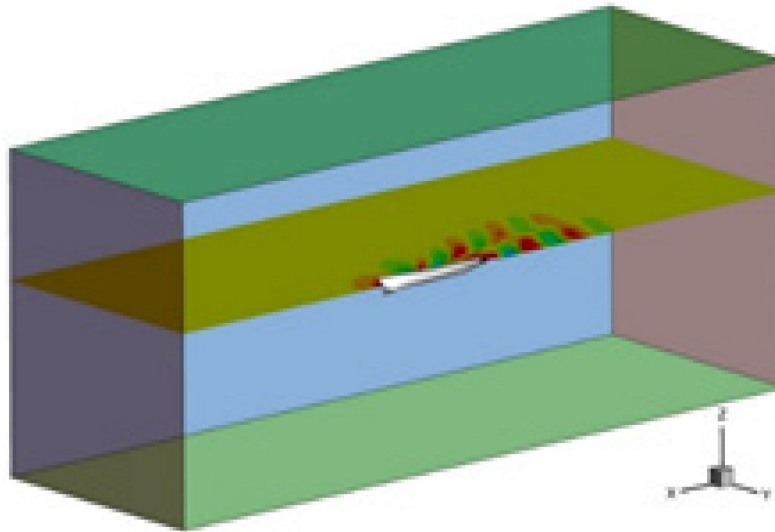


Figure 12-2: ISIS-CFD Computational Domain and Boundaries with a Computed Free Surface.

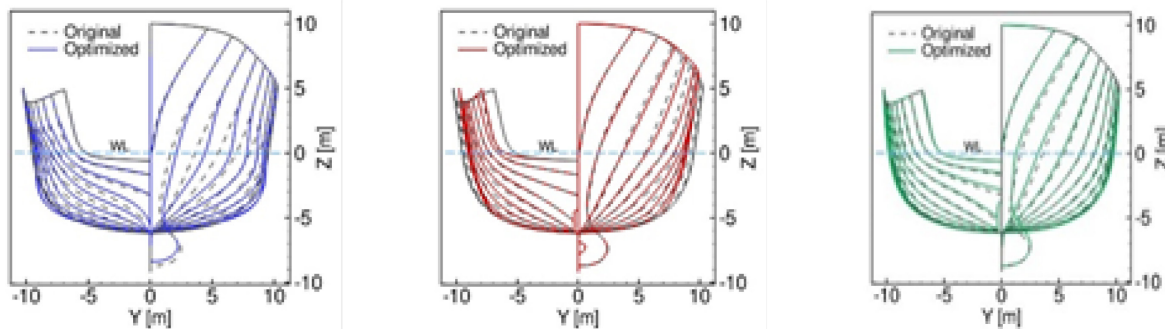


Figure 12-3: Optimized and Original Hull Stations (Left: INSEAN/UI (NK-WC); Middle: ITU; Right: NTUA).

The seakeeping calculations using URANS code were limited and the achieved changes on the vertical dynamic responses were quite limited.

Figure 12-4 and Figure 12-5 show the wave elevation patterns evaluated by ISIS-CFD at $Fr = 0.28$ (used for comparison with experimental data available for the original hull) and $Fr = 0.41$, respectively. A summary of the results is presented in Table 12-1.

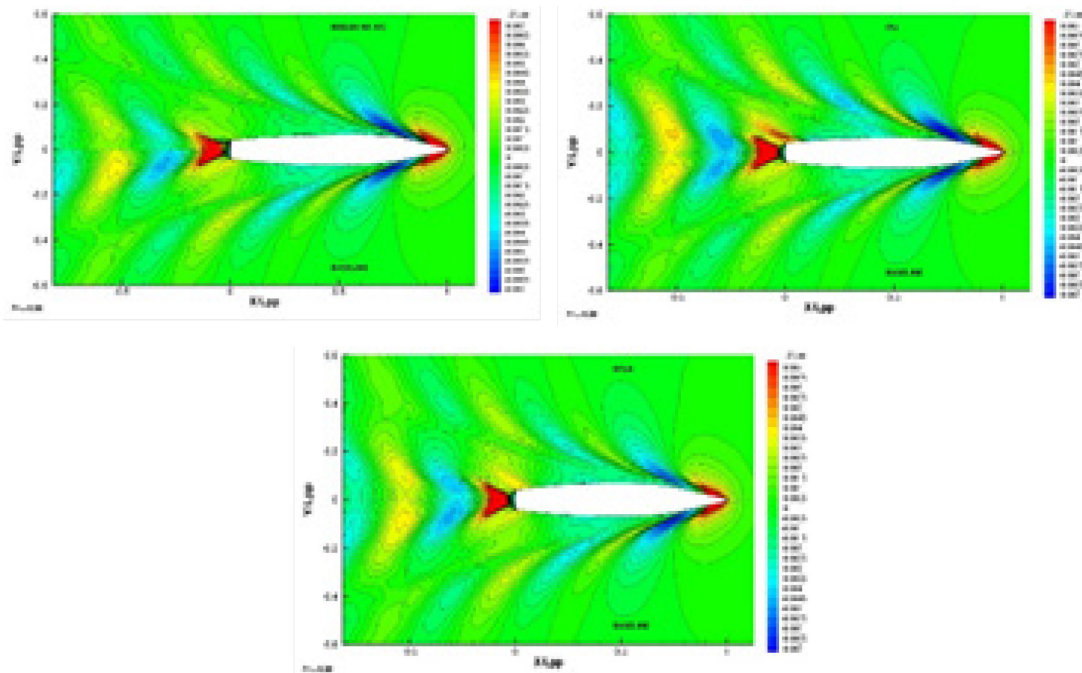


Figure 12-4: Optimized and Original Wave Elevations Distribution for Calm Water at $Fr = 0.28$ Stations (Left: INSEAN/UI (NK-WC); Right: ITU; Below: NTUA).

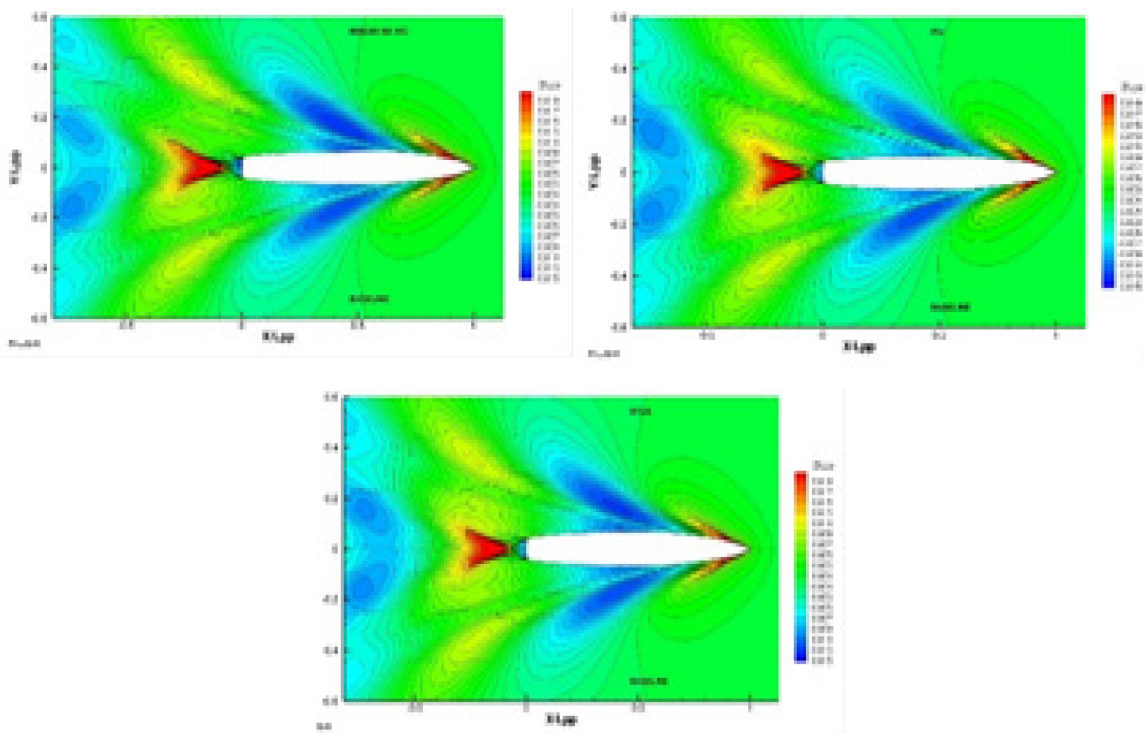


Figure 12-5: Optimized and Original Wave Elevations Distribution for Calm Water at $Fr = 0.41$ Stations (Left: INSEAN/UI (NK-WC); Right: ITU; Below: NTUA).

Table 12-1: Optimization Results Summary – RANS Validation of PF-Based Optimal Solutions.

Geometry	$C_T \times 10^{-3}$ [-] Fr = 0.25	$C_T \times 10^{-3}$ [-] Fr = 0.41	Δf_1 %	RMS(\mathbf{az}) [m/s²] 180 deg	RMS(φ) [rad] 30 deg	Δf_2 %
Original	2.702	4.960	–	1.296	0.018	–
INSEAN/UI	3.018	5.314	9.3	1.254	0.020	3.1
NTUA	2.435	5.112	-6.1	1.314	0.019	0.7
ITU	2.801	5.043	6.2	1.275	0.019	1.2

12.1.5.1 Propeller Optimization for Optimized Hull Form

TUHH team used the in-house boundary element solver panMARE (a typical grid is shown in Figure 12-6) and the wake field provided by ECN-CNRS CFD-code ISIS to design the propeller. The latter always works in an inhomogeneous wake field due to the presence of the ship’s hull in front of the propeller. This wake field is a major design factor for the propeller. Although the propeller is usually designed on the basis of the calm water condition, it has to cope with the real operation conditions where the wake field is unsteady due to the incoming waves and the ship motions. The unsteady field can be a reason for increasing the power demand and the pressure fluctuation amplitudes. Within this study advanced optimization algorithms are used to design propellers with improved characteristics in seaways. The varying wake field is considered at four cases within a cycle of a regular wave, propeller on the crest or the trough and at a wave node moving up or downwards.

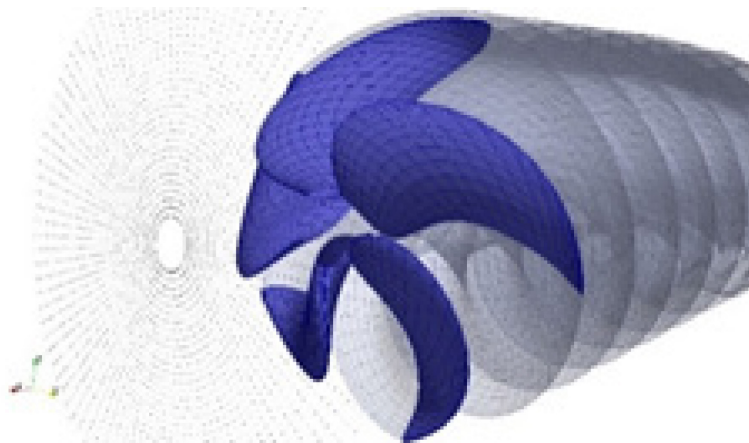


Figure 12-6: panMARE Computational Grid.

The variant propeller designs were evaluated in two stages. The aim of the first stage is to develop geometries, which satisfy the demand for averaged delivered thrust with a minimum value of required torque. In a second stage, a number of most successful designs are investigated regarding their cavitation behaviour.

The goal of this study is to design an optimal propeller for unsteady operating conditions. After a number of simplifications, a numerical setup is achieved that allows for considering the most important physical aspects of the problem. The setup is used to evaluate the individuals generated within a defined search space. The number of individuals which satisfy the imposed constraint is gradually increased with the evolutionary

progress of the optimization. In addition, the propeller efficiency also shows a considerable improvement. The shape of the optimized propeller and the pressure distribution are shown in Figure 12-7. The analysis of the optimized geometries shows that the pitch is reduced at the tip to limit the tip vortex circulation. Accordingly, a slight increase in camber is present. For mid-section parameters, slow convergence behaviour has been observed. The influence of the evolutionary algorithm settings on the results should therefore be studied with regard to accelerating the convergence while retaining the converging character. In a second simulation stage, the best individuals from the evolutionary run are evaluated concerning cavitation probability. Many geometries show little thin cavitating line near the leading edge in the investigated operating conditions. Further numerical studies based on RANS-simulations are needed to check whether phenomena like leading edge vortex may be the reason for local separation in this area. Details may be found in Ref. [1].

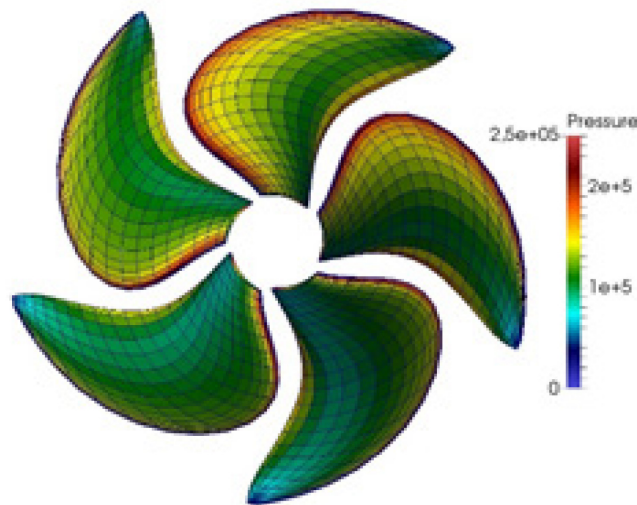


Figure 12-7: Shape and Pressure Distribution on the Optimal Propeller.

12.1.5.2 Initial Design (Design Variables, Objectives, Constraint Values)

Not available.

12.1.5.3 Optimized Design (Design Variables, Objectives, Constraint Values)

Not available.

12.1.5.4 Observations

A multi-objective hull form and propeller optimization of the DTMB 5415 (specifically the MARIN variant 5415M, with skeg only) was investigated using low- and high-fidelity solvers, performed by different research team (INSEAN/UI, ITU, NTUA, ECN-CNRS, and TUHH). Overall, optimization achievements by low-fidelity solvers were found significant, with an average improvement for calm-water resistance and seakeeping performances of 10 and 9% respectively. The most promising designs show up to 16% improvement for the calm-water resistance and 14% for the seakeeping merit factor. The design-space size ranged from two to twelve and the optimized designs show a quite large variability and different characteristic.

INSEAN/UI defined six design spaces with dimensionality ranging from two to six, using a linear expansion of orthogonal basis functions for the modification of the DTMB 5415 bare hull. The optimization was performed by a multi-objective extension of the deterministic particle swarm optimization algorithm. ITU produced 250 hull form variants of the 5415M using Akima's surface generation, with randomly distributed relaxation coefficients at control points over the body surface. The optimization procedure combined an artificial neural network with a sequential quadratic programming algorithm, which is fed with aggregate objective functions. NTUA used the parametric modelling of the CAESES/FRIENDSHIP-Framework for the design modification of the 5415M, representing the hull form by a set of basic curves, providing topological information, and defining a set of 19 sections. The hull surface was parametrized by ten design variables. The NSGA II code was used for the optimization procedure. ECN-CNRS verified parent and optimal hulls, using an in-house high-fidelity solver (ISIS-CFD). The geometry provided by NTUA was selected as the best candidate, providing a 6.1% reduction of the calm water resistance (weighted average at $Fr = 0.25$ and 0.41). TUHH performed the propeller optimization considering the unsteady wake field in waves. Finally, further investigations on the effects of potential flow formulation/linearization on the multi-objective optimization were proposed by INSEAN/UI, along with a RANS-based optimization.

The methodologies proposed have been found a viable option for SBDO. Low-fidelity solvers have shown some limitations in the prediction of the objective trends (especially for the resistance). High-fidelity solvers should be used, whenever possible. SBDO techniques are mature for extension to more complex aspects of the hydrodynamics of naval combatants (maneuvering, intact and dynamic stability, etc.) as well as other items/disciplines (structures, operations, economic management, weight, etc.). Moving to more complex, real-world, multi-disciplinary problems, particular attention should be paid to the trade-off between computational accuracy and cost, and the interplay among the different elements and disciplines involved. Finally, SBDO research would benefit from experimental fluid dynamics (EFD) of original and optimized designs, whenever possible.

12.1.6 Technical and Financial Improvements/Benefits of Using MDO vs. Traditional Design Methods

Unknown.

12.1.7 References; Web Resources; Science Connect Link; and Validation Data Location

Details on the benchmark may be found in:

- [1] NATO STO (2016). NATO STO Task Group AVT-204 Tech. Rep. (STO-TR-AVT-204), Assessing the ability to optimize hull forms of sea vehicles for best performance in sea environment.
- [2] Serani, A., Leotardi, C., Iemma, U., Campana, E.F., Fasano, G. and Diez, M. (2016). Parameter selection in synchronous and asynchronous deterministic particle swarm optimization for ship hydrodynamics problems, *Applied Soft Computing*, 49, pp. 313-334.
- [3] Pellegrini, R., Campana, E. F., Diez, M., Serani, A., Rinaldi, F., Fasano, G., Iemma, U., Liuzzi, G., Lucidi, S. and Stern, F. (2014). Application of derivative-free multi-objective algorithms to reliability-based robust design optimization of a high-speed catamaran in real ocean environment, *Engineering Optimization IV*, EngOpt 2014, Lisbon, Portugal.

- [4] Deb, K., Pratap, A., Agarwal, S. and Meyarivan, T. (2002). A fast and elitist multiobjective genetic algorithm: NSGA-II, *Evolutionary Computation*, IEEE Transactions, 6 (2), pp. 182-197.

No Science Connect link is available.

No validation data are available.

Chapter 13 – BENCHMARK: RELIABILITY-BASED AEROELASTIC OPTIMIZATION OF THE AGARD 445.6 WING

Melike Nikbay
Istanbul Technical University
TURKEY

This multidisciplinary benchmark study was accomplished during the research project titled “Analysis and Reliability Based Design Optimization of Fluid-Structure Interaction Problems Subject to Instability Phenomena” between the years of 2006 – 2010 and was supported by the Scientific and Technological Research Council of Turkey (TUBITAK) through the 3501 National Young Researchers Career Development under grant No. 105M235.

13.1 BENCHMARK EXECUTIVE SUMMARY

13.1.1 Qualitative Optimization Problem Statement

This benchmark study presents a reliability-based multidisciplinary design optimization framework applied to the aeroelastic optimization of the AGARD 445.6 wing. In this framework, an in-house reliability analysis code is coupled with the high-fidelity aeroelastic solutions. The optimization criteria include both deterministic and probabilistic constraints with both structural and aerodynamic uncertainties, such as in the yield strength, Mach number, and angle of attack.

In this framework, a finite volume-based flow solver is used to solve inviscid three-dimensional Euler equations, while three-dimensional solid models are updated using Catia parametrically through optimization. For fluid-structure interaction, a Mesh-based Parallel Code Coupling Interface (MPCCI), is used to exchange the pressure and displacement information between Fluent and Abaqus to perform a loosely coupled aeroelastic analysis.

The reliability-based multidisciplinary optimization process is proven to be fully automatic, modular, and practical, so it can be employed for more advanced applications concerning military vehicle design.

13.1.1.1 Design Variables

The AGARD 445.6 wing is a swept-back wing with a quarter-chord sweep angle of 45 degrees as shown in Figure 13-1. Cross sections of the wing are NACA 65A004 airfoils. The wing has a taper ratio of 0.66 and an aspect ratio of 1.65. Moreover, it is a wall-mounted model made with laminated mahogany. The wing parametric CAD model which is prepared by using Catia-V5 is shown in Figure 13-1.

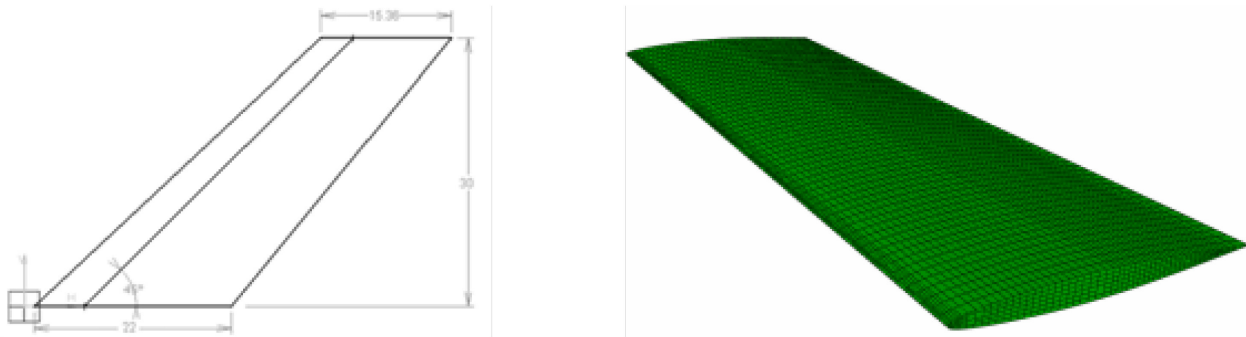


Figure 13-1: Wing Geometry (Length in Inches).

There are two models of the AGARD 445.6 wing in the literature [1]: the solid and the weakened model. In this study the weakened model of the wing is used. The optimization variables are chosen to be the taper ratio and the sweep angle at the quarter-chord. We consider a set of random variables for fluid and structural domain in the reliability analysis which are yield strength, Mach number and angle of attack.

13.1.1.2 Objective Function(s)

This problem is considered to be a multi-objective optimization problem with two objective functions which are the mass of the wing structure and the lift/drag ratio from aerodynamic loads. The first objective function depends only on the deterministic optimization variables while the second objective function depends on both the deterministic optimization variables and the random variables so it becomes a probabilistic objective.

13.1.1.3 Constraint Function(s)

The optimization problem is subject to two reliability based constraints governing the maximum displacement of the wing and the maximum Von Mises stress on the wing.

13.1.2 Description of Analyses/Disciplines/Theory/Fidelities Involved

The aeroelastic analysis and optimization framework involves simultaneous coupling of a solid modeler, a fluid mesh generator, a flow solver (Computational Fluid Dynamics (CFD) discipline), a structural solver (Computational Structural Dynamics (CSD) discipline), a fluid-structure interaction interface and a multidisciplinary optimization driver.

Modefrontier 4.0 is used as a multi-objective and multidisciplinary optimization software to automate the workflow. Here, the finite volume-based flow solver Fluent 6.3.26 is used to solve inviscid three-dimensional Euler equations, three-dimensional parametric solid models are updated using Catia V5-R16 and Gambit is used to generate the fluid domain mesh. The finite element analysis software, Abaqus 6.7.1 was used as a three-dimensional linear, static structural solver to compute the structural response of the aeroelastic system.

The finite element model in Abaqus is composed of 19,610 linear hexahedral structural elements. The computational grid of the flow domain was constructed in Gambit with 691,000 tetrahedral elements and 1.35 million faces. The flow is modeled with the Euler equations. This is a valid approximation for the high Reynolds number flows according to the Prandtl's boundary-layer analysis. Moreover, inviscid flow models give acceptable results for maximizing the lift/drag optimization problems in transonic cruise conditions.

MPCCI 3.0.6 (Mesh-based Parallel Code Coupling Interface) was employed to exchange the pressure and displacement information between Fluent and Abaqus. The advantage of using MPCCI is that it facilitates the exchange of data between nonmatching mesh interfaces of CFD and CSD codes. The staggered algorithm used in this study is demonstrated in Figure 13-2.

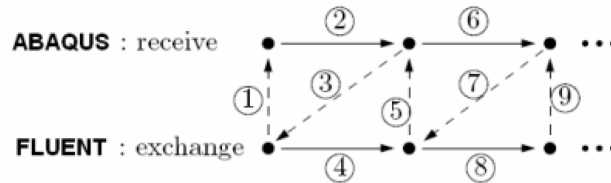


Figure 13-2: Staggered Algorithm for the Aeroelastic Coupling.

13.1.3 MDO Approach (Algorithm/Architecture)

When uncertainties are included in a design optimization problem; a Reliability Based Design Optimization (RBDO) model is formulated as below:

$$\begin{aligned}
 & \text{Minimize : } f(\mathbf{b}) \\
 & \text{Subject to : } P_{fi} = P_i[g_i(\mathbf{b}, \mathbf{X}) < 0] \leq P_{Ri}, i = 1, \dots, m \\
 & h_j^{det}(\mathbf{b}) < 0, j = 1, \dots, n
 \end{aligned}
 \tag{13-1}$$

where $g_i(\cdot)$ represents the performance function, $h_j^{det}(\cdot)$ represents a set of deterministic constraints, \mathbf{b} is the vector of deterministic design variables, and \mathbf{X} is the random parameters of the system. P_{fi} is the probability of failure of the i^{th} probabilistic constraint. P_i is the probability function of the i^{th} probabilistic constraint. P_{Ri} is the required probability of failure level of the i^{th} probabilistic constraint. Here, m is the number of probabilistic constraints and n is the number of deterministic constraints. The probabilistic constraints are defined by the performance functions $g_i(\mathbf{b}, \mathbf{X})$, their probabilistic models, and their required probability of failure levels P_{Ri} . For a given performance function $g_i(\mathbf{b}, \mathbf{X})$, $g_i(\mathbf{b}, \mathbf{X}) < 0$ denotes the failure region, where $g_i(\mathbf{b}, \mathbf{X}) = 0$ is the failure surface and $g_i(\mathbf{b}, \mathbf{X}) > 0$ represents the safe region, as shown in Figure 13-3.

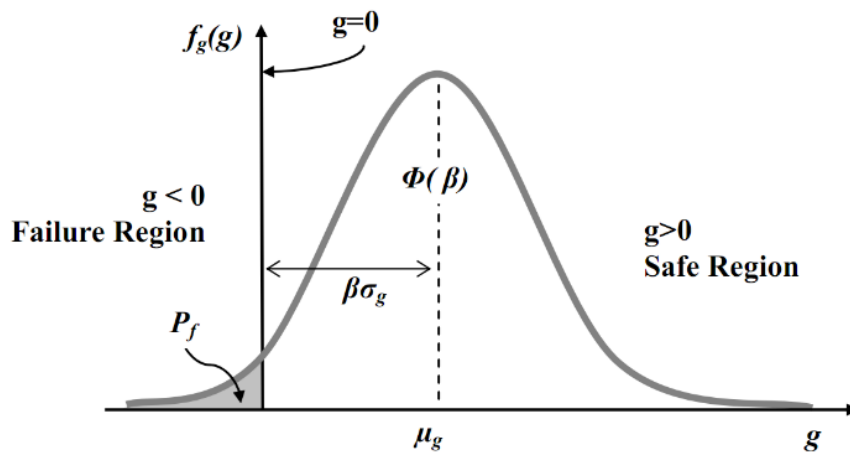


Figure 13-3: Probability Density Function (PDF) for Limit-State Function $g(\cdot)$

The statistical description of the failure of the performance function $g_i(\mathbf{b}, \mathbf{X})$ is characterized by its CDF (Cumulative Distribution Function) $F_{g_i}(0)$ as follows:

$$F_{g_i}(0) = P_i[g_i(\mathbf{b}, \mathbf{X}) < 0] = \int_{g_i(\mathbf{b}, \mathbf{X}) < 0} \dots \int f_X(x) dx_1 \dots dx_n, i = 1, \dots, m \quad (13-2)$$

The evaluation of Equation (13-2) requires reliability analysis where a multiple integration is involved. Some approximate probability integration methods have been developed to provide efficient solutions, such as the First Order Reliability Method (FORM) or Second Order Reliability Method (SORM). FORM often provides adequate accuracy and is widely used for RBDO applications [2] as long as the curvature is not too large. FORM also requires the transformation of the random variables vector \mathbf{X} into the standard normal space as follows:

$$\mathbf{u} = T(\mathbf{X})$$

After the transformation shown in Figure 13-4 is performed, the components of \mathbf{u} are normally distributed with zero means and unit variance and are statistically independent. Thus, Rosenblatt transformation is preferred in this work among possible approaches as follows:

$$u_i = \frac{X_i - \mu_{X_i}}{\sigma_{X_i}} \quad (13-3)$$

where μ_{X_i} and σ_{X_i} represent the mean (first moment) and the standard deviation (second moment) of X_i . As shown in Figure 13-4, the reliability index, β is the shortest distance from the origin to the failure surface in the standard normalized coordinate system.

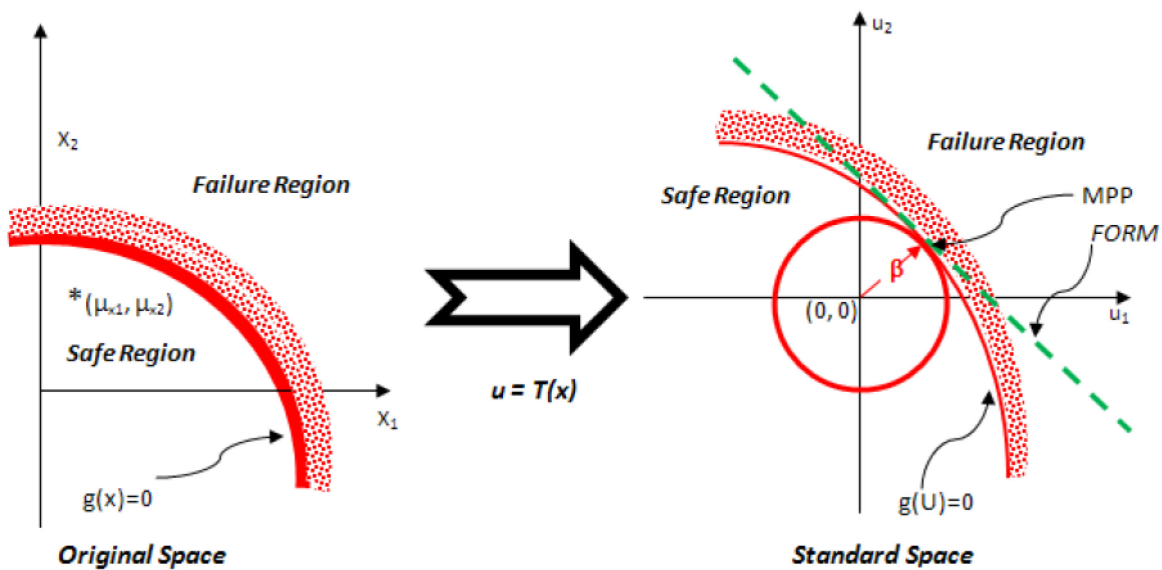


Figure 13-4: Transformation of Random Variables to Standard Normal Space.

$$\beta_s = \min_{\mathbf{u} \in g(\mathbf{u}) = 0} \left\{ (\mathbf{u}^T \mathbf{u})^{\frac{1}{2}} \right\} = \min_{\mathbf{u} \in g(\mathbf{u}) = 0} \{ \|\mathbf{u}\|_2 \} \quad (13-4)$$

Each required probability of failure level of the system P_{Ri} is often represented by the target reliability index as $\beta_{t_i} = -\Phi^{-1}(P_{Ri})$ where Φ is the standard normal cumulative distribution function. Hence, any probabilistic constraint in Equation (13-1) can be rewritten using Equation (13-2) as:

$$F_{g_i}(0) \leq \Phi(-\beta_{t_i}) \quad (13-5)$$

which can also be expressed in two ways through inverse transformations [3] as:

$$\beta_{s_i} = -\Phi^{-1}(F_{g_i}(0)) \geq \beta_{t_i} \quad (13-6)$$

$$g_{p_i} = F_{g_i}^{-1}(\Phi(-\beta_{t_i})) \geq 0 \quad (13-7)$$

where β_{s_i} and g_{p_i} are respectively called the reliability index and the probabilistic performance measure for the i^{th} probabilistic constraint. Equation (13-5) can be employed to describe the probabilistic constraint in Equation (13-1) by using the reliability index and it is called the Reliability Index Approach (RIA). At a given design, the evaluation of reliability index β_{s_i} for RIA is performed using reliability analysis. Using RIA, Equation (13-1) can be rewritten as:

$$\begin{aligned} & \text{Minimize : } f(\mathbf{b}) \\ & \text{Subject to : } \beta_{s_i} \geq \beta_{t_i}, i = 1, \dots, m \\ & h_j^{det}(\mathbf{b}) < 0, j = 1, \dots, n \end{aligned} \quad (13-8)$$

Equation (13-6) can be employed to describe the probabilistic constraint in Equation (13-1) by using the probabilistic performance measure and it is called the Performance Measure Approach (PMA). At a given design, the evaluation of probabilistic performance measure g_{p_i} for PMA is performed using inverse reliability analysis. Using PMA, Equation (13-1) can be rewritten as:

$$\begin{aligned} & \text{Minimize : } f(\mathbf{b}) \\ & \text{Subject to : } g_{p_i} \geq 0, i = 1, \dots, m \\ & h_j^{det}(\mathbf{b}) < 0, j = 1, \dots, n \end{aligned} \quad (13-9)$$

In this benchmark study, probabilistic constraints are evaluated with the Reliability Index Approach (RIA). The following Equation (13-10) presents the Hasofer and Lind (HL) [4] iteration method which is employed to solve the optimization problem in RIA:

$$\beta_s = \frac{\mu_{\tilde{g}}}{\sigma_{\tilde{g}}} = \frac{g(\mathbf{u}^*) - \sum_{i=1}^n \frac{\partial g(\mathbf{u}^*)}{\partial x_i} \sigma_{x_i} u_i^*}{\sqrt{\sum_{i=1}^n \left(\frac{\partial g(\mathbf{u}^*)}{\partial x_i} \right)^2 \sigma_{x_i}^2}} \quad (13-10)$$

Within the MDO benchmark problem, there are two objective functions which are maximizing the $\frac{L}{D}$ (lift/drag) ratio and minimizing the weight as shown in Equation (13-11). The random variables; yield strength σ_{yield} , free stream Mach number M and the angle of attack α are modeled with normal distributions assuming $N(8, 0.4)$ MPa , $N(0.85, 0.03)$ and $N(5, 0.25)$ respectively. The random variable vector at any state is:

$\mathbf{X}_R = [\sigma_{yield}, M, \alpha]$ while the mean value vector of random variables is: $\bar{\mathbf{X}} = [\bar{\sigma}_{yield}, \bar{M}, \bar{\alpha}]$. Then, the multi-objective optimization problem is formulated as:

$$\begin{aligned} & \min_{\mathbf{s} \in \mathcal{S}} M(\mathbf{s}), \max_{\mathbf{s} \in \mathcal{S}} \frac{L}{D}(\mathbf{X}_R, \mathbf{s}) \\ & P \left[g_1^{prob}(\mathbf{X}_R, \mathbf{s}) = \frac{\sigma_{yield}(\mathbf{X}_R)}{\sigma_{max}(\mathbf{X}_R, \mathbf{s})} - 1 \leq 0 \right] \leq 10^{-7}, g_1^{prob}(\mathbf{X}_R, \mathbf{s}) \in \mathbb{R} \\ & P \left[g_2^{prob}(\mathbf{X}_R, \mathbf{s}) = \frac{u_0}{u_{max}(\mathbf{X}_R, \mathbf{s})} - 1 \leq 0 \right] \leq 10^{-7}, g_2^{prob}(\mathbf{X}_R, \mathbf{s}) \in \mathbb{R} \\ & \mathcal{S} = \{\mathbf{s} \in \mathbb{R} | \mathbf{s}_L \leq \mathbf{s} \leq \mathbf{s}_U\} \mathbf{s} = \left(\lambda, \Lambda_{\frac{c}{4}} \right) 0.1 \leq \lambda \leq 0.5 \ 0^\circ \leq \Lambda_{\frac{c}{4}} \leq 50^\circ \end{aligned} \quad (13-11)$$

where $M(\mathbf{s})$ is the total mass of the wing, $\frac{L}{D}(\mathbf{X}_R, \mathbf{s})$ is the lift over drag value for the wing, $g_i^{prob}(\mathbf{X}, \mathbf{s})$ are the probabilistic constraints, $u_{max}(\mathbf{X}_R, \mathbf{s})$ and $\sigma_{max}(\mathbf{X}_R, \mathbf{s})$ are the maximum tip displacement and maximum Von Mises stress of the wing structure. The optimization variables are λ , the taper ratio which is defined as $\lambda = \frac{c_{tip}}{c_{root}}$ and $\Lambda_{\frac{c}{4}}$, the sweep value at the quarter chord. $u_0 = 76$ mm is chosen as reference value to constrain the tip displacement in static aeroelastic response. \mathcal{S} is the set of optimization parameters with lower bound \mathbf{s}_L and upper bound \mathbf{s}_U . In terms of reliability index, the above optimization problem can be expressed as:

$$\begin{aligned} & \min_{\mathbf{s} \in \mathcal{S}} M(\mathbf{s}), \max_{\mathbf{s} \in \mathcal{S}} \frac{L}{D}(\bar{\mathbf{X}}, \mathbf{s}) \\ & g_1^{prob}(\beta_{Stress}) = \beta_{Stress} - \beta_{Target Stress} \geq 0, g_1^{prob}(\beta_{Stress}) \in \mathbb{R} \\ & g_2^{prob}(\beta_{Disp}) = \beta_{Disp} - \beta_{Target Disp} \geq 0, g_2^{prob}(\beta_{Disp}) \in \mathbb{R} \\ & \mathcal{S} = \{\mathbf{s} \in \mathbb{R} | \mathbf{s}_L \leq \mathbf{s} \leq \mathbf{s}_U\} \mathbf{s} = \left(\lambda, \Lambda_{\frac{c}{4}} \right) 0.1 \leq \lambda \leq 0.5 \ 0^\circ \leq \Lambda_{\frac{c}{4}} \leq 50^\circ \end{aligned} \quad (13-12)$$

Here, $\beta_{Target Stress}$ and $\beta_{Target Disp}$ are the target reliability indexes for stress and displacement constraints and chosen as to be 5.1993 for a probability of failure of 10^{-7} . The actual reliability index values for the current design at each optimization iteration is calculated and passed to the outer optimization loop as a constraint. The workflow for the above probabilistic optimization problem is given in Figure 13-5.

13.1.4 Implementation Details

13.1.4.1 Analysis Software

At each optimization iteration, Catia V5 node updates the optimization variables by using the parametric 3D CAD model. Then, the new geometric model is transferred to Gambit in “iges” format. Gambit uses a journal file to prepare the fluid mesh and to update the boundary conditions and then transfers the mesh file to the Fluent node. Fluent updates the optimization variables and imports the mesh files. Next, Fluent prepares the flow model and sets boundary conditions through a journal file and transfers the “case” file to Mpcci for the aeroelastic analysis. In CSD preprocessing, the CATIA V5 node updates the optimization variables by using the parametric 3D CAD model. Abaqus updates the structural model by using a Phyton script and transfers the input file to Mpcci for the aeroelastic analysis. Then Mpcci performs the coupling by using the Fluent and Abaqus models in batch mode. This aeroelastic analysis produces a result file that contains the aerodynamic and structural criteria. At each

optimization iteration, an inner loop for reliability analysis is performed at the MATLAB node for probabilistic constraint check. Modefrontier controls the constraint violation for both deterministic and probabilistic criteria and if needed, new iteration process starts.

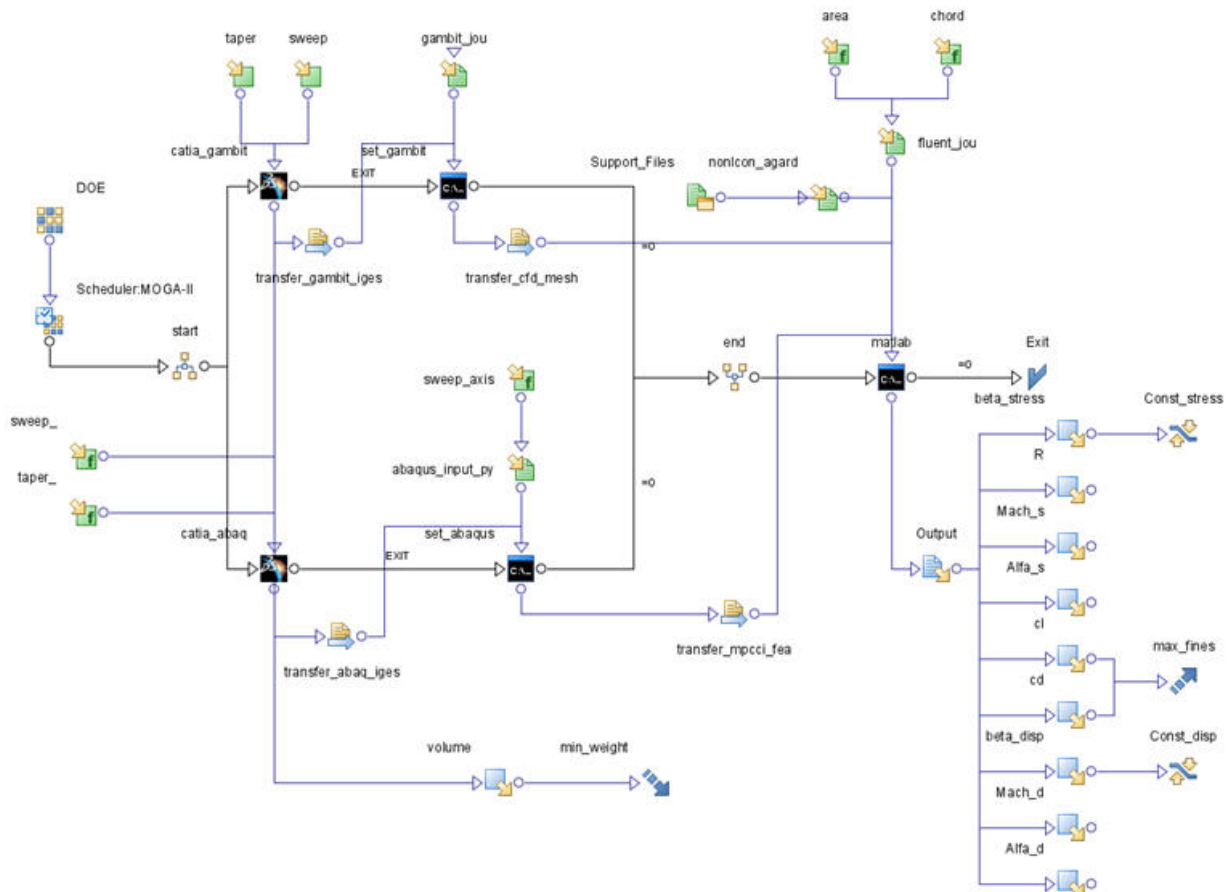


Figure 13-5: Reliability-Based Aeroelastic Optimization Workflow: AGARD 445.6 Wing.

13.1.4.2 Optimization Software

Modefrontier 4.0 is used as a multiobjective and multidisciplinary optimization software. In order to perform an optimization study a work flow should be prepared in Modefrontier to control the optimization process. In this work flow the optimization variables (their limits and increments), scheduler, design of experiments, objectives, constraints, output variables and the software are defined. Optimization work flow is prepared to automate the multi-objective multidisciplinary optimization problem. Once the work flow is run, it controls the optimization process automatically by using the well prepared script files and models.

13.1.4.3 Hardware

Solution of the problem took about 215 hours 40 minutes on a workstation with Intel(R) Core(TM) 2 Quad CPU 6700@2.40 GHz processor, with 2 GB of RAM on a Microsoft Windows XP operating system.

13.1.4.4 Human Effort

The human effort was not quantified.

13.1.5 Results

13.1.5.1 Initial Design (Design Variables, Objectives, Constraint Values)

The original AGARD 445.6 wing has a quarter-chord sweep angle of 45 degrees and has a taper ratio of 0.66. The initial objective function values are: mass 1.831 kg and the lift/drag ratio is 11.4589.

13.1.5.2 Optimized Design (Design Variables, Objectives, Constraint Values)

The workflow shown in Figure 13-5 was let to run with 12 Design Of Experiments (DOE) with “Sobol Sequence” where MOGA-II (Multi Objective Genetic Algorithm II) was used as the optimization algorithm. Finally, a total number of 43 designs were generated for the optimization problem. Twenty-three feasible designs and 20 unfeasible designs were found. As a result, 6 designs are found in the pareto front set for this optimization problem. These paretos are demonstrated in Table 13-1. The design which corresponds to Pareto 3 in Table 13-1 is chosen as the optimum design due to its minimum mass value, satisfactory $\frac{L}{D}$ ratio, while still satisfying the target reliability index constraints.

Table 13-1: Paretos of AGARD 445.6 Wing Aeroelastic Optimization with RBDO.

Variables and criteria	1	2	3	4	5	6
Sweep	8	16	8	10	10	18
Taper	0.225	0.275	0.200	0.225	0.250	0.325
C_D	0.039	0.038	0.040	0.039	0.039	0.037
C_L	0.454	0.447	0.457	0.454	0.451	0.438
β_{Stress}	6.133	5.444	6.323	6.045	5.858	5.233
σ_{yield} (MPa)	6.109	6.484	6.031	6.152	6.221	6.628
M_{Stress}	0.913	0.927	0.911	0.912	0.910	0.933
α_{Stress}	5.823	5.740	5.853	5.828	5.809	5.703
β_{Disp}	5.923	5.296	5.374	5.555	6.057	5.209
M_{Disp}	0.928	1.009	0.924	0.928	0.928	0.936
α_{Disp}	6.333	5.000	6.193	6.228	6.369	6.087
L/D	11.539	11.713	11.534	11.561	11.576	11.767
Mass, kg	1.116	1.182	1.085	1.116	1.149	1.252
Improvement of mass	-39.0%	-35.4%	-40.7%	-39.0%	-37.2%	-31.6%
Improvement of L/D	+0.7%	+2.2%	+0.7	+0.9%	+1.0%	+2.7%

The selected pareto design 3 gives approximately a 40.7% decrease in mass and 0.7% increase in L/D ratio with respect to the reference values of 1.831 kg and 11.4589. All feasible designs are shown in mass vs. L/D ratio space in Figure 13-6, where the regression line, which shows the relationship between objective functions for the feasible design points, is demonstrated. As it is seen from the regression line in Figure 13-6 the L/D values are increasing while mass values are increasing.

13.1.5.3 Observations

In this work, a Reliability Index Approach (RIA) is implemented in an in-house developed RBDO code and integrated into a multidisciplinary optimization framework composed of high-fidelity commercial software. In this computational framework, a finite volume based flow solver Fluent is used to solve inviscid 3D Euler equations and Catia is treated as a parametric 3D solid modeler. Abaqus, a structural finite element method solver, is driven to compute the structural response of the aeroelastic system. Mpcci, mesh based parallel code coupling interface, is utilized to exchange the pressure and displacement information between Fluent and Abaqus to perform a loosely coupled aeroelastic analysis. Modefrontier is employed as a multi-objective and multi-disciplinary optimization driver to control the optimization workflow.

The optimization criteria include probabilistic constraints with both structural and aerodynamic uncertainties. A first order reliability analysis method, Hasofer-Lind iteration method is implemented in MATLAB to compute MPP (Most Probable Failure Point) solution.

The presented reliability based multidisciplinary optimization process is proven to be fully-automatic, modular and practical which could find potential applications in industrial problems with even larger sizes.

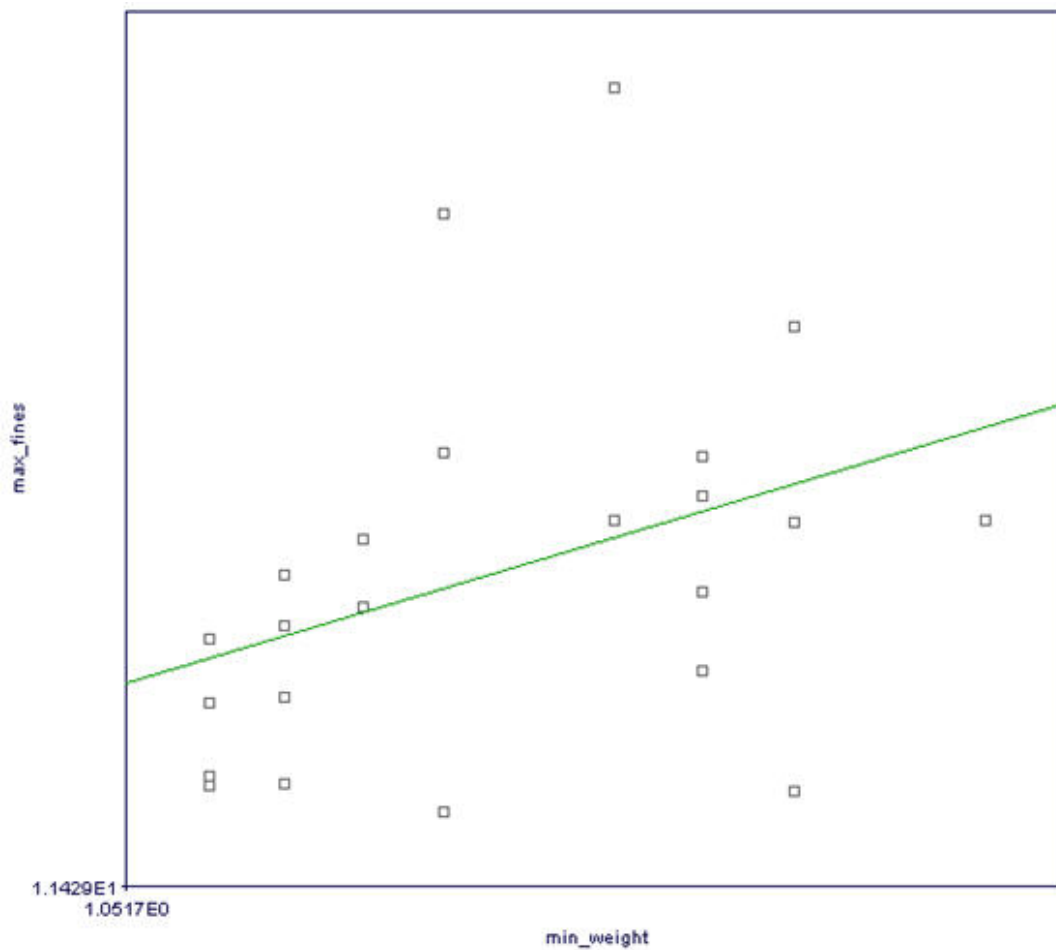


Figure 13-6: Mass vs. L/D Ratio Space.

13.1.6 Technical and Financial Improvements/Benefits of Using MDO vs. Traditional Design Methods

As compared to traditional design methods, this aeroelastic optimization benchmark study demonstrated the important aspects such as fluid-structure coupling, multi-objective optimization through pareto optimal designs and reliability based design optimization as a probabilistic advancement to deterministic optimization. Further details of this framework can be found in Refs. [5] and [6].

13.1.7 References; Web Resources; Science Connect Link; and Validation Data Location

- [1] Yates, E. (1985). AGARD Standard Aeroelastic Configurations for Dynamic Response I-Wing 445.6, AGARD Report No.765.
- [2] Youn, B., Choi, K., and Park, Y. (2003). Hybrid Analysis Method for Reliability-Based Design Optimization. *Journal of Mechanical Design*, Vol. 125.
- [3] Madsen, H.O., Krenk, S., and Lind, N.C. (1986). *Methods of Structural Safety*, Prentice-Hall, Englewood Cliffs, NJ.
- [4] Choi, S.-K., Grandhi, R. and Canfield, R. (2007). *Reliability-Based Structural Optimization*, Springer.
- [5] Nikbay, M. and Kuru, M.N. (2013). Reliability Based Multidisciplinary Optimization of Aeroelastic Systems with Structural and Aerodynamic Uncertainties, *AIAA Journal of Aircraft*, Vol. 50, No.3, pp. 708-715, DOI 10.2514/1.C031693.
- [6] Nikbay, M., Oncu, L., and Aysan, A. (2009). Multidisciplinary Code Coupling for Analysis and Optimization of Aeroelastic Systems, *AIAA Journal of Aircraft*, December 2009, Vol. 46, No.6, pp. 1938-1944, DOI:10.2514/1.41491.

No Science Connect link available.

No validation data are available.

Chapter 14 – BENCHMARK: THE MALE UAV CASE STUDIES AT AIRBUS MILITARY AIRCRAFT

Johannes Schweiger
Airbus Military Aircraft
GERMANY

The Medium Altitude Long Endurance (MALE) UAV, Figure 14-1, reference case was selected at Airbus Military Aircraft for various MDO related activities. The main objective was the fast creation of analytical models in early stages of the (conceptual) design process and the ability to quickly modify those models.

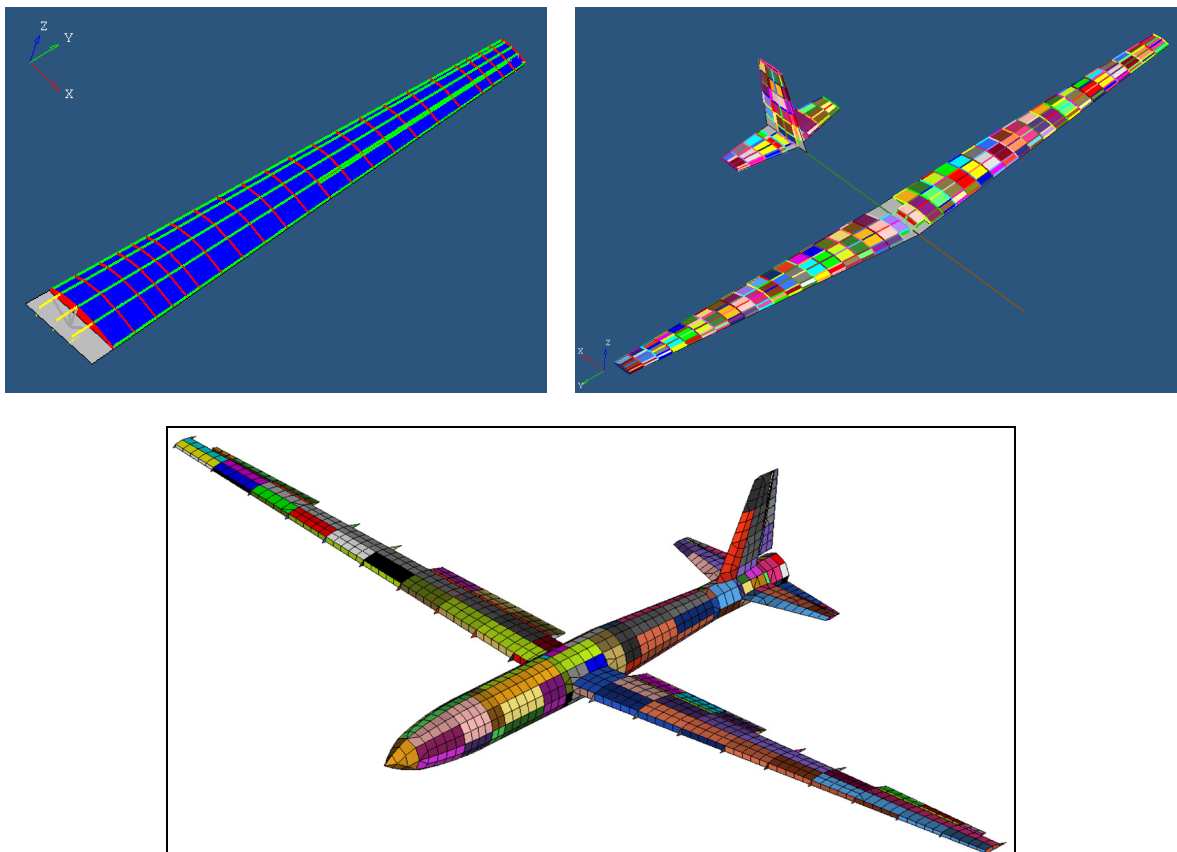


Figure 14-1: The MALE UAV.

Besides MDO-related questions and answers, this document reports on the challenges that exist in the development of the appropriate models, use the tools properly, process and interpret results, draw the right conclusions, and use them to develop alternative ideas for design improvements by alternative configurations.

A few hints are given at the end with respect to the proper simulation of body freedom flutter. Several types of configurations (high aspect ratio, long and slender configurations, flying wings, forward swept wings) are prone for this severe instability, which can usually only be fixed by extensive modifications in the early design process.

This summary report is stored at <https://scienceconnect.sto.nato.int/apps/23705> (AVT-237 data base). The activities and findings are documented in several thesis reports (most of them in German language) and conference papers which are also stored in the AVT-237 benchmarks database.

Additional information can be requested directly via the author of this report.

14.1 BENCHMARK EXECUTIVE SUMMARY

14.1.1 Qualitative Optimization Problem Statement

Structural and multidisciplinary optimizations have a long tradition at Airbus Military Aircraft and its predecessor companies (Cassidian, EADS, DASA, MBB). Starting with the tools FASTOP and TSO, which were developed for and distributed by the US Air Force Research Lab in the late 1970s, were first used and extended, before the inhouse tool LAGRANGE development started in the mid-1980s [1]. Since then LAGRANGE was continuously extended and modernized.

The Medium Altitude Long Endurance (MALE) UAV reference case is depicted in Figure 14-2 for one possible configuration by a mock-up.



Figure 14-2: MALE UAV Mock-Up (Airbus Talarion).

Related activities date back to several earlier efforts in the Airbus Military Aircraft department for Structural Dynamics and Aeroelasticity. Because aeroelastic effects like control effectiveness or flutter stability have essential impacts on the vehicle performance and the required structural stiffness, and because the magnitude of these effects is dominated by the external shape and placement of the vehicle's heavy internal and external equipment, it is essential to perform related analytical investigations as early as possible in the design process.

In most cases, however, the traditional or “official” approach in the aerospace industry today is:

- 1) Conceptual design without analytical structural efforts and without considerations with respect to aeroelastic effects;
- 2) Establishment of the “official” structural analytical model and related load cases;
- 3) Modification of the model for structural dynamic needs (integration of masses, corrections for the proper representation of stiffness); and
- 4) Perform aeroelastic analysis tasks.

This approach typically lasts more than a year – after the end of the conceptual design freeze! The most time-consuming task is the creation of the analytical model, which is usually performed on the basis of a CAD model.

For this reason, Airbus Military Aircraft started efforts in the disciplinary departments (aeroelasticity, tools development) and in conceptual design in the early 2000s to resolve this problem.

In a first effort, an Excel-based tool was created in the structural dynamics and aeroelastic department for the fast creation of analytical structural and aerodynamic models for main aerodynamic surfaces. Figure 14-3 from Ref. [3] shows an example for a wing with various tip surfaces.

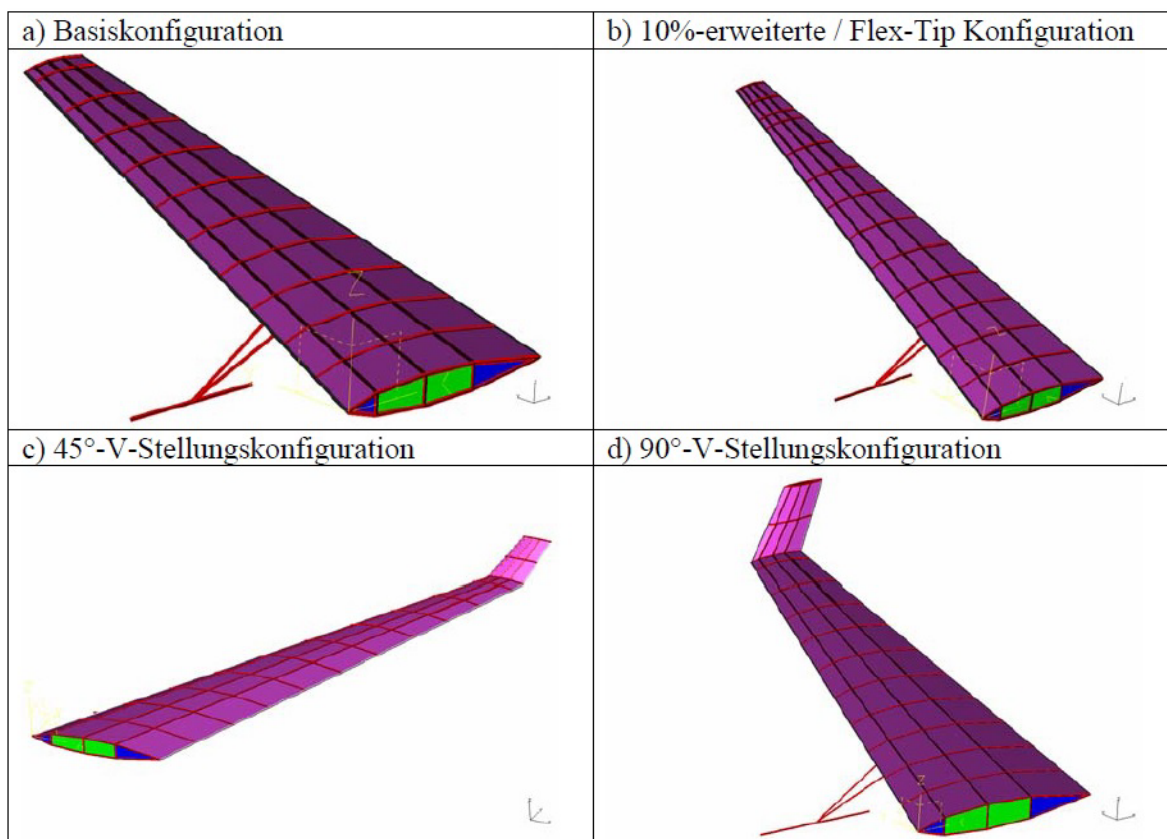


Figure 14-3: Excel-Based Creation of Wing Models with Different Tip Surfaces.

Because conceptual design activities are usually performed before disciplinary departments get involved, at least for structural design and related tasks, it was decided in 2011 to implement the MDO process in the conceptual design department. It was the initial intention to perform this task in collaboration with the (structural) analytical tools development department where LAGRANGE and related tools are hosted. Unfortunately, the ideas about the architecture of the analytical model creation process diverged between both departments and resulted in different approaches. But it was agreed that the MALE configuration will be used as a reference case for both approaches. These efforts are reported here.

It was not intended to investigate the impacts from changing design requirements on a design, or to improve or optimize a specific concept. The MALE UAV only served as a reference case to develop or improve tools, and investigate their proper and efficient use.

The reference configuration, depicted in Figure 14-4, is a classic 3-surface design with a rear horizontal stabilizer attached to a single vertical tail at its bottom, mid, or top position (T-tail) and two engines attached to the wings or to the rear fuselage, as well as one or on or two large payloads attached to the wings and/or carried in an internal bay. The figure also shows the different main zones for the model, which are used for the model creation process. See Table 14-1, Table 14-2, and Table 14-3 for aircraft design data.

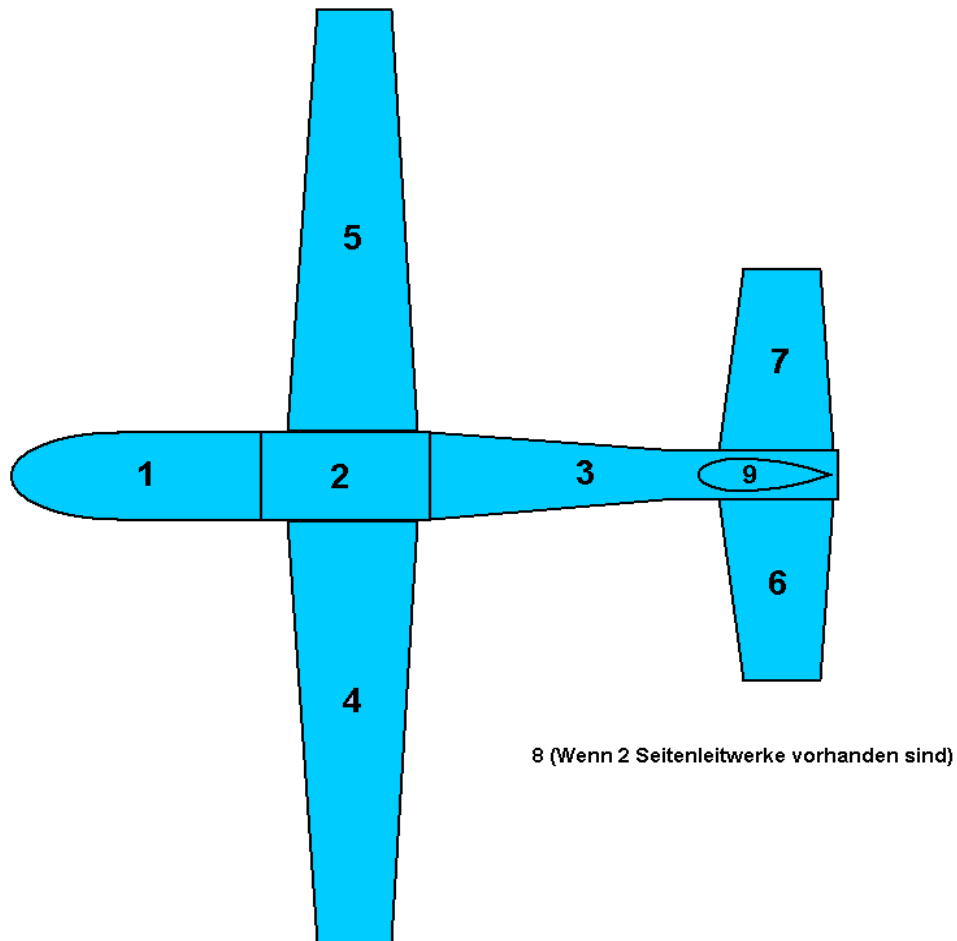


Figure 14-4: Model Geometry and Zoning.

Table 14-1: Main Geometry Data for the Reference Configuration.

	Wing	Horizontal Tail	Vertical Tail
Span	32 m	6 m	3,2 m
Area	52.4 m ²	8,5 m ²	6,0 m ²
Aspect ratio	19,5	4,2	3,4
Taper ratio	0,38	0,56	0,49
Leading edge sweep angle	4,5°	10,5°	30,0°
Trailing edge sweep angle	-0,77°	-5,0°	10,0°
Dihedral	2,0°	0°	(90°)
Airfoil	Laminar airfoil; 15,2% thickness	NACA64A010; 10% thickness	NACA64A010; 10% thickness
Root coordinates	(6,3/0/0) m	(13,5/0/0) m	(13/0/0) m
Estimated structural mass	1300 kg	100 kg	90 kg

Table 14-2: Additional Design Data.

Fuselage	15.5 m length
	1.6 m diameter at wing root
	1.0 m diameter at stabilizers attachment
	3000 kg estimated mass for structure and equipment
Total Aircraft	CG at 41% MAC (7,4/0/0) m
	800 kg payload
	5300 kg estimated OW
	4700 kg max. fuel
	10000 kg estimated MTOW
	Mach 0.6 max. speed

Table 14-3: Airfoil Data.

Upper Surface			Lower Surface	
x/c	y/c		x/c	y/c
0	0		0	0
0,001621	0,01707		0,001621	-0,001976
0,006475	0,026197		0,006475	-0,00493
0,014529	0,036312		0,014529	-0,007513
0,025732	0,04699		0,025732	-0,01001
0,04001	0,057142		0,04001	-0,012525

**BENCHMARK: THE MALE UAV CASE
STUDIES AT AIRBUS MILITARY AIRCRAFT**



Upper Surface			Lower Surface	
x/c	y/c		x/c	y/c
0,057272	0,066677		0,057272	-0,014983
0,077405	0,075746		0,077405	-0,017226
0,100279	0,084202		0,100279	-0,019318
0,125745	0,092004		0,125745	-0,021214
0,153638	0,099088		0,153638	-0,022877
0,183777	0,105433		0,183777	-0,024304
0,215968	0,110974		0,215968	-0,025466
0,25	0,115663		0,25	-0,026357
0,285654	0,119458		0,285654	-0,026977
0,322698	0,122299		0,322698	-0,027302
0,360891	0,124114		0,360891	-0,02733
0,399987	0,124809		0,399987	-0,027065
0,439732	0,124264		0,439732	-0,026505
0,479867	0,122351		0,479867	-0,025652
0,520133	0,118919		0,520133	-0,024494
0,560268	0,113813		0,560268	-0,023028
0,600013	0,106947		0,600013	-0,021274
0,639109	0,098407		0,639109	-0,019239
0,677302	0,088455		0,677302	-0,016865
0,714346	0,077492		0,714346	-0,014081
0,75	0,06623		0,75	-0,010938
0,784032	0,055549		0,784032	-0,007663
0,816223	0,046102		0,816223	-0,004646
0,846362	0,037889		0,846362	-0,00213
0,874255	0,030724		0,874255	-0,000215
0,899721	0,024801		0,899721	0,001069
0,922595	0,020019		0,922595	0,001761
0,942728	0,015794		0,942728	0,001957
0,95999	0,01182		0,95999	0,001782
0,974268	0,008107		0,974268	0,001378
0,985471	0,004834		0,985471	0,000884
0,993525	0,002244		0,993525	0,000429
0,998379	0,000577		0,998379	0,000113
1	0		1	0

14.1.1.1 Design Variables

Structural element gages. Limited efforts for aerodynamic shape. External geometry variables are treated by parametric variations.

14.1.1.2 Objective Function(s)

In addition to the aircraft mass, the required time and efforts for the creation of analytical models, preparation of inputs for analysis and optimization, as well as the proper approaches for results evaluation were the main non-technical objectives.

In addition, the versatility of the methods and tools for more or less massive changes of the analytical models with respect to basic configuration, structural concept, and top-level design requirements were essential to set up the tools and processes. See Table 14-4 for a summary of time requirements for MDO process.

Table 14-4: Time Requirements for the MDO Process.

Time to prepare the first model and analysis/optimization inputs for a completely new configuration	4 days or less
Assessment of first results	1 day
Computing time for a typical optimization	Below 15 minutes
Computing time for an analysis	Below 2 minutes
Prepare and perform additional analysis or optimization with modified inputs	1 hour
Major change to the baseline configuration	Below one day

14.1.1.3 Constraint Function(s)

Static strength (and buckling), flutter stability, aeroelastic (roll) effectiveness.

14.1.2 Description of Analyses/Disciplines/Theory/Fidelities Involved

The main objective of the various activities was the implementation of analytical structural (FEM) and multidisciplinary analysis and optimization in the conceptual design department. This requires simple and robust analytical models (FEM, non-structural masses, steady and unsteady aero, coupling method), creation of the analysis and optimization input data, definition of load cases, performance of analytical tasks, and results evaluation. It was agreed to use the Airbus Military Aircraft inhouse MDA&O tool. Because only one person is usually tasked in conceptual design for this purpose, the process has to be simple, and only a limited set of software tools should be required. However, the required knowledge in the involved disciplines and software tools still requires a lot of experience or learning efforts. The intended approach was a joint effort by conceptual design and the analytical tools department. The activities however ended up in two parallel approaches – by conceptual design as well as by the tools specialists.

14.1.3 MDO Approach (Algorithm/Architecture)

The Airbus tool LAGRANGE has a set of different optimization methods available, among them RQP, SLP, CONLIN, SCP, NLPQL.

14.1.4 Implementation Details

The new model and analysis input data creation tool and process in the conceptual design department was named “CMC” for Concept Model Creator. The alternative approach by the (structural analysis) tools development department uses an “OPEN CASCADE” approach, which, among others requires the creation of a CAD model (CATIA) in order to create the parametrized structural and aerodynamic models. Both approaches then use the Doublet Lattice method for the creation of unsteady and steady aerodynamic influence coefficient matrices.

The conceptual design department approach is based on a C++ programme which allows setting up the complete input for steady and unsteady aerodynamic models, FE model (NASTAN bulk data deck), aero-structure coupling, non-structural masses, LAGRANGE analysis and optimization inputs based on an Excel sheet with very few information about the baseline model and the desired model discretization. The programme, called Conceptual Model Creator (CMC), developed by Moritz Büsing, is described in his diploma thesis report [4] and in an AIAA paper [5].

14.1.4.1 Analysis Software

Figure 14-5 depicts the global model creation process. An excel file is used to summarize the required model definition data. These are then used by the core program “CMC” to prepare the so-called strip models (“Streifenmodell”) for spanwise sections of the main components, the inputs for the definitions of individual elements, and to process the airfoil data for the z-coordinates. CMC then generates the inputs for:

- 1) The finite element model;
- 2) Design variables;
- 3) Aerodynamic model definitions; and
- 4) Aero-structure coupling procedure.

Figure 14-6 shows the numbering scheme for structural and aerodynamic sub-components. The individual elements within one strip are arranged as shown in Figure 14-7.

The structural analysis tools development department approach is very well documented in Ref. [7]. The main differences to the conceptual design department approach are:

- A 3-D CAD model must first be established from the basic input data; and
- The fuselage is represented by a 3-D body which creates at least the same amount of additional finite elements as those required for the aerodynamic surfaces.

Compared with the conceptual design department approach, this one required effort for model creation, analysis time, post-processing, and model modifications, which are higher by factors between 100 and 1000 – definitely much too long for conceptual design activities with respect to available time, budget, and manpower.

The effort especially required to create a CAD model first and the approach for a 3-D fuselage model are not appropriate for conceptual design purposes.

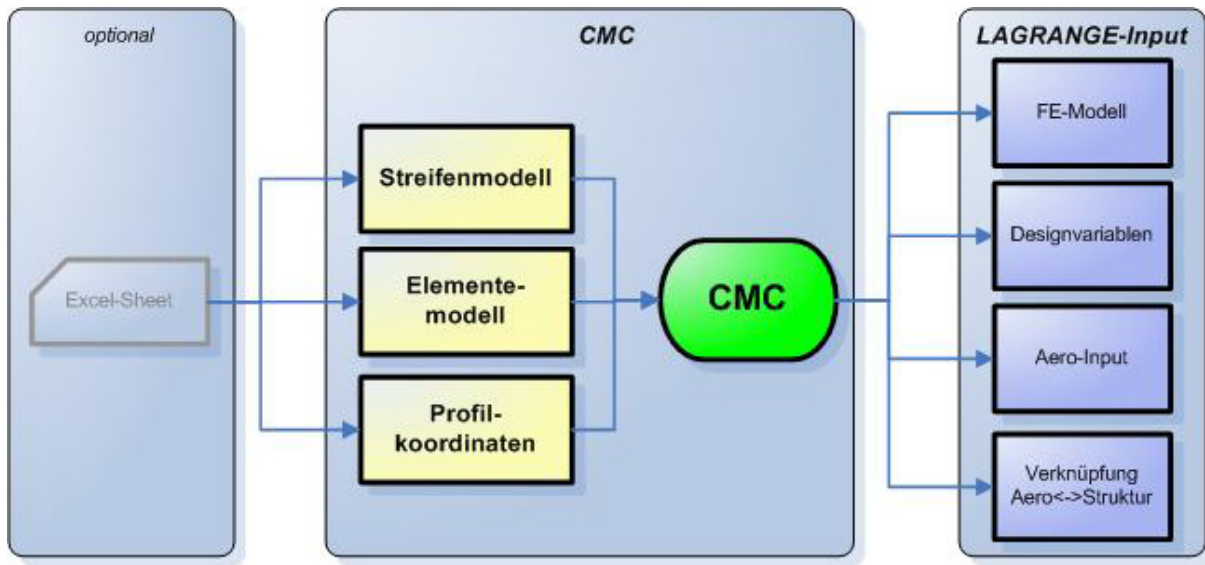


Figure 14-5: Model Creation Process.

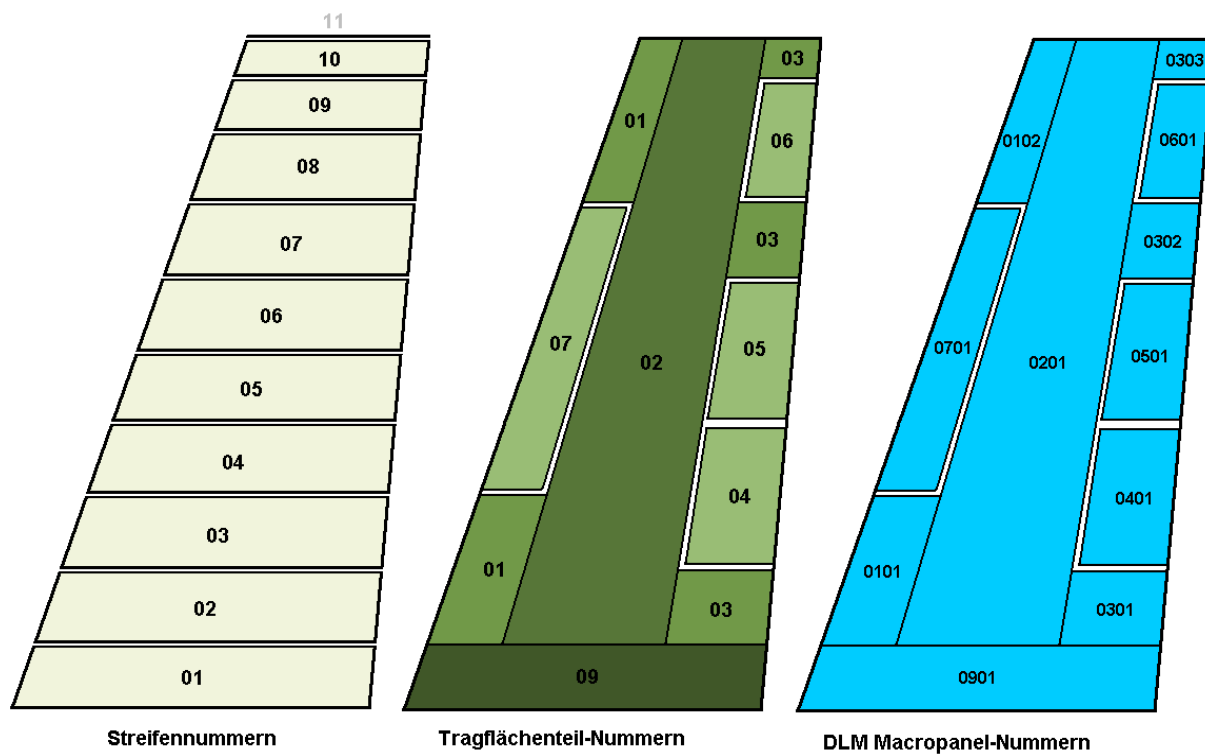
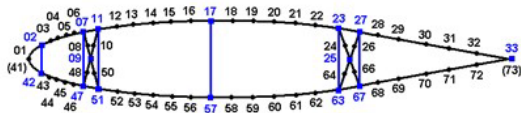


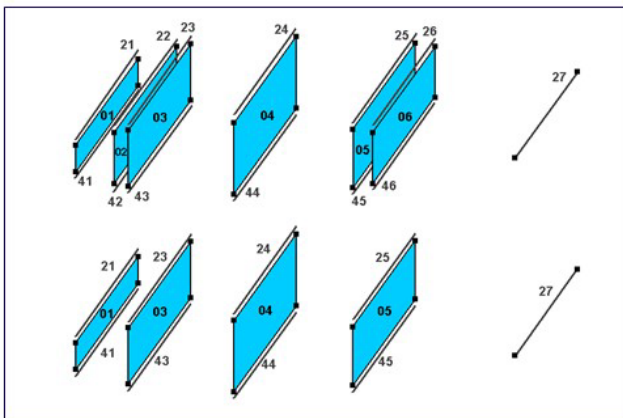
Figure 14-6: Numbering Scheme for Structural and Aerodynamic Sub-Components.

Definition der Struktur eines Streifens

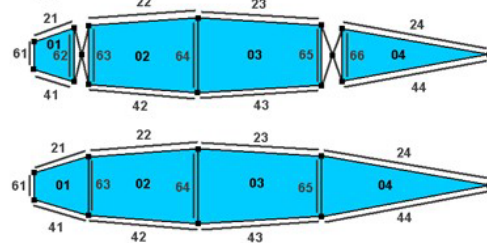
Nummerierung der Knotenpunkte eines Profilschnitts



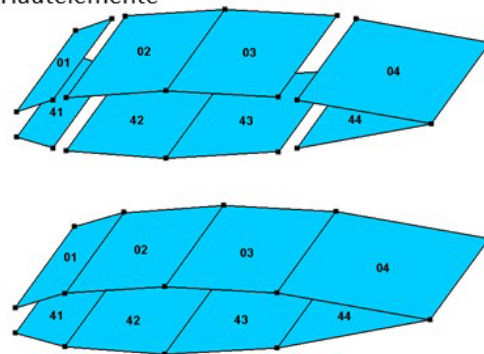
Holm-/Spantelemente



Rippenelemente



Hautelemente



Dipl.-Ing. Max Mustermann
Kurztitel Vortrag

Lehrstuhl für Luftfahrttechnik
27.11.2017, Folie 7

Figure 14-7: Structural Elements Numbering Scheme Within One Strip.

The application of this approach to two different concepts (MALE and a flying wing UCAV configuration, shown in Figure 14-8) revealed another weakness by creating the complete model without any 1-D-elements! This resulted in completely unrealistic optimization results.

14.1.4.2 Optimization Software

It is essential for successful and efficient MDO applications that a set of different optimization methods is available – to “jump across” local minima gaps as well as for acceptable computing times. Any single method will never do it right! It is therefore extremely important that the user try several methods for each individual problem.

14.1.4.3 Hardware

Various (main frame computers, work stations (LINUX), PCs).

14.1.4.4 Human Effort

A few days (if user is experienced) for the first approach, weeks/months for the second (more complex models, additional effort for CAD model creation, more time for running and data evaluation).

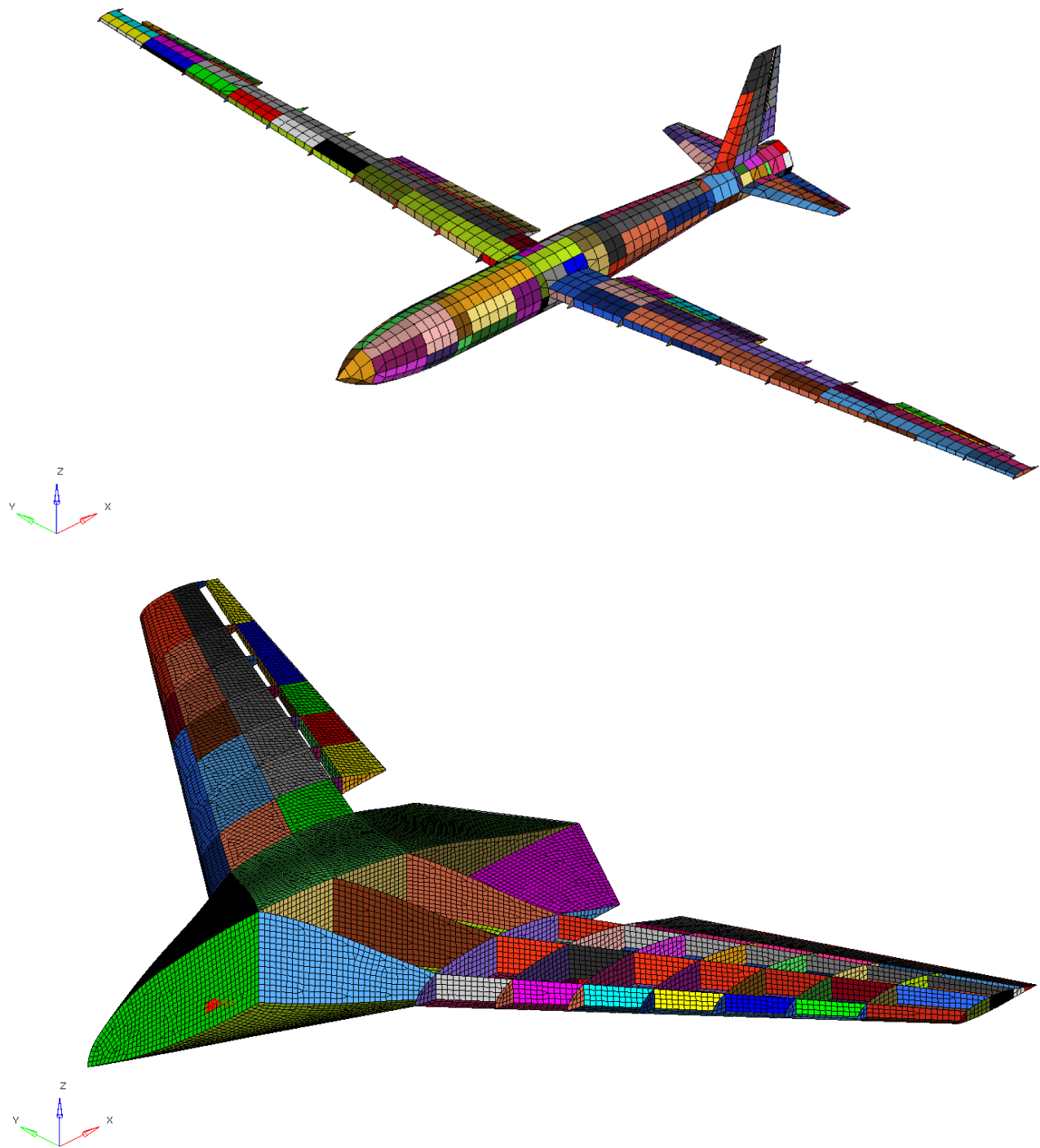


Figure 14-8: Two Models Created by the Structural Analysis Department Method.

14.1.5 Results

A computing time comparison for different sets of design variable elements is given in Table 14-5. Whereas Ref. [4] mainly deals with the development of the method, Ref. [2] describes efforts to incorporate an alternative aerodynamic method (AVL code), mainly for flight mechanic simulations, and Ref. [6] investigates the capabilities of the tool to find and optimize alternative design options.

Table 14-5: Computing Time Comparison for Different Sets of Design Variables.

Elementeset	1	2	3	4
Anzahl der Elemente	2412	2412	1509	1509
Anzahl der Freiheitsgrade	2055	2055	3771	3771
Anzahl der Designvariablen	747	1455	659	1367
Anzahl der Nebenbedingungen	4738	7306	2932	8924
Ausgelegte Strukturmasse [t]	1.376	0.617	1.341	0.707
Rechenzeit bis zur Konvergenz [sec]	1127	1655	547	276
Rechenzeit bis 101% der Endmasse [sec]	874	388	384	127

As an example, and to demonstrate the versatility of the method, several wing tip configurations were compared. Figure 14-9 shows these 15 sets with different sweep and dihedral angles.

In addition, a passive, movable tip was investigated in order to reduce the gust and manoeuvre loads by rotating about a spanwise axis. The rotation is restrained by a torsion spring to maintain a planar shape with the main wing at cruise conditions. Figure 14-10 shows this model.

This study showed the importance of efficient model modification capabilities, the need to simulate all essential constraints (static loads, static aeroelastic effectiveness, flutter stability), and the importance of looking for alternative design concepts.

14.1.5.1 Initial Design (Design Variables, Objectives, Constraint Values)

Initial designs for both approaches are not defined. The user can easily create various start versions for external geometry, structural and aerodynamic meshes, and structural gages.

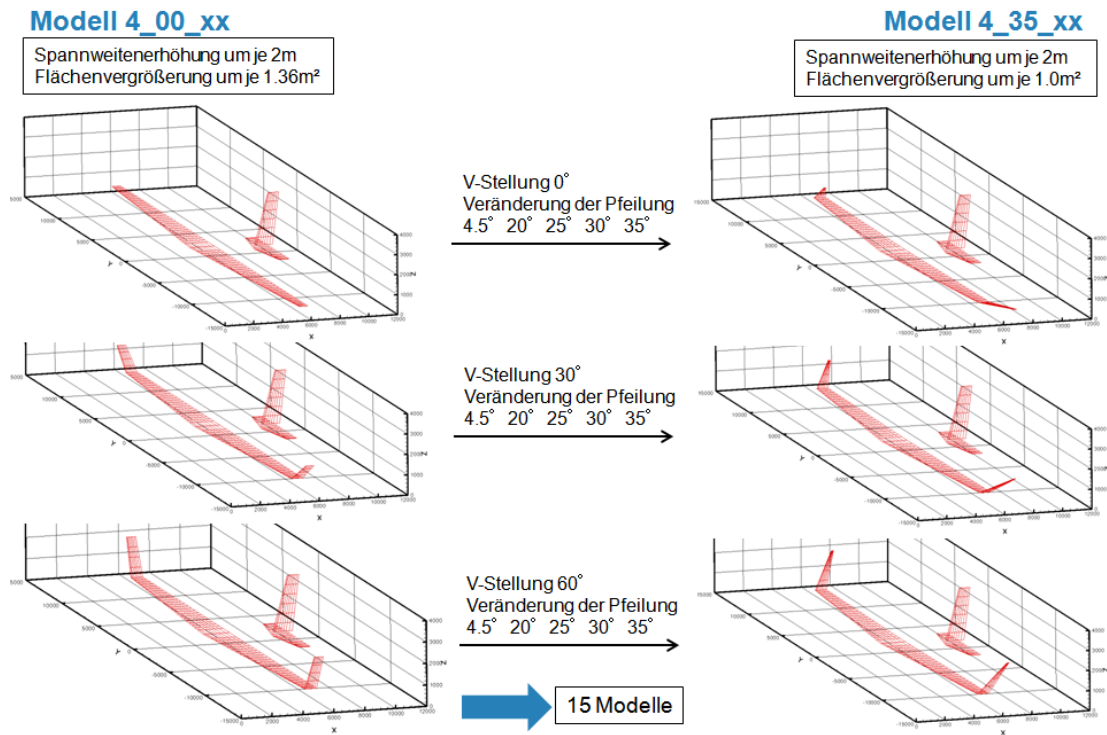


Figure 14-9: Sets of Different Wing Tip Configurations.

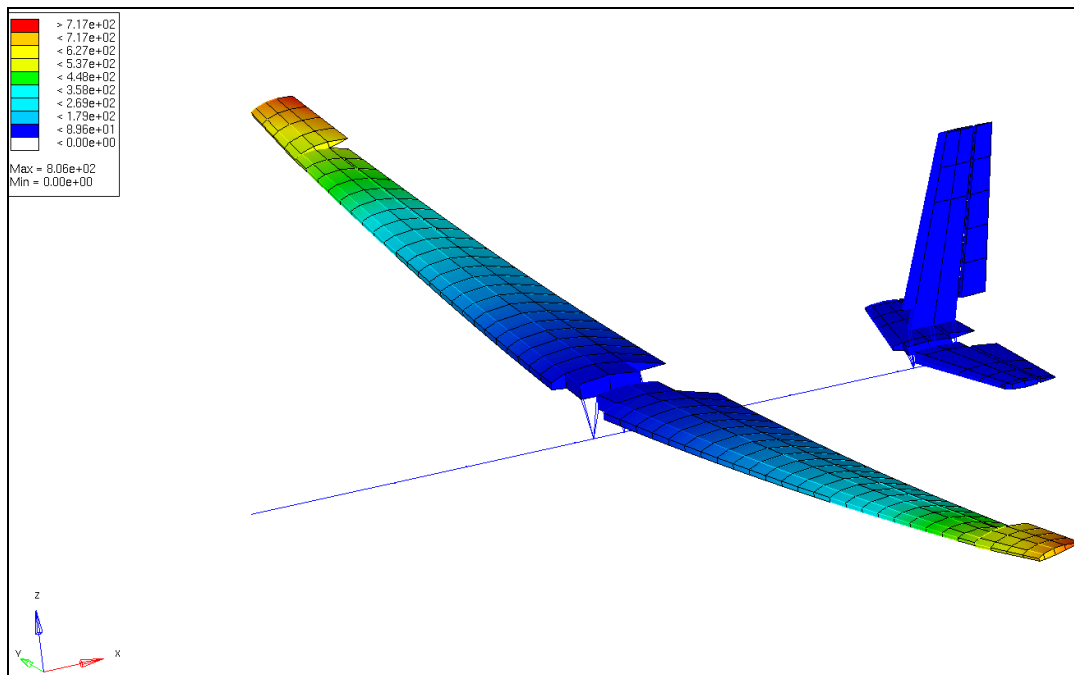


Figure 14-10: Model with Flexing Wing Tips.

14.1.5.2 Optimized Design (Design Variables, Objectives, Constraint Values)

Various results – for fixed external geometry, as well as for parametric variations of the geometry – and for variations of the requirements. The first model creation approach was also used to investigate an adaptive structure solution by a passive movable wingtip for load alleviation.

Figure 14-11 shows the optimization results for a MALE model created with the CMC tool. CONLIN is clearly the best method in this case by approaching the optimum after few minutes, whereas NLPQL, which is currently the one and only preferred method in the structural analysis tools department, is not yet converging after two hours, for this rather simple model. SLP quickly shows a low mass but the results are oscillating in the infeasible domain without a trend towards converging. Past experience shows that CONLIN results usually contain small violations of a few design constraints. To overcome this weakness, a few restart steps by RQP1 (or RQP2) are usually sufficient.

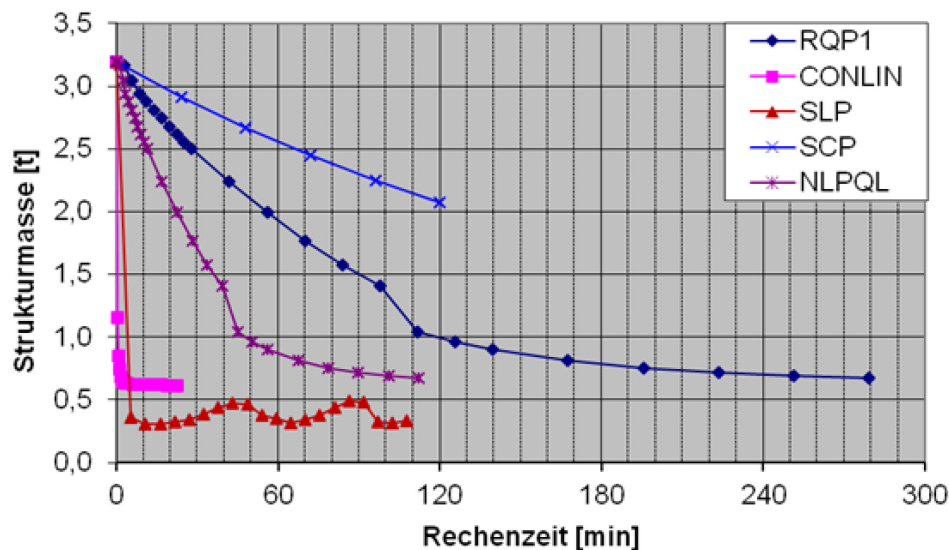


Figure 14-11: MALE Optimization Results with Different Optimization Methods.

The author observed in this context and in publications about external MDO modelling efforts that many tool developers and users seem to like the idea of attaching heavy and large (lumped) masses in the model to a great number of surrounding structural grid points, as indicated in Figure 14-12 for one mass in the forward fuselage of the model. While this makes sense for distributed masses like fuel, it is not correct for heavy equipment. Their Eigenmodes will not show up, which therefore gives incorrect results for the structural modes, and local loads from these masses do not act at the proper locations.

14.1.5.3 Observations

The ability to quickly create a large number of different analytical models permits the discovery of optimal feasible solutions for variations of design requirements. It also enables the user to investigate novel design concepts like adaptive structures (for load alleviation and/or aerodynamic drag reduction).

AVT task 251 is called “Multi-Disciplinary Design and Performance Assessment of Effective, Agile NATO Air Vehicles”. It deals with a flying wing UCAV configuration. This specific configuration shows the short-comings

of the CMC approach, above, as well as those of the parametric modelling approach via a CAD model. The main characteristic of this configuration is given by large equipment items inside the wing, which require discontinuities in the structure (holes in the bottom skin, no space for carry-through spars).

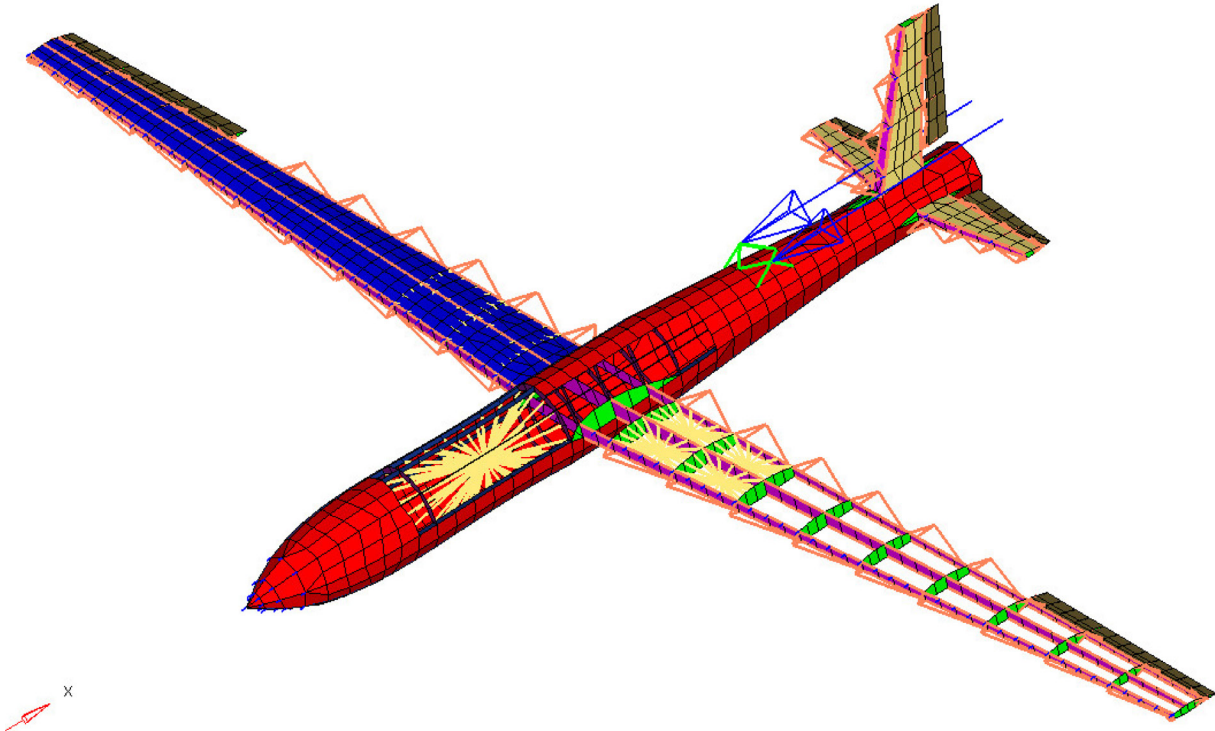


Figure 14-12: “Spider Web” Attachment for a Lumped Mass in the Forward Fuselage.

Body Freedom Flutter (BFF) is most likely the severest design challenge for this type of configuration. In order to simulate it correctly, it is essential that the user understands how to handle the flutter analysis and manipulate the analytical model. Because BFF involves a rigid body motion of the aircraft model, the so-called short period mode, which is composed of a combined motion in heave and pitch, the following facts must be understood:

- a) Rigid body modes have frequency zero at zero airspeed. Flutter analysis usually starts at a finite speed and a finite frequency. The rigid body modes (or at least one of them) is therefore often lost or remains at zero frequency. The real motion is however a combination of both modes (heave and pitch). In order to catch them, it is helpful to fix the model near or at its CG (or AC) in all degrees of freedom and attach two soft springs there for z-translation and rotation about the y-axis.
- b) The model must have a realistic mass moment of inertia about the pitch axis.
- c) The aerodynamic model must be capable to simulate the pitch and heave motions properly.

There are some inherent conflicts for the efficient application of MDO methods and tools:

- Engineers with a lot of experience in aircraft design usually have no experience in the application of MDO tools, and the tool world is getting more and more complex.
- MDO tool specialists usually have only limited experience in aircraft design.

- Resources and time for conceptual design efforts, when formal MDO would be most efficient, are usually very limited.
- MDO tools specialists, when asked to apply their tools for conceptual design applications, usually tend to over-emphasize the refinement of the analytical models and go into details too much for a single discipline while ignoring or under-estimating other effects.

Because software tools are very complex, and because new projects often require extensions to the existing tools, it is essential to have the expertise and ability to quickly create those extensions in-house.

Because of the increasing complexity of tools – not only for the MDO process itself (structural and aerodynamic analysis, materials, lightweight design principles, structural dynamics, aeroelasticity, optimization methods), but also CAD, pre- and post-processing, the required knowledge of the involved disciplines and “practical” aircraft design experience, it is very difficult to create the proper tool-set, which can be handled by a single person in conceptual design and deliver reliable results after just a few days.

It is rather easy to create a tool set for a set of similar configurations (like transport aircraft families with always the same basic geometry and structural concept), but it is almost impossible to create such tool that fits all kinds of unusual configurations. Both approaches described above showed deficiencies when applied to a flying wing configuration like the UCAV from CSO AVT-task 251 (MULDICON configuration), where large internal equipment items and holes in the external structure for access and payload doors require rather irregular structural concepts.

14.1.6 Technical and Financial Improvements/Benefits of Using MDO vs. Traditional Design Methods

Not available.

14.1.7 References; Web Resources; Science Connect Link; and Validation Data Location

- [1] Schweiger, J., Krammer, J., and Hörnlein, H. (1996). Development and application of the integrated structural design tool LAGRANGE. 6th AIAA/NASA/ISSMO Symposium on Multidisciplinary Analysis and Optimization. CP-4169, Seattle, WA, 1996.
- [2] Feger, J. (2012). Weiterentwicklung eines multidisziplinären Flugzeugvorentwurfs-prozesses. Diploma Thesis, Technical University Munich, Lehrstuhl für Luftfahrtsysteme.
- [3] Vidy, C. (2006). Erstellung und Analyse generischer Flügelmodelle für aeroelastische Problemstellungen. Diploma Thesis, Technical University Munich, Lehrstuhl für Aerodynamik.
- [4] Büsing, M. (2011). Multidisziplinäre Optimierung in der Vorentwicklung. Diploma Thesis at the “Lehrstuhl für Luftfahrtsysteme” LS-DA-11/11-EX, Technische Universität München.
- [5] Schweiger, J., Büsing, M., and Feger, J. (2012). A Novel Approach to Improve Conceptual Air Vehicle Design by Multidisciplinary Analysis and Optimization Models and Methods. 12th AIAA Aviation Technology, Integration, and Operations (ATIO) Conference and 14th AIAA/ISSM conference, 17 – 19 September 2012, Indianapolis, Indiana. AIAA 2012-5450.

- [6] Paßler, A. (2013). Einsatz eines multidisziplinären Analyse- und Optimierungsverfahrens zur Auslegung neuer Konzepte im Vorentwurf. Diploma Thesis at the “Lehrstuhl für Luftfahrtsysteme. Technische Universität München.
- [7] Maierl, R. (2012). Automatic Generation of Multidisciplinary Analysis Models based on a Parametric Geometry Description. Diploma Thesis at the Institute of Lightweight Structures, TUM-MW65/1216-DA, Technische Universität München.
- [8] Schweiger, J., Büsing, M., and Feger, J. (2012). Multidisciplinary Analysis and Optimization in the Conceptual Aircraft Design Phase to Support Early Mass Predictions. SAWE Paper No. 3566. 71st Annual Conference of the Society of Allied Weight Engineers, Inc., Bad Gögging and Manching, Germany, 5 – 10 May 2012.
- [9] Schweiger, J. and Munzinger, C. (2012). Rückblick und Ausblick auf Multidisziplinäre Analyse und Optimierung im Flugzeugentwurf Bei Cassidian. German Aerospace Congress, Berlin, Germany 2012.

The Science Connect link is <https://scienceconnect.sto.nato.int/apps/382763>.

No validation data are available.



REPORT DOCUMENTATION PAGE			
1. Recipient's Reference	2. Originator's References	3. Further Reference	4. Security Classification of Document
	STO-TR-AVT-237 AC/323(AVT-237)TP/862	ISBN 978-92-837-2186-4	PUBLIC RELEASE
5. Originator	Science and Technology Organization North Atlantic Treaty Organization BP 25, F-92201 Neuilly-sur-Seine Cedex, France		
6. Title	Benchmarks in Multidisciplinary Optimization and Design for Affordable Military Vehicles		
7. Presented at/Sponsored by	Final Report of NATO AVT-237.		
8. Author(s)/Editor(s)	Multiple	9. Date	September 2019
10. Author's/Editor's Address	Multiple	11. Pages	208
12. Distribution Statement	There are no restrictions on the distribution of this document. Information about the availability of this and other STO unclassified publications is given on the back cover.		
13. Keywords/Descriptors	Aeroelasticity Benchmark Multidisciplinary Optimization		
14. Abstract	<p>The task group objectives were to develop documentation standards for multidisciplinary design optimization (MDO) bench marks and to apply those standards to a number of MDO problems to form a repository to facilitate future research. The driving principal behind the standards was to develop standards that would provide a researcher the necessary information to understand and implement the vehicle optimization performed in a benchmark problem. Specifically, the goals of the standards were to:</p> <ul style="list-style-type: none"> • Describe pertinent aspects of MDO problem; • Contain enough information to duplicate MDO results; and • Document the technical and financial improvement by using MDO in design relative to a traditional design process. <p>The documentation standards were developed and refined over the course of the AVT-237 effort, edited and approved by the entire AVT-237 team, and used to document several MDO benchmark problems. Science Connect was used as a repository for corresponding computer models, files, supporting documents, etc., to provide future researchers with the information necessary to reproduce the benchmark results.</p>		





BP 25

F-92201 NEUILLY-SUR-SEINE CEDEX • FRANCE
Télécopie 0(1)55.61.22.99 • E-mail mailbox@cs.o.nato.int



DIFFUSION DES PUBLICATIONS
STO NON CLASSIFIEES

Les publications de l'AGARD, de la RTO et de la STO peuvent parfois être obtenues auprès des centres nationaux de distribution indiqués ci-dessous. Si vous souhaitez recevoir toutes les publications de la STO, ou simplement celles qui concernent certains Panels, vous pouvez demander d'être inclus soit à titre personnel, soit au nom de votre organisation, sur la liste d'envoi.

Les publications de la STO, de la RTO et de l'AGARD sont également en vente auprès des agences de vente indiquées ci-dessous.

Les demandes de documents STO, RTO ou AGARD doivent comporter la dénomination « STO », « RTO » ou « AGARD » selon le cas, suivi du numéro de série. Des informations analogues, telles que le titre et la date de publication sont souhaitables.

Si vous souhaitez recevoir une notification électronique de la disponibilité des rapports de la STO au fur et à mesure de leur publication, vous pouvez consulter notre site Web (<http://www.sto.nato.int/>) et vous abonner à ce service.

CENTRES DE DIFFUSION NATIONAUX

ALLEMAGNE

Streitkräfteamt / Abteilung III
Fachinformationszentrum der Bundeswehr (FIZBw)
Gorch-Fock-Straße 7, D-53229 Bonn

BELGIQUE

Royal High Institute for Defence – KHID/IRSD/RHID
Management of Scientific & Technological Research
for Defence, National STO Coordinator
Royal Military Academy – Campus Renaissance
Renaissancelaan 30, 1000 Bruxelles

BULGARIE

Ministry of Defence
Defence Institute "Prof. Tsvetan Lazarov"
"Tsvetan Lazarov" bul no.2
1592 Sofia

CANADA

DGSIST 2
Recherche et développement pour la défense Canada
60 Moodie Drive (7N-1-F20)
Ottawa, Ontario K1A 0K2

DANEMARK

Danish Acquisition and Logistics Organization
(DALO)
Lautrupbjerg 1-5
2750 Ballerup

ESPAGNE

Área de Cooperación Internacional en I+D
SDGPLATIN (DGAM)
C/ Arturo Soria 289
28033 Madrid

ESTONIE

Estonian National Defence College
Centre for Applied Research
Riia str 12
Tartu 51013

ETATS-UNIS

Defense Technical Information Center
8725 John J. Kingman Road
Fort Belvoir, VA 22060-6218

FRANCE

O.N.E.R.A. (ISP)
29, Avenue de la Division Leclerc
BP 72
92322 Châtillon Cedex

GRECE (Correspondant)

Defence Industry & Research General
Directorate, Research Directorate
Fakinos Base Camp, S.T.G. 1020
Holargos, Athens

HONGRIE

Hungarian Ministry of Defence
Development and Logistics Agency
P.O.B. 25
H-1885 Budapest

ITALIE

Ten Col Renato NARO
Capo servizio Gestione della Conoscenza
F. Baracca Military Airport "Comparto A"
Via di Centocelle, 301
00175, Rome

LUXEMBOURG

Voir Belgique

NORVEGE

Norwegian Defence Research
Establishment
Attn: Biblioteket
P.O. Box 25
NO-2007 Kjeller

PAYS-BAS

Royal Netherlands Military
Academy Library
P.O. Box 90.002
4800 PA Breda

POLOGNE

Centralna Biblioteka Wojskowa
ul. Ostrobramska 109
04-041 Warszawa

PORTUGAL

Estado Maior da Força Aérea
SDFA – Centro de Documentação
Alfragide
P-2720 Amadora

REPUBLIQUE TCHEQUE

Vojenský technický ústav s.p.
CZ Distribution Information Centre
Mladoboleslavská 944
PO Box 18
197 06 Praha 9

ROUMANIE

Romanian National Distribution
Centre
Armaments Department
9-11, Drumul Taberei Street
Sector 6
061353 Bucharest

ROYAUME-UNI

Dstl Records Centre
Rm G02, ISAT F, Building 5
Dstl Porton Down
Salisbury SP4 0JQ

SLOVAQUIE

Akadémia ozbrojených síl gen.
M.R. Štefánika, Distribučné a
informačné stredisko STO
Demänová 393
031 01 Liptovský Mikuláš 1

SLOVENIE

Ministry of Defence
Central Registry for EU & NATO
Vojkova 55
1000 Ljubljana

TURQUIE

Milli Savunma Bakanlığı (MSB)
ARGE ve Teknoloji Dairesi
Başkanlığı
06650 Bakanlıklar – Ankara

AGENCES DE VENTE

**The British Library Document
Supply Centre**
Boston Spa, Wetherby
West Yorkshire LS23 7BQ
ROYAUME-UNI

**Canada Institute for Scientific and
Technical Information (CISTI)**
National Research Council Acquisitions
Montreal Road, Building M-55
Ottawa, Ontario K1A 0S2
CANADA

Les demandes de documents STO, RTO ou AGARD doivent comporter la dénomination « STO », « RTO » ou « AGARD » selon le cas, suivie du numéro de série (par exemple AGARD-AG-315). Des informations analogues, telles que le titre et la date de publication sont souhaitables. Des références bibliographiques complètes ainsi que des résumés des publications STO, RTO et AGARD figurent dans le « NTIS Publications Database » (<http://www.ntis.gov/>).



BP 25
F-92201 NEUILLY-SUR-SEINE CEDEX • FRANCE
Télécopie 0(1)55.61.22.99 • E-mail mailbox@cs.o.nato.int



**DISTRIBUTION OF UNCLASSIFIED
STO PUBLICATIONS**

AGARD, RTO & STO publications are sometimes available from the National Distribution Centres listed below. If you wish to receive all STO reports, or just those relating to one or more specific STO Panels, they may be willing to include you (or your Organisation) in their distribution.

STO, RTO and AGARD reports may also be purchased from the Sales Agencies listed below.

Requests for STO, RTO or AGARD documents should include the word 'STO', 'RTO' or 'AGARD', as appropriate, followed by the serial number. Collateral information such as title and publication date is desirable.

If you wish to receive electronic notification of STO reports as they are published, please visit our website (<http://www.sto.nato.int/>) from where you can register for this service.

NATIONAL DISTRIBUTION CENTRES

BELGIUM

Royal High Institute for Defence –
KHID/IRSD/RHID
Management of Scientific & Technological
Research for Defence, National STO
Coordinator
Royal Military Academy – Campus
Renaissance
Renaissancelaan 30
1000 Brussels

BULGARIA

Ministry of Defence
Defence Institute "Prof. Tsvetan Lazarov"
"Tsvetan Lazarov" bul no.2
1592 Sofia

CANADA

DSTKIM 2
Defence Research and Development Canada
60 Moodie Drive (7N-1-F20)
Ottawa, Ontario K1A 0K2

CZECH REPUBLIC

Vojenský technický ústav s.p.
CZ Distribution Information Centre
Mladoboleslavská 944
PO Box 18
197 06 Praha 9

DENMARK

Danish Acquisition and Logistics Organization
(DALO)
Lautrupbjerg 1-5
2750 Ballerup

ESTONIA

Estonian National Defence College
Centre for Applied Research
Riia str 12
Tartu 51013

FRANCE

O.N.E.R.A. (ISP)
29, Avenue de la Division Leclerc – BP 72
92322 Châtillon Cedex

GERMANY

Streitkräfteamt / Abteilung III
Fachinformationszentrum der
Bundeswehr (FIZBW)
Gorch-Fock-Straße 7
D-53229 Bonn

GREECE (Point of Contact)

Defence Industry & Research General
Directorate, Research Directorate
Fakinos Base Camp, S.T.G. 1020
Holargos, Athens

HUNGARY

Hungarian Ministry of Defence
Development and Logistics Agency
P.O.B. 25
H-1885 Budapest

ITALY

Ten Col Renato NARO
Capo servizio Gestione della Conoscenza
F. Baracca Military Airport "Comparto A"
Via di Centocelle, 301
00175, Rome

LUXEMBOURG

See Belgium

NETHERLANDS

Royal Netherlands Military
Academy Library
P.O. Box 90.002
4800 PA Breda

NORWAY

Norwegian Defence Research
Establishment, Attn: Biblioteket
P.O. Box 25
NO-2007 Kjeller

POLAND

Centralna Biblioteka Wojskowa
ul. Ostrobramska 109
04-041 Warszawa

PORTUGAL

Estado Maior da Força Aérea
S DFA – Centro de Documentação
Alfragide
P-2720 Amadora

ROMANIA

Romanian National Distribution Centre
Armaments Department
9-11, Drumul Taberei Street
Sector 6
061353 Bucharest

SLOVAKIA

Akadémia ozbrojených síl gen
M.R. Štefánika, Distribučné a
informačné stredisko STO
Demänová 393
031 01 Liptovský Mikuláš 1

SLOVENIA

Ministry of Defence
Central Registry for EU & NATO
Vojkova 55
1000 Ljubljana

SPAIN

Área de Cooperación Internacional en I+D
SDGPLATIN (DGAM)
C/ Arturo Soria 289
28033 Madrid

TURKEY

Milli Savunma Bakanlığı (MSB)
ARGE ve Teknoloji Dairesi Başkanlığı
06650 Bakanlıklar – Ankara

UNITED KINGDOM

Dstl Records Centre
Rm G02, ISAT F, Building 5
Dstl Porton Down, Salisbury SP4 0JQ

UNITED STATES

Defense Technical Information Center
8725 John J. Kingman Road
Fort Belvoir, VA 22060-6218

SALES AGENCIES

The British Library Document Supply Centre

Boston Spa, Wetherby
West Yorkshire LS23 7BQ
UNITED KINGDOM

Canada Institute for Scientific and Technical Information (CISTI)

National Research Council Acquisitions
Montreal Road, Building M-55
Ottawa, Ontario K1A 0S2
CANADA

Requests for STO, RTO or AGARD documents should include the word 'STO', 'RTO' or 'AGARD', as appropriate, followed by the serial number (for example AGARD-AG-315). Collateral information such as title and publication date is desirable. Full bibliographical references and abstracts of STO, RTO and AGARD publications are given in "NTIS Publications Database" (<http://www.ntis.gov>).